

**High resolution records of black carbon
and other aerosol constituents from the
Lomonosovfonna 2009 ice core**

Inauguraldissertation

der Philosophisch-naturwissenschaftlichen Fakultät

der Universität Bern

vorgelegt von

Isabel Alexandra Wendl

aus Deutschland

Leiterin der Arbeit:

Prof. Dr. Margit Schwikowski

Departement für Chemie und Biochemie der Universität Bern

**High resolution records of black carbon
and other aerosol constituents from the
Lomonosovfonna 2009 ice core**

Inauguraldissertation
der Philosophisch-naturwissenschaftlichen Fakultät
der Universität Bern

vorgelegt von

Isabel Alexandra Wendl

aus Deutschland

Leiterin der Arbeit:

Prof. Dr. Margit Schwikowski

Departement für Chemie und Biochemie der Universität Bern

Von der philosophisch-naturwissenschaftlichen Fakultät angenommen:

Bern,

Der Dekan:

Prof. Dr. G. Colangelo

Summary

Black carbon (BC) is one of the short-lived atmospheric constituents whose radiative forcing is not yet fully understood and quantified. It has recently gained attention in the climate discussion because BC mitigation is expected to result in a climate effect within the next few decades, thus much earlier than that following from CO₂ reduction.

BC is a by-product of the incomplete combustion of biomass and fossil fuels that affects climate due to its light-absorbing properties. It has a direct warming effect in the atmosphere as well as an indirect effect once deposited on snow and ice. Deposited BC reduces the surface albedo which results in more absorption of the incoming solar radiation and thus in accelerated melting of snow and ice. This is of particular importance to the Polar Regions that comprise vast areas of snow-and ice-covered surfaces. The Arctic is already among the regions that are most affected by climate change because climate effects there are amplified. Over the past 100 years, Arctic temperatures have increased at almost twice the global average rate, with an increase in annual average surface air temperatures of 2-3°C in Alaska and Siberia from 1954 to 2003. This is accompanied by an earlier onset of the spring melt, a lengthening of the melt season, changes in the mass balance of the Greenland ice sheet, and a reduced sea ice extent.

BC data from the Arctic are sparse and the existing global climate models often underestimate the effects in the Arctic. In order to understand today's role of BC for the Arctic, climate information on past BC concentrations is needed. Instrumental observations cover only the most recent years and studies on Arctic snow extend back only several decades. Thus, natural archives, such as ice cores, provide an invaluable source of information on temperature, moisture, and atmospheric composition that extend beyond instrumental observations. Ice core research in the Arctic has so far mainly focused on the large ice sheet of Greenland. However, the high-altitude Greenland sites are affected by pollution from the low latitudes, which is contrary to the low-altitude sites outside of Greenland that are partly influenced by pollution sources located in the high latitudes. In order to get a more complete picture, it is also important to gain palaeo-climate information from sites outside of Greenland that have often been neglected because they are affected by seasonal melt.

In this work, the ice core from Lomonosovfonna, Svalbard, drilled in 2009 (Lomo09), was analysed for BC and other atmospheric constituents in order to reconstruct the climate and environmental history of a low-altitude Arctic site. Because Lomonosovfonna has been proven to be less affected by melt, the atmospheric signal is better preserved than at other Arctic sites.

The Lomo09 ice core was dated by applying a multiple parameter approach. This included detection of reference horizons, annual layer counting based on the pronounced seasonality of $\delta^{18}\text{O}$ and Na^+ concentration, nuclear dating with ^{210}Pb , and a simple glacier flow model. This resulted in a robust chronology assigning the ice at the depth of 149.5 m to the year 1222. The core was sampled at high resolution (3-4 cm) so that even for the oldest ice annual resolution was obtained.

In order to compile a highly time-resolved BC record of the Lomo09 core, the method for the BC analysis in discrete snow and ice samples using a single particle soot photometer (SP2) was optimised. The SP2 requires a nebulization step for the analysis of liquid snow or ice samples because it only analyses airborne samples. The method improvement thus involved the comparison of three different nebulizer types: (1) the ultrasonic nebulizer (CETAC) applied in previous studies, (2) the newly introduced jet nebulizer system APEX-Q, and (3) a PSI-in-house built Collison-type nebulizer. The APEX-Q was identified as the least size-dependent nebulizer in the BC particle diameter range of 100–1000 nm, whereas the advantage of the CETAC remained that air and liquid flows can be monitored continuously. The Collison-type nebulizer consumes large sample volumes and was considered not applicable for ice core analysis where sample volume is limited. All nebulizer types require calibration with BC standards for the determination of the BC mass concentration in unknown liquid samples. Aquadag, an industrial lubricant, was chosen as suitable material for the preparation of those standards. The method for BC analysis was further optimised by evaluating the best sample treatment for fresh discrete snow and ice samples. This showed that the samples are best kept frozen until analysis. Once melted, they are best treated in an ultrasonic bath for around 25 min to destroy potential agglomerates, and then immediately analysed while being stirred with a magnetic stir bar. Refreezing of the samples should be avoided because it caused particle loss. This method was then applied to obtain a BC mass concentration record of the Lomo09 core that covers the time period between 1950 and 2005. The BC concentrations were observed to be in the range of those from Greenland ice rather than the much higher concentrations detected in Svalbard snow or ice. This can partly be explained by the different methods applied to the previous Svalbard samples. Furthermore, the increase in BC concentrations in the last 30 years observed in another ice core from Svalbard is not reflected in the Lomo09 BC record. The decreasing concentrations in the Lomo09 BC record from 1950 to 2005 resemble the decreasing trend observed in Greenland ice cores as well as in atmospheric measurements in the Arctic. This decrease is probably caused by BC emissions from the source region of Eurasia that have decreased constantly over the last 50 years. In some years, however, the Lomo09 BC record is influenced by additional emissions from North America.

The Lomo09 was further analysed for water soluble major ions, including the two nitrogen species of nitrate (NO_3^-) and ammonium (NH_4^+). Those species were examined for emission sources and the influence of melt on the ion records. The record for annual melt percent of the Lomo09 core was obtained by visually identifying melt features during the core sampling process. In order to account for dating uncertainties and potential smoothing effects by melt-water relocation, only 10-year-averaged data was used. Both the NO_3^- and the NH_4^+ record reveal a clear anthropogenic influence in the 20th century, which is attributed to Eurasian emission sources. On decadal timescales, pre-industrial NO_3^- correlates with methane-sulphonate (MSA), a species linked to ocean productivity. This connection is explained by a fertilising effect where the deposition of atmospheric NO_3^- leads to increased marine phytoplankton growth resulting in elevated MSA concentrations in the atmosphere. Based on the data, the source for pre-industrial NO_3^- could not be identified but is thought to be Eurasia as for industrial NO_3^- . This is different for pre-industrial NH_4^+ , which was found to originate from biogenic ammonia (NH_3) emissions from the Siberian boreal forests. The ion records do not correlate with the melt record. Thus, melt is excluded from having affected the decadal variations of the NO_3^- and NH_4^+ records used for this investigation.

The Lomo09 core was drilled only 4.6 km south of the 1997 Lomonosovfonna ice core (Lomo97) that has been studied in great detail. This provides an excellent opportunity to investigate the spatial representativeness of the climate reconstruction from the cores. The general ion composition and the temporal trends of the ion records of the two cores agree well. The anthropogenic influence is clearly visible in the NO_3^- and SO_4^{2-} records. However, the correlation of NO_3^- and MSA observed in the Lomo09 core was not detected in the Lomo97 core, where NO_3^- is correlated with Ca^{2+} instead. The $\delta^{18}\text{O}$ records are also very similar, with a decreasing trend from 1200 to around 1880, and highest values between 1900 and 1950. Thus, it is assumed that the Lomo09 $\delta^{18}\text{O}$ record also represents temperature changes, with the coldest temperatures occurring between 1760 and 1880. Like for the Lomo97 core, the Lomo09 $\delta^{18}\text{O}$ record is assumed to be representative of Longyearbyen air temperature. Moreover, prior to 1800, the two records of the melt index of $\ln(\text{Na}^+/\text{Mg}^{2+})$ agree very well. After 1800, the Lomo09 $\ln(\text{Na}^+/\text{Mg}^{2+})$ record resembles that of another Svalbard ice core from Holtedahlfonna, drilled in 2005. The largest discrepancy between the Lomo09 and the Lomo97 core is observed in the dating of the lowermost core section. In both cases, the sulphate peak detected in this part of the core was assigned to a certain major volcanic eruption; in case of the Lomo09 core this is Samalas in 1257/58 and for the Lomo97 core it is Hekla in 1104 or 1158. Based on the data, whether one or the other attribution was correct could not be resolved. This is because in either case, the annual accumulation rate to fit the particular other major volcanic eruption would be

out of range. This first comparison of the two most recent ice cores from Lomonosovfonna revealed that the climate and environmental reconstruction from one ice core may be representative of a single glacier, but not necessarily of an entire region such as Svalbard.

A snow pit study conducted in March/April 2010 revealed that BC concentrations as well as concentrations of chloride, an ionic species mainly derived from sea salt, are more than a factor of two lower at Lomonosovfonna than at Foxfonna and Tellbreen, two glaciers located in the vicinity of Longyearbyen and the ocean. This difference was explained by the greater distance of Lomonosovfonna to local BC sources and the ocean.

This thesis provides high resolution records of BC and other aerosol constituents from the Lomo09 ice core enabling a reconstruction of the climate and environmental history. Although many aspects have been considered, future work is needed. This mainly concerns the BC record that should be extended for the whole core and the detailed comparison of the Lomo09 and Lomo97 ice cores.

Please note that this PhD thesis is written in British English apart from chapter 3 that is written in American English due to the journal requirements.

Contents

Summary	i
Contents	v
List of abbreviations	ix
1 Introduction	1
1.1 Climate change	1
1.2 Black carbon (BC) and climate change.....	3
1.3 The Arctic	4
1.3.1 Transport pathways to the Arctic/ Arctic Haze.....	5
1.4 Svalbard	7
1.4.1 Setting and climate.....	7
1.4.2 State of the art in ice core research.....	10
1.4.3 Influence of melt on records of chemical species.....	11
1.5 Lomonosovfonna.....	11
1.5.1 The Lomonosovfonna 1997 ice core.....	12
1.6 Motivation of the study.....	13
References	14
2 Methods	23
2.1 Drilling.....	23
2.2 Sample preparation.....	24
2.3 Annual melt percent.....	26
2.4 Water stable isotope ratios ($\delta^{18}\text{O}$ and δD).....	26
2.4.1 Isotopic ratio mass spectrometry (IRMS)	28
2.4.2 Wavelength-scanned cavity ring down spectrometry (WS-CRDS).....	29
2.5 Ion chromatography (water soluble major ions).....	31
2.6 Black carbon (BC).....	34
2.7 Dating of the Lomo09 ice core	35
2.7.1 Liquid scintillation counting (^3H)	36

2.7.2	Volcanic reference horizons.....	37
2.7.3	α -spectroscopy (^{210}Pb).....	39
2.7.4	Annual layer counting (ALC).....	41
2.7.5	Glacier flow model	42
	References	43
3	Optimized method for black carbon analysis in ice and snow using the Single Particle Soot Photometer.....	47
	Abstract.....	48
3.1	Introduction	48
3.2	Experimental.....	49
3.2.1	Nebulizer/SP2-setup.....	50
3.2.2	Internal Calibration	53
3.2.3	Approaches to determine the BC mass concentration of an aqueous sample	53
3.2.4	Standard preparation.....	57
3.3	Results and discussion	58
3.3.1	Nebulizer comparison	58
3.3.2	Uncertainty of external calibration approach and choice of BC standard material...	62
3.3.3	Repeatability of external calibration.....	64
3.3.4	Sample treatment.....	66
3.4	Summary.....	69
	Appendix A: Instrumental setup	71
	Appendix B: BC standards.....	72
	Appendix C: Sample storage.....	73
	References	75
	Supplementary Material	78

4	800 year ice-core record of nitrogen deposition in Svalbard linked to ocean productivity and biogenic emissions	109
	Abstract.....	110
4.1	Introduction	110
4.2	Methods.....	113
4.2.1	Drilling site and meteorological setting.....	113
4.2.2	Sampling and analyses	113
4.2.3	Ice-core dating	114
4.2.4	Calculation of annual melt percent	115
4.3	Results and discussion	115
4.3.1	Nitrate and methane-sulphonate (NO ₃ ⁻ and MSA).....	119
4.3.2	Ammonium (NH ₄ ⁺).....	124
4.4	Summary.....	126
	References	127
	Supplementary Material	135
5	Is the climate and environmental reconstruction from one ice core representative of an entire region? - A case study from Lomonosovfonna, Svalbard	137
	Abstract.....	138
5.1	Introduction	138
5.2	Drilling and methods	139
5.3	Results and discussion	142
5.3.1	Dating.....	142
5.3.2	Ion chemistry	145
5.3.3	Annual accumulation rate.....	151
5.3.4	Water stable isotope ratio δ ¹⁸ O	152
5.3.5	Melt indices stratigraphic melt index and ln(Na ⁺ /Mg ²⁺).....	153
5.4	Summary and conclusions.....	156
	References	158
	Supplementary Material	163

6	Black carbon in the Lomonosovfonna 2009 ice core	169
6.1	Introduction	169
6.2	Results and discussion	171
6.3	Summary and outlook.....	176
	References	178
7	Snow pit study on black carbon concentrations in Svalbard	183
7.1	Introduction	183
7.2	Methods.....	184
7.3	Results and discussion	185
7.4	Summary.....	186
	References	188
8	Outlook	189
8.1	Black carbon (BC).....	189
8.2	Ice core chemistry.....	189
8.3	Dating methods	190
	References	191
9	Appendix	193
	Acknowledgements	205
	Curriculum Vitae	209

List of abbreviations

ALC	Annual layer counting
AMAP	Arctic Monitoring and Assessment Programme
APEX-Q	APEX-Q jet nebulizer
AQ	Aquadag
BC	Black Carbon
BS	Barents Sea
CETAC	CETAC ultrasonic nebulizer
CWU	Central Washington University
DMS	Dimethyl-sulphide
Eq.	Equation
FELICS	Fast Electromechanical Lightweight Ice Coring System
Holte05	Holtedahlfonna 2005 ice core
IC	Ion chromatography
IPCC	Intergovernmental Panel on Climate Change
IRMS	Isotope ratio mass spectrometry
ISSW	Integrating Sphere/ Integrating Sandwich Spectrophotometer
LIA	Little Ice Age
Lomo09	Lomonosovfonna 2009 ice core
Lomo97	Lomonosovfonna 1997 ice core
m asl	Meter above sea level
MLR	Multiple linear regression analysis
MQ	MilliQ water (ultrapure water)
MSA	Methane-sulphonate
m weq	Meter water equivalent
MWP	Medieval Warm Period
Nss	Non-sea-salt
OC	Organic Carbon
PC	Principal component
PCA	Principal component analysis
PFA	Polyfluoralkoxy-polymer
PMT	Photomultiplier tube
PP	Polypropylene
PSI	Paul Scherrer Institut

PSL	Polystyrene latex spheres
SP2	Single Particle Soot Photometer
TU	Tritium units
UNFCC	United Nations Framework Convention on Climate Change
VSMOW	Vienna Standard Mean Ocean Water
WS-CRDS	Wavelength-Scanned Cavity Ring Down Spectrometry

1 Introduction

1.1 Climate change

Climate is defined as the average weather including the variability of its parameters like temperature, wind, clouds, etc., over time periods of decades or longer (Cubasch et al., 2013). It undergoes changes and thus has been of interest for a long time. Nowadays, the awareness of changes in climate has not only increased in science but also amongst the public and in politics. The annual United Nations Framework Convention on Climate Change (UNFCCC) conferences as well as the assessment reports, published every five to six years by the Intergovernmental Panel on Climate Change (IPCC), are highly discussed and not only show the great public interest but also point out the uncertainties and raise questions regarding climate change. How much has the climate changed in the past? How much will it change in the future? Is this change natural? Where will it lead to? Who is to blame? Most of these questions still remain unresolved.

The Earth's climate is controlled by solar radiation and the resulting radiation balance. It involves a complex interplay of incoming shortwave and outgoing longwave radiation. The Earth's radiation balance can thus be perturbed by natural and anthropogenic changes in the atmosphere, land, ocean, biosphere, and cryosphere which result in a radiative forcing that affects climate (Cubasch et al., 2013).

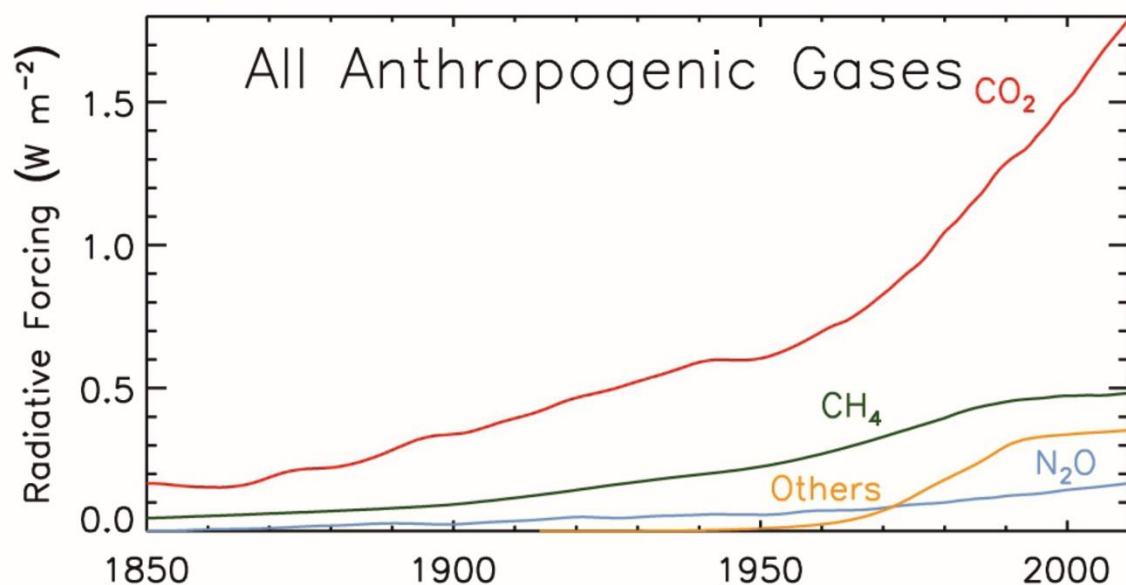


Figure 1.1 Radiative forcing caused by the main anthropogenic gases (modified after Myhre et al., 2013). CO₂ = carbon dioxide; CH₄ = methane; N₂O = nitrous oxide.

Instrumental observations cover the time period back to around 1850 (Hartmann et al., 2013). They reveal that in the last 150 years anthropogenic emissions have resulted in increased

1 Introduction

concentrations of the greenhouse gases carbon dioxide (CO_2), methane (CH_4) and nitrous oxide (N_2O) that highly affect the Earth's radiation balance (Myhre et al., 2013) (Figure 1.1). However, in order to place those changes into the perspective of the natural variability that occurred on geological timescales of millions of years, we need climate information from natural archives. These archives include tree rings, marine and terrestrial sediment cores, and ice cores that cover the time period prior to instrumental observations. These archives incorporated a strong climatic signal into their structure in the past, so that their physical or chemical characteristics can be used as proxy data for temperature, moisture, etc. in historical times, thus providing palaeoclimate records (Bradley et al., 2003).

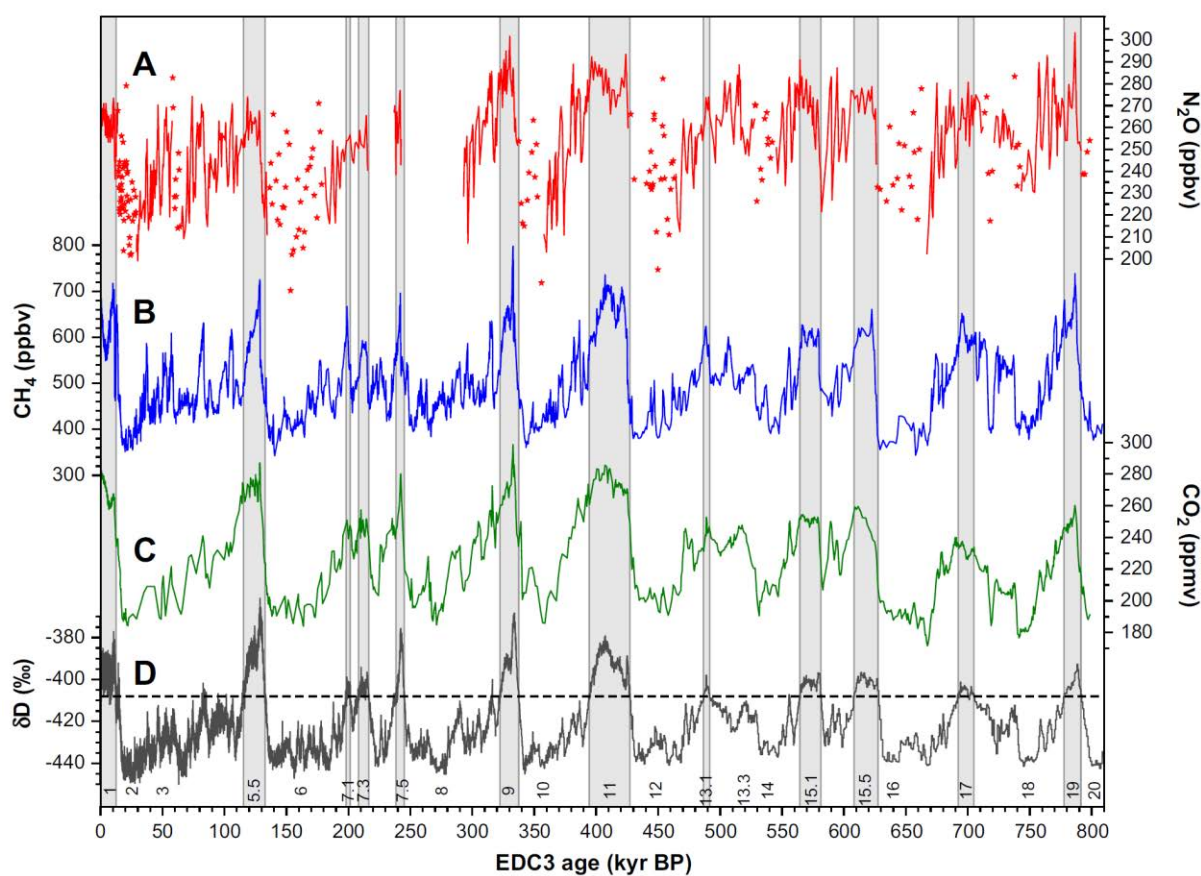


Figure 1.2 Reconstructed greenhouse gas concentrations from Antarctic ice cores (Schilt et al., 2010). A: N_2O from EPICA Dome C; B: CH_4 from EDC; C: CO_2 from Vostok between 20 and 390 kyr BP, EDC elsewhere; D: δD EDC; grey shaded areas mark interglacials.

Ice cores provide an invaluable climate archive that has largely contributed to the understanding of the Earth's climate. Up to now, the oldest ice retrieved is that of the EPICA Dome C core, Antarctica, which covers the last 800,000 years (Schilt et al., 2010). These extensive records, displayed in Figure 1.2, depict the natural variability of the observed parameters. It can be seen that in the past, the concentrations of CO_2 , CH_4 and N_2O were high at certain times, especially during the interglacials. In the past, CO_2 concentrations never exceeded

300 ppm, however, today we are at a level of 390.5 ppm (Masson-Delmotte et al., 2013). Based on ice core studies, present-day (2011) CO₂ concentrations as well as the concentration range of CH₄ and N₂O can be seen to exceed that of the past 800,000 years (Masson-Delmotte et al., 2013). At present we are in the Holocene, an interglacial period that up to now has lasted for approximately 11,500 years (Mayewski et al., 2004). Interglacials are characterised by high temperatures. The higher δD values depicted in Figure 1.2 are good indicators of this. δD , the ratio of the hydrogen isotopes ¹H and ²H (details in chapter 2.4), was found to be temperature-dependent and thus can be used as a palaeo-thermometer (e.g., Dansgaard, 1953; Wolff et al., 2006).

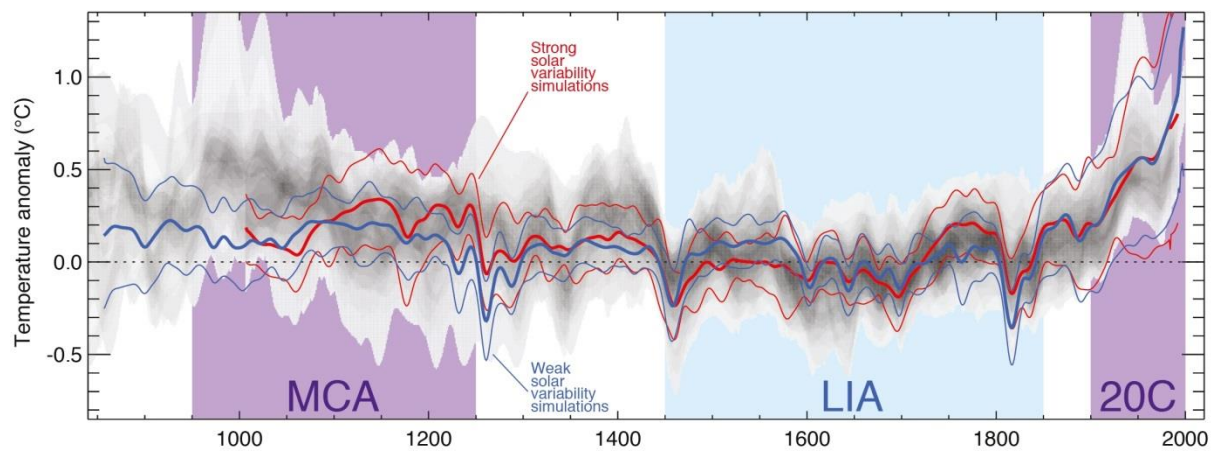


Figure 1.3 Reconstructed (grey) and simulated (red/blue) Northern Hemispheric temperature (Masson-Delmotte et al., 2013). MCA = Medieval Climate Anomaly; LIA = Little Ice Age; 20C = 20th century.

In order to reveal the current trends in atmospheric composition and temperature we have to focus on the more recent past of the last one or two millennia (Mayewski et al., 2004). The last millennium in the Northern Hemisphere features three distinct phases (Figure 1.3): (1) the Medieval Climate Anomaly (MCA) from around 950 to 1250 with elevated temperatures in many regions and reduced glacier extent (Grove and Switsur, 1994; Hughes and Diaz, 1994), (2) the Little Ice Age (LIA) from around 1450 to 1850 with lower temperatures and glacier advances (e.g., Bradley and Jones, 1993; Mann et al., 2009), and (3) the recent warming trend since around 1850 (Hartmann et al., 2013). It is still under debate if those periods were a global phenomenon or if they mainly affected the Northern Hemisphere (e.g., Broecker, 2001). Nevertheless, understanding the mechanisms behind warm and cold phases such as the MWP and the LIA is important in understanding the mechanisms that are at work in recent times.

1.2 Black carbon (BC) and climate change

The long-lived greenhouse gases, such as CO₂, and their radiative forcing are relatively well understood and simulated (Myhre et al., 2013). On the contrary, the climate forcing of short-

1 Introduction

lived atmospheric aerosols is less defined and quantified, mainly due to their complex interaction with clouds (Myhre et al., 2013). Black carbon (BC) is one of those short-lived aerosols that have recently gained attention because their mitigation is expected to result in a climate effect much earlier than that expected from the mitigation of CO₂ (AMAP, 2011a).

BC is a by-product of incomplete combustion of biomass and fossil fuels. Due to its black colour it strongly absorbs solar radiation. BC affects the climate through several mechanisms (AMAP, 2011a; Bond et al., 2013; Myhre et al., 2013). First, atmospheric BC directly warms the atmosphere by absorbing the solar radiation that would otherwise have been absorbed by the surface or reflected back into space. Second, BC that is deposited on snow- or ice-covered surfaces causes the reduction of the albedo thus increasing the absorption of solar radiation at the surface. This indirect climate effect of BC gives rise to earlier snow and ice melt. Third, BC interacts with clouds thus affecting their distribution, lifetime and properties. So far, the estimates of the climate effect of BC show large differences between different studies (Bond et al., 2013). The reasons behind these differences remain unresolved (Bond et al., 2013). The latest estimates for the radiative forcing are 0.60 W/m² for the direct effect and 0.04 W/m² for the forcing by the snow/ice albedo effect (Myhre et al., 2013). The interaction of BC with clouds is very complex and thus not yet fully quantified (Myhre et al., 2013).

Sidenote: The terms soot and elemental carbon are also used for this fraction of particulate matter that results from incomplete combustion. There is still a lack of a universally accepted nomenclature (Petzold et al., 2013). In this thesis, the term black carbon (BC) is used in order to emphasise the absorption of solar radiation and its resulting climate effects.

1.3 The Arctic

The Arctic has become known as the 'early warning system' of climate change because the globally observed changes are amplified in this region (AMAP, 2011a; Miller et al., 2010). Over the past 100 years, Arctic temperatures have increased at almost twice the global average rate, with an increase in annual average surface air temperatures of 2-3°C in Alaska and Siberia from 1954 to 2003 (AMAP, 2011a). This is accompanied by an earlier onset of the spring melt, a lengthening of the melt season, changes in the mass balance of the Greenland ice sheet, and reduced sea ice extent (AMAP, 2011a, 2011b). Loss of highly reflective ice and snow surfaces causes a reduced surface albedo due to the underlying darker and more absorbing surfaces being exposed (AMAP, 2011a; Cubasch et al., 2013). The increased absorption then leads to further warming. This so-called ice albedo feedback is one of the reasons why the Arctic is highly affected by temperature changes (AMAP, 2011a; Cubasch et al., 2013).

The snow- and ice-covered parts of the Arctic are dominated by the large Greenland ice sheet which has been subject to research for a long time. The first ice core drilled to bedrock was that from Camp Century in 1966 (Dansgaard et al., 1969). Since that time many more deep ice cores have been retrieved from Greenland, including those from NGRIP and NEEM. These contain ice from as far back as the last part of the Eemian interglacial at around 130,000 to 118,000 years ago and thus are the two cores that provide the longest palaeoclimate records from Greenland (Rasmussen et al., 2013; Wolff et al., 2010). The Greenlandic ice cores have been studied extensively, providing annual resolution for some parameters for the last 100,000 years (Alley, 2000; Johnsen et al., 2001). Due to continuous flow analysis, it is possible to obtain even sub-seasonal resolution (McConnell et al., 2007; Rhodes et al., 2013; Sigl et al., 2013).

1.3.1 Transport pathways to the Arctic/ Arctic Haze

The Arctic has long been thought to be more or less free of pollutants due to its remote location and a lack of local sources (AMAP, 2011a). However, the Arctic troposphere is largely influenced by pollution sources from outside the Arctic. This was first discovered in the 1950's when pilots faced heavily reduced visibility over the American Arctic that was accompanied by high levels of gaseous air pollutants (Greenaway, 1950). This was observed regularly since then and referred to as Arctic Haze (Barrie, 1986; Shaw, 1995). In the Arctic the low surface temperatures lead to a thermally stable stratification of the air with strong surface inversions (Shaw, 1995; Stohl, 2006). As a result, a dome of cold stratified air over the Arctic is produced which acts as a transport barrier for warm air masses from lower latitudes. This barrier is called Arctic or Polar Front which shifts position from summer to winter due to temperature (Figure 1.4). In summer, the Polar Front is located at around 65°N because only the more northern parts of the Northern Hemisphere are cold enough to cause a stable stratification of the atmosphere. In winter, temperatures in more southern parts become cold enough to shift the Arctic Front as far south as 40°N. At this point, transport of pollution from high polluting areas such as Eurasia and North America, is facilitated because of their inclusion in the Arctic dome. In winter, both dry and wet depositions are reduced within the Arctic dome. This results in very long aerosol lifetimes once they reach the Arctic dome (Stohl et al. 2006).

Three transport pathways have been identified that enable pollutants from the mid-latitudes to reach the Arctic (Stohl, 2006; Figure 1.5): (1) Rapid (within four days) low-level transport into the Arctic followed by uplift at the Polar Front. This happens when and where the Arctic Front is located far north. (2) Low-level transport of air masses that are cold enough to penetrate the Polar Dome. This transport that takes around ten to fifteen days occurs mainly in winter because it involves surface cooling of air masses travelling over snow-covered surfaces. (3)

1 Introduction

Pollutants ascend south of the Arctic and slowly descend into the Polar Dome from the stratosphere due to radiational cooling. Stohl (2006) observed that European pollution follows all three pathways in winter and pathways one and three in summer. Pollution originating from North America and Asia is only transported by pathway three.

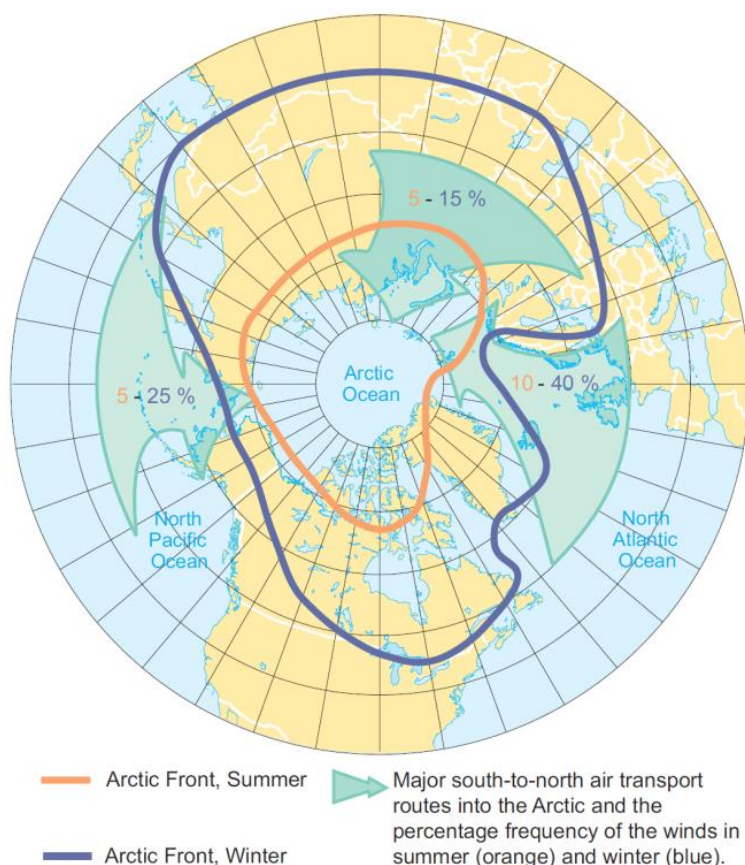


Figure 1.4 Location of the Arctic front in summer (orange) and winter (blue) (AMAP, 1998).

The varied transport pathways result in different source regions of pollutants found in the Arctic for locations near the surfaces and those in the middle and upper troposphere (Hirdman et al., 2010). On the one hand, the inland plateau of Greenland (around 3,000 m asl) does not receive low-level transport and is instead more directly connected to transport from lower latitudes (AMAP, 2011a), mainly following pathway three described above. On the other hand, low-altitude Arctic sites are more influenced by low-level transport of pollutants from high-latitude Eurasia (AMAP, 2011a; Hirdman et al., 2010). This means that the small ice caps and glaciers outside of Greenland add important information to the palaeoclimate reconstruction of the Arctic. Due to their higher annual accumulation they also provide palaeoclimate data at high time resolution (Van der Wel et al., 2011; Tarussov, 1992). Hence, ice cores from locations outside of Greenland are well suited for studying the impacts and source histories of pollutants during the last centuries.

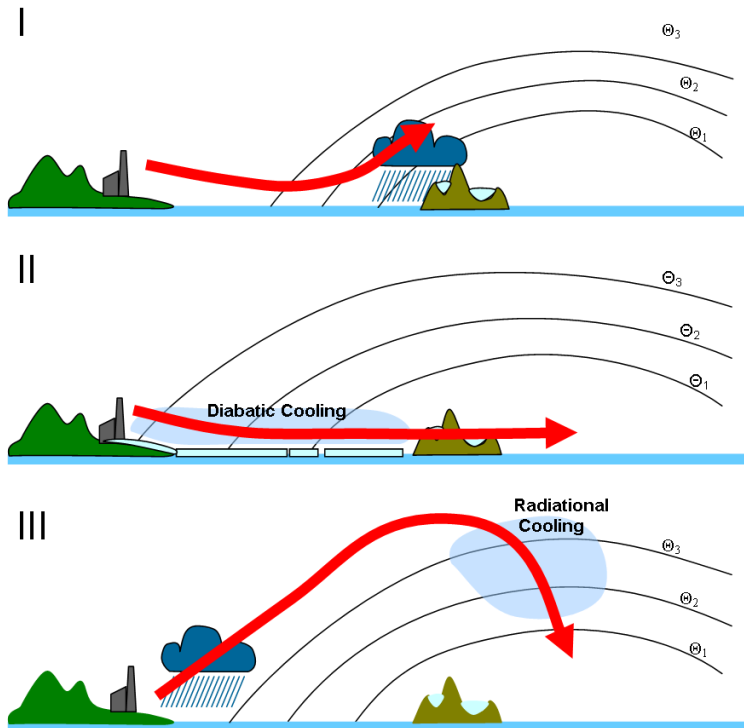


Figure 1.5 Transport pathways to the Arctic as described by Stohl (2006). $\theta_{1,2,3}$ = potential temperature at altitude 1,2 and 3. Graph adopted from Kühnel (2013).

1.4 Svalbard

1.4.1 Setting and climate

Svalbard is an archipelago of around 61,000 km² in the Eurasian Arctic which belongs to Norway. It is covered by glacier to about 60% (Hisdal, 1998) and consists mainly of four islands: Spitsbergen, Nordaustlandet, Edgeøya, and Barentsøya. Svalbard is surrounded by the Arctic Ocean, the Barents Sea and the North Atlantic and is situated at the southerly edge of the permanent Arctic sea ice. The climate in this area is highly variable because it is influenced by two different weather regimes. First, the atmospheric circulation is controlled by the low pressure system over Iceland and the high pressure system over Greenland and the Arctic Ocean. This results in mild air from the mid-latitudes reaching the archipelago with westerly and south-westerly winds (Hisdal, 1998; Isaksson et al., 2003; Samyn et al., 2012). The second regime mainly affecting the northern part of Svalbard is dominated by easterly and north-easterly winds that originate from the Barents Sea and the Siberian coast (Hisdal, 1998; Isaksson et al., 2003; Samyn et al., 2012). Svalbard is further characterised by relatively mild average winter temperatures which result from the warm Atlantic Waters that flow northward as continuation of the Gulf Stream and lead to open waters to the west of the archipelago (Hisdal, 1998; Skeie and Gronas, 2000). In general, winter temperatures vary more than summer temperatures (Figure 1.6), and western Svalbard, with mean temperatures in the

1 Introduction

coldest months (January-March) around -8 to -16°C , is less cold in winter and less warm in summer than the eastern parts of the archipelago (Hisdal, 1998). On Spitsbergen the lowest recorded temperature is -49.4°C at Green Harbour in March 1917 (Førland et al., 2009). The amount of precipitation in Svalbard is low, with an annual average of well under 500 mm on the west coast of Spitsbergen (Hisdal, 1998). The east side of the islands receive the most precipitation with annual values of up to 1,000 mm (Hisdal, 1998). Spring and early summer are typically the driest months (Hisdal, 1998). As an example the climate diagram of Svalbard airport (=lufthavn) is shown in Figure 1.7.

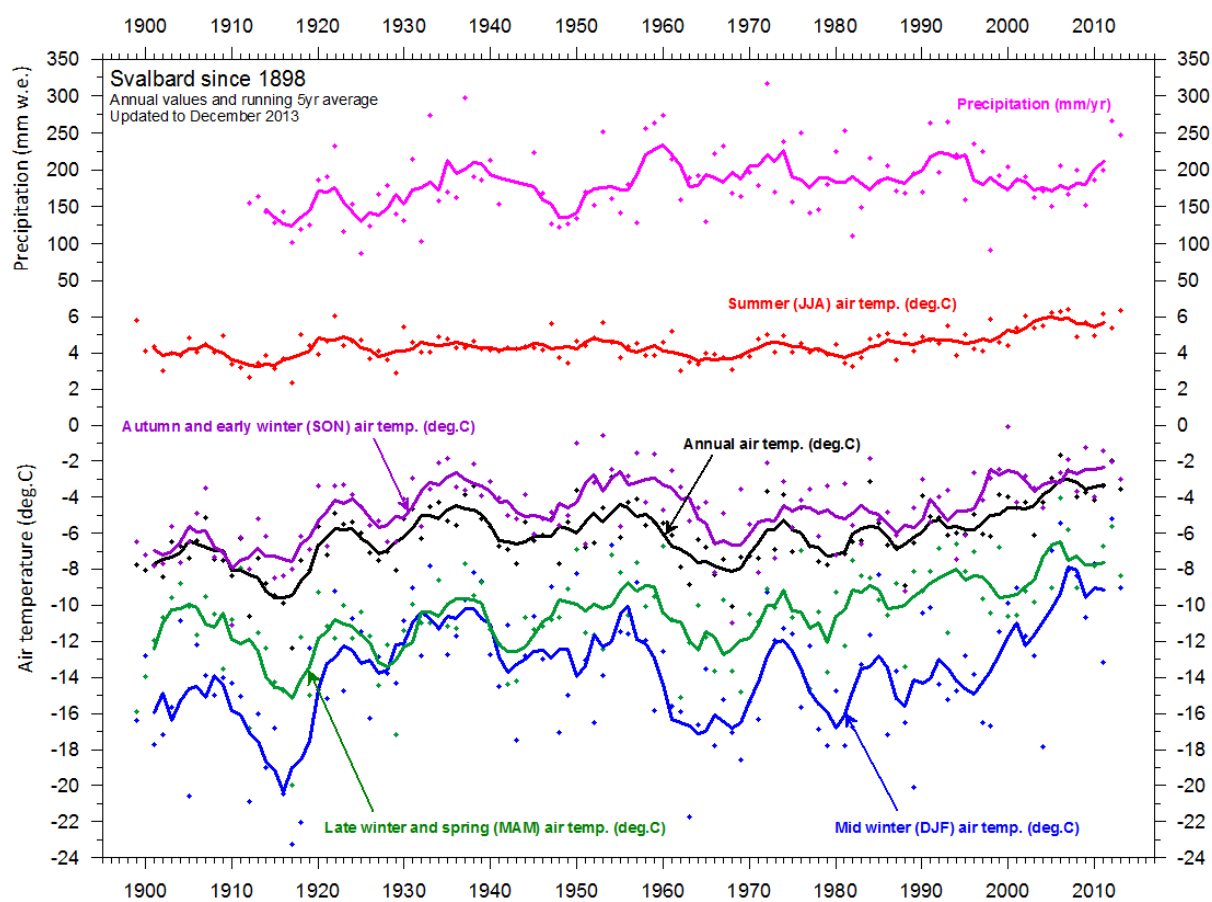


Figure 1.6 Meteorological observations from Svalbard; dots indicate annual and seasonal averages; lines are five-year-running-means (www.climate4you.com).

Additionally, Svalbard is situated relatively close to some of the major sources of anthropogenic pollution. Tunved et al. (2013) found the pollutant source areas for Svalbard to vary throughout the year with Atlantic air dominating in summer while air masses from Siberia, Eurasia and partly Asia dominating for the rest of the year.

The climate in Svalbard is changing. In the 20th century, Arctic air temperatures were at the highest level in the past 400 years (Serreze et al., 2000). In Svalbard, temperature has been measured since 1911, with the Svalbard airport composite temperature series providing one of

the few long-term instrumental temperature records from the high Arctic (Nordli, 2010; Nordli et al., 1996). This series has recently been extended back to 1898 by including observations from hunting and scientific expeditions (Nordli et al., 2014). Førland and Hanssen-Bauer (2003) identified three sub-periods within the last 100 years of temperature record (Figure 1.6): (1) a positive trend from the 1910s to the late 1930s, (2) a decrease from the 1930s to the 1960s, and (3) a significant increase from the 1960s to the present, with annual temperatures that still remained lower than in the 1930s. Nordli et al. (2014) also discuss this temperature increase from the 1960s, but report further that the present temperature level is significantly higher than at any earlier period in the instrumental record. The annual precipitation has increased since the beginning of the 20th century (Figure 1.6), e.g. at Svalbard airport by a rate of more than 2.5% per decade (Førland and Hanssen-Bauer, 2003). The annual fraction of solid precipitation has decreased during the last decades, which partly explains the increase in precipitation that is caused by a minimised undercatch of the gauges that are used for measuring precipitation (Førland and Hanssen-Bauer, 2003).

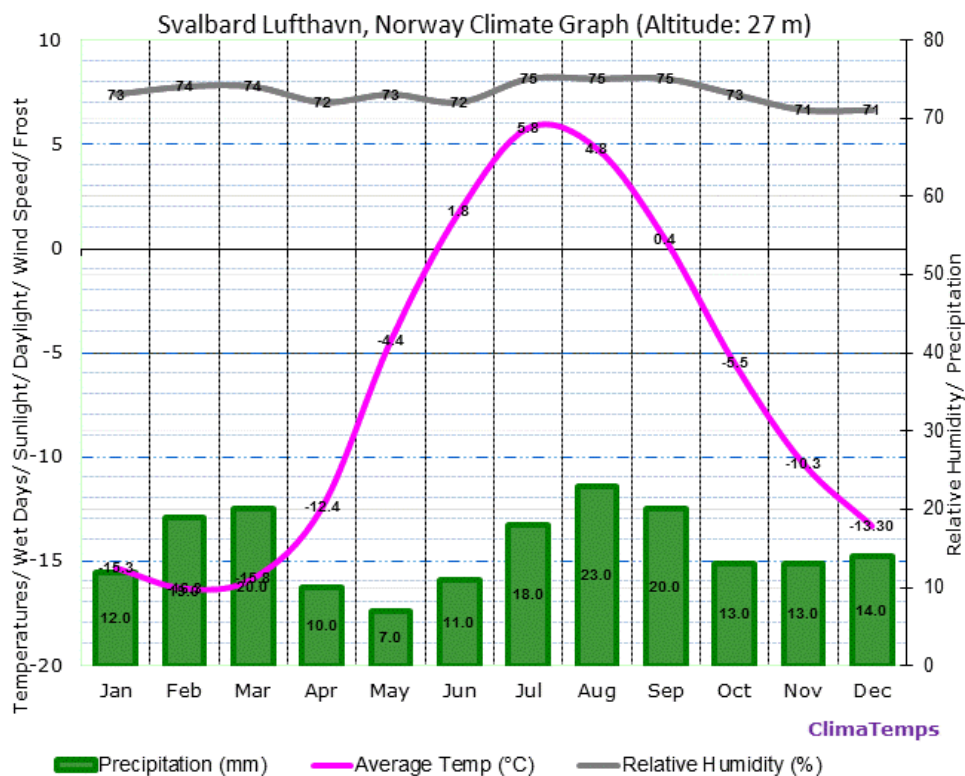


Figure 1.7 Climate diagram from Svalbard Lufthavn (www.svalbard-aero.climatemps.com).

Sea ice has a considerable effect on the climate in Svalbard: an ice-free state results in relatively mild and humid conditions, heavy sea ice is accompanied by cold and dry conditions because the ice isolates from the latent and sensible heat sources of the sea (Førland et al., 2009).

1.4.2 State of the art in ice core research

Due to its interesting location Svalbard has for some decades been subject to environmental research on aerosols, snow and ice (e.g., Beine et al., 1996; Eleftheriadis et al., 2009; Forsström et al., 2009; Kotlyakov et al., 2004; Tarussov, 1992; Teinilä et al., 2003; Virkkunen et al., 2007). Ice core studies offer the unique possibility to retrieve long climatic and environmental records that extend far back in time. The first ice core studies were performed by groups from the former Soviet Union who drilled seven cores between 1974 and 1987 (Tarussov, 1992). In 1987 Japanese groups also started ice core studies in Svalbard (Motoyama et al., 2008). The glaciers sampled include among others Vestfonna, Austfonna, and Lomonosovfonna by the Soviets, as well as Høghetta Ice Cap, Snøfjellafonna, Åsgårdfonna, Brøggerbreen and also Vestfonna and Austfonna by the Japanese (Fujii et al., 1990; Gordiyenko et al., 1981; Goto-Azuma and Koerner, 2001; Iizuka et al., 2002; Kameda et al., 1993; Motoyama et al., 2008; Punning et al., 1987; Tarussov, 1992; Uchida et al., 1996; Watanabe et al., 2001). The early Soviet studies were mostly of a stratigraphic nature and included only minor ion analyses. The Japanese did study the ion chemistry but only few results were published until now (Goto-Azuma and Koerner, 2001; Iizuka et al., 2002; Isaksson et al., 2003; Matoba et al., 2002; Motoyama et al., 2000; Watanabe et al., 2001). The main problem of all studies was determining how much the records were altered by melt. Furthermore, dating of the cores was in many cases hampered by a combination of melting, crude sampling and few analysed chemical species (Isaksson et al., 2003). One of the few exceptions is the core from Lomonosovfonna drilled in 1997 (Lomo97) which will be discussed in chapter 1.5.1. The major finding of the studies listed above is an increase in nitrate and sulphate concentrations from the middle of the 20th century, that is due to anthropogenic emissions seen at Snøfjellafonna (Goto-Azuma and Koerner, 2001), Austfonna and Vestfonna (Matoba et al., 2002; Watanabe et al., 2001). Iizuka et al. (2002) further identified the ratio of magnesium to sodium (Mg^{2+}/Na^+) as best melt indicator at Austfonna. A list of all the ice cores from the Eurasian Arctic drilled until 2004 is given in Kotlyakov et al. (2004). The latest ice core- except the 2009 Lomonosovfonna core- is that retrieved from Holtedahlfonna in 2005, which covers the last 300 years (Holte05; Beaudon et al., 2013). So far, several studies have been published on this core: van der Wel et al. (2011) used the high-resolution tritium profiles of the Lomo97 and Holte05 ice cores to observe that melt results in better preservation of the annual isotope signal; Divine et al. (2011) reconstructed 1000 years of winter air temperature using the isotopic records of the Lomo97 and Holte05 cores; Hermanson et al. (2010) and Ruggirello et al. (2010) focused on the deposition of brominated flame retardant compounds and other pesticides; Moore et al. (2012) found the Holte05 core to lack a clear volcanic record applying a statistical extraction method; Sjögren et al. (2007) presented a new method for deriving a high-resolution density record for the firn part of the core; and Beaudon

et al. (2013) focused on the ion chemistry in detail and compared it with the Lomo97 ice core. The findings of Beaudon et al. (2013) are discussed further in chapter 5.

1.4.3 Influence of melt on records of chemical species

Arctic glaciers outside of Greenland are affected by seasonal melt. In a review of ice cores from Arctic sites, Koerner (1997) showed that at least 50% of the ice column of these cores is clear ice formed by surface melt, infiltration and refreezing. The ratio of ice affected by melt to that not affected is used as a melt index (Koerner and Fisher, 1990). The higher the melt index the larger the portion of melt. Melt clearly affects the distribution of water-soluble chemical species within the ice so that some ionic species are removed easier than others (Brimblecombe et al., 1985; Davies et al., 1982; Moore and Grinsted, 2009; Pohjola et al., 2002a; Virkkunen et al., 2007). At Penny Ice Cap, Canadian Arctic, with an average melt index of 50%, previous studies showed that the atmospheric signals are preserved with annual to biannual resolution (Grumet et al., 1998). At Austfonna, Svalbard, with a melt index of 67% the chemical records were smoothed to three to ten years (Tarussov, 1992). This indicates that at least on decadal time scales, reliable ion records can be retrieved from ice cores influenced by melt. However, doubts remain in the interpretation of the records at higher resolution (Moore et al., 2005).

1.5 Lomonosovfonna

Lomonosovfonna is one of the highest ice fields in Svalbard (1250 m asl; Figure 2.1). It has a cupola shape with an approximate radius of 500 m (Isaksson et al., 2001). At the summit the glacier has a depth of 126.5 m as indicated by radar measurements (Isaksson et al., 2001). The accumulation area of Lomonosovfonna is about 600 km², including the glaciers of Nordenskjöldbreen, Grusdievbreen and Mittag-Lefflerbreen which are the major glaciers through which the ice field drains to sea level (Isaksson et al., 2001). At present, Lomonosovfonna has a negative mass balance like most of the Svalbard glaciers (Nuth et al., 2010). There are only a few direct air-temperature measurements from Lomonosovfonna (Gordiyenko et al., 1981; Isaksson et al., 2001; Pohjola et al., 2002a). Borehole temperatures at the Lomo97 drilling site were at a mean of -2.8°C with a nearly isothermal profile (Van de Wal et al., 2002). Furthermore, Lomonosovfonna is close to the coal mining villages of Pyramiden (35 km; in operation 1947-1998) and Longyearbyen (100 km; in operation since 1911) (Isaksson et al., 2001).

Due to its high elevation, Lomonosovfonna was thought to experience less melt than other Svalbard sites and is thus a suitable location for ice core studies. Up to now, Lomonosovfonna has been drilled three times, in 1976 and 1982 by the Soviets and in 1997 by a multi-national

1 Introduction

team. The early studies, that mainly focused on the stratigraphy, already indicated that Lomonosovfonna has a better preserved stratigraphy than other Svalbard sites (Gordiyenko et al., 1981).

1.5.1 The Lomonosovfonna 1997 ice core

In 1997, a 121.6 m ice core was retrieved from the summit of Lomonosovfonna (1250 m asl; 78°51'53"N, 17°25'30"E; Figure 2.1). This core (Lomo97) has been studied extensively for melt effects (Van der Wel et al., 2011; Grinsted et al., 2006; Moore and Grinsted, 2009; Moore et al., 2005; Pohjola et al., 2002a; Virkkunen et al., 2007), ion chemistry (Beaudon et al., 2013; Grinsted et al., 2006; Isaksson et al., 2001, 2003, 2005a; Jauhiainen et al., 1999; Kekonen et al., 2002, 2004, 2005a; Moore and Grinsted, 2009; Moore et al., 2005, 2006, 2012; O'Dwyer et al., 2000; Vehvilainen et al., 2002; Virkkunen et al., 2007), water stable isotopes (Divine et al., 2011, 2008; Isaksson et al., 2001, 2003, 2005b, 2005c; Pohjola et al., 2002b), tritium (Van der Wel et al., 2011), radioactive layers (Pinglot et al., 1999), volcanic tephra (Kekonen et al., 2005b), fly ash, charcoal and pollen (Hicks and Isaksson, 2006).

The Lomo97 covers the period of 770±150 to 1997 (Divine et al., 2011), with a dating uncertainty back to 1613 of ±1 year in the vicinity of the tiepoints and roughly ±5 years between the dating horizon. Please note that most of the publications cited above include the old chronology of Kekonen et al. (2005a). The mean accumulation rate at the site is 0.36 m weq, with varying values for different segments: 0.42 m weq (1997-1963), 0.32 m weq (1963-1903), 0.37 m weq (1903-1783), and 0.36 m weq below 1783 (Divine et al., 2011). The core was sampled at 5-10 cm resolution (e.g., Isaksson et al., 2001; Jauhiainen et al., 1999) and partly resampled at 2.5 cm resolution to obtain the updated chronology by Divine et al. (2011). Divine et al. (2011) further reconstructed 1000 years of winter surface air temperature using the high-resolution Lomo97 $\delta^{18}\text{O}$ record. The core suffers from modest seasonal melt but the records of the water stable isotopes are nearly unaffected and the ion records are mainly preserved. The percolation length does not exceed two to eight annual layers and even melt percentages of 80% cause little disturbance to the chemical stratigraphy (Moore et al., 2005; Pohjola et al., 2002a). Nitrate (NO_3^-) and sulphate (SO_4^{2-}) were found to elute the easiest, and ammonium (NH_4^+) to elute the least (Moore and Grinsted, 2009; Pohjola et al., 2002a). The ion budget is dominated (>70%) by the sea salt species of sodium (Na^+), chloride (Cl^-), potassium (K^+) and Mg^{2+} (Kekonen et al., 2005a). After the mid-20th century a clear anthropogenic impact is seen in the ion records of NO_3^- and SO_4^{2-} (Kekonen et al., 2005a). Further details of the studies on the Lomo97 core and a comparison with the Lomo09 are given in chapter 5.

1.6 Motivation of the study

The source region of pollutants reaching the high-altitude ice sheet of Greenland and those reaching the low-altitude regions such as Svalbard differ as a result of the transport pathways (chapter 1.3.1). This emphasises the importance in obtaining long-term past climate and environmental records from other Arctic sites besides Greenland. In Svalbard, Lomonosovfonna was shown to be a suitable location for ice core studies due to its well preserved stratigraphy in comparison to other sites.

Although the Lomo97 was studied in great detail, there remained uncertainty about the dating of the core part below 81 m (Kekonen et al., 2005a). This was recently reduced by resampling of the core section between 74 and 90 m depth, resulting in the updated chronology of Divine et al. (2011). However, the precise dating of the lowermost part of the Lomo97 core remains hampered by discontinuities in the chemical stratigraphy (Divine et al., 2011). Moreover, the Lomo97 core was sampled at a resolution of 5 cm, with no adjustment to layer thinning due to ice flow further down the core. Thus, the resolution in the lowermost core part was less than annual. Additionally, there was no material left of the Lomo97 core and BC, one of the short-lived atmospheric aerosols that have a large effect on global climate, had not been analysed.

This study on the 2009 ice core from Lomonosovfonna intends to close the gap of a BC record on historical timescales, and to improve the chemical stratigraphy by adjusting the sample resolution along the core to obtain annually resolved records for the entire core length.

References

- Alley, R. B.: Ice-core evidence of abrupt climate changes, *Proceedings of the National Academy of Sciences*, 97(4), 1331, 2000.
- AMAP: Arctic Monitoring and Assessment Programme (AMAP) Assessment Report: Arctic pollution issues, Oslo, Norway, 1998.
- AMAP: The impact of black carbon on Arctic climate, Arctic Monitoring and Assessment Programme (AMAP), Oslo, 2011a.
- AMAP: Snow, Water, Ice and Permafrost in the Arctic (SWIPA): Climate change and the cryosphere, Arctic Monitoring and Assessment Programme (AMAP), Oslo, Norway, 2011b.
- Barrie, L. A.: Arctic air pollution: An overview of current knowledge, *Atmospheric Environment* (1967), 20(4), 643–663, doi:10.1016/0004-6981(86)90180-0, 1986.
- Beaudon, E., Moore, J. C., Martma, T., Pohjola, V. A., van de Wal, R. S. W., Kohler, J. and Isaksson, E.: Lomonosovfonna and Holtedahlfonna ice cores reveal east–west disparities of the Spitsbergen environment since AD 1700, *Journal of Glaciology*, 59(218), 1069–1083, doi:10.3189/2013JoG12J203, 2013.
- Beine, H. J., Engardt, M., Jaffe, D. A., Hov, Ø., Holmén, K. and Stordal, F.: Measurements of NO_x and aerosol particles at the Ny-Ålesund Zeppelin mountain station on Svalbard: Influence of regional and local pollution sources, *Atmospheric Environment*, 30(7), 1067–1079, doi:10.1016/1352-2310(95)00410-6, 1996.
- Bond, T. C., Doherty, S. J., Fahey, D. W., Forster, P. M., Berntsen, T., DeAngelo, B. J., Flanner, M. G., Ghan, S., Kärcher, B., Koch, D., Kinne, S., Kondo, Y., Quinn, P. K., Sarofim, M. C., Schultz, M. G., Schulz, M., Venkataraman, C., Zhang, H., Zhang, S., Bellouin, N., Guttikunda, S. K., Hopke, P. K., Jacobson, M. Z., Kaiser, J. W., Klimont, Z., Lohmann, U., Schwarz, J. P., Shindell, D., Storelvmo, T., Warren, S. G. and Zender, C. S.: Bounding the role of black carbon in the climate system: A scientific assessment, *Journal of Geophysical Research: Atmospheres*, 118(11), 5380–5552, doi:10.1002/jgrd.50171, 2013.
- Bradley, R. S. and Jones, P. D.: “Little Ice Age” summer temperature variations: their nature and relevance to recent global warming trends, *The Holocene*, 3(4), 367–376, doi:10.1177/095968369300300409, 1993.
- Bradley, R. S., Briffa, K. R., Cole, J., Hughes, M. K. and Osborn, T. J.: The climate of the last millennium, in *Paleoclimate, global change and the future*, pp. 105–141, Springer, 2003.
- Brimblecombe, P., Tranter, M., Abrahams, P. W., Blackwood, I., Davies, T. D. and Vincent, C. E.: Relocation and preferential elution of acidic solute through the snowpack of a small, remote, high-altitude Scottish catchment, *Annals of Glaciology*, 7, 141–147, 1985.
- Broecker, W. S.: Was the Medieval Warm Period global?, *Science*, 291(5508), 1497–1499, doi:10.1126/science.291.5508.1497, 2001.

- Cubasch, U., Wuebbles, D., Chen, D., Facchini, M. C., Frame, D., Mahowald, N. and Winther, J.-G.: Introduction, in *Climate Change 2013: The Physical Science Basis. Contribution of Working Group I to the Fifth Assessment Report of the Intergovernmental Panel on Climate Change*, edited by T. F. Stocker, D. Qin, G.-K. Plattner, M. Tignor, S. K. Allen, J. Boschung, A. Nauels, Y. Xia, V. Bex, and P. M. Midgley, Cambridge University Press, Cambridge, United Kingdom and New York, NY, USA., 2013.
- Dansgaard, W.: The abundance of O¹⁸ in atmospheric water and water vapour, *Tellus*, 5(4), 461–469, doi:10.1111/j.2153-3490.1953.tb01076.x, 1953.
- Dansgaard, W., Johnsen, S. J., Møller, J. and Langway, C. C.: One thousand centuries of climatic record from Camp Century on the Greenland ice sheet, *Science*, 166(3903), 377–380, 1969.
- Davies, T. D., Vincent, C. E. and Brimblecombe, P.: Preferential elution of strong acids from a Norwegian ice cap, *Nature*, 300(5888), 161–163, doi:10.1038/300161a0, 1982.
- Divine, D. V., Isaksson, E., Pohjola, V., Meijer, H., van de Wal, R. S. W., Martma, T., Moore, J., Sjögren, B. and Godtliobsen, F.: Deuterium excess record from a small Arctic ice cap, *Journal of Geophysical Research*, 113, D19104, 2008.
- Divine, D., Isaksson, E., Martma, T., Meijer, H. A. ., Moore, J., Pohjola, V., van de Wal, R. S. W. and Godtliobsen, F.: Thousand years of winter surface air temperature variations in Svalbard and northern Norway reconstructed from ice core data, *Polar Research*, 30(0), 2011.
- Eleftheriadis, K., Vratolis, S. and Nyeki, S.: Aerosol black carbon in the European Arctic: measurements at Zeppelin station, Ny-Ålesund, Svalbard from 1998–2007, *Geophysical Research Letters*, 36(2), L02809, 2009.
- Førland, E. J. and Hanssen-Bauer, I.: Past and future climate variations in the Norwegian Arctic: overview and novel analyses, *Polar Research*, 22(2), 113–124, 2003.
- Førland, E. J., Benestad, R. E., Flatøy, F., Hanssen-Bauer, I., Haugen, J. E., Isaksen, K., Sorteberg, A. and Ådlandsvik, B.: Climate development in North Norway and the Svalbard region during 1900–2100, Rapportserie Nr. 128, April 2009, Norsk Polarinstitut, Polarmiljøsenderet, 9296 Tromsø, 2009.
- Forsström, S., Ström, J., Pedersen, C. A., Isaksson, E. and Gerland, S.: Elemental carbon distribution in Svalbard snow, *Journal of Geophysical Research: Atmospheres*, 114(D19), doi:10.1029/2008JD011480, 2009.
- Fujii, Y., Kamiyama, K., Kawamura, T., Kameda, T., Izumi, K., Satow, K., Enomoto, H., Nakamura, T., Hagen, J. O., Gjessing, Y. and Watanabe, O.: 6000-year climate records in an ice core from the Hoggsetta ice dome in northern Spitsbergen, *Annals of Glaciology*, 14, 85–89, 1990.
- Gordiyenko, F. G., Kotlyakov, V. M., Punning, Y. -K. M. and Vairmäe, R.: Study of a 200-m core from the Lomonosov ice plateau on Spitsbergen and the paleoclimatic implications, *Polar Geography and Geology*, 5(4), 242–251, doi:10.1080/10889378109388695, 1981.
- Goto-Azuma, K. and Koerner, R. M.: Ice core studies of anthropogenic sulfate and nitrate trends in the Arctic, *Journal of Geophysical Research*, 106, 4959–4969, 2001.

1 Introduction

Greenaway, K. R.: Experience with Arctic flying weather, Royal Meteorological Society, Canadian Branch, Toronto, Canada, 1950.

Grinsted, A., Moore, J. C., Pohjola, V., Martma, T. and Isaksson, E.: Svalbard summer melting, continentality, and sea ice extent from the Lomonosovfonna ice core, *Journal of Geophysical Research*, 111, D07110, 2006.

Grove, J. M. and Switsur, R.: Glacial geological evidence for the medieval warm period, *Climatic Change*, 26(2-3), 143–169, doi:10.1007/BF01092411, 1994.

Grumet, N. S., Wake, C. P., Zielinski, G. A., Fisher, D., Koerner, R. and Jacobs, J. D.: Preservation of glaciochemical time-series in snow and ice from the Penny Ice Cap, Baffin Island, *Geophysical Research Letters*, 25(3), 357–360, doi:10.1029/97GL03787, 1998.

Hartmann, D. L., Klein Tank, A. M. G., Rusticucci, M., Alexander, L. V., Brönnimann, S., Charabi, Y., Dentener, F. J., Dlugokencky, E. J., Easterling, D. R., Kaplan, A., Soden, B. J., Thorne, P. W., Wild, M. and Zhai, P. M.: *Observations: Atmosphere and Surface*, edited by T. F. Stocker, D. Qin, G.-K. Plattner, M. Tignor, S. K. Allen, J. Boschung, A. Nauels, Y. Xia, V. Bex, and P. M. Midgley, Cambridge University Press, Cambridge, United Kingdom and New York, NY, USA., 2013.

Hermanson, M. H., Isaksson, E., Forsström, S., Teixeira, C., Muir, D. C. G., Pohjola, V. A. and van de Wal, R. S. V.: Deposition history of brominated flame retardant compounds in an ice core from Høltedahlfonna, Svalbard, Norway, *Environmental Science & Technology*, 44(19), 7405–7410, doi:10.1021/es1016608, 2010.

Hicks, S. and Isaksson, E.: Assessing source areas of pollutants from studies of fly ash, charcoal, and pollen from Svalbard snow and ice, *Journal of Geophysical Research- Atmospheres*, 111(D2), doi:10.1029/2005JD006167, 2006.

Hirdman, D., Sodemann, H., Eckhardt, S., Burkhardt, J. F., Jefferson, A., Mefford, T., Quinn, P. K., Sharma, S., Ström, J. and Stohl, A.: Source identification of short-lived air pollutants in the Arctic using statistical analysis of measurement data and particle dispersion model output, *Atmospheric Chemistry and Physics*, 10, 669–693, 2010.

Hisdal, V.: *Svalbard : nature and history*, Norsk Polarinstitut, 1998.

Hughes, M. K. and Diaz, H. F.: Was there a “medieval warm period”, and if so, where and when?, *Climatic Change*, 26(2-3), 109–142, doi:10.1007/BF01092410, 1994.

Iizuka, Y., Igarashi, M., Kamiyama, K., Motoyama, H. and Watanabe, O.: Ratios of Mg^{2+}/Na^+ in snowpack and an ice core at Austfonna ice cap, Svalbard, as an indicator of seasonal melting, *Journal of Glaciology*, 48(162), 452–460, 2002.

Isaksson, E., Pohjola, V., Jauhiainen, T., Moore, J., Pinglot, J. F., Vaikmaa, R., van de Wal, R. S. ., Hagen, J. O., Ivask, J., Karlöf, L., Martma, T., Meijer, H. A. J., Mulvaney, R., Thomassen, M. and van den Broeke, M.: A new ice-core record from Lomonosovfonna, Svalbard: viewing the 1920-97 data in relation to present climate and environmental conditions, *Journal of Glaciology*, 47(157), 335–345, 2001.

Isaksson, E., Hermanson, M., Hicks, S., Igarashi, M., Kamiyama, K., Moore, J., Motoyama, H., Muir, D., Pohjola, V., Vaikmäe, R., van de Wal, R. S. W., Watanabe, O.: Ice cores from Svalbard—useful

archives of past climate and pollution history, *Physics and Chemistry of the Earth, Parts A/B/C*, 28(28-32), 1217–1228, 2003.

Isaksson, E., Kekonen, T., Moore, J. and Mulvaney, R.: The methanesulfonic acid (MSA) record in a Svalbard ice core, *Annals of Glaciology*, 42(1), 345–351, 2005a.

Isaksson, E., Divine, D., Kohler, J., Martma, T., Pohjola, V., Motoyama, H. and Watanabe, O.: Climate oscillations recorded in Svalbard ice core $\delta^{18}\text{O}$ records between AD 1200 and 1997, *Geografiska Annaler: Series A, Physical Geography*, 87(1), 203–214, 2005b.

Isaksson, E., Kohler, J., Pohjola, V., Moore, J., Igarashi, M., Karlöf, L., Martma, T., Meijer, H., Motoyama, H., Vaikmäe, R. and van de Wal, R. S. W.: Two ice-cored $\delta^{18}\text{O}$ records from Svalbard illustrating climate and sea-ice variability over the last 400 years, *Holocene*, 15(4), 501–509, doi:10.1191/0959683605hl820rp, 2005c.

Jauhiainen, T., Moore, J., Perämäki, P., Derome, J. and Derome, K.: Simple procedure for ion chromatographic determination of anions and cations at trace levels in ice core samples, *Analytica Chimica Acta*, 389(1-3), 21–29, 1999.

Johnsen, S. J., Dahl-Jensen, D., Gundestrup, N., Steffensen, J. P., Clausen, H. B., Miller, H., Masson-Delmotte, V., Sveinbjörnsdóttir, A. E. and White, J.: Oxygen isotope and palaeotemperature records from six Greenland ice-core stations: Camp Century, Dye-3, GRIP, GISP2, Renland and NorthGRIP, *Journal of Quaternary Science*, 16(4), 299–307, doi:10.1002/jqs.622, 2001.

Kameda, T., Takahashi, S., Goto-Azuma, K., Kohshima, S., Watanabe, O. and Hagen, J. O.: First report of ice core analyses and borehole temperatures on the highest icefield on western Spitsbergen in 1992, *Bulletin of Glacier Research*, 11, 51–61, 1993.

Kekonen, T., Moore, J. C., Mulvaney, R., Isaksson, E., Pohjola, V. and van de Wal, R. S. W.: A 800 year record of nitrate from the Lomonosovfonna ice core, Svalbard, *Annals of Glaciology*, 35(1), 261–265, 2002.

Kekonen, T., Perämäki, P. and Moore, J. C.: Comparison of analytical results for chloride, sulfate and nitrate obtained from adjacent ice core samples by two ion chromatographic methods, *Journal of Environmental Monitoring*, 6(2), 147–152, 2004.

Kekonen, T., Moore, J., Perämäki, P., Mulvaney, R., Isaksson, E., Pohjola, V. and van de Wal, R. S. W.: The 800 year long ion record from the Lomonosovfonna (Svalbard) ice core, *Journal of Geophysical Research*, 110, D07304, 2005a.

Kekonen, T., Moore, J., Perämäki, P. and Martma, T.: The Icelandic Laki volcanic tephra layer in the Lomonosovfonna ice core, Svalbard, *Polar Research*, 24(1-2), 33–40, doi:10.1111/j.1751-8369.2005.tb00138.x, 2005b.

Koerner, R. M.: Some comments on climatic reconstructions from ice cores drilled in areas of high melt, *Journal of Glaciology*, 43, 90–97, 1997.

Koerner, R. M. and Fisher, D. A.: A record of Holocene summer climate from a Canadian high-Arctic ice core, *Nature*, 343(6259), 630–631, doi:10.1038/343630a0, 1990.

1 Introduction

Kotlyakov, V. M., Arkhipov, S. M., Henderson, K. A. and Nagornov, O. V.: Deep drilling of glaciers in Eurasian Arctic as a source of paleoclimatic records, *Quaternary Science Reviews*, 23(11), 1371–1390, 2004.

Kühnel, J. R.: Reactive Nitrogen: Transport to and deposition at the high Arctic site Ny-Ålesund, Svalbard, PhD thesis, University of Oslo, Oslo, Norway, 2013.

Mann, M. E., Zhang, Z., Rutherford, S., Bradley, R. S., Hughes, M. K., Shindell, D., Ammann, C., Faluvegi, G. and Ni, F.: Global signatures and dynamical origins of the Little Ice Age and Medieval Climate Anomaly, *Science*, 326(5957), 1256–1260, doi:10.1126/science.1177303, 2009.

Masson-Delmotte, V., Schulz, M., Abe-Ouchi, A., Beer, J., Ganopolski, A., Gonzalez Rouco, J. F., Jansen, E., Lambeck, K., Luterbacher, J., Naish, T., Osborn, T., Otto-Bliesner, B., Quinn, T., Ramesh, R., Rojas, M., Shao, X. and Timmermann, A.: *Information from Paleoclimate Archives*, edited by T. F. Stocker, D. Qin, G.-K. Plattner, M. Tignor, S. K. Allen, J. Boschung, A. Nauels, Y. Xia, V. Bex, and P. M. Midgley, Cambridge University Press, Cambridge, United Kingdom and New York, NY, USA., 2013.

Matoba, S., Narita, H., Motoyama, H., Kamiyama, K. and Watanabe, O.: Ice core chemistry of Vestfonna ice cap in Svalbard, Norway, *Journal of Geophysical Research*, 107(D23), 4721, 2002.

Mayewski, P. A., Rohling, E. E., Curt Stager, J., Karlén, W., Maasch, K. A., David Meeker, L., Meyerson, E. A., Gasse, F., van Kreveld, S. and Holmgren, K.: Holocene climate variability, *Quaternary Research*, 62(3), 243–255, 2004.

McConnell, J. R., Edwards, R., Kok, G. L., Flanner, M. G., Zender, C. S., Saltzman, E. S., Banta, J. R., Pasteris, D. R., Carter, M. M. and Kahl, J. D. W.: 20th-century industrial black carbon emissions altered Arctic climate forcing, *Science*, 317(5843), 1381–1384, doi:10.1126/science.1144856, 2007.

Miller, G. H., Alley, R. B., Brigham-Grette, J., Fitzpatrick, J. J., Polyak, L., Serreze, M. C. and White, J. W. C.: Arctic amplification: can the past constrain the future?, *Quaternary Science Reviews*, 29(15–16), 1779–1790, doi:10.1016/j.quascirev.2010.02.008, 2010.

Moore, J. C. and Grinsted, A.: Ion fractionation and percolation in ice cores with seasonal melting, in *Physics of ice core records II*, vol. 68, edited by Institute of Low Temperature Science, Hokkaido University, pp. 287–298, Hokkaido University Press, Sapporo, Japan, 2009.

Moore, J. C., Grinsted, A., Kekonen, T. and Pohjola, V.: Separation of melting and environmental signals in an ice core with seasonal melt, *Geophysical Research Letters*, 32(10), L10501, 2005.

Moore, J., Kekonen, T., Grinsted, A. and Isaksson, E.: Sulfate source inventories from a Svalbard ice core record spanning the industrial revolution, *Journal of Geophysical Research*, 111(D15), 2006.

Moore, J. C., Beaudon, E., Kang, S., Divine, D., Isaksson, E., Pohjola, V. A. and van de Wal, R. S. W.: Statistical extraction of volcanic sulphate from nonpolar ice cores, *Journal of Geophysical Research*, 117(D3), D03306, 2012.

- Motoyama, H., Kamiyama, K., Igarashi, M., Nishio, F. and Watanabe, O.: Distribution of chemical constituents in superimposed ice from Austre Brøggerbreen, Spitsbergen, *Geografiska Annaler: Series A, Physical Geography*, 82(1), 33–38, doi:10.1111/j.0435-3676.2000.00003.x, 2000.
- Motoyama, H., Watanabe, O., Fujii, Y., Kamiyama, K., Igarashi, M., Matoba, S., Kameda, T., Goto-Azuma, K., Izumi, K., Narita, H., Yoshinori Ilzuka and Isaksson, E.: Analyses of ice core data from various sites in Svalbard glaciers from 1987 to 1999, 2008.
- Myhre, G., Shindell, D., Bréon, F.-M., Collins, W., Fuglestedt, J., Huang, J., Koch, D., Lamarque, J.-F., Lee, D., Mendoza, B., Nakajima, T., Robock, A., Stephens, G., Takemura, T. and Zhang, H.: Anthropogenic and natural radiative forcing, in *Climate Change 2013: The Physical Science Basis. Contribution of Working Group I to the Fifth Assessment Report of the Intergovernmental Panel on Climate Change*, edited by T. F. Stocker, D. Qin, G.-K. Plattner, M. Tignor, S. K. Allen, J. Boschung, A. Nauels, Y. Xia, V. Bex, and P. M. Midgley, Cambridge University Press, Cambridge, United Kingdom and New York, NY, USA., 2013.
- Nordli, Ø.: The Svalbard airport temperature series, *Bulletin of Geography. Physical Geography Series*, (3), 5–25, 2010.
- Nordli, Ø., Przybylak, R., Ogilvie, A. E. J. and Isaksen, K.: Long-term temperature trends and variability on Spitsbergen: the extended Svalbard Airport temperature series, 1898–2012, *Polar Research*, 33(0), doi:10.3402/polar.v33.21349, 2014.
- Nordli, P. Ø., Hanssen-Bauer, I. and Førland, E. J.: Homogeneity analyses of temperature and precipitation series from Svalbard and Jan Mayen, *Norske meteorologiske institutt*, 1996.
- Nuth, C., Moholdt, G., Kohler, J., Hagen, J. O. and Käab, A.: Svalbard glacier elevation changes and contribution to sea level rise, *Journal of Geophysical Research*, 115, F01008, 2010.
- O'Dwyer, J., Isaksson, E., Vinje, T., Jauhiainen, T., Moore, J., Pohjola, V., Vaikmae, R. and van de Wal, R. S. W.: Methanesulfonic acid in a Svalbard ice core as an indicator of ocean climate, *Geophysical Research Letters*, 27(8), 1159–1162, 2000.
- Petzold, A., Ogren, J. A., Fiebig, M., Laj, P., Li, S.-M., Baltensperger, U., Holzer-Popp, T., Kinne, S., Pappalardo, G., Sugimoto, N., Wehrli, C., Wiedensohler, A. and Zhang, X.-Y.: Recommendations for reporting “black carbon” measurements, *Atmospheric Chemistry and Physics*, 13(16), 8365–8379, doi:10.5194/acp-13-8365-2013, 2013.
- Pinglot, J. F., Pourchet, M., Lefauconnier, B., Hagen, J. O., Isaksson, E., Vaikmäe, R. and Kamiyama, K.: Accumulation in Svalbard glaciers deduced from ice cores with nuclear tests and Chernobyl reference layers, *Polar Research*, 18(2), 315–321, 1999.
- Pohjola, V. A., Moore, J. C., Isaksson, E., Jauhiainen, T., van de Wal, R. S. W., Martma, T., Meijer, H. A. J. and Vaikmäe, R.: Effect of periodic melting on geochemical and isotopic signals in an ice core from Lomonosovfonna, Svalbard, *Journal of Geophysical Research*, 107(10.1029), 2002a.
- Pohjola, V. A. , Martma, T. A., Meijer, H. A. ., Moore, J. C., Isaksson, E., Vaikmae, R. and van de Wal, R. S. W.: Reconstruction of three centuries of annual accumulation rates based on the record of stable isotopes of water from Lomonosovfonna, Svalbard, *Annals of Glaciology*, 35(1), 57–62, 2002b.

1 Introduction

Punning, J.-M., Vaikmäe, R. and Tóugu, K.: Variations of $\delta^{18}\text{O}$ and Cl⁻ in the ice cores of Spitsbergen, *Journal de Physique*, 48(C1), C1-619-C1-624, doi:10.1051/jphyscol:1987185, 1987.

Rasmussen, S. O., Abbott, P. M., Blunier, T., Bourne, A. J., Brook, E., Buchardt, S. L., Buizert, C., Chappellaz, J., Clausen, H. B., Cook, E., Dahl-Jensen, D., Davies, S. M., Guillevic, M., Kipfstuhl, S., Laepple, T., Seierstad, I. K., Severinghaus, J. P., Steffensen, J. P., Stowasser, C., Svensson, A., Vallelonga, P., Vinther, B. M., Wilhelms, F. and Winstrup, M.: A first chronology for the North Greenland Eemian Ice Drilling (NEEM) ice core, *Climate of the Past*, 9(6), 2713-2730, doi:10.5194/cp-9-2713-2013, 2013.

Rhodes, R. H., Faïn, X., Stowasser, C., Blunier, T., Chappellaz, J., McConnell, J. R., Romanini, D., Mitchell, L. E. and Brook, E. J.: Continuous methane measurements from a late Holocene Greenland ice core: Atmospheric and in-situ signals, *Earth and Planetary Science Letters*, 368, 9-19, doi:10.1016/j.epsl.2013.02.034, 2013.

Ruggirello, R. M., Hermanson, M. H., Isaksson, E., Teixeira, C., Forsström, S., Muir, D. C. G., Pohjola, V., van de Wal, R. and Meijer, H. A. J.: Current use and legacy pesticide deposition to ice caps on Svalbard, Norway, *Journal of Geophysical Research*, 115(D18), D18308, doi:10.1029/2010JD014005, 2010.

Samyn, D., Vega, C. P., Motoyama, H. and Pohjola, V. A.: Nitrate and sulfate anthropogenic trends in the 20th century from five Svalbard ice cores, *Arctic, Antarctic, and Alpine Research*, 44(4), 490-499, doi:10.1657/1938-4246-44.4.490, 2012.

Schilt, A., Baumgartner, M., Blunier, T., Schwander, J., Spahni, R., Fischer, H. and Stocker, T. F.: Glacial-interglacial and millennial-scale variations in the atmospheric nitrous oxide concentration during the last 800,000 years, *Quaternary Science Reviews*, 29(1-2), 182-192, doi:10.1016/j.quascirev.2009.03.011, 2010.

Serreze, M. C., Walsh, J. E., Chapin Iii, F. S., Osterkamp, T., Dyurgerov, M., Romanovsky, V., Oechel, W. C., Morison, J., Zhang, T. and Barry, R. G.: Observational evidence of recent change in the northern high-latitude environment, *Climatic Change*, 46(1-2), 159-207, 2000.

Shaw, G. E.: The arctic haze phenomenon, *Bulletin of the American Meteorological Society*, 76, 2403-2414, 1995.

Sigl, M., McConnell, J. R., Layman, L., Maselli, O., McGwire, K., Pasteris, D., Dahl-Jensen, D., Steffensen, J. P., Vinther, B., Edwards, R., Mulvaney, R. and Kipfstuhl, S.: A new bipolar ice core record of volcanism from WAIS Divide and NEEM and implications for climate forcing of the last 2000 years, *Journal of Geophysical Research: Atmospheres*, doi:10.1029/2012JD018603, 2013.

Sjögren, B., Brandt, O., Nuth, C., Isaksson, E., Pohjola, V., Kohler, J. and van de Wal, R. S. W.: Determination of firn density in ice cores using image analysis, *Journal of Glaciology*, 53(182), 413-419, doi:10.3189/002214307783258369, 2007.

Skeie, P. and Gronas, S.: Strongly stratified easterly flows across Spitsbergen, *Tellus A*, 52(5), 473-486, doi:10.1034/j.1600-0870.2000.01075.x, 2000.

Stohl, A.: Characteristics of atmospheric transport into the Arctic troposphere, *Journal of Geophysical Research*, 111(D11), D11306, 2006.

Tarussov, A.: The Arctic from Svalbard to Severnaya Zemlya: climatic reconstructions from ice cores, in *Climate Since A.D. 1500*, edited by R. S. Bradley and P. D. Jones, pp. 505–516, Routledge, 1992.

Teinilä, K., Hillamo, R., Kerminen, V.-M. and Beine, H. J.: Aerosol chemistry during the NICE dark and light campaigns, *Atmospheric Environment*, 37(4), 563–575, doi:10.1016/S1352-2310(02)00826-9, 2003.

Tunved, P., Ström, J. and Krejci, R.: Arctic aerosol life cycle: linking aerosol size distributions observed between 2000 and 2010 with air mass transport and precipitation at Zeppelin station, Ny-Ålesund, Svalbard, *Atmospheric Chemistry and Physics*, 13(7), 3643–3660, doi:10.5194/acp-13-3643-2013, 2013.

Uchida, T., Kamiyama, K., Fujii, Y., Takahashi, A., Suzuki, T., Yoshimura, Y., Igarashi, M. and Watanabe, O.: Ice core analyses and borehole temperature measurements at the drilling site on Asgardfonna, Svalbard, in 1993 (scientific paper), *Memoirs of National Institute of Polar Research. Special issue*, 51, 377–386, 1996.

Vehvilainen, J., Isaksson, E. and Moore, J. C.: A 20th-century record of naphthalene in an ice core from Svalbard, *Annals of Glaciology*, 35(1), 257–260, 2002.

Virkkunen, K., Moore, J. C., Isaksson, E., Pohjola, V., Peramaki, P., Grinsted, A. and Kekonen, T.: Warm summers and ion concentrations in snow: comparison of present day with Medieval Warm Epoch from snow pits and an ice core from Lomonosovfonna, Svalbard, *Journal of Glaciology*, 53(183), 623–634, 2007.

Watanabe, O., Motoyama, H., Igarashi, M., Kamiyama, K., Matoba, S., Goto-Azuma, K., Narita, H. and Kameda, T.: Studies on climatic and environmental changes during the last few hundred years using ice cores from various sites in Nordaustlandet, Svalbard, *Memoirs of National Institute of Polar Research. Special Issue*, 54(227-242), 2001.

Van de Wal, R. S. W., Mulvaney, R., Isaksson, E., Moore, J. C., Pinglot, J. F., Pohjola, V. A. and Thomassen, M.: Reconstruction of the historical temperature trend from measurements in a medium-length borehole on the Lomonosovfonna plateau, Svalbard, *Annals of Glaciology*, 35(1), 371–378, 2002.

Van der Wel, L. G., Streurman, H. J., Isaksson, E., Helsen, M. M., van de Wal, R. S. W., Martma, T., Pohjola, V. A., Moore, J. C. and Meijer, H. A. J.: Using high-resolution tritium profiles to quantify the effects of melt on two Spitsbergen ice cores, *Journal of Glaciology*, 57(206), 1087–1097, 2011.

Wolff, E. W., Chappellaz, J., Blunier, T., Rasmussen, S. O. and Svensson, A.: Millennial-scale variability during the last glacial: The ice core record, *Quaternary Science Reviews*, 29(21–22), 2828–2838, doi:10.1016/j.quascirev.2009.10.013, 2010.

Wolff, E. W., Fischer, H., Fundel, F., Ruth, U., Twarloh, B., Littot, G. C., Mulvaney, R., Röthlisberger, R., De Angelis, M., Boutron, C. F., Hansson, M., Jonsell, U., Hutterli, M. A., Lambert, F., Kaufmann, P.,

1 Introduction

Stauffer, B., Stocker, T. F., Steffensen, J. P., Bigler, M., Siggaard-Andersen, M. L., Udisti, R., Becagli, S., Castellano, E., Severi, M., Wagenbach, D., Barbante, C., Gabrielli, P. and Gaspari, V.: Southern Ocean sea-ice extent, productivity and iron flux over the past eight glacial cycles, *Nature*, 440(7083), 491–496, 2006.

Internet:

<http://www.climate4you.com/SvalbardTemperatureSince1912.htm#SvalbardSince1912%20simple>; last access: July 11th 2014.

<http://www.svalbard-aero.climateps.com/graph.php>; last access: July 11th 2014.

2 Methods

In this chapter, information on the methods applied to the Lomo09 ice core is provided. First, the drilling campaign is described (chapter 2.1), followed by the sample preparation (chapter 2.2), the description of determining the annual melt percent (chapter 2.3), and specifications on the analysis of the water stable isotopes (chapter 2.4). Chapter 2.5 discusses the ion chromatography used for the analysis of the major water soluble ions, and chapter 2.6 describes the method for the analysis of black carbon (BC). The method section ends with chapter 2.7 that specifies all methods applied to attribute a certain depth in the ice core to a certain age, establishing the core chronology.

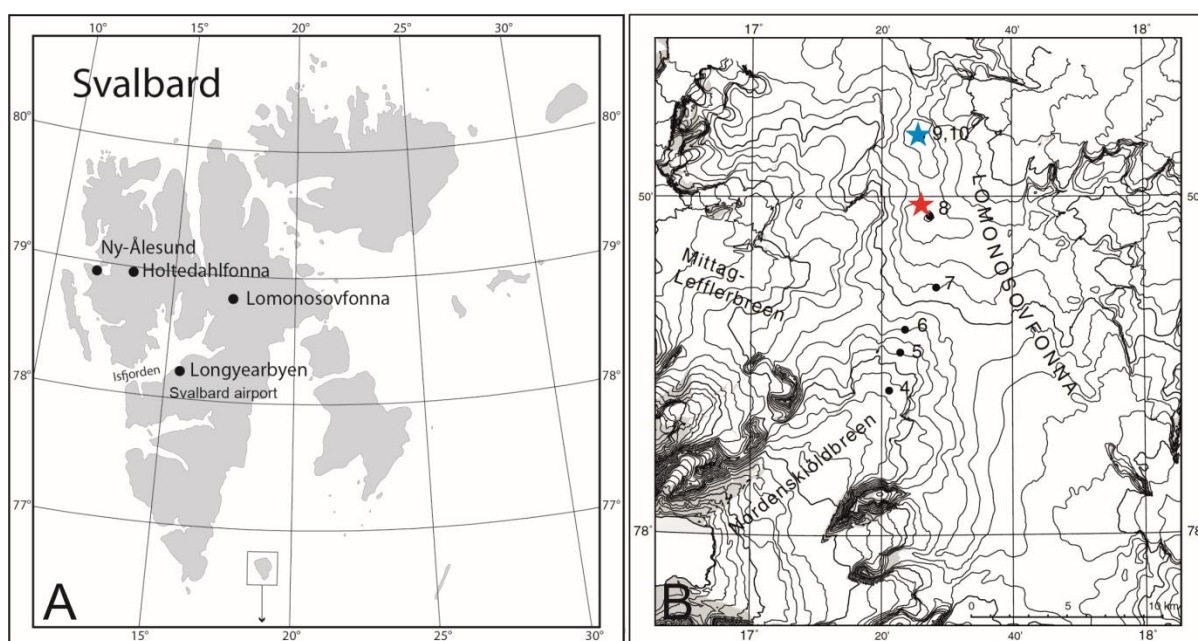


Figure 2.1 (A) Map of Svalbard with the location of Lomonosovfonna (courtesy of the Norwegian Polar Institute). (B) Map indicating the Lomonosovfonna drilling sites in 1997 (blue) and 2009 (red). Graph B is modified after Isaksson et al. (2001).

2.1 Drilling

In March 2009 a team of eight people from Switzerland, Norway, and Sweden drilled two ice cores of 149.5 m and 37 m depth, respectively, on Lomonosovfonna (1202 m asl; 78°49'24.4" N; 17°25'59.2"E; Figures 2.1 and 2.2), Svalbard, Norway, using the Fast Electromechanical Lightweight Ice Coring System (FELICS, Ginot et al., 2002). The drilling site was located 4.6 km south of that in 1997 (Isaksson et al. 2001; both locations are displayed in Figure 2.1). It was not possible to obtain a second core from the 1997 drilling site due to a large crevasse that had opened in the area of the 1997 drilling just before the 2009 expedition. This crevasse probably

2 Methods

disturbed the records, making the 1997 site unsuitable for further ice core studies. During the 10-days-expedition in 2009 bedrock could not be reached because the drill got stuck at 149.5 m depth. A later conducted ground penetrating radar survey suggests bedrock to be at around 200 m depth (Pettersen, unpublished data). The ice temperatures ranged from -1.8°C at 12 m to -2.2°C at 42 m depth, the deepest point where temperature was measured.

The long ice core was shipped to the Paul Scherrer Institut (PSI), Switzerland, in frozen state, whereas the short ice core was stored at the Norwegian Polar Institute, Norway.



Figure 2.2 The 2009 drilling site on Lomonosovfonna with the drilling tent on the left and the camp in the background (Photography by M. Björkman).

2.2 Sample preparation

The ice core from Lomonosovfonna was drilled in 243 segments of mainly 60-74 cm and around 8.1 cm diameter. In total, the segments represent 149.5 m of the glacier thickness. The ice segments were packed in polyethylene tubing and shipped in frozen state in insulated boxes to PSI, Switzerland. There they were processed in a cold room (-20°C) as follows. Each segment was unpacked, weighed and measured in length and diameter to calculate an average density for each core segment. Stratigraphy including melt features, coloured layers, core breaks as well as missing core pieces was noted while the segment being backlit on a light bench. Missing pieces of a segment were accounted for in the density calculation (see Figure 9.1 for density profile).

The core segment was cut as displayed in Figure 2.3 using a band saw with a Teflon coated tabletop (Eichler et al., 2000). The saw and tabletop were cleaned regularly with acetone and polyethylene gloves were worn during all handling, both to avoid contamination. The samples

for the more sensitive analyses, such as ion chromatography (IC) and black carbon (BC) analysis, were taken from the inner part of the core to avoid contamination as much as possible. For practical reasons, the ion chromatography sample was also used for mass spectrometry for water stable isotopes. The outer parts of the core were used for the analysis of ^{210}Pb and ^3H that are not as sensitive to potential contamination. About half of each core segment was repacked in polyethylene tubing and archived for future analysis.

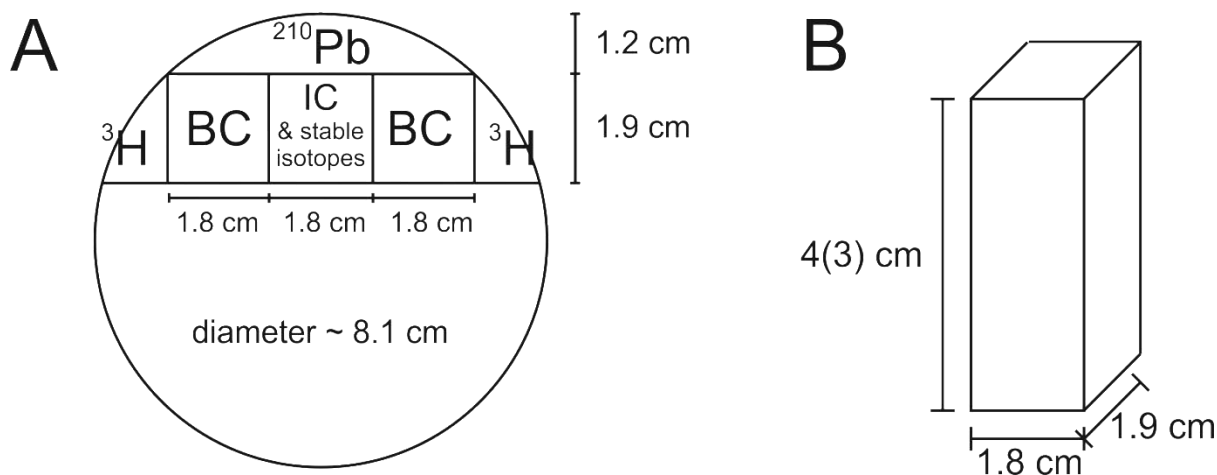


Figure 2.3 Cutting scheme of the Lomo09 ice core. (A) Cross-section of the core with the core parts labelled for the different analyses. Stable isotopes = water stable isotopes. (B) Dimensions of a single sample for IC analysis.

Figure 2.3B displays a single sample for IC analysis with the outer dimensions of approximately 1.9 x 1.8 x 3-4 cm. The sampling resolution was adjusted to account for layer thinning due to ice flow further down the core. In order to have sufficient volume for the analysis, two parallel samples were combined in one 50 mL polypropylene (PP) sample vial for BC analysis, whereas only one sample of the same depth was used for IC. For water stable isotope analysis using mass spectrometry an aliquot of 1-1.5 mL was taken from the melted IC sample. In total, the sampling resulted in 3997 samples for IC/mass spectrometry and 4046 samples for BC analysis. The difference in sample number results from the length of the 50 mL PP sample vials which in some cases was not sufficient to hold two parallel BC samples. In these cases, the BC samples needed to be cut in higher resolution, resulting in sample lengths of less than 3 or 4 cm, respectively.

During the core cutting potentially missing ice parts were respected. This means that when the two sides around a core break did not fit well, the samples were cut to contain only ice from one side of the break. Including ice from both sides of such a break would have resulted in a wrong depth attributed to the sample.

2.3 Annual melt percent

Melt features such as ice layers poor or free of air bubbles are formed by percolation and refreezing of melt water which occurs when surface snow melts. The melt water percolates deeper into the snow pack and fills the pores. There the melt water refreezes under the formation of ice layers. The percentage of annual melt in the Lomo09 core was calculated from the melt features observed during processing of the core (Figure 2.4), similar to Henderson et al. (2006). When the core is backlit, clear and bubbly ice appears as transparent area. The procedure by Henderson et al. (2006) was changed as such that the melt features were not categorised but it was accounted for to what extent the melt affected the core diameter. This was done by multiplying the length of the melt feature with the percentage of the affected core diameter. For instance, if a melt feature was 20 cm long but affected only one fifth of the core diameter, this melt feature equals a melt feature of four centimetre length affecting the whole core diameter. In order to calculate the annual melt percent, the observed melt features of one year were summed up.

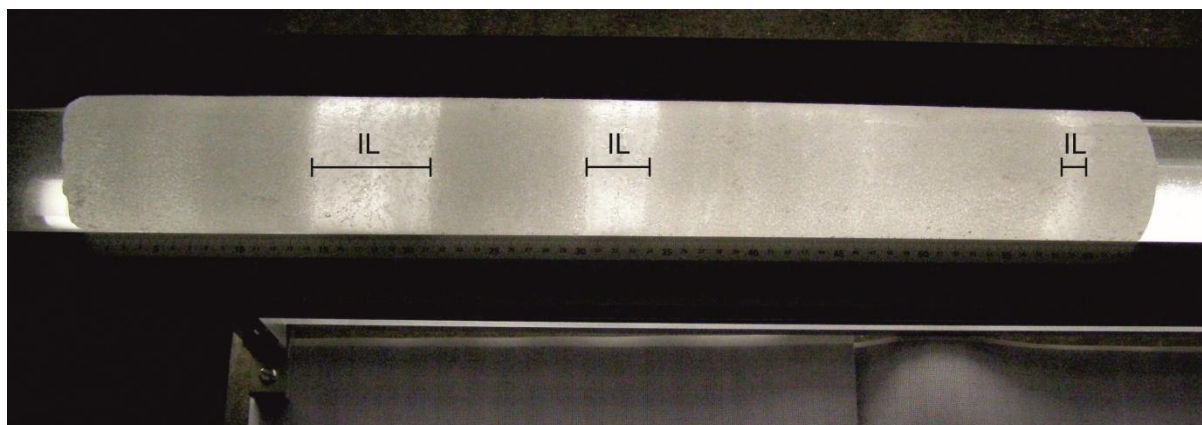


Figure 2.4 Example of a core section on the light bench in the cold room at PSI. Major melt features are indicated. IL = Ice lens.

2.4 Water stable isotope ratios ($\delta^{18}\text{O}$ and δD)

The water molecule can be formed naturally by combinations of the stable isotopes of the two hydrogen isotopes ^1H and ^2H (or D, deuterium) and the three oxygen isotopes ^{18}O , ^{17}O and ^{16}O . Paleoclimatology focuses on the following three combinations (called isotopologues), listed according their abundance: (1) H_2^{16}O , (2) H_2^{18}O , and (3) HDO .

During phase changes in the hydrological cycle, such as evaporation and condensation, the relative concentration of the water molecules containing the stable isotopes ^{18}O and ^{16}O as well as D and ^1H changes due to the differences in vapour pressure. The molecules with the lighter (heavier) isotopes have a higher (lower) vapour pressure and thus will evaporate (condensate)

more easily. This so-called isotopic fractionation is temperature-dependent, so the ratio of $^{18}O/^{16}O$ or $^2H/^1H$ in precipitation can be used as temperature-proxy e.g. in ice cores where precipitated water is stored for a long time. The ratios of $^{18}O/^{16}O$ and $^2H/^1H$ are commonly reported as $\delta^{18}O$ and δD , respectively, indicating their deviation in per mill from an international standard, the Vienna Standard Mean Ocean Water (VSMOW) index. The value $\delta^{18}O$ (δD) used as temperature proxy is calculated as follows:

$$\delta^{18}O [\text{‰}] = \frac{r_{sample} - r_{VSMOW}}{r_{VSMOW}} = \frac{\left(\frac{^{18}O}{^{16}O}\right)_{sample} - \left(\frac{^{18}O}{^{16}O}\right)_{VSMOW}}{\left(\frac{^{18}O}{^{16}O}\right)_{VSMOW}} * 1000 \quad (2-1)$$

With

$$r_{VSMOW} = \left(\frac{^{18}O}{^{16}O}\right)_{VSMOW} = (2005.2 \pm 0.45) * 10^{-6} \quad (\text{Baertschi, 1976}) \quad (2-2)$$

$$\delta D [\text{‰}] = \frac{r_{sample} - r_{VSMOW}}{r_{VSMOW}} = \frac{\left(\frac{D}{H}\right)_{sample} - \left(\frac{D}{H}\right)_{VSMOW}}{\left(\frac{D}{H}\right)_{VSMOW}} * 1000 \quad (2-3)$$

With

$$r_{VSMOW} = \left(\frac{D}{H}\right)_{VSMOW} = (155.95 \pm 0.08) * 10^{-6} \quad (\text{de Wit et al., 1980}) \quad (2-4)$$

In the Lomonosovfonna 2009 ice core $\delta^{18}O$ and δD were determined in samples taken from the inner part of the core (Figure 2.3A) for practical reasons although not being sensitive to contamination. The samples represent an aliquot of 1.0 to 1.5 mL of the samples for ion chromatography and were given into 2 mL glass vials with a PP screw top and a silicon/PTFE septum (Infochroma AG, Zug, Switzerland) directly after melting the ice. The analysis was partly accomplished by Tõnu Martma at the Institute of Geology, Tallinn University of Technology, Estonia (samples #1-1370 and #3224-3997), and partly at PSI (samples #1371-3223). The samples were measured with varying instruments as indicated in Table 2.1. Further details on the instruments are given in the next two sub-chapters. Some values are missing completely or were not used further (Table 2.2) due to non-availability of the instrument and/or too large errors.

2 Methods

Table 2.1 Details on $\delta^{18}\text{O}$ and δD analyses.

Parameter	Sample #	Instrument	Precision [‰]	Location
$\delta^{18}\text{O}$	1-221	GasBench-IRMS	0.1	Tallinn
	330, 331, 370, 571			University
	577-830			
	222-576	WS-CRDS		Tallinn
	831-1370			University
	3224-3997			
	1371-3223	WS-CRDS	0.1	PSI
δD	222-570	WS-CRDS		Tallinn
	572-576			University
	831-1370			
	3224-3997			
	571	TC/EA-IRMS	1	Tallinn
	577-830			University
	1371-3223	WS-CRDS	0.5	PSI

Table 2.2 Missing or not further used values of $\delta^{18}\text{O}$ and δD .

Parameter	Sample #
$\delta^{18}\text{O}$	17, 171, 192, 258, 286, 341, 1062, 1367, 1389, 2972, 3739
δD	1-221, 258, 286, 330, 331, 341, 370, 1062, 1367, 1389, 2972, 3739

2.4.1 Isotopic ratio mass spectrometry (IRMS)

At Tallinn University $\delta^{18}\text{O}$ and δD of the first samples of the Lomo09 core (Table 2.1) were both analysed with an isotopic ratio mass spectrometer (IRMS, Delta V Advantage, Thermo Fisher Scientific, Bremen, Germany), which separates the different isotopes by their mass/charge ratio. In order to obtain values with the highest precision possible the IRMS was combined with an On-Line Gas Preparation Multiple Loop Injection system (GasBench II, Thermo Fisher Scientific, Bremen, Germany) for $\delta^{18}\text{O}$ analysis, for δD analysis it was connected with a High Temperature Conversion Elemental Analyzer (TC/EA, Thermo Fisher Scientific, Bremen, Germany).

For $\delta^{18}\text{O}$ analysis with the GasBench-IRMS 0.5 mL of each sample is transferred into a 12 mL screw top vial (Labco Limited, Lampeter, Ceredigion, UK) using disposable pipettes. After sealing the 12 mL vials with septa all air is removed by an automated, autosampler-assisted (HTC-xt PAL, LEAP Technologies, Carrboro, NC, USA) flushing procedure using a mixture of 0.3% CO_2 in 99.7% helium (He) at 90 mL/min. The CO_2 here functions as equilibration gas. After 24 hours of equilibrium time the gaseous He/ CO_2 mixture is flushed out of the vial by a He stream at 0.5 mL/min. Potential water is removed before the gases are separated by an isothermal gas chromatograph and before the sample is introduced to the IRMS, where $^{12}\text{C}^{16}\text{O}^{16}\text{O}$ and $^{12}\text{C}^{18}\text{O}^{16}\text{O}$ are separated by their mass of 44 and 46, respectively. The CO_2 /He-mixture of each sample is injected ten times (100 μL per injection), of which only the last six injections are used for calculating the $\delta^{18}\text{O}$ of each sample to avoid potential memory effects. In order to monitor stability and potential drifts of the setup the measurement of three in-house standards (TLN-A, TLN-B and TLN-D; see Table 2.3 for isotopic values) is followed by five samples. The overall precision (1σ) of the $\delta^{18}\text{O}$ analysis with the GasBench-IRMS is $\pm 0.1\%$.

The original 2 mL sample vials are placed in the autosampler of the TC/EA for δD analysis. For each injection $\sim 0.1 \mu\text{L}$ of water is transferred to a glassy carbon tube with glassy carbon filling with a 0.5 μL syringe (SGE Europe Ltd, Crownhill, Milton Keynes, UK). There it is pyrolysed at 1400°C , where hydrogen (^1H and D) contained in the sample is converted to H_2 or HD (and oxygen (^{16}O or ^{18}O) to $^{12}\text{C}^{16}\text{O}$ and $^{12}\text{C}^{18}\text{O}$). A He-stream then transports the H_2 and HD (and $^{12}\text{C}^{16}\text{O}/^{12}\text{C}^{18}\text{O}$) to a gas chromatography column where they are separated before being introduced to the IRMS. There H_2 and HD are separated by their different masses of 2 and 3, respectively. Each sample is injected four times, of which the last three are used to calculate the mean δD of the sample. The same standards as for GasBench-IRMS were measured after every fourth sample to monitor stability and potential drifts. The overall precision (1σ) of the δD analysis with the TC/EA-IRMS is $\pm 1\%$.

Table 2.3 Isotopic values of the three in-house laboratory standards at Tallinn University of Technology.

Name of standard	$\delta^{18}\text{O}$ [‰]	δD [‰]
TLN-A	-9.73	-74.7
TLN-B	-21.09	-158,9
TLN-D	-14.73	-111.4

2.4.2 Wavelength-scanned cavity ring down spectrometry (WS-CRDS)

The rest of the samples of the Lomo09 core (Table 2.1) were analysed with a wavelength-scanned cavity ring down spectrometer (WS-CRDS, Picarro L2130-i (PSI) and Picarro L2120-i

2 Methods

(Tallinn University), Picarro Inc., Santa Clara, CA, USA) for $\delta^{18}\text{O}$ and δD at both PSI and Tallinn University. The instruments were purchased in 2011 and 2010, respectively.

The WS-CRDS is based on the Lambert-Beer law and infrared (IR) spectroscopy. The Lambert-Beer law states that the intensity of light travelling through a medium decreases due to the interaction with the medium. The IR spectroscopy uses the different near-infrared absorption spectra of the analysed water molecules for identification of the different isotopologues. The WS-CRDS uses an IR laser that enters a cavity holding the evaporated water sample. The cavity contains three mirrors with an exceptional high reflectivity (>99.999%) which extend the mean path length of photons in the cavity by a factor of 10^5 . The light intensity leaving the cavity is detected with a photo-detector. When the detector signal reaches a steady state, the laser is shut off and the light starts to decay. Since the mirrors do not have 100% reflectivity, the light intensity in the cavity leaks out and this ring-down (decay) is measured with the photo-detector in real-time. If the cavity holds a sample, this intensity decrease is faster due to absorption of the IR light by the water molecules. The time of the decay and its final total absorption is detected and enables calculation of the sample concentration. The laser scans different wavelengths, enabling the differentiation between various compounds with similar absorption lines, such as water isotopologues.

At PSI the WS-CRDS setup includes an autosampler (HTC-xt PAL, LEAP Technologies, Carrboro, NC, USA), a vaporiser (A0211, Picarro Inc., Santa Clara, CA, USA), and two wash stations (one with ultrapure water (MilliQ, 18 M Ω cm, hereafter called MQ), the other with a methylpyrrolidinone solution) for pre- and post-cleaning of the syringe. The methylpyrrolidinone solution was added because it was found to reduce the friction of the plunger, thus considerably prolonging the syringe's lifetime. At Tallinn University the same setup is used but the syringe is rinsed once with the next sample and cleaned manually every morning and evening with a methylpyrrolidinone solution.

For $\delta^{18}\text{O}$ and δD analysis at PSI 2.1 μL and at Tallinn University 1.2 μL are injected into the vaporiser kept at 110°C using a 10 μL syringe (model 203206, Hamilton, Reno, NV, USA) at PSI and a 5 μL syringe (SGE Europe Ltd, Crownhill, Milton Keynes, UK) at Tallinn University. High purity N_2 then carries the water vapour to the cavity kept at 80°C and 67 hPa. The laser builds up in tenth of microseconds and is then shut off. The decay time is determined for a selected wavelength, then the laser is tuned to a different wavelength, scanning the range from 1.3888 μm to 1.3889 μm in order to detect the three major water isotopologues H_2^{16}O , H_2^{18}O and HDO. At PSI six injections are performed for each sample, of which the first three are discarded due to memory effects and the average of the last three injections is taken as real

value. Potential instrumental drift is monitored by measuring the three in-house standards Scuol, Rueras and Labwater after every 10th sample (see Table 2.4 for isotopic values). If a drift in the Rueras standard, the one with intermediate isotopic values, occurred the values of $\delta^{18}\text{O}$ and δD were drift-corrected. At Tallinn University samples are also injected six times of which the last four are used for calculation. The same standards as for IRMS are used and measured after every 9th sample. The $\delta^{18}\text{O}$ and δD values were drift-corrected if a drift in the standards appeared. The analytical uncertainty of the WS-CRDS at PSI is $<0.1\text{‰}$ for $\delta^{18}\text{O}$ and $<0.5\text{‰}$ for δD (Mariani, 2013).

Table 2.4 Isotopic values of the three PSI in-house standards (Mariani, 2013). The standards were split each into two separate bottles, so the isotopic values of bottle 1 and 2 differ slightly.

Name of standard	$\delta^{18}\text{O}$ [‰]	δD [‰]
Scuol1	-23.77±0.03	-181.0±0.3
Scuol2	-23.77±0.03	-181.6±0.3
Rueras1	-17.08±0.02	-124.2±0.2
Rueras2	-17.10±0.02	-124.0±0.2
Labwater1	-9.96±0.02	-70.8±0.2
Labwater2	-9.93±0.02	-70.4±0.2

In order to check the reliability of the results obtained at PSI and Tallinn University, we performed an inter-laboratory comparison for 20 Lomo09 ice core samples, all six PSI in-house standards Scuol 1 and 2, Rueras 1 and 2, and Labwater 1 and 2, and two standards from Tallinn University (TLN-A2 and TLN-B2; Table 2.5). The values for $\delta^{18}\text{O}$ and δD in the ice samples differed by maximum $\pm 1\%$. The discrepancy for the in-house standards was slightly higher, with a discrepancy of maximum $\pm 2.4\%$. This proves that the values determined in the two laboratories are comparable and can be used without further adjustment.

Table 2.5 Isotopic values of the in-house laboratory standards at Tallinn University of Technology used for the inter-laboratory comparison.

Name of standard	$\delta^{18}\text{O}$ [‰]	δD [‰]
TLN-A2	-10.15	-77.53
TLN-B2	-21.95	-162.51

2.5 Ion chromatography (water soluble major ions)

Water soluble major ions (hereafter called major ions) are analysed in ice cores to reconstruct air composition and pollution on historical timescales, allowing e.g. to identify varying sources

2 Methods

of the air masses reaching the glacier. The major ions determined in the Lomonosovfonna 2009 ice core include the following thirteen species: the five cations of sodium (Na^+), ammonium (NH_4^+), potassium (K^+), magnesium (Mg^{2+}), and calcium (Ca^{2+}) and the eight anions of fluoride (F^-), acetate (CH_3COO^-), formate (HCOO^-), methane-sulphonate (CH_3SO_3^- ; MSA), chloride (Cl^-), nitrate (NO_3^-), sulphate (SO_4^{2-}), and oxalate ($\text{C}_2\text{O}_4^{2-}$). The cutting described in chapter 2.2 resulted in 3997 samples for IC from the inner part of the ice core. The inner part is used because major ions in ice cores occur at very low concentrations ($<<1\text{ppm}$), which is why they are sensitive to contamination. Thus, the 50 mL PP sample vials were pre-cleaned by laying them in MQ for 24 hours, which was repeated five times with fresh MQ. In order to obtain a procedure blank and monitor potential contamination by processing the samples, MQ was frozen in blocks and processed identically to the ice core samples. Further care was taken to avoid contamination by laboratory air when melting the ice samples. Therefore, the vials containing the samples were flushed with nitrogen gas (N_2) when the samples were still in frozen condition. Then the samples were melted at room temperature.

Major ions were analysed with a Metrohm 850 Professional IC combined with an 872 Extension Module and an autosampler (858 Professional Sample Processor). The anions were determined by a step-wise elution, beginning with a lower concentrated eluent (A) followed by a higher concentrated one (B). This procedure was found to give the best results in terms of separation of the single ions and measuring time. Details on the single components and chemicals used for analysis are given in Table 2.6. Calibration with different dilutions of in-house reference solutions of 10 ppm was performed for every sample batch separately, except for NH_4^+ (see further details below). In order to monitor potential drifts e.g. in the calibration, one of the reference solutions and an in-house standard (snow from the Jungfrauoch, Switzerland) were measured after every $\sim 20^{\text{th}}$ sample. The raw data were then processed with the MagICNet 1.1 software. The precision of the method is around 5%. The detection limits, blanks and procedure blanks for the single ionic species are given in Table 2.7. The blank values were determined analysing MQ; the procedure blanks result from the analysis of MQ that had been frozen to blocks that were then processed the same way as the Lomo09 samples. The Lomo09 ion concentrations were not blank-corrected. Concentrations below the detection limit were substituted with a concentration of half the detection limit.

Table 2.6 Components and chemicals used for major ion analysis with the Metrohm 850 Professional IC.

	Cations	Anions
Eluent	2.8 mM HNO ₃	A: 1.5 mM Na ₂ CO ₃ / 0.3 mM NaHCO ₃ B: 8 mM Na ₂ CO ₃ / 1.7 mM NaHCO ₃
Flow rate	1 mL/min	0.9 mL/min
Loop	500 µL	500 µL
Separation column	Metrosep C4	Metrosep A Supp 10
Guard column		Metrosep A Supp 5
Suppression	-	0.05 M H ₂ SO ₄ + 12 g oxalic acid
Detection	conductivity	conductivity

Table 2.7 Detection limits, precision and blank values [ppb] for the ions analysed with the Metrohm 850 Professional IC. DL = Detection limit. Blank = MQ. PBlank = Procedure blank, MQ ice processed equally to the samples.

Anions	Cations				Cations		
	DL	Blank	PBlank		DL	Blank	PBlank
F ⁻	0.1	0.3	0.1	Na ⁺	0.4	1.1	1.1
CH ₃ COO ⁻	0.7	1.1	3.4	NH ₄ ⁺	0.3	0.6	1.0
HCOO ⁻	0.8	1.9	2.5	K ⁺	0.8	1.6	1.9
MSA	0.5	0.3	0.3	Mg ²⁺	0.4	5.6	9.1
Cl ⁻	0.6	4.8	3.9	Ca ²⁺	0.9	2.7	6.0
NO ₃ ⁻	0.6	3.8	3.8				
SO ₄ ²⁻	1.0	2.8	3.0				
C ₂ O ₄ ²⁻	0.8	0.6	0.6				

The analysis of NH₄⁺ is difficult because it is prone to contamination during analysis (Jauhiainen et al., 1999; Kaufmann et al., 2010; Legrand et al., 1984, 1993, 1999; Udisti et al., 1994). The solution of NH₃ from laboratory air results in artificially increased NH₄⁺ concentrations in the sample. This artefact occurred especially in the low standards analysed for the Lomo09 IC samples, thus highly affecting the NH₄⁺ calibration curve in the low concentration range (1-10 ppb). In general, the NH₄⁺ concentrations in the Lomo09 samples are low (median of 10 ppb) and hence sensitive to the modified calibration curve in the low concentration range. Thus for NH₄⁺ one calibration that was least influenced by contamination was applied to all 3997 samples. This procedure was tested with the concentration of Na⁺, one of the species that account for >30% of the ion budget in the Lomo09 core and that is not sensitive to contamination by laboratory air. The Na⁺ concentrations determined using just one calibration

2 Methods

for all samples was within $\pm 6\%$ of the Na^+ concentrations calculated with a calibration performed for every sample batch (Figure 2.5). This is almost within the precision of the analysis. Thus, the application of this calibration procedure for NH_4^+ was justified.

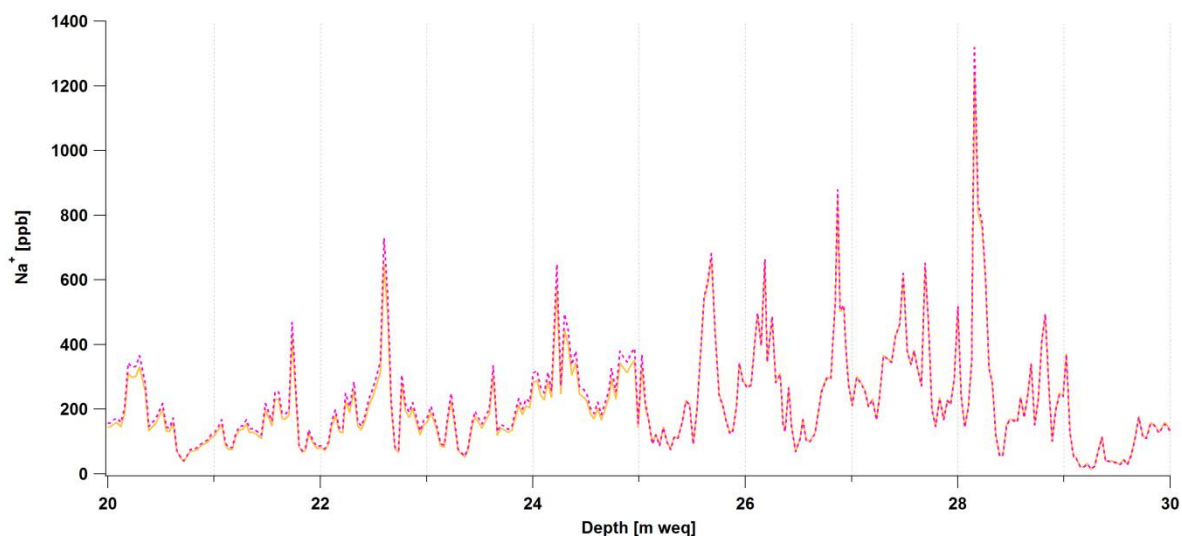


Figure 2.5 Na^+ records of the Lomo09 ice core in the depth range of 20 to 30 m weq; the yellow line represents the concentrations calculated with a calibration for every sample batch; the dashed pink line represents the concentrations calculated with one calibration for all samples.

2.6 Black carbon (BC)

The cutting described in chapter 2.2 resulted in 4046 samples for black carbon (BC) analysis from the inner part of the ice core. The 50 mL PP sample vials were cleaned similarly to those for IC analysis but a threefold repetition was found to be sufficient. Procedure blanks and potential contamination by processing the samples was monitored by analysing MQ that was frozen in blocks and processed identically to the ice core samples. Similar to the IC samples the BC samples were flushed with N_2 gas to avoid potential contamination by laboratory air when still in frozen condition and melted at room temperature.

BC was analysed with a setup including a Single Particle Soot Photometer (SP2, Droplet Measurement Technology, Inc., Boulder, CO, USA, Schwarz et al., 2006) combined with an APEX-Q jet nebulizer system (High Sensitivity Sample Introduction System, Elemental Scientific Inc., Omaha, NE, USA). The SP2 is an instrument widely applied in aerosol science and analyses only airborne samples. Thus for the analysis of ice core samples a nebulisation step is required. Here, only a brief description of the method is given, details can be found in chapter 3.

The SP2 measures the mass concentration and size distribution of single BC-containing particles using the principle of laser-induced incandescence. A continuous-wave Nd:YAG-laser heats individual BC-containing particles to their boiling point (~ 4200 K). The resulting peak intensity

of the thermal radiation is proportional to the BC mass in the particle (Schwarz et al., 2006). The APEX-Q nebuliser system (hereafter APEX-Q) can be operated in self-aspirating mode, where the liquid sample flow is defined by the flow of the carrier gas, the diameter and length of the capillary and the geometry of the nebuliser nozzle. A jet nebuliser aerosolises the aqueous sample into a heated (100°C) glass cyclonic spray chamber. In order to remove the remaining water vapor before being introduced into the SP2 the aerosol is afterwards cooled (2°C) in a Peltier-cooled multipass condenser (Elemental Scientific Inc., 2013).

The setup used for BC analysis in the Lomo09 ice core samples includes an APEX-Q PFA-ST MicroFlow nebulizer (ES-2040-7000) and a 1.5 m long PFA capillary with an inner diameter of 0.25 mm (ES-2042; both Elemental Scientific Inc., Omaha, NE, USA). The optimal purge airflow was found to be 1 L/min. The calibration of the SP2 (internal calibration) as well as that of the whole nebuliser/SP2-setup were performed using Aquadag (AQ), an industrial lubricant consisting of a colloidal suspension of aggregates of graphitic carbon in water with $\sim 70.5\% \pm 1.0\%$ (1σ) BC content of the dry mass (76% in Gysel et al., 2011).

For the determination of BC mass concentration in an aqueous sample via SP2 measurement of the nebulized aerosol it is important to account for the nebulizer efficiency. This was done by relating the measurement of the unknown sample to the measurement of an aqueous BC standard with known concentration (external calibration). The nebulizer efficiency was assumed to remain stable between measurement of the sample and the standard. BC mass concentrations in the ice core samples C_{SP2}^{S1} were then calculated as follows:

$$C_{SP2}^{S1} = c_{SP2} \frac{C_{liq}^*}{c_{SP2}^*} \quad (2-5)$$

where c_{SP2} and c_{SP2}^* are the BC mass concentrations measured by the SP2 for the aerosols from the nebulised aqueous sample and aqueous standard, respectively, and C_{liq}^* is the BC mass concentration of the aqueous standard.

2.7 Dating of the Lomo09 ice core

The Lomo09 core was dated with a combination of different methods including the identification of reference horizons such as the tritium peak indicating the year 1963 (chapter 2.7.1) and major volcanic eruptions (chapter 2.7.2), ^{210}Pb decay (chapter 2.7.3), annual layer counting (chapter 2.7.4), and a simple glacier flow model (chapter 2.7.5).

2.7.1 Liquid scintillation counting (^3H)

Tritium (^3H) is the radioactive isotope of hydrogen with a half-life of 12.3 years. It is naturally produced in the atmosphere by cosmic-ray induced neutrons that react with atmospheric nitrogen ($n + ^{14}\text{N} \rightarrow ^{12}\text{C} + ^3\text{H}$). By interaction with stratospheric oxygen, tritium is incorporated in the water molecule and thus the water cycle. Tritium has a very low natural background level with concentrations in precipitation in the order of a few tritium units (TU; $1 \text{ TU} = 10^{-18} [^3\text{H}]/[\text{H}]$) (Michel, 2005). However, since 1951 above-ground nuclear weapon tests have resulted in an increased production of tritium which was only stopped by the US-Soviet Test Ban Treaty in 1963. Until then a large amount of tritium had been released into the atmosphere ($2.4 \cdot 10^{14}$ Bq, Clark and Fritz, 1997). Because this atmospheric tritium has been precipitated onto and incorporated in glacial ice, its temporal trend can be used for dating purposes, with the highest levels indicating the year 1963 when there was the highest level of tritium in the atmosphere.

The samples for tritium analysis were taken from the outer part of the Lomonosovfonna 2009 ice core (Figure 2.3A) because tritium is less affected by contamination than e.g. the water soluble ions. First, a series of samples was cut with low resolution (one sample per ice core segment, $\sim 60\text{-}74\text{cm}$) to detect the approximate depth of the tritium peak that indicates the year 1963. Then, a second series was cut at higher resolution (22 cm) to refine the depth of the tritium peak (Figure 2.6). The samples were analysed by liquid scintillation counting.

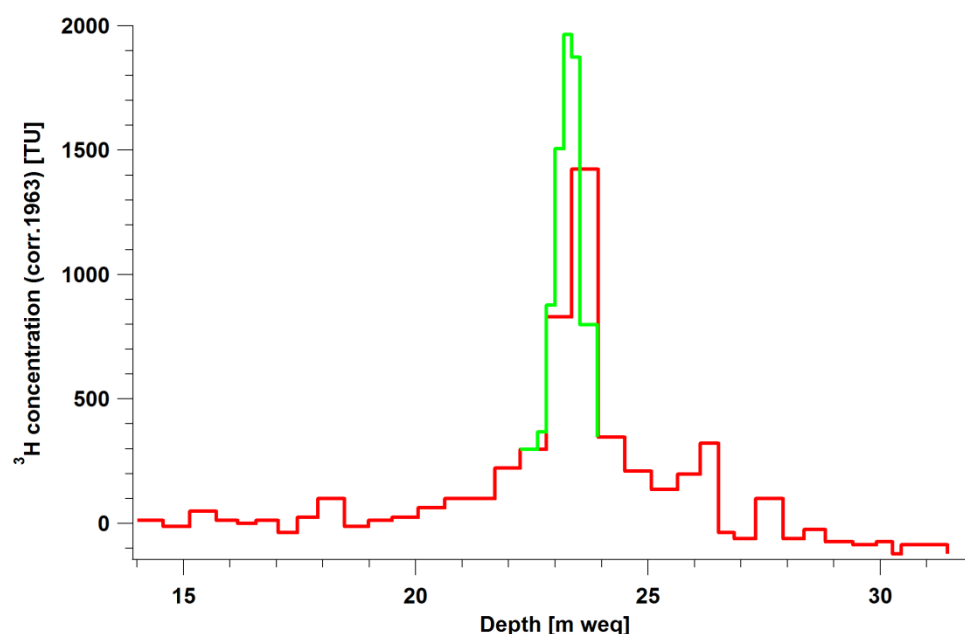


Figure 2.6 Tritium (^3H) peak in the Lomonosovfonna 2009 ice core. Values are given in tritium units (TU) and are decay-corrected to the year 1963 for easier comparison with other records. The red curve indicates the coarse sample resolution of 60-74 cm; the green curve indicates the high sample resolution of ~ 22 cm for more precise depth determination of the peak.

The samples were melted at room temperature; then 10 mL of each sample were mixed with a solvent plus scintillator for the analysis. By decaying the tritium in the samples emits beta-rays that transmit energy to the scintillator. The scintillator then converts the absorbed energy into photons whose fluorescence leads to an electrical pulse in the photomultiplier tubes (PMT) of the counter (TriCarb 2770 SLL/BGO counter, Packard SA, Meriden, USA). This electrical pulse that is converted to a digital value is proportional to the number of photons. The detection limit of the setup is 9.65 TU. The counting time was 1200 min with a blank level of 0.61-0.63 counts per minute. The results were decay-corrected to the year 1963 to facilitate the comparison with other records. The analysis was performed by Jost Eikenberg and Max Rüthi of the Radioanalytics Group at PSI.

The tritium peak in the Lomonosovfonna 2009 ice core was detected at an approximate depth of 23.18 m weq which was assigned to the year 1963 and used as a reference horizon for dating the core.

2.7.2 Volcanic reference horizons

Large volcanic eruptions emit sulphur dioxide (SO_2) that is oxidised to sulphuric acid (H_2SO_4) in the stratosphere or troposphere. Thus, the eruptions can affect the SO_4^{2-} budget on a global scale, leading to increased atmospheric SO_4^{2-} concentrations 1-2 years after an eruption. Therefore, the SO_4^{2-} peaks detected in e.g. ice cores can be used as reference horizons for dating purposes. This approach has been applied successfully in a variety of ice cores (e.g., Legrand and Mayewski, 1997; Sigl et al., 2013). In order to identify volcanic reference horizons in the Lomo09 core we applied a method similar to that in Moore et al. (2012).

2 Methods

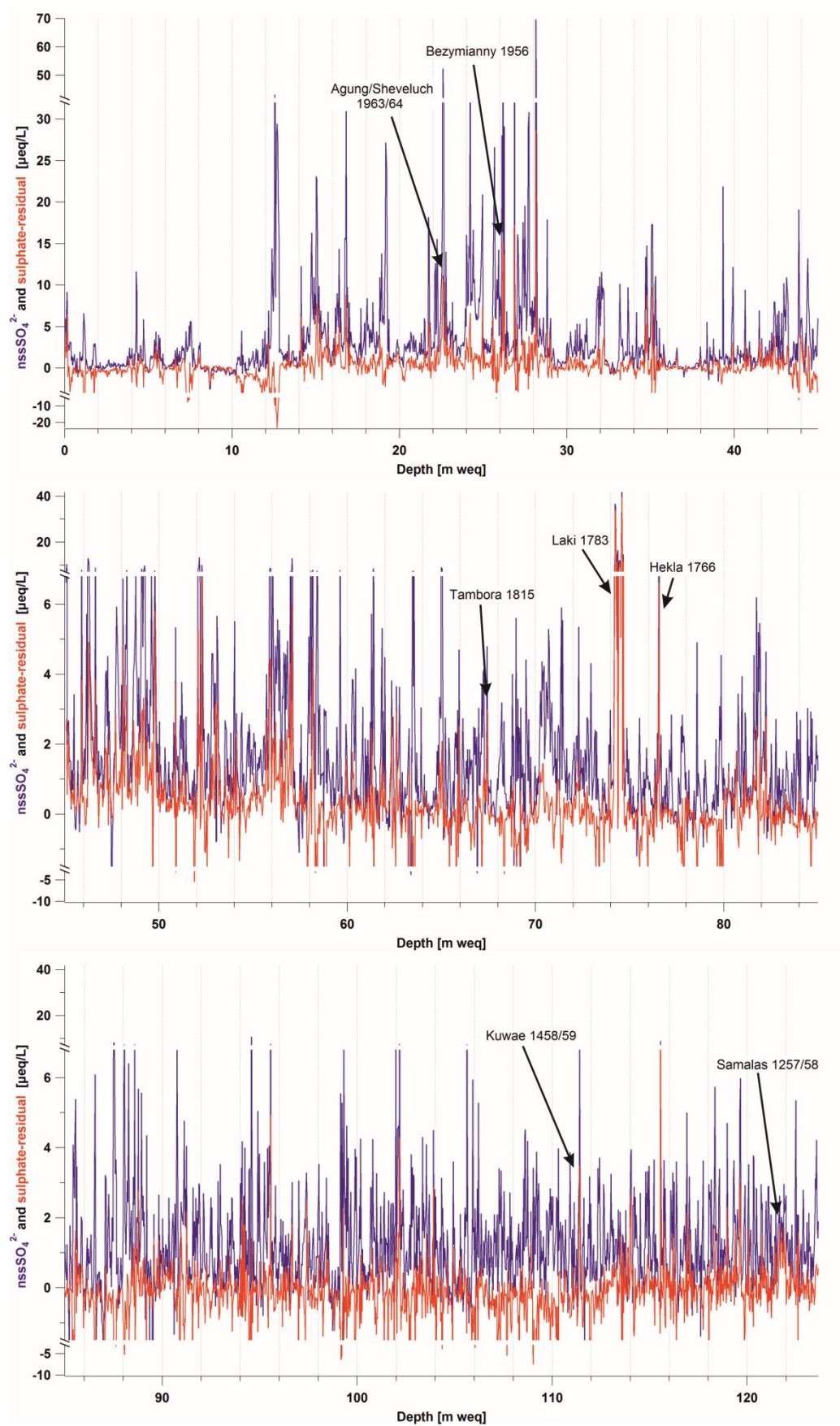


Figure 2.7 The records of nss-sulphate (nssSO₄²⁻) (blue) and sulphate (SO₄²⁻)-residual (red) of the Lomo09 ice core. The volcanic eruptions identified are indicated.

SO₄²⁻ detected in ice cores can have several sources: (1) sea salt, (2) mineral dust, (3) anthropogenic and biogenic SO₂ emissions, including volcanic eruptions (Legrand and Mayewski, 1997). Among the ionic species standardly analysed in ice cores only SO₄²⁻ has partly a volcanic source. Thus the part of the SO₄²⁻ budget that cannot be explained by any of the other ionic species is thought to come from a volcanic source. This residual was estimated by a multiple linear regression analysis (MLR) between SO₄²⁻ and the other ionic species analysed in the ice core, similar as in Moore et al. (2012). Different from these authors we used the raw data and did not apply a moving window but split the ionic record at a depth of 45 m weq and performed a MLR for both parts separately to avoid a bias in preindustrial times when there was no anthropogenic SO₄²⁻ input. The record of the SO₄²⁻-residual was compared with the non-sea-salt sulphate (nssSO₄²⁻) record (Figure 2.7). NssSO₄²⁻ is the part of the SO₄²⁻ corrected for the contribution by sea salt. It is calculated by subtracting the proportional amount of Na⁺ from the SO₄²⁻ according to the sea water ratio of Na⁺ to SO₄²⁻ (in µeq/L) (Eq. 2-6) because at Lomonosovfonna Na⁺ originates mainly from sea salt. This is supported by the mean Cl⁻ to Na⁺ ratio of 1.21 that is very close to the bulk sea water ratio of 1.16 (Keene et al., 1986).

$$nssSO_4^{2-} = SO_4^{2-} - 0.12 * Na^+ \quad [\mu\text{eq/L}] \quad (2-6)$$

The two records of nssSO₄²⁻ and the SO₄²⁻-residual agree well for the sharp peaks (Figure 2.7). Those were then matched to the volcanic eruptions given in Table 2.8.

Table 2.8 Volcanic eruptions identified in the Lomo09 ice core. Year gives the year of eruption. For the Kuwae eruption we applied the updated eruption year of Sigl et al. (2013); for the Samalas eruption we refer to Lavigne et al. (2013).

Depth [m weq]	Volcanic eruption	Year
22.6	Agung/ Sheveluch	1963/64
26.2	Bezymianny	1956
42.4	Katmai	1912
67.45	Tambora	1815
74.5 (74.2-74.7)	Laki	1783
76.55	Hekla	1766
111.4	Kuwae	1458/59
121.78 (121.65-121.9)	Samalas	1257/58

2.7.3 α-spectroscopy (²¹⁰Pb)

²¹⁰Pb is a naturally occurring radioactive isotope with a half-life of 22.3 years that belongs to the ²³⁸U decay chain. ²³⁸U is a natural radioactive isotope in the earth's crust which decays over several intermediate isotopes to ²²²Rn. ²²²Rn has a half-life of 3.8 days and because it is a gas it

2 Methods

emanates constantly from the earth's crust into the atmosphere (Figure 2.8). There ^{222}Rn decays over several intermediate isotopes to ^{210}Pb , which attaches to aerosols and settles onto the glacier surface by dry or wet deposition within a few days to weeks. Due to its radioactive decay the activity of ^{210}Pb decreases in firn and ice with depth and can therefore be used for dating purposes. The time period accessible for dating depends mainly on the half-life of 22.3 years and was found to be on a century time-scale (Gäggeler et al., 1983). This is the case for (1) constant accumulation of ^{210}Pb in the ice and (2) if no relocation of the initial ^{210}Pb occurred (Gäggeler et al., 1983). High initial activity and low blank values give access to longer time periods of up to 200 years (Herren et al., 2013). The activity of ^{210}Pb is measured indirectly by its decay product ^{210}Po which has a half-life of 138 days and emits α -radiation.

In the Lomonosovfonna ice core, the outer parts of two segments (Figure 2.3A) were combined to one sample of 180-220 g for measuring the ^{210}Pb activity, because α -spectroscopy is not sensitive to contamination and combining two core segments largely increases the signal to noise ratio. Hydrochloric acid (HCl) and a ^{209}Po ($T_{1/2} = 102$ yr) standard were added to the frozen samples. Then the samples were melted and heated to 90-95°C when they were bubbled with sulphur dioxide (SO_2) for three minutes to adjust the pH to remove Fe^{3+} that would affect the following steps. A silver plate was then placed in the hot sample solution for seven hours to allow deposition of ^{210}Po on the plate (electroplating). After the plate was rinsed with MQ and dried, it was analysed by α -spectroscopy (Euertec Schlumberger, Type 7164 with PIPS detector) by measuring the α -activities of ^{209}Po and ^{210}Po . The ^{209}Po is used to correct for the efficiency of the chemical separation. Edith Vogel of the Laboratory of Radiochemistry and Environmental Chemistry prepared the silver plates which were then measured by Leonhard Tobler at PSI.

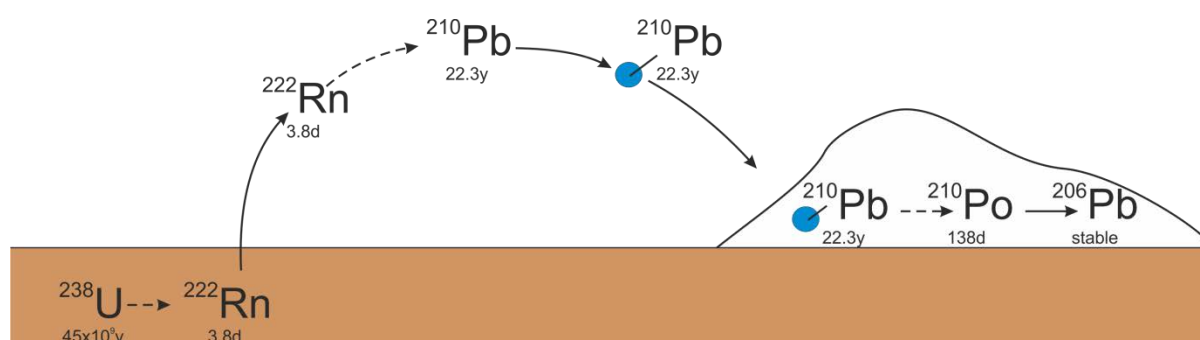


Figure 2.8 Decay chain of ^{210}Pb .

The ^{210}Pb activity in the Lomonosovfonna 2009 ice core ranges from 0.4 to 49.8 mBq/kg, blank-corrected with a background activity of ~ 2.5 mBq/kg. This accords well with the values found in the Lomonosovfonna 1997 core (Pinglot et al., 2003). In contrast to the values of the 1997 core that did not show a clear depth-age relation, the higher depth-resolved ^{210}Pb data from the

Lomonosovfonna 2009 core nicely reflect the depth-age relation, with decreasing activity with increasing depth (Figure 5.3). The data show a large scatter which can be explained by the low concentrations as well as the probably non-constant accumulation of ^{210}Pb on the glacier. Nevertheless, the depth-age relation resulting from the ^{210}Pb -dating agrees well with the other dating methods (Figure 4.2).

2.7.4 Annual layer counting (ALC)

Some ionic species show concentrations that vary with season and show maximum (minimum) concentrations in a particular season and low (high) concentrations throughout the rest of the year. Those cycles can then be used for dating purposes counting single years from maximum to maximum (minimum to minimum).

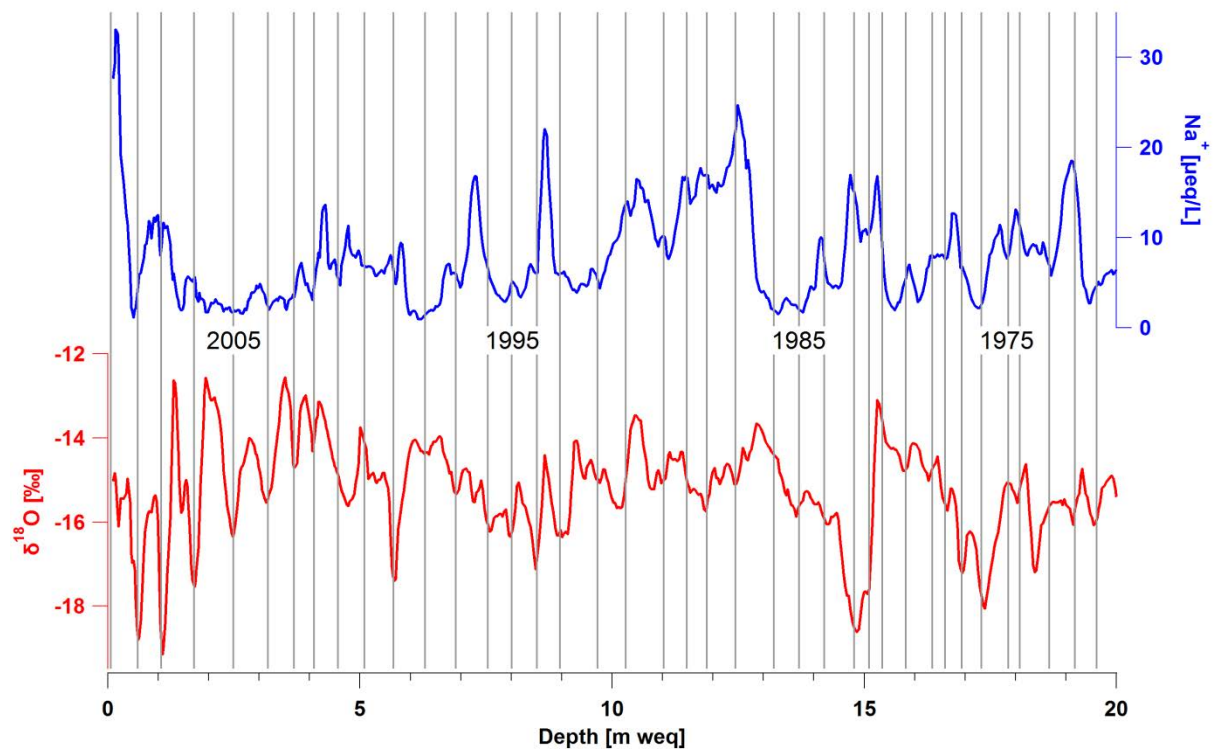


Figure 2.9 Example for annual layer counting (ALC) for the core section between 0 and 20 m weq using the records of $\delta^{18}\text{O}$ and Na^+ concentration. Data are five-point-moving averages. Grey vertical lines indicate the single counted years; numbers within the graph give the resulting year.

The water stable isotope ratio of $\delta^{18}\text{O}$ also shows cyclicity. This is caused by the temperature-dependence of the ratio with higher values at higher temperatures and lower values at lower temperatures. Since the temperatures within a year also follow the cycle of warmer temperatures in summer and lower temperatures in winter, this temperature-dependence can be used for counting years. This so-called annual layer counting (ALC) in the Lomo09 was performed using pronounced seasonality of the $\delta^{18}\text{O}$ record and, where it was critical to identify

single years, additionally the Na⁺ record which shows higher values in summer due to more open water that can lead to sea spray formation (Figure 2.9). It was possible to count years down to a depth of 79.86 m weq which was attributed to the year 1749 AD. Below that depth it was difficult to identify the annual cycles. One year is represented by 3 to 32 samples. In order to obtain an age for each sample, the age of the samples in between full years was linearly interpolated.

2.7.5 Glacier flow model

A simple glacier flow model (Thompson et al., 1998) was fitted through the volcanic reference horizons. This was used to date the core below a depth of 79.7 m weq (= 1750) where ALC was limited due to strong layer thinning. The glacier flow model accounts for layer thinning due to increasing compression with depth and is described by Eq. 2-7.

$$z(t) = H \left[1 - \left(\frac{t * b * p}{H} - 1 \right)^{1/p} \right] \quad (2-7)$$

With H as glacier thickness (~170 m weq = 200 m total depth), z the depth in m weq, t the time, b the modelled averaged accumulation rate in m/year, and p a constant (Thompson et al., 1998). The parameters b and p were determined by fitting the following data into Eq. 2-7: ALC data back to 1766 and the two volcanic reference horizons at 111.4 and 121.78 m weq attributed to the years 1458/59 and 1257/58 AD, respectively. This resulted in $b = 0.5832$ m/year and $p = 1.015$ with an R^2 of 0.9997.

Combining the dating methods described above resulted in the dating of the Lomo09 ice core displayed in Figure 4.2. Thus the core covers the time period of 1222 to 2009. The dating uncertainty for the core down to a depth of ~68 m weq is estimated to be ± 1 year within ± 10 years of the reference horizons and increases to ± 3 years in between. Down to a depth of ~80 m weq the dating uncertainty enlarges to ± 3 years also in proximity of the reference horizons, and below ~80 m weq it increases to ± 10 years. This dating uncertainty was calculated by comparing the year of the volcanic eruptions with the modelled date.

References

- Baertschi, P.: Absolute ^{18}O content of standard mean ocean water, *Earth and Planetary Science Letters*, 31(3), 341–344, doi:10.1016/0012-821X(76)90115-1, 1976.
- Clark, I. D. and Fritz, P.: *Environmental isotopes in hydrogeology*, CRC Press, 1997.
- Eichler, A., Schwikowski, M., Gäggeler, H. W., Furrer, V., Synal, H.-A., Beer, J., Saurer, M. and Funk, M.: Glaciochemical dating of an ice core from upper Grenzgletscher (4200 m a.s.l.), *Journal of Glaciology*, 46(154), 507–515, doi:10.3189/172756500781833098, 2000.
- Elemental Scientific Inc.: Apex Q High Sensitivity Sample Introduction System, Product Overview, available at: <http://www.icpms.com/pdf/ApexQ-ESI.pdf>, last access: 10 December, 2013.
- Gäggeler, H., Von Gunten, H. R., Rössler, E., Oeschger, H. and Schotterer, U.: ^{210}Pb -dating of cold alpine firn/ice cores from Colle Gnifetti, Switzerland, *Journal of Glaciology*, 29(101), 165–177, 1983.
- Ginot, P., Stampfli, F., Stampfli, D., Schwikowski, M. and Gäggeler, H. W.: FELICS, a new ice core drilling system for high-altitude glaciers, *Memoirs of National Institute of Polar Research. Special Issue*, 56, 38–48, 2002.
- Gysel, M., Laborde, M., Olfert, J. S., Subramanian, R. and Groehn, A. J.: Effective density of Aquadag and fullerene soot black carbon reference materials used for SP2 calibration, *Atmospheric Measurement Techniques*, 4(12), 2851–2858, doi:10.5194/amt-4-2851-2011, 2011.
- Henderson, K., Laube, A., Gäggeler, H. W., Olivier, S., Papina, T. and Schwikowski, M.: Temporal variations of accumulation and temperature during the past two centuries from Belukha ice core, Siberian Altai, *Journal of Geophysical Research*, 111(D3), D03104, 2006.
- Herren, P.-A., Eichler, A., Machguth, H., Papina, T., Tobler, L., Zapf, A. and Schwikowski, M.: The onset of Neoglaciation 6000 years ago in western Mongolia revealed by an ice core from the Tsambagarav mountain range, *Quaternary Science Reviews*, 69, 59–68, doi:10.1016/j.quascirev.2013.02.025, 2013.
- Isaksson, E., Pohjola, V., Jauhiainen, T., Moore, J., Pinglot, J. F., Vaikmaa, R., van de Wal, R. S. W., Hagen, J. O., Ivask, J., Karlöf, L., Martma, T., Meijer, H. A. J., Mulvaney, R., Thomassen, M. and van den Broeke, M.: A new ice-core record from Lomonosovfonna, Svalbard: viewing the 1920–97 data in relation to present climate and environmental conditions, *Journal of Glaciology*, 47(157), 335–345, 2001.
- Jauhiainen, T., Moore, J., Perämäki, P., Derome, J. and Derome, K.: Simple procedure for ion chromatographic determination of anions and cations at trace levels in ice core samples, *Analytica Chimica Acta*, 389(1-3), 21–29, 1999.
- Kaufmann, P., Fundel, F., Fischer, H., Bigler, M., Ruth, U., Udisti, R., Hansson, M., de Angelis, M., Barbante, C., Wolff, E. W., Hutterli, M. and Wagenbach, D.: Ammonium and non-sea salt sulfate in

2 Methods

the EPICA ice cores as indicator of biological activity in the Southern Ocean, *Quaternary Science Reviews*, 29(1–2), 313–323, doi:10.1016/j.quascirev.2009.11.009, 2010.

Keene, W. C., Pszenny, A. A. P., Galloway, J. N. and Hawley, M. E.: Sea-salt corrections and interpretation of constituent ratios in marine precipitation, *Journal of Geophysical Research*, 91(D6), 6647–6658, doi:10.1029/JD091iD06p06647, 1986.

Lavigne, F., Degeai, J.-P., Komorowski, J.-C., Guillet, S., Robert, V., Lahitte, P., Oppenheimer, C., Stoffel, M., Vidal, C. M., Surono, Pratomo, I., Wassmer, P., Hajdas, I., Hadmoko, D. S. and Belizal, E. de: Source of the great A.D. 1257 mystery eruption unveiled, Samalas volcano, Rinjani Volcanic Complex, Indonesia, *Proceedings of the National Academy of Science*, 110(42), 16742–16747, doi:10.1073/pnas.1307520110, 2013.

Legrand, M. and Mayewski, P.: Glaciochemistry of polar ice cores: a review, *Reviews of Geophysics*, 35, 219–244, 1997.

Legrand, M., de Angelis, M. and Delmas, R. J.: Ion chromatographic determination of common ions at ultratrace levels in Antarctic snow and ice, *Analytica Chimica Acta*, 156, 181–192, doi:10.1016/S0003-2670(00)85549-X, 1984.

Legrand, M., De Angelis, M. and Maupetit, F.: Field investigation of major and minor ions along Summit (Central Greenland) ice cores by ion chromatography, *Journal of Chromatography A*, 640(1–2), 251–258, doi:10.1016/0021-9673(93)80188-E, 1993.

Legrand, M., Wolff, E. and Wagenbach, D.: Antarctic aerosol and snowfall chemistry: implications for deep Antarctic ice-core chemistry, *Annals of Glaciology*, 29(1), 66–72, doi:10.3189/172756499781821094, 1999.

Mariani, I.: Water stable isotopes in Alpine ice cores as proxies for temperature and atmospheric circulation, PhD thesis, University of Bern, Bern, Switzerland, 2013.

Michel, R. L.: Tritium in the hydrologic cycle, in *Isotopes in the water cycle*, edited by P. K. Aggarwal, J. R. Gat, and K. F. O. Froehlich, pp. 53–66, Springer Netherlands, 2005.

Moore, J. C., Beaudon, E., Kang, S., Divine, D., Isaksson, E., Pohjola, V. A. and van de Wal, R. S. W.: Statistical extraction of volcanic sulphate from nonpolar ice cores, *Journal of Geophysical Research*, 117(D3), D03306, 2012.

Pinglot, J. F., Vaikmae, R. A., Kamiyama, K., Igarashi, M., Fritzsche, D., Wilhelms, F., Koerner, R., Henderson, L., Isaksson, E., Winther, J. G., van de Wal, R. S. W., Fournier, M., Bouisset, P. and Meijer, H. A. J.: Ice cores from Arctic sub-polar glaciers: chronology and post-depositional processes deduced from radioactivity measurements, *Journal of Glaciology*, 49(164), 149–158, 2003.

Schwarz, J. P., Gao, R. S., Fahey, D. W., Thomson, D. S., Watts, L. A., Wilson, J. C., Reeves, J. M., Darbeheshti, M., Baumgardner, D. G., Kok, G. L., Chung, S. H., Schulz, M., Hendricks, J., Lauer, A., Kärcher, B., Slowik, J. G., Rosenlof, K. H., Thompson, T. L., Langford, A. O., Loewenstein, M. and Aikin, K. C.: Single-particle measurements of midlatitude black carbon and light-scattering

aerosols from the boundary layer to the lower stratosphere, *Journal of Geophysical Research*, 111(D16), 207, 2006.

Sigl, M., McConnell, J. R., Layman, L., Maselli, O., McGwire, K., Pasteris, D., Dahl-Jensen, D., Steffensen, J. P., Vinther, B., Edwards, R., Mulvaney, R. and Kipfstuhl, S.: A new bipolar ice core record of volcanism from WAIS Divide and NEEM and implications for climate forcing of the last 2000 years, *Journal of Geophysical Research: Atmospheres*, doi:10.1029/2012JD018603, 2013.

Thompson, L. G., Davis, M. E., Mosley-Thompson, E., Sowers, T. A., Henderson, K. A., Zagorodnov, V. S., Lin, P.-N., Mikhailenko, V. N., Campen, R. K., Bolzan, J. F., Cole-Dai, J. and Francou, B.: A 25,000-year tropical climate history from Bolivian ice cores, *Science*, 282(5395), 1858–1864, doi:10.1126/science.282.5395.1858, 1998.

Udisti, R., Bellandi, S. and Piccardi, G.: Analysis of snow from Antarctica: a critical approach to ion-chromatographic methods, *Fresenius Journal of Analytical Chemistry*, 349(4), 289–293, doi:10.1007/BF00323205, 1994.

De Wit, J. C., van der Straaten, C. M. and Mook, W. G.: Determination of the absolute hydrogen isotopic ratio of V-SMOW and SLAP, *Geostandards Newsletter*, 4(1), 33–36, doi:10.1111/j.1751-908X.1980.tb00270.x, 1980.

3 Optimized method for black carbon analysis in ice and snow using the Single Particle Soot Photometer

I. A. Wendl^{1,2,3,*}, J. A. Menking^{4,*}, R. Färber⁵, M. Gysel⁵, S. D. Kaspari⁴, M. J. G. Laborde⁵, M. Schwikowski^{1,2,3}

¹Laboratory of Radiochemistry and Environmental Chemistry, Paul Scherrer Institut, 5232 Villigen PSI, Switzerland

²Oeschger Centre for Climate Change Research, University of Bern, Switzerland

³Department of Chemistry and Biochemistry, University of Bern, Switzerland

⁴Department of Geological Sciences, Central Washington University, Ellensburg, WA, USA

⁵Laboratory of Atmospheric Chemistry, Paul Scherrer Institut, 5232 Villigen PSI, Switzerland

*These authors contributed equally to this work

Published in Atmospheric Measurement Techniques

Abstract

In this study we attempt to optimize the method for measuring black carbon (BC) in snow and ice using a Single Particle Soot Photometer (SP2). Beside the previously applied ultrasonic (CETAC) and Collison-type nebulizers we introduce a jet (Apex Q) nebulizer to aerosolize the aqueous sample for SP2 analysis. Both CETAC and Apex Q require small sample volumes (a few milliliters) which makes them suitable for ice core analysis. The Apex Q shows the least size-dependent nebulizing efficiency in the BC particle diameter range of 100–1000 nm. The CETAC has the advantage that air and liquid flows can be monitored continuously. All nebulizer-types require a calibration with BC standards for the determination of the BC mass concentration in unknown aqueous samples. We found Aquadag to be a suitable material for preparing calibration standards. Further, we studied the influence of different treatments for fresh discrete snow and ice samples as well as the effect of storage. The results show that samples are best kept frozen until analysis. Once melted, they should be sonicated for 25 min, immediately analyzed while being stirred and not be refrozen.

3.1 Introduction

Light-absorbing impurities in snow and ice play an important role in the Earth's radiative balance and thus climate change. The main absorbers of visible solar radiation are atmospheric black carbon (BC) particles, emitted by incomplete combustion of biomass and fossil fuels. When deposited on snow or ice, BC lowers the albedo of the surface, leading to accelerated melt. Recently, Bond et al. (2013) reported a radiative forcing between 0.01 and 0.09 Wm⁻² for the snow albedo effect of BC. Furthermore, the efficacy of this forcing was found to be up to three times greater than the forcing by CO₂ (Flanner et al., 2007).

Traditionally, BC concentration in snow and ice has been analyzed by filter-based methods, such as optical or thermal–optical techniques (Clarke and Noone, 1985; Dou et al., 2012; Lavanchy et al., 1999). These methods require large sample volumes usually not available from ice cores. Ice cores offer a unique medium to study the variability of BC concentrations over long time periods, but analyses that require large sample volumes result in low time (or depth) resolution. Furthermore, the filter-based methods have the potential to over- or underestimate the BC mass concentration due to analytical artifacts, such as charring of organic carbon (Soto-García et al., 2011), dust interference (Wang et al., 2012) or filter efficiency (Torres et al., 2014).

The Single Particle Soot Photometer (SP2, Droplet Measurement Technology, Inc., Boulder, CO, USA; Schwarz et al., 2006) has been used in snow and ice research in a variety of studies (Bisiaux et al., 2012a, b; Kaspari et al., 2011; McConnell et al., 2007; Sterle et al., 2013). The SP2

does not require a filtration step, which makes it less time-consuming than the traditional methods and enables its use in a continuous flow analysis system. The SP2 analysis requires very little sample volume, which allows obtaining highly time-resolved data series, even from ice cores. However, the SP2 requires an aerosolization step because it analyzes only airborne samples. This step can be incorporated in a continuous flow system (McConnell et al., 2007) or in batch analysis (Ohata et al., 2011). The SP2 response is BC-specific and not affected by particle morphology or coatings (Cross et al., 2010; Laborde et al., 2012; Moteki and Kondo, 2007; Slowik et al., 2007), though there is a small positive artifact caused by high dust loadings (Schwarz et al., 2012), which are rarely found in ice cores. Furthermore, the SP2 returns the size distribution of BC particles in addition to their mass concentration. Mainly continuous flow systems have been used for measuring BC in ice, but the importance of discrete samples must not be underestimated because (1) poor ice core quality might make it impossible to cut undisturbed ice columns needed for continuous flow systems, (2) high dust content may cause clogging of the continuous melting system and (3) sonication of samples with high dust content, which helps to detach BC from the dust particle surfaces, is not easily performed with a continuous flow setup. Finally, snow sampling always results in discontinuous samples.

This study aims to provide SP2 users with a method for analyzing discrete liquid snow and ice samples. This includes the discussion of (1) the aerosolization of the aqueous samples focusing on (a) differences between the three nebulizer systems tested (ultrasonic (CETAC), jet (Apex Q) and Collison-type) and (b) the quantification of the nebulizer efficiency and BC losses in the system using aqueous BC reference standards; (2) the calibration of the SP2 for aqueous sample analysis; and (3) the best methods of sample treatment and sample storage.

Different terms are found in the literature for the most refractory and light-absorbing component of carbonaceous aerosols depending on the applied experimental method (e.g., black carbon (BC) or elemental carbon (EC)). In this study we applied an SP2, which utilizes laser-induced incandescence for quantitative measurements of refractory black carbon (rBC) in single particles, which we denote BC throughout this manuscript.

3.2 Experimental

In this section we describe the SP2-setup for analysis of aqueous samples (particularly snow and ice) with emphasis on the use of a nebulizer to transform BC particles from an aqueous sample into a dry aerosol and transport them to the SP2. Furthermore, we describe the internal calibration of the SP2 and the basic principle for determining the BC mass concentration of an unknown aqueous sample.

3.2.1 Nebulizer/SP2-setup

The SP2 is an instrument widely applied in aerosol science; it uses the principle of laser-induced incandescence to measure the mass concentration and size distribution of BC on a particle-by-particle basis. Individual BC particles are heated to their boiling point (~ 4200 K) by a continuous-wave Nd:YAG-laser. The peak intensity of the thermal radiation is proportional to the BC mass in the particle (Schwarz et al., 2006). The thermal radiation is detected with two photomultiplier tubes covering different wavelength ranges (broadband: ~ 350 – 800 nm; narrowband: ~ 630 – 800 nm). Each detector has two different electronic signal amplification gains (high and low). We run the broadband and narrowband detectors with staggered gains and combine the signals from the high-gain broadband output with the low-gain narrowband output in order to maximize the detectable BC mass (per particle) range. The band ratio, calculated from the ratio of the broadband to narrowband signals, depends on the boiling-point temperature and the spectral emissivity of the incandescent material, thus providing information to distinguish BC particles from, e.g., metal particles (Stephens et al., 2003). The calibration of the SP2 was conducted up to a mass of 70 fg BC. The measured calibration curve was linearly extrapolated to cover the full dynamic range of the incandescence detector (up to ~ 500 fg, which corresponds to a BC mass equivalent diameter of ~ 810 nm). Moteki and Kondo (2010) showed that the SP2 calibration curves can deviate from linearity for larger BC mass, depending on the effective density of the particles. In this study, no deviation from linearity was observed up to a BC mass of 70 fg BC and the doubly charged particles indicated that this still holds with little uncertainty up to 140 fg BC. Sensitivity analyses using an empirical power law calibration curve for the BC mass range above 100 fg, in a similar manner as applied by Schwarz et al. (2012), indicated deviations from the linear calibration approach well below the general calibration uncertainty of the SP2. This confirms that choosing a linear calibration curve is appropriate for this study. However, this would not necessarily hold, when a substantial fraction of the BC mass is detected at BC mass equivalent diameters above $1 \mu\text{m}$.

The BC analysis of aqueous samples with the SP2 requires a nebulizer to aerosolize and dry the liquid before it can be measured. Primarily Collison-type and ultrasonic nebulizers have been used with the SP2. Here, we also discuss a jet nebulizer system, the Apex Q (High Sensitivity Sample Introduction System, Elemental Scientific Inc., Omaha, NE, USA). The three systems not only vary in their nebulizing principle but also in their efficiencies, i.e., the fraction of water-insoluble particles of the injected liquid sample that is successfully nebulized and ends up in the aerosol provided at the outlet of the nebulizer. In the following we describe the three nebulizer/SP2-setups (Fig. A1).

3.2.1.1 Ultrasonic nebulizer (CETAC)

The ultrasonic nebulizer (U5000 AT, CETAC Technologies, Omaha, NE, USA), characterized by high efficiency and low sample consumption, has been used in several previous SP2 studies of BC in aqueous samples (Bisiaux et al., 2012a, b; Kaspari et al., 2011; McConnell et al., 2007; Ohata et al., 2011, 2013; Sterle et al., 2013). In the CETAC/SP2-setup (Fig. A1a), the aqueous sample is pumped (peristaltic pump, polyfluoroalkoxy-polymer (PFA) tubing) to a glass spray chamber where contact with an ultrasonic transducer causes the liquid containing the solid BC particles to become suspended as aerosol. A carrier gas (compressed air, BC-free) transports the aerosol through a heating and a cooling element, removing the liquid so that only dry particles are introduced into the SP2.

The primary benefit of the CETAC is that it allows the continuous monitoring of the maximally possible nebulizer efficiency (η_{\max} , Eq. S12, in the Supplement). This is accomplished by using flow monitors to measure the rate at which the sample is introduced into the nebulizer and the rate at which that sample drains from the aerosol chamber. This drainage includes sample that was not nebulized as well as sample that impacted on the glass walls of the aerosol chamber before reaching the drying chamber. Characterizing the nebulizer efficiency is necessary because the performance of the ultrasonic transducer may vary during use. However, potential particle losses ($\varepsilon_{\text{loss}}(D)$, Eq. S13, in the Supplement) cannot be quantified. Thus the CETAC has to be calibrated with a standard (hereafter referred to as external calibration as in Bisiaux et al., 2012b).

Experiments performed on the CETAC at Central Washington University (CWU), WA, USA, indicate that the optimal settings for BC analysis of snow and ice samples are 0.75 L min^{-1} purge airflow and 0.5 mL min^{-1} liquid-sample inflow. The aerosol is heated to 140°C and cooled to 3°C to remove the water. The operating temperatures are based on recommendations from the manufacturer and are restricted because of the need to fully dry the aerosol before introducing it into the SP2. Minor temperature adjustments ($140\text{-}160^\circ\text{C}$ heating, $1\text{-}3^\circ\text{C}$ cooling) did not result in significant changes in the BC concentrations ($C_{\text{SP2,low}}^\eta$, Eq. S32, in the Supplement) derived from SP2 measurements. Altering the airflow to higher and lower values resulted in 10–33% lower BC concentrations compared to normal flow. Similarly, sample inflows of 0.55 mL min^{-1} and higher caused steadily decreasing BC concentrations with up to 34% reduction. Changing these parameters may lead to inefficient nebulization of BC particles or to inefficient transport of BC particles to the SP2.

3 Optimized method for BC analysis

Repeated measurements of the same sample showed a standard deviation within 10% of the mean over time periods of days to weeks, though changes in the performance of the transducer over longer periods of months to years could lead to larger differences in BC concentration.

3.2.1.2 Jet nebulizer (Apex Q)

The Apex Q can be operated in self-aspirating mode, where the flow of the carrier gas (particle-free compressed air), the diameter and length of the capillary, and the geometry of the nebulizer nozzle define the liquid-sample flow. The aqueous sample is aerosolized into a heated (100°C) glass cyclonic spray chamber with a jet nebulizer. The aerosol is then cooled (2°C) in a Peltier-cooled multipass condenser to remove the remaining water vapor before being introduced into the SP2 (Elemental Scientific Inc., 2013).

The Apex Q as applied at the Paul Scherrer Institut (PSI), Switzerland, can be run with liquid-sample flows between 10 and 700 $\mu\text{L min}^{-1}$, requiring small sample volumes (see Sect. 3.1.2). The maximal nebulizer efficiency (η_{max} , Eq. S12, in the Supplement) is unknown for the Apex Q because most of the liquid not nebulized is evaporated from the heated spray chamber walls. Thus an external calibration is indispensable for quantitative liquid BC mass concentration determinations.

The optimal Apex Q/SP2-setup (Fig. A1b) includes an Apex Q PFA-ST MicroFlow nebulizer (ES-2040-7000) and a 1.5 m long PFA capillary with an inner diameter of 0.25 mm (ES-2042; both Elemental Scientific Inc., Omaha, NE, USA). The optimal purge airflow is 1 L min^{-1} , which for our MicroFlow nebulizer (serial no. Apex Q PFA-ST 1322) results in a liquid-sample inflow of 0.13 mL min^{-1} to the Apex Q, but may vary with time and nebulizer. Other settings and options, e.g., higher air inflow, use of a glass nebulizer and different diameters of tubing, did not result in higher BC concentrations and/or shorter measuring time even with higher sample consumption. The flow parameters of the Apex Q/SP2-setup are monitored manually and adjusted if necessary.

Repeated measurements of the same sample varied within one standard deviation of 15% of the mean, indicating the setup is stable.

3.2.1.3 Collision-type nebulizer

In the PSI Collision-type nebulizer, built in-house, a pressurized air stream that expands through a critical orifice causes the aqueous sample to be aspirated through a tube. The aqueous sample hits the air stream orthogonally and is sheared into droplets that are subsequently dried in a diffusion dryer and transported to the SP2 (Fig. A1c).

Collision-type systems can be built in-house which makes them inexpensive compared to other nebulizers. However, they have a high percentage of drain and thus, if no recirculation of the sample is performed, require relatively large sample volumes (>50 mL). Additionally, in the current design at PSI there is no control on how much sample is used because the sample is moved passively.

The Collision-type nebulizer built at PSI is run with an air pressure of 2.5 bar. The sample flow was not determined.

3.2.2 Internal Calibration

The SP2 needs empirical calibration to assign a BC mass to a given SP2 response, hereafter referred to as internal calibration. Unfortunately, the sensitivity of the SP2 differs substantially between different BC-types (Laborde et al., 2012; Moteki and Kondo, 2010). For atmospheric applications the SP2 is calibrated according to its sensitivity to BC that is typically found in ambient and diesel engine exhaust particles. This is commonly done with mass-selected fullerene soot or Aquadag (AQ) particles, applying appropriate scaling factors as recommended in Baumgardner et al. (2012). Two aspects are important for accurate quantification of BC mass in liquid samples. First, the SP2 must be calibrated according to its sensitivity to the BC-type under investigation. The BC-type contained in the aqueous BC standard may differ from that, e.g., in an ice core sample. Thus, it may be necessary to apply different SP2 calibration curves for the analysis of the BC standard and the ice core samples, so that the most suitable SP2 calibration is used for either BC-type. Second, it is important to account for potential non-BC matter in the SP2 calibration material in a consistent manner (see next section and Sects. S.4 and S.5 in the Supplement for details).

3.2.3 Approaches to determine the BC mass concentration of an aqueous sample

The nebulizer efficiency must be accounted for when determining the BC mass concentration in an aqueous sample via SP2 measurement of the nebulized aerosol. This can be done in two ways: (1) by determining the nebulizer efficiency or (2) by relating the measurement of the unknown sample to the measurement of an aqueous BC standard with known concentration (external calibration).

3.2.3.1 Using known nebulizer efficiency

If the overall nebulizer efficiency is known for all BC particle sizes, it is possible to directly infer the BC mass concentration in a liquid sample from the BC mass size distribution measured by the SP2 for the nebulized sample by using Eq. (S27) (in the Supplement). The only errors introduced with this approach arise from a potential SP2 calibration bias and missing BC mass

3 Optimized method for BC analysis

from particles with a BC mass outside the detection range of the SP2 (Eq. S28, in the Supplement). However, this approach has to our knowledge not been used so far as the nebulizer efficiency is typically not exactly known.

The overall nebulizer efficiency depends on the fraction of nebulized sample, the liquid and air flow rates as well as the BC particle losses in the system. An upper limit for the nebulizer efficiency η_{\max} can be calculated from the relevant flow rates (Eq. S12, in the Supplement), with the assumption that no BC particle losses occur. A lower limit for the BC mass concentration in the aqueous sample $C_{\text{SP2,low}}^{\eta}$ is then obtained with the following (Eq. S32, in the Supplement):

$$C_{\text{SP2,low}}^{\eta} = \frac{1}{\eta_{\max}} c_{\text{SP2}}, \quad (1)$$

where c_{SP2} is the BC mass concentration of the nebulized sample measured by the SP2. This approach has previously been applied by Kaspari et al. (2011). Based on analysis of aqueous BC standards, $C_{\text{SP2,low}}^{\eta}$ determined using the CETAC/SP2-setup at CWU underestimates BC concentration by at least 50% (see also Sect. S.3.2 in the Supplement). Using this method without external calibration is not advised.

3.2.3.2 Using external calibration

Commonly (Bisiaux et al., 2012a, b; Sterle et al., 2013), the nebulizer efficiency is implicitly accounted for by relating the SP2 measurement of a nebulized sample to that of an aqueous BC standard of known concentration. Two slightly different approaches can be chosen.

Approach 1

The nebulizer efficiency is assumed to remain stable between measurement of the sample and the standard. With this approach, the BC mass concentration in the aqueous sample under investigation $C_{\text{SP2}}^{\text{S1}}$ is calculated as follows (Eq. S35, in the Supplement):

$$C_{\text{SP2}}^{\text{S1}} := c_{\text{SP2}} \frac{C_{\text{liq}}^*}{c_{\text{SP2}}^*}, \quad (2)$$

where c_{SP2} and c_{SP2}^* are the BC mass concentrations measured by the SP2 for the aerosols from the nebulized aqueous sample and aqueous standard, respectively, and C_{liq}^* is the BC mass concentration of the aqueous standard.

This approach can be applied for any nebulizer with a stable efficiency, e.g., the Apex Q and the Collison-type. The inferred, C_{SP2}^{S1} , and true, C_{liq} , BC mass concentrations of the aqueous sample relate to each other as follows (Eq. S42 in the Supplement):

$$C_{SP2}^{S1} = C_{liq} \frac{f_{bias}}{f_{bias}^*} k_{S1}. \quad (3)$$

The result is biased if the sensitivity of the SP2 to the BC-types in the sample and/or standard is unknown; thus, the respective SP2 calibration bias factors f_{bias} and/or f_{bias}^* will be different from unity (see Eq. S16 in the Supplement for definition of f_{bias}). This restricts the choice of internal calibration standards to BC-types for which the SP2 sensitivity is known ($\Rightarrow f_{bias}^* = 1$). The factor f_{bias} only becomes unity if the sensitivity of the SP2 to the BC-type in the sample is known, therefore potentially leaving some uncertainty. Note that it does not matter whether the SP2's sensitivity is equal or different for the standard and sample nor does it have any influence on the resulting uncertainty of the method if appropriate calibration curves are chosen for the analysis of both measurements. The reason for this is that, in this approach, the measurement of the standard is solely used to quantify the efficiency of the nebulizer, while it is not used to quantify the sensitivity of the SP2.

The factor k_{S1} in Eq. (3) is given in Eq. (S43) (in the Supplement). It shows that additional errors can potentially be introduced due to the following two reasons: (1) if a substantial portion of the BC mass size distribution of the sample and/or the standard falls outside the detection range of the SP2 or (2) if the nebulizer efficiency depends on the size of the BC particles. The bias introduced by the latter only disappears if the nebulizer efficiency is independent of size or if the BC size distributions of the sample and standard have equal shape. The stronger the size-dependence of the nebulizer efficiency and the more different the size distribution shapes, the larger the bias introduced by the second reason (see Sect. S.2 in the Supplement for details).

This approach is applied to the Apex Q/SP2- and the Collison-type/SP2-setups at PSI.

Approach 2

Drifts of the liquid sample and/or air flow rates between the measurement of the standard and the sample will result in a drift of the nebulizer efficiency. If these flows are monitored, this can be accounted for by using the following equation to infer the BC mass concentration C_{SP2}^{S2} of the liquid sample (Eq. S37, in the Supplement):

3 Optimized method for BC analysis

$$C_{\text{SP2}}^{\text{S2}} := C_{\text{SP2,low}}^{\eta} \frac{C_{\text{liq}}^*}{C_{\text{SP2,low}}^{\eta,*}}, \quad (4)$$

where $C_{\text{SP2,low}}^{\eta}$ and $C_{\text{SP2,low}}^{\eta,*}$ are the lower limit of the BC mass concentration in the aqueous sample and standard, respectively, as inferred using Eq. (1).

This approach is applied for the CETAC/SP2-setups at CWU and PSI.

The approaches 1 and 2 are identical if the flow rates do not drift, and the caveats made for approach 1 regarding biases introduced by using an external calibration also apply to approach 2 (see also Eqs. S44 and S45 in the Supplement). The external calibration factor $C_{\text{liq}}^* / C_{\text{SP2,low}}^{\eta,*}$ for approach 2 (or $C_{\text{liq}}^* / c_{\text{SP2}}^*$ SP2 for approach 1) can be determined with a single measurement of a suitable standard. We determined this ratio from a series of measurements of different standards with concentrations in the range of $C_{\text{liq}}^* = 0.5$ to $\sim 14 \mu\text{g L}^{-1}$ (for details on the preparation, see Sect. 2.4.1). The results are given in Table 3.1, where the values correspond to the slope of the linear regression through the correlation of C_{liq}^* with $C_{\text{SP2,low}}^{\eta,*}$ for each standard, using the internal SP2 calibration as indicated in the column header.

Table 3.1 External calibration factor ($C_{\text{liq}}^* / C_{\text{SP2,low}}^{\eta,*}$) for the CETAC determined by using various BC-like materials. n.a. stands for not applicable.

	Linear fit of $C_{\text{liq}}^* / C_{\text{SP2,low}}^{\eta,*}$	Linear fit of $C_{\text{liq}}^* / C_{\text{SP2,low}}^{\eta,*}$
BC-like Material	(mean \pm 1 σ) internal calibration with AQ	(mean \pm 1 σ) internal calibration with fullerene soot
AQ	3.4 ± 0.7	n.a.
Aquablack	5.0 ± 2.4	3.0 ± 1.3
Cabojet	3.9 ± 0.6	2.2 ± 0.3
Flame soot	4.5 ± 0.5	2.3 ± 0.3
Fullerene soot	n.a.	2.0 ± 0.3

3.2.4 Standard preparation

3.2.4.1 BC standards

In order to determine uncertainties associated with using the external calibration approach and to identify the suitable materials as standard for external calibration we prepared standards with C_{liq}^* ranging from 0.5 to 14 $\mu\text{g L}^{-1}$ using different BC-like materials (AQ, Aquablack 162, Cabojet 200, flame soot and fullerene soot), similar to the procedure described below for AQ. The actual BC content of each material was considered in the calculation of the concentration: ~71% for AQ, 74% for Aquablack, 88% for Cabojet and 100% for fullerene (Gysel et al., 2011; S. Ohata, personal communication, 2013) and flame soot (T. Kirchstetter, personal communication, 2012) (Table B1).

AQ is an industrial lubricant consisting of a colloidal suspension of aggregates of graphitic carbon in water with $70.5\% \pm 1.0\%$ (1σ) BC content of the dry mass (76% in Gysel et al., 2011). The dry mass needs to be determined for each batch because the moisture content may vary between batches and AQ can dry over time.

We prepared a stock with a BC mass concentration of 2500 $\mu\text{g L}^{-1}$ in a 1 L glass volumetric flask. The standards were diluted by mass from this stock immediately prior to analysis. After sonicating the 2500 $\mu\text{g L}^{-1}$ stock for 20 min, we prepared a 100 $\mu\text{g L}^{-1}$ stock in a 50 mL polypropylene (PP) vial. Then we created standards of 0.5–14 $\mu\text{g L}^{-1}$ BC in individual 50 mL PP vials ($\geq 5 \mu\text{g L}^{-1}$ standard diluted from the 2500 $\mu\text{g L}^{-1}$ stock; $\leq 2 \mu\text{g L}^{-1}$ standard diluted from the 100 $\mu\text{g L}^{-1}$ stock).

3.2.4.2 Polystyrene latex sphere (PSL) standards

In order to investigate the size-dependence of the nebulizer efficiency (Sect. 3.1), we prepared standards of polystyrene latex spheres (PSL). We used PSLs with diameters of 100, 150, 269, 350, 450, 600, 800 and 1000 nm (Duke Scientific Corp., CA, USA) at PSI and diameters of 220, 356, 505, 771 and 1025 nm (Polyscience Inc., Warrington, PA, USA) at CWU. For a known PSL number concentration in water, we used the solid weight percentage determined by drying (on average $1.2\% \pm 0.2\%$ for the Duke PSLs) and provided by the manufacturer (7% for the Polyscience PSLs; Schwarz et al., 2012) and calculated the number concentrations according to Eq. (1) in Schwarz et al. (2012). These ranged from 2.65×10^6 to 2.48×10^9 particles cm^{-3} for the Duke PSL standards, which were diluted further (at least 1:5) for analysis with the CETAC and Apex Q/SP2-setups. The Polyscience PSLs ranged from 1.5×10^5 to 7.9×10^5 particles cm^{-3} .

3.2.4.3 Snow and ice samples

We used several snow and ice samples to monitor the stability of the setup and to test the optimal method on real samples. The so-called internal snow standards were prepared from fresh snow from Blewett Pass, WA, USA, and from Ewigschneefeld, Switzerland. A large amount of fresh snow was melted and kept in a glass bottle in the refrigerator ($\sim 5^{\circ}\text{C}$). The ice core samples used for testing the optimal method include two core segments from an ice core from Tsambagarav Glacier, Mongolian Altai, drilled at 4130 m a.s.l. in 2009, and two core segments from Lomonosovfonna, Svalbard, Norway, drilled at 1202 m a.s.l. in 2009. Those two ice cores are thought to represent the extremes in terms of mineral dust content with the Mongolian core being highly influenced by dust from the nearby deserts and the Svalbard core being remote from any large dust source. The dust content was estimated based on the average calcium concentration in the core segments.

3.3 Results and discussion

First, we compare the three different nebulizers tested regarding their nebulizer efficiency, which was previously indicated to be size-dependent (Ohata et al., 2013; Schwarz et al., 2012), followed by the differences in sample consumption. Second, we discuss the choice of a standard material for the external calibration. Third, we quantify the repeatability of the external calibration. Finally, we focus on (1) sample treatment, (2) sample storage and (3) recovery of BC in stored samples.

3.3.1 Nebulizer comparison

3.3.1.1 Size-dependence of the nebulizer efficiency

The nebulizer efficiencies for different particle sizes were determined by measuring the PSL standards of known number concentration described in Sect. 2.4.2 with the three nebulizer/SP2-setups (Eq. S5 in the Supplement). We extend previous studies (Ohata et al., 2013; Schwarz et al., 2012) by introducing a jet nebulizer and analyzing BC standards. At PSI all three nebulizer-types were tested, whereas only a CETAC was tested at CWU.

As illustrated in Fig. 3.1a the CETAC has a decreased efficiency not only in the large (>500 nm) (Schwarz et al., 2012) but also in the small size range (<200 – 250 nm), similar to findings by Ohata et al. (2013). The Collison-type nebulizer shows a decreased efficiency in the large size range, whereas the Apex Q gives a size-independent efficiency for the tested size range from 100 to 1000 nm within the variability of the whole setup (15%).

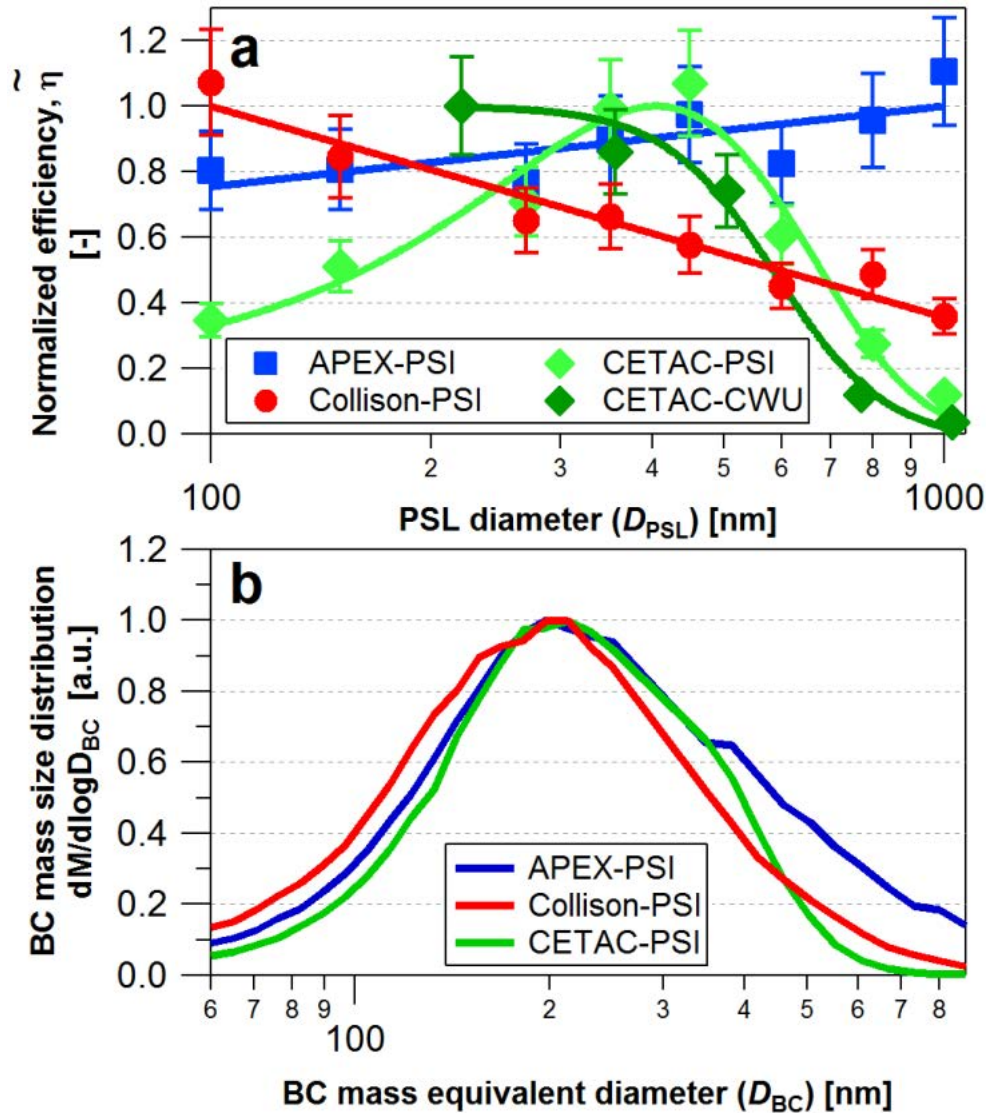


Figure 3.1 Comparison of the nebulizer efficiencies for the three different setups (CETAC, Apex Q and Collision-type nebulizer) for particle diameters from 100 to ~ 1000 nm. **(a)** Nebulizer efficiency for PSL standards of known number concentration; curves normalized to their maximum. **(b)** BC mass size distribution of polydisperse Aquadag as measured in the three setups; curves normalized to their maximum. a.u. stands for arbitrary units.

We further tested the three nebulizers in terms of behavior towards a commercially available BC standard, namely AQ. The BC mass size distribution of polydisperse AQ, normalized to the maximum, as measured with the three setups (Fig. 3.1b), shows that the Collision-type nebulizer skews the BC mass concentration towards smaller sizes, compared to the Apex Q with a size-independent efficiency, and the CETAC reduces the tails of the size distribution at either end. This indicates that the size-dependence of the nebulizer efficiencies determined for PSLs (Fig. 3.1a) also applies to AQ particles, at least qualitatively. Relating the shape of the AQ size distribution measured by the Collision-type nebulizer to that measured by the Apex Q allows

3 Optimized method for BC analysis

estimating the nebulizer efficiency of the Collison-type nebulizer for AQ as a function of BC mass equivalent diameter (Eq. S67 in the Supplement) and mobility diameter (Eq. S72 in the Supplement), making use of the weak size-dependence of the Apex Q nebulizer efficiency, which justifies the respective assumptions made in Eqs. (S66) and (S71) in the Supplement. Figure 3.2a shows that the efficiency of the Collison-type nebulizer for BC is equal to that for PSLs within the repeatability of this approach, whereas the relevant particle diameter that determines the losses for the BC particles is likely somewhere between the mass equivalent and the mobility diameter. Based on this finding it would be justified to use the nebulizer efficiency inferred from PSL measurements to quantify the BC mass concentration of an unknown sample by using the approach of Sect. 2.3.1.

The efficiency of the PSI-CETAC for BC was determined in the same manner. Figure 3.2b reveals that the nebulizer efficiency has the same shape and magnitude for BC and PSLs. However, there is a substantial and size-dependent shift in diameter both when using the mass equivalent or the mobility diameter for BC particles. This makes it difficult to impossible to accurately infer the efficiency for BC from that for PSLs. Thus, applying Eq. (S27) (in the Supplement) to quantify the BC mass concentration of an unknown sample would be associated with considerable uncertainty when using a nebulizer with a very strongly size-dependent efficiency such as the CETAC.

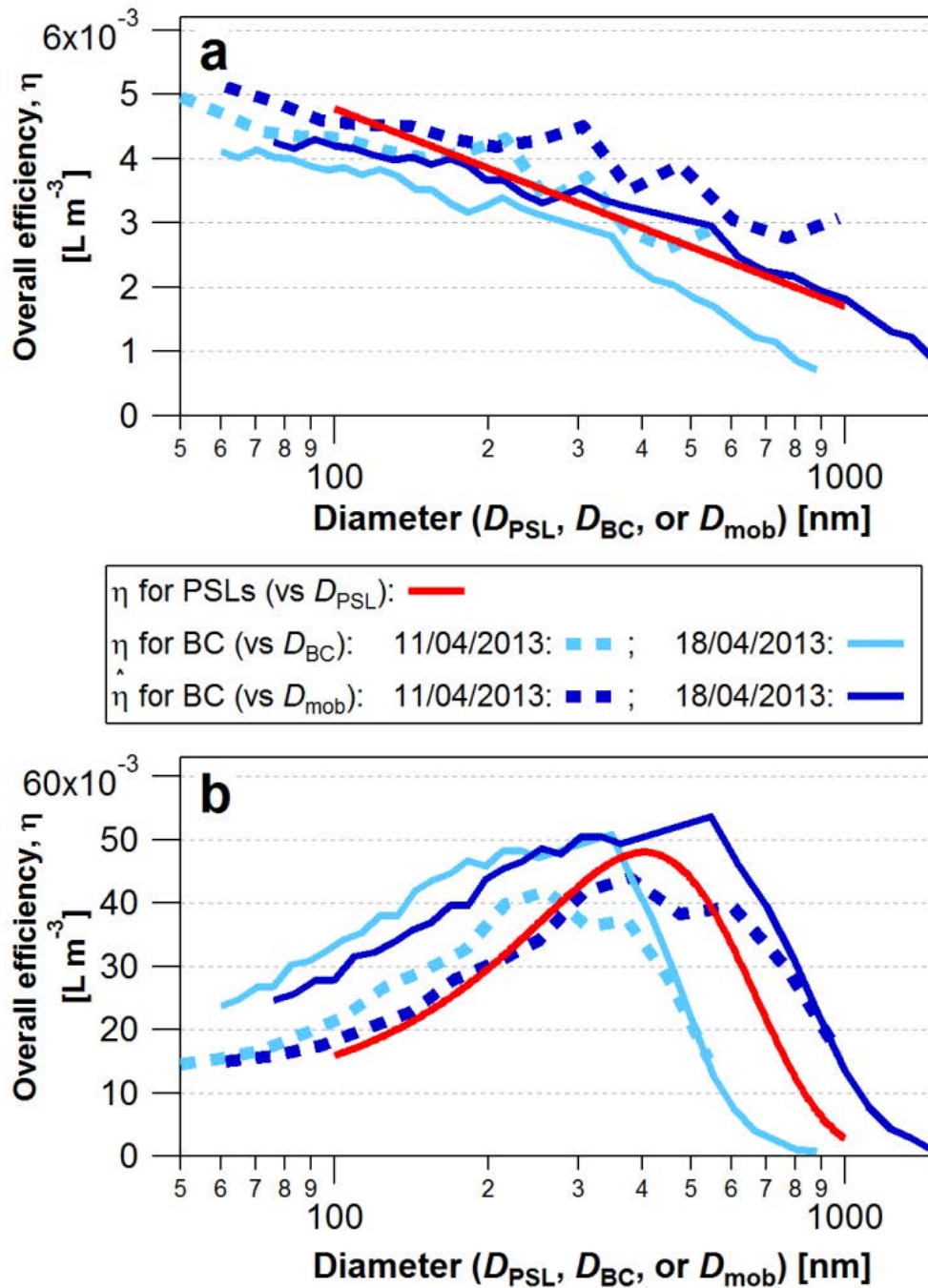


Figure 3.2 Overall nebulizer efficiency of **(a)** the Collision-type nebulizer and **(b)** the PSI-CETAC nebulizer for PSLs and polydisperse Aquadag (AQ) relative to that of the Apex Q on two different days. D_{PSL} represents PSL diameter; D_{BC} stands for BC mass equivalent diameter; D_{mob} is mobility diameter.

3.3.1.2 Sample consumption

Sample consumption is crucial, especially when working with ice cores of limited volume. The Collision-type nebulizer at PSI requires sample volumes >50 mL, whereas both the CETAC and Apex Q need relatively small sample volumes. In the case of our AQ standards this was <3 mL, which can be used as a guide value, although it may vary depending on whether the particle size distribution of the sample differs strongly from that of AQ.

Generally, the amount of sample volume required is determined by the recommendation to record $\sim 10\,000$ BC-containing particles (Schwarz et al., 2012) to ensure statistical precision of the measurement. We can only support this recommendation although it may take more than an hour to record 10 000 particles with the Apex Q. If this is not feasible with one sample in terms of available sample volume and measuring time, it is possible to combine adjacent samples at the expense of temporal resolution.

The comparison of the three nebulizers suggests the Apex Q to have the most size-independent nebulizing efficiency, making it the most suitable nebulizer for BC analysis of snow and ice samples using a nebulizer/SP2-setup. However, the nebulizing efficiency of the Apex Q has to be assumed to be constant, whereas with the CETAC it can be continuously monitored.

Later on in the paper, we exclude the Collision-type nebulizer from the discussion because its high sample consumption makes it unsuitable for the analysis of snow and ice samples.

3.3.2 Uncertainty of external calibration approach and choice of BC standard material

The standards of different BC-like materials (AQ, Aquablack 162, Cabojet 200, flame soot and fullerene soot; see Sect. 2.4.1 for preparation procedure) were analyzed with the CETAC/SP2-setup at CWU to determine the external calibration factor $C_{\text{liq}}^* / C_{\text{SP2,low}}^{\eta,*}$ for the second approach of external calibration (Sect. 2.3, Eq. 4), which accounts for flow rate drifts.

The sensitivity of the SP2 to the BC-type in Aquablack, Cabojet and flame soot is not known; therefore, cSP2 was determined with both AQ and fullerene soot internal calibration data (Sects. 2.2 and S.5 in the Supplement). Thus two columns with different $C_{\text{liq}}^* / C_{\text{SP2,low}}^{\eta,*}$ are given in Table 3.1. In the cases of AQ and fullerene soot only the AQ and fullerene soot internal calibration, respectively, were applied. The BC content of AQ (71% BC) was accounted for in the AQ internal calibration applied to obtain the values in the first data column of Table 3.1. The BC content was also accounted for in the calculation of C_{liq}^* for the AQ standards in order to treat it consistently (see Sect. S.4 in the Supplement). Fullerene soot standards were analyzed 1 year after the AQ, Aquablack, Cabojet and flame soot standards. AQ standards analyzed at the same time as fullerene soot indicated a shift with time in the losses ($\varepsilon_{\text{loss}}(D)$, Eq. S9 in the Supplement) occurring in the CETAC nebulizer. The $C_{\text{liq}}^* / C_{\text{SP2,low}}^{\eta,*}$ reported for fullerene soot in Table 3.1 is adjusted based on the shift of $C_{\text{liq}}^* / C_{\text{SP2,low}}^{\eta,*}$ of AQ analyzed during both experiments.

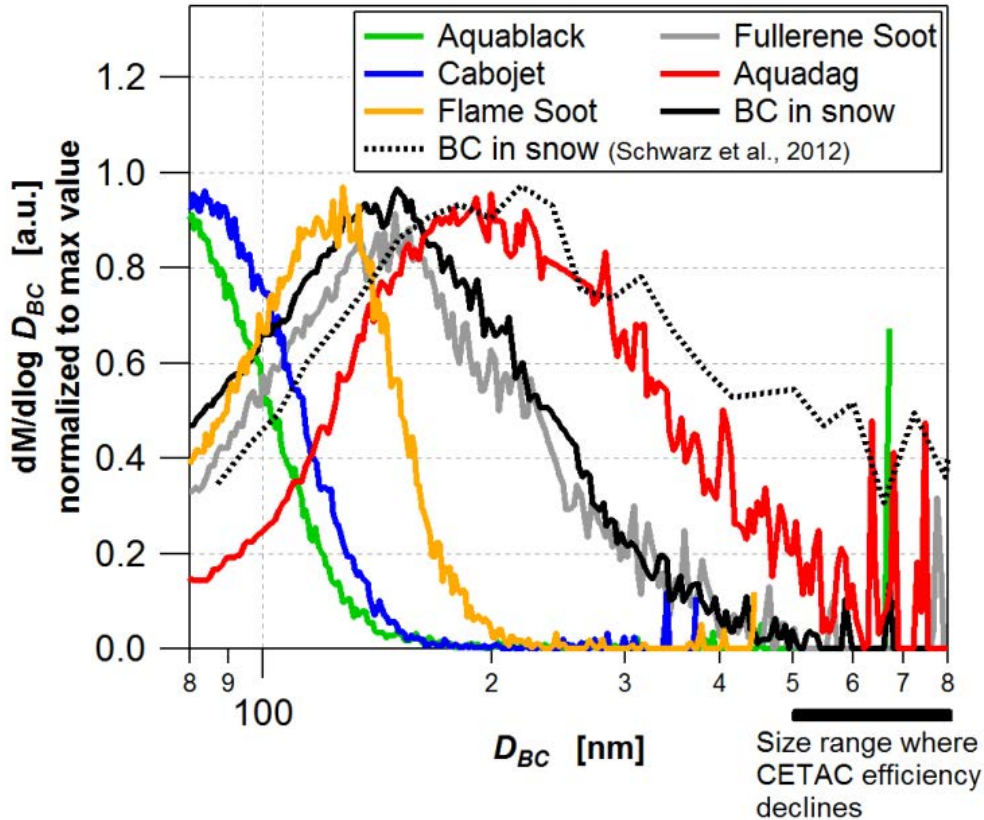


Figure 3.3 Average mass size distributions of various BC materials measured with the CETAC/SP2-setup at CWU – Aquadag, Cabojet 200, Aquablack 162, flame soot, fullerene soot and BC in snow (Blewett Pass, WA, USA). Large particles were allowed to settle out of the fullerene soot sample prior to measurement according to Schwarz et al. (2012). The curve from Schwarz et al. (2012) is added to illustrate the variability of the BC mass size distribution in snow. The lower limit of the horizontal axis is set at 80 nm because this is the lower limit of reliable internal calibration and detection efficiency of the SP2.

The values reported in Table 3.1 reveal that the external calibration factor of the CETAC determined with different standards spans a range of more than a factor of two. Consequently, the BC mass concentrations determined for an unknown aqueous BC sample by using the nebulizer/SP2-setup and the external calibration approach are potentially associated with large uncertainties. The reasons for this spread arise, e.g., from SP2 calibration uncertainties, detection range limitations of the SP2 and the size-dependence of nebulizer losses (quantified by k_{S2} / f_{bias}^* in Eq. (S44) (in the Supplement), which is essentially equal to Eq. 3). Uncertainties in standard preparation, i.e., in C_{liq}^* , also contribute though the exact share remains unknown without a method to independently determine the true C_{liq}^* .

The sensitivity of the SP2 to the BC-type in Aquablack, Cabojet and flame soot is unknown, introducing a difference of a factor of ~ 1.8 between possible external calibration values,

3 Optimized method for BC analysis

assuming that the extremes of SP2 sensitivity are represented by fullerene soot and that AQ accounted for the non- BC fraction. Therefore, Aquablack, Cabojet and flame soot are not recommended as calibration standard.

Even if the SP2 sensitivity was known, Aquablack and Cabojet would remain unsuitable for external calibration as ~50% or more of the BC mass is associated with BC core sizes below the lower detection limit of the SP2 (Fig. 3.3). This results in underestimation of $C_{SP2,low}^{\eta,*}$, overestimation of the external calibration factor and thus also the BC concentration that would be inferred for an unknown sample by using Eq. (4).

For both AQ and fullerene soot the SP2 sensitivity is known and the dominant fraction of their mass size distributions lies between the upper and lower detection limit of the SP2 in terms of BC core size. Despite this, the external calibration factor determined for the CETAC is ~70% smaller for the fullerene soot compared to the AQ standard. This difference is mainly caused by the strong size-dependence of the CETAC nebulizer efficiency with a sharp drop above ~500 nm. AQ has a larger contribution of bigger BC particles compared to fullerene soot (Fig. 3.3) and thus the external calibration factor shown in Table 3.1, which is essentially an inverted average of the nebulizer losses $\varepsilon_{loss}^*(D_{BC})$ integrated over all diameters with the shape of the BC mass size distribution of the standard as a weighting function (see Eq. S74 in the Supplement), becomes larger for AQ. This influence of the shape of the BC mass size distribution of the standard disappears for a nebulizer with a size-independent efficiency, such as the Apex Q, thereby strongly reducing the uncertainties associated with the external calibration approach. If a nebulizer with a strongly size-dependent efficiency, such as the CETAC, is used, it is important to choose a standard which best matches the shape of the BC mass size distribution of the sample, in order to minimize the uncertainties associated with size effects. This can sometimes be AQ and sometimes fullerene soot (Fig. 3.3). One advantage of AQ is that it does not exhibit any batch-to-batch variability of the corresponding internal SP2 calibration curves like fullerene soot does (Gysel et al., 2011; Laborde et al., 2012).

We chose AQ to prepare the aqueous BC standards because (1) its mass equivalent diameter distribution falls almost entirely into the detection range of the SP2 (~70–700 nm), (2) besides fullerene soot, AQ is the only standard which extends to BC diameters above ~200 nm as is expected in snow and ice samples (Fig. 3.3) and (3) it is easy to weigh, suspend and dilute.

3.3.3 Repeatability of external calibration

The external calibration of the nebulizer efficiency is crucial when quantifying the BC mass concentration in a liquid sample by measurement of BC in the nebulized aerosol. We

determined the repeatability of the external calibration by analyzing freshly prepared AQ standards from two different concentrated $2500 \mu\text{g L}^{-1}$ stocks over a period of 2 months, using both the CETAC/SP2- and Apex Q/SP2-setups. The reproducibility was within $\sim 19\%$. This includes the uncertainty in concentrations of the stock and the diluted standards and the uncertainty of the whole nebulizer/SP2-setup. These tests also revealed that the $2500 \mu\text{g L}^{-1}$ stocks remained stable over the whole 2 months, whereas the $100 \mu\text{g L}^{-1}$ stocks experienced significant BC losses within as little as 1 day. This demonstrates the need to prepare lower concentration stocks and standards immediately prior to analysis.

Importantly, the SP2 response to AQ scaled linearly with concentration for both systems. The external calibration factor $C_{\text{liq}}^* / C_{\text{SP2,low}}^{\eta,*}$ for approach 2, applied with the CETAC, was determined from the slope of the regression line through C_{liq}^* vs. $C_{\text{SP2,low}}^{\eta,*}$ each time a dilution series was measured (and likewise $C_{\text{liq}}^* / c_{\text{SP2}}^*$ for approach 1 with the Apex Q). These “averaged” external calibration factors of each dilution series varied in the 2 months by $\sim 22\%$ for the CETAC and by $\sim 8\%$ for the Apex Q. Additionally, environmental snow samples from Blewett Pass, WA, USA, and Ewigschneefeld, Switzerland, were used to track the stability of the CETAC/SP2-setup at CWU to identify whether day-to-day variations in the AQ external calibration factors were due to changes in nebulizer efficiency and/or SP2 response or errors in gravimetric AQ standard preparation. It is not known why the variability of AQ calibration curve slopes is higher for the CETAC than the Apex Q, but the liquid BC mass concentration of the environmental snow samples varied less than the AQ standards ($<9\%$, $2.56 \pm 0.21 \mu\text{g L}^{-1}$ for Blewett snow and $1.03 \pm 0.09 \mu\text{g L}^{-1}$ for Ewigschneefeld snow), indicating that some portion of the 22% calibration variability may be due to errors in AQ standard production rather than variability in the CETAC/SP2-setup. SP2 users are therefore advised to use a combination of AQ and environmental snow standards and perform a calibration at least once per week. For the Apex Q/SP2-setup a weekly calibration with AQ seems sufficient.

Blank values for the CETAC/SP2-setup are $0.01 \pm 0.0 \mu\text{g L}^{-1}$ for ultrapure water and $0.03 \pm 0.01 \mu\text{g L}^{-1}$ for ultrapure ice, prepared with the same cutting process as the ice core samples. The corresponding blanks for the Apex Q/SP2-setup are $0.07 \pm 0.07 \mu\text{g L}^{-1}$ and $0.10 \pm 0.01 \mu\text{g L}^{-1}$ for ultrapure ice.

The calibration factors discussed in this section are unique to each nebulizer/SP2-setup and may shift over time due to changes in the nebulizer efficiency. As such, the relationship between $C_{\text{SP2,low}}^{\eta}$ or c_{SP2} and C_{liq}^* must be monitored regularly. For nebulizers with a strongly size-

3 Optimized method for BC analysis

dependent efficiency such as the CETAC, it may be necessary to choose between different standard materials to match the BC size distribution of the samples under investigation as well as possible (see Sect. 3.2).

3.3.4 Sample treatment

3.3.4.1 Treatment of fresh samples

In order to optimize the BC analysis with the SP2 several methods of sample treatment were tested, keeping all other parameters, e.g., liquid and air flows as well as pressure, stable. The results shown are applicable to freshly melted or prepared discrete samples and may not be relevant for continuous flow systems. The gains or losses in signal reported below are always relative to the signal without treatment.

First, we tested different vial materials including glass, PFA, PP, Nalgene® -PP and high-density polyethylene (PEHD). Dilution series of the AQ standard were created in each type of material using the same material from the high-concentration stock to the lowest AQ standard ($0.5 \mu\text{g L}^{-1}$). Each stock was sonicated for 20 min before dilution. The diluted AQ standards were then sonicated again for 25 min directly prior to analysis. Both standard creation and analysis was done within 1 day. The different vial materials resulted in <10% variability. The CETAC did not nebulize liquids that had been sonicated in PFA vials. So far, we do not understand this effect. Maybe a change of surface tension of the sample in the PFA vial hinders the sample from being nebulized with the ultrasonic membrane.

Second, we investigated the effect of stirring AQ standards as well as snow and ice core samples during the measurement with a magnetic stir bar. Stirring is assumed to result in more representative sampling because it hampers settling. The ice core samples originate from Svalbard and Mongolia, and each location provided a sample with a high (92.9 and $425.9 \mu\text{g L}^{-1}$) and a low (24.5 and $157 \mu\text{g L}^{-1}$) calcium concentration, representing two extremes of mineral dust content. Nevertheless, the dust was not visible by eye in any sample. The results of agitating the samples were inconclusive, although previous results recommended the use of a stir bar, especially for samples with high dust loads (Kaspari et al., 2011). The effect of stirring might vary in the case of samples with even higher dust content.

Third, we tested the same samples for the effect of sonication prior to analysis by varying the sonication time from 0 to 50 min. Sonication can break down agglomerates which might cause interferences in the SP2. The results showed that 25 min sonication increases the BC mass concentration insignificantly ($\sim 5\% \pm 22\%$) and that sonication for different amounts of time gave inconclusive results.

Fourth, we examined the effect of a combination of stirring and sonication with the same samples as above. A $\sim 15\% \pm 21\%$ increase in the measured BC mass concentration indicates the optimal treatment to be the combination of sonication for 25 min and stirring.

Fifth, we investigated the effect of acidification of the samples to 0.5 M with 65% suprapur nitric acid (HNO_3) as proposed by Kaspari et al. (2011). This effect may depend on the sample composition, as indicated by varying results with AQ standards and snow and ice samples. Since precise sample composition is not known for snow or ice samples and acidification causes $\sim 22\% \pm 14\%$ lower measured BC mass concentrations, we do not advise acidification.

These results indicate that the vial material used for fresh samples may be chosen based on practicability. We use PP vials that are (1) easy to handle in the cold room, (2) large enough to hold the obtained ice samples, (3) lighter and safer in the field than glass and (4) low-cost, which is important especially if sampling at high resolution. Since all tests beside that of the sonication for different time periods include 25 min sonication (Kaspari et al. (2011) suggested 15 min), we recommend sonicating the samples for 25 min plus stirring of the samples with a magnetic stir bar during sample analysis.

3.3.4.2 Sample storage

Repeated measurements of previously melted snow samples indicate that the BC concentration of samples stored in the liquid phase are not stable over time. We assessed the stability of liquid samples and determined the most stable conditions for their storage prior to SP2 analysis. In some cases it might be desirable to measure the BC concentration of aqueous samples that have been previously melted, e.g., archived samples or samples from remote locations that melted during retrieval. Furthermore, it is preferable to store BC standards created in the liquid phase for repeat use if they remain stable.

Liquid suspensions of the BC-like materials AQ, Aquablack, Cabojet and flame soot as well as environmental snow samples were stored in PP and glass vials at 25 and 2°C. The liquid BC mass concentration of the samples was measured immediately after standard creation or melting of the snow, using the CETAC/SP2-setup. The concentrations were monitored for 18 days. Samples stored in glass vials at 2°C showed no significant losses, whereas samples stored in PP vials at 25°C showed the highest losses of 30–80 %. Samples stored in glass vials at 25°C and PP vials at 2°C experienced variable BC losses (0–20 %). These results were consistent for all BC reference materials as well as the snow samples (see Appendix C for data and details). We assume that BC losses in aqueous samples are due to particles adhering to vial walls or agglomerating to larger sizes outside of the SP2 detection range.

3 Optimized method for BC analysis

Melted ice core samples are often refrozen for preservation after the first measurement. Aqueous samples of snow were refrozen to see if this procedure affects BC stability during storage. Refreezing and thawing snow samples after the first melt resulted in BC losses of up to 60%. A second freeze–thaw cycle resulted in further losses of the same magnitude. Losses from refreezing may be due to the agglomeration of BC particles to larger sizes not entering the system or not being detected by the SP2 when the particles are rejected by the matrix of ice crystals (Schwarz et al., 2013). However, like Schwarz et al. (2012), we did not observe significant shifts in the mass size distribution of samples that underwent freeze–thaw cycles.

We also tested whether acidification affected sample stability during storage. We acidified snow samples and samples of AQ of ~ 4 , ~ 10 and $\sim 24 \mu\text{g L}^{-1}$ BC to 0.5 M using 65% suprapur HNO_3 immediately after melting (snow) or preparing (AQ) the samples. The BC concentration of each sample was measured directly after acidification and during the following 13 days. We found that acidification did not halt or slow BC losses when those samples were stored in the liquid phase. Additionally, acidification caused immediate losses of up to $\sim 35\%$ in all of our AQ samples.

Overall, we advise keeping snow and ice samples frozen until prior to BC analysis with the SP2. If this cannot be fulfilled, samples should be stored in glass vials at cold temperature ($\sim 2^\circ\text{C}$), though monitoring samples for longer than 18 days (multiple months) suggests that losses might still occur under these conditions (results not shown). Thus measurements of samples stored in the liquid phase may underestimate the actual BC mass concentration. Samples should further not be refrozen or acidified since these procedures lead to BC losses.

3.3.4.3 Recovery of BC in stored samples

We tested whether the BC mass concentration of samples could be recovered after undergoing losses in storage. Samples that had experienced BC losses during storage were treated with (1) acid (HNO_3) and (2) a dispersing agent (sodium pyrophosphate decahydrate). Kaspari et al. (2011) suggested acidifying samples in order to recover BC lost during refreezing, but our results do not support acidification. Sixteen samples were acidified to 0.5 M with 65% suprapur HNO_3 , of which six responded with between 10 and 100% recovery of the lost BC, and ten samples showed no recovery or further losses of 10–40%. We observed that all samples for which acidification caused some BC recovery were stored in PP vials, whereas samples stored in glass vials showed no recovery or even further losses. Since vial-type seems to affect the amount of BC that could be recovered after acidification, we suspect that the addition of HNO_3 helped to desorb BC from the walls of the PP vials. Schwarz et al. (2012) noted a shift towards smaller particle sizes after acidification and surmised that acid helped to break up agglomerated

particles. We did not observe any significant shift in the particle size distributions of samples after acidification. No distinct difference in BC recovery after acidification was evident based on different sample composition (AQ versus snow samples).

As in the case of fresh samples, we do not recommend acidification of stored samples or standards prior to BC analysis due to the variable effects of acidification on BC concentration seen in this study and the shift in particle size distribution observed by others (Schwarz et al., 2012). Similar to acid, treatment with the dispersing agent yielded varying results with BC recovery in some samples and further BC losses in others. Thus we do not recommend the use of a dispersing agent to treat fresh or stored samples.

3.4 Summary

We compared three different nebulizer/SP2-setups to optimize the method for measuring BC in discrete aqueous, namely snow and ice, samples using an SP2. Both the jet (Apex Q) and ultrasonic (CETAC) nebulizer were found to be suitable for ice core analysis because they require small sample volumes of a few milliliters, whereas the Collison-type requires more than 50mL sample. The nebulizing efficiency in the BC particle diameter range expected in snow and ice samples (100–1000 nm) is least size-dependent for the Apex Q. However, the air and liquid flows can only be monitored continuously with the CETAC. For all nebulizer-types we recommend an external calibration with BC standards for the determination of the BC mass concentration in unknown aqueous samples. The choice of the BC-like standard material is crucial since it was found to potentially introduce large uncertainties into the determination of the BC mass concentrations of an unknown aqueous BC sample. Aquablack, Cabojet and flame soot are not recommended as external calibration standards because the sensitivity of the SP2 to their BC-type is not known, thus introducing a difference of a factor of ~1.8 between possible external calibration values. Furthermore, ~50% or more of the BC mass in Aquablack and Cabojet is associated with BC core sizes below the lower detection limit of the SP2 which results in an overestimation of the BC concentration in the analyzed sample. The SP2 sensitivity to AQ and fullerene soot is known and their main mass is within the detection limits of the SP2. This implies that for a nebulizer with a size-independent efficiency such as the Apex Q either AQ or fullerene soot can be used for external calibration. If a nebulizer with a strongly size-dependent efficiency such as the CETAC is used, it is in some cases better to use AQ and in others better to use fullerene soot, depending on which standard best matches the shape of the BC mass size distribution of the sample. We chose AQ to prepare the aqueous BC standards because (1) it does not exhibit any batch-to-batch variability of the corresponding internal SP2 calibration

3 Optimized method for BC analysis

curves like fullerene soot does (Gysel et al., 2011; Laborde et al., 2012) and (2) it is easy to weigh, suspend and dilute.

We further investigated different treatments for fresh discrete snow and ice samples, the effect of sample storage and the best method to recover BC in stored samples. The samples can be kept in PP vials, which are easy to handle and are low-cost. Prior to analysis the samples should be sonicated for 25 min and then immediately be analyzed while being stirred with a magnetic stir bar. Acidification is not recommended. The samples should best stay frozen until just prior to analysis. If this cannot be fulfilled, the samples are best kept in glass vials at a cold temperature ($\sim 2^{\circ}\text{C}$), although this might lead to BC losses. Refreezing or acidifying samples that need to be stored should be avoided. Further, the recovery of BC in stored samples cannot be improved by the use of acid or a dispersing agent.

Appendix A: Instrumental setup

Figure A1 displays the instrumental setup of the three different nebulizer/SP2-systems.

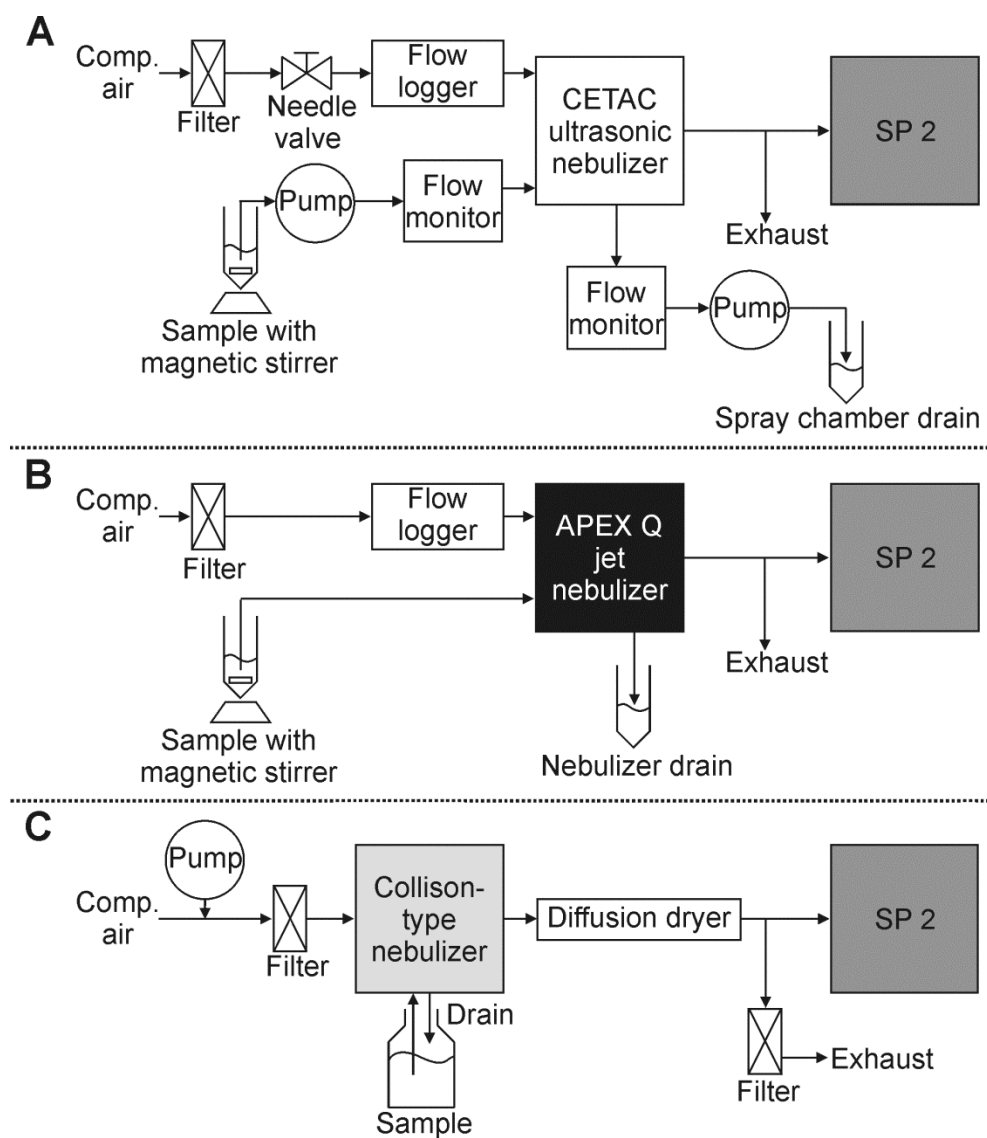


Figure A1. Instrumental setup for black carbon analysis of aqueous samples with the SP2: **(A)** ultrasonic (CETAC), **(B)** jet (Apex Q) and **(C)** Collison-type (PSI, built in-house) setup. Comp. air stands for compressed air.

Appendix B: BC standards

In Table B1 the various BC materials are given with their properties.

Table B1 Various BC materials mentioned in this manuscript.

Material and lot no. (if available)	Manufacturer and source	BC material	BC (EC) portion of solid mass	Source of BC content information	Confidence in BC portion
Aquadag no. N/A	Acheson Industries Inc, Port Huron, MI	Graphite	0.71*-0.76#	Sunset thermal-optical analyses # (Gysel et al, 2011; R. Subramanian, personal communication, 2013) *this study (PSI)	High due to multiple results from different laboratories
Aquablack 162 no. N/A	Tokai Carbon Co. Ltd., Tokyo, Japan	Carbon black	0.74	Sunset thermal-optical analysis, this study (CWU)	Low, due to large spread in data ($\sigma = 0.1$)
Cabojet 200 no. 1312497	Cabot Corp., Boston, USA	Carbon black	0.88	Sunset thermal-optical analysis, this study (CWU)	High, due to small spread in data ($\sigma = 0.01$)
Fullerene soot no. F12S011 (filtered)	Sigma-Aldrich Corp., St. Louis, MO, USA	Carbon black and fullerenes	1.0	(Gysel et al, 2011; S. Ohata, personal communication, 2013)	Not analyzed by thermal-optical
Flame soot	Lawrence-Berkeley National Laboratory (Kirchstetter and Novakov, 2007)	Flame-generated soot	1.0	(T. Kirchstetter, personal communication, 2012)	Not analyzed by thermal-optical

Appendix C: Sample storage

Here we present in greater detail the results of the storage experiments discussed in the main text. Note that these storage tests were conducted with the CETAC/SP2-setup, so were subject to the nebulizer efficiency issues described in Sect. 3.1.1.

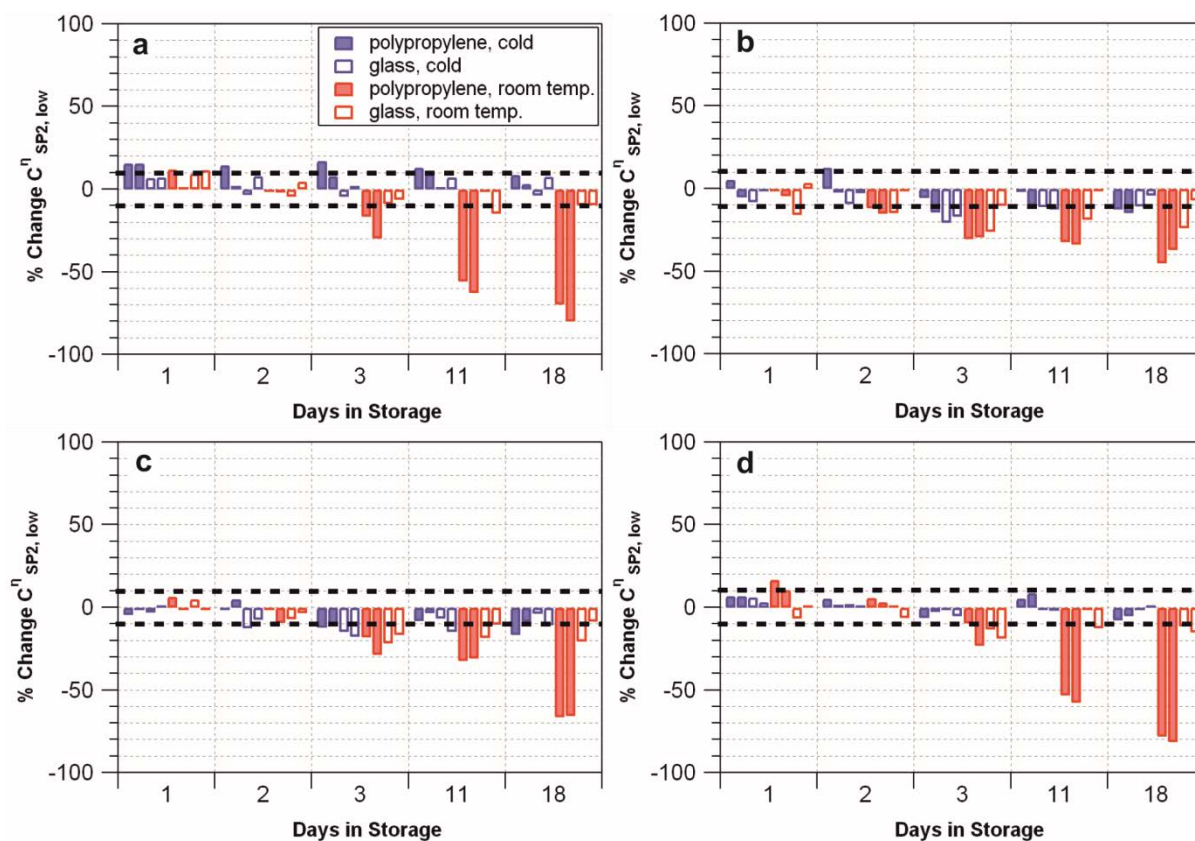


Figure C1 BC concentrations in (a) environmental snow, (b) AQ $\sim 15 \mu\text{g L}^{-1}$, (c) AQ $\sim 10 \mu\text{g L}^{-1}$ and (d) AQ $\sim 3 \mu\text{g L}^{-1}$ samples tracked for 18 days in various storage conditions. The bars express the BC concentration on a given day as a percentage of the original BC concentration (before any losses due to storage; not shown). Each bar represents one sample. Black dotted lines indicate the repeatability of the SP2, assuming no sample changes.

Samples were stored in polypropylene (PP) and glass vials at 25 and 2°C and monitored over time. Teflon vials were not used in the experiment because samples stored in Teflon vials did not nebulize properly after sonication. Sample stability for AQ and environmental snow samples over an 18-day period suggests that storing samples at 25°C in PP vials results in substantial BC losses compared to storage in glass vials or storage at a cold temperature (Fig. C1). Samples stored in glass vials at cold temperatures remained near stable for 18 days.

In addition, these experiments indicate that the magnitude of BC losses in storage may be related to sample concentration. After 18 days, AQ samples stored in PP vials at 25°C showed 80,

3 Optimized method for BC analysis

65 and 40% losses for low-concentration ($\sim 2 \mu\text{g L}^{-1}$), medium-concentration ($\sim 8 \mu\text{g L}^{-1}$) and high-concentration ($\sim 14 \mu\text{g L}^{-1}$) samples, respectively (Fig. C1). This result would imply that the magnitude of losses is higher for low-concentration samples compared to high-concentration samples, but we caution that the total BC mass lost in the low-concentration samples ($\sim 1 \mu\text{g L}^{-1}$ equivalent) is less than the mass of BC lost in the medium- and high-concentration samples ($\sim 3 \mu\text{g L}^{-1}$ equivalent). It seems that while BC losses may be proportionally higher for low-concentration samples, total BC mass lost in storage is greater in samples that are more concentrated. This would imply that relative differences between samples may appear smaller than they actually are if the samples have undergone BC losses in storage.

Acknowledgements

The authors would like to thank J. P. Schwarz for providing a batch of fullerene soot and PSLs from Polyscience Inc., Warrington, PA, USA, and T. Kirchstetter for providing a batch of flame soot.

Supplementary Material

The supplementary material contains all the equations and details for the calculations.

References

- Baumgardner, D., Popovicheva, O., Allan, J., Bernardoni, V., Cao, J., Cavalli, F., Cozic, J., Diapouli, E., Eleftheriadis, K., Genberg, P. J., Gonzalez, C., Gysel, M., John, A., Kirchstetter, T.W., Kuhlbusch, T. A. J., Laborde, M., Lack, D., Müller, T., Niessner, R., Petzold, A., Piazzalunga, A., Putaud, J. P., Schwarz, J., Sheridan, P., Subramanian, R., Swietlicki, E., Valli, G., Vecchi, R., and Viana, M.: Soot reference materials for instrument calibration and intercomparisons: a workshop summary with recommendations, *Atmospheric Measurement Techniques*, 5, 1869–1887, doi:10.5194/amt-5-1869-2012, 2012.
- Bisiaux, M. M., Edwards, R., McConnell, J. R., Albert, M. R., Anschütz, H., Neumann, T. A., Isaksson, E., and Penner, J. E.: Variability of black carbon deposition to the East Antarctic Plateau, 1800–2000 AD, *Atmospheric Chemistry and Physics*, 12, 3799–3808, doi:10.5194/acp-12-3799-2012, 2012a.
- Bisiaux, M. M., Edwards, R., McConnell, J. R., Curran, M. A. J., Van Ommen, T. D., Smith, A. M., Neumann, T. A., Pasteris, D. R., Penner, J. E., and Taylor, K.: Changes in black carbon deposition to Antarctica from two high-resolution ice core records, 1850–2000 AD, *Atmospheric Chemistry and Physics*, 12, 4107–4115, doi:10.5194/acp-12-4107-2012, 2012b.
- Bond, T. C., Doherty, S. J., Fahey, D. W., Forster, P. M., Berntsen, T., DeAngelo, B. J., Flanner, M. G., Ghan, S., Kärcher, B., Koch, D., Kinne, S., Kondo, Y., Quinn, P. K., Sarofim, M. C., Schultz, M. G., Schulz, M., Venkataraman, C., Zhang, H., Zhang, S., Bellouin, N., Guttikunda, S. K., Hopke, P. K., Jacobson, M. Z., Kaiser, J. W., Klimont, Z., Lohmann, U., Schwarz, J. P., Shindell, D., Storelvmo, T., Warren, S. G., and Zender, C. S.: Bounding the role of black carbon in the climate system: A scientific assessment, *Journal of Geophysical Research-Atmospheres*, 118, 5380–5552, doi:10.1002/jgrd.50171, 2013.
- Clarke, A. D. and Noone, K. J.: Soot in the Arctic snowpack: A cause for perturbations in radiative transfer, *Atmospheric Environment*, 1967, 19, 2045–2053, 1985.
- Cross, E. S., Onasch, T. B., Ahern, A., Wrobel, W., Slowik, J. G., Olfert, J., Lack, D. A., Massoli, P., Cappa, C. D., Schwarz, J. P., Spackman, J. R., Fahey, D. W., Sedlacek, A., Trimborn, A., Jayne, J. T., Freedman, A., Williams, L. R., Ng, N. L., Mazzoleni, C., Dubey, M., Brem, B., Kok, G., Subramanian, R., Freitag, S., Clarke, A., Thornhill, D., Marr, L. C., Kolb, C. E., Worsnop, D. R., and Davidovits, P.: Soot particle studies – instrument intercomparison – project overview, *Aerosol Science & Technology*, 44, 592–611, 2010.
- Dou, T., Xiao, C., Shindell, D. T., Liu, J., Eleftheriadis, K., Ming, J., and Qin, D.: The distribution of snow black carbon observed in the Arctic and compared to the GISS-PUCCINI model, *Atmospheric Chemistry and Physics*, 12, 7995–8007, doi:10.5194/acp-12-7995-2012, 2012.
- Elemental Scientific Inc.: Apex Q High Sensitivity Sample Introduction System, Product Overview, available at: <http://www.icpms.com/pdf/ApexQ-ESI.pdf>, last access: 10 December, 2013.
- Flanner, M. G., Zender, C. S., Randerson, J. T., and Rasch, P. J.: Present-day climate forcing and response from black carbon in snow, *Journal of Geophysical Research-Atmospheres*, 112, D11202, doi:10.1029/2006JD008003, 2007.

3 Optimized method for BC analysis

Gysel, M., Laborde, M., Olfert, J. S., Subramanian, R., and Gröhn, A. J.: Effective density of Aquadag and fullerene soot black carbon reference materials used for SP2 calibration, *Atmospheric Measurement Techniques*, 4, 2851–2858, doi:10.5194/amt-4-2851-2011, 2011.

Kaspari, S. D., Schwikowski, M., Gysel, M., Flanner, M. G., Kang, S., Hou, S., and Mayewski, P. A.: Recent increase in black carbon concentrations from a Mt. Everest ice core spanning 1860–2000 AD, *Geophysical Research Letters*, 38, L04703, doi:10.1029/2010GL046096, 2011.

Kirchstetter, T. W. and Novakov, T.: Controlled generation of black carbon particles from a diffusion flame and applications in evaluating black carbon measurement methods, *Atmospheric Environment*, 41, 1874–1888, 2007.

Laborde, M., Mertes, P., Zieger, P., Dommen, J., Baltensperger, U., and Gysel, M.: Sensitivity of the Single Particle Soot Photometer to different black carbon types, *Atmospheric Measurement Techniques*, 5, 1031–1043, doi:10.5194/amt-5-1031-2012, 2012.

Lavanchy, V. M. H., Gäggeler, H. W., Schotterer, U., Schwikowski, M., and Baltensperger, U.: Historical record of carbonaceous particle concentrations from a European high-alpine glacier (Colle Gnifetti, Switzerland), *Journal of Geophysical Research*, 104, 21227–21236, 1999.

McConnell, J. R., Edwards, R., Kok, G. L., Flanner, M. G., Zender, C. S., Saltzman, E. S., Banta, J. R., Pasteris, D. R., Carter, M. M., and Kahl, J. D. W.: 20th-century industrial black carbon emissions altered Arctic climate forcing, *Science*, 317, 1381–1384, doi:10.1126/science.1144856, 2007.

Moteki, N. and Kondo, Y.: Effects of mixing state on black carbon measurements by laser-induced incandescence, *Aerosol Science & Technology*, 41, 398–417, 2007.

Moteki, N. and Kondo, Y.: Dependence of laser-induced incandescence on physical properties of black carbon aerosols: Measurements and theoretical interpretation, *Aerosol Science & Technology*, 44, 663–675, 2010.

Ohata, S., Moteki, N., and Kondo, Y.: Evaluation of a method for measurement of the concentration and size distribution of black carbon particles suspended in rainwater, *Aerosol Science & Technology*, 45, 1326–1336, doi:10.1080/02786826.2011.593590, 2011.

Ohata, S., Moteki, N., Schwarz, J., Fahey, D., and Kondo, Y.: Evaluation of a method to measure black carbon particles suspended in rainwater and snow Samples, *Aerosol Science & Technology*, 47, 1073–1082, doi:10.1080/02786826.2013.824067, 2013.

Schwarz, J. P., Gao, R. S., Fahey, D. W., Thomson, D. S., Watts, L. A., Wilson, J. C., Reeves, J. M., Darbeheshti, M., Baumgardner, D. G., Kok, G. L., Chung, S. H., Schulz, M., Hendricks, J., Lauer, A., Kärcher, B., Slowik, J. G., Rosenlof, K. H., Thompson, T. L., Langford, A. O., Loewenstein, M., and Aikin, K. C.: Single-particle measurements of midlatitude black carbon and light-scattering aerosols from the boundary layer to the lower stratosphere, *Journal of Geophysical Research*, 111, D16207, doi:10.1029/2006JD007076, 2006.

Schwarz, J. P., Doherty, S. J., Li, F., Ruggiero, S. T., Tanner, C. E., Perring, A. E., Gao, R. S., and Fahey, D. W.: Assessing Single Particle Soot Photometer and Integrating Sphere/Integrating Sandwich Spectrophotometer measurement techniques for quantifying black carbon concentration in

snow, *Atmospheric Measurement Techniques*, 5, 2581–2592, doi:10.5194/amt-5-2581-2012, 2012.

Schwarz, J. P., Gao, R. S., Perring, A. E., Spackman, J. R., and Fahey, D. W.: Black carbon aerosol size in snow, *Scientific Reports* 3: 1356, doi:10.1038/srep01356, 2013.

Slowik, J. G., Cross, E. S., Han, J. H., Davidovits, P., Onasch, T. B., Jayne, J. T., Williams, L. R., Canagaratna, M. R., Worsnop, D. R., Chakrabarty, R. K., Moosmüller, H., Arnott, W. P., Schwarz, J. P., Gao, R.-S., Fahey, D. W., Kok, G. L., and Petzold, A.: An inter-comparison of instruments measuring black carbon content of soot particles, *Aerosol Science & Technology*, 41, 295–314, 2007.

Soto-García, L. L., Andreae, M. O., Andreae, T. W., Artaxo, P., Maenhaut, W., Kirchstetter, T., Novakov, T., Chow, J. C., and Mayol-Bracero, O. L.: Evaluation of the carbon content of aerosols from the burning of biomass in the Brazilian Amazon using thermal, optical and thermal-optical analysis methods, *Atmospheric Chemistry and Physics*, 11, 4425–4444, doi:10.5194/acp-11-4425-2011, 2011.

Stephens, M., Turner, N., and Sandberg, J.: Particle identification by laser-induced incandescence in a solid-state laser cavity, *Applied Optics*, 42, 3726–3736, 2003.

Sterle, K. M., McConnell, J. R., Dozier, J., Edwards, R., and Flanner, M. G.: Retention and radiative forcing of black carbon in eastern Sierra Nevada snow, *The Cryosphere*, 7, 365–374, doi:10.5194/tc-7-365-2013, 2013.

Torres, A., Bond, T. C., Lehmann, C. M. B., Subramanian, R., and Hadley, O. L.: Measuring organic carbon and black carbon in rainwater: evaluation of methods, *Aerosol Science & Technology*, 15, 239–250, doi:10.1080/02786826.2013.868596, 2014.

Wang, M., Xu, B., Zhao, H., Cao, J., Joswiak, D., Wu, G., and Lin, S.: The influence of dust on quantitative measurements of black carbon in ice and snow when using a thermal optical method, *Aerosol Science & Technology*, 46, 60–69, 2012.

Supplementary Material

Equations and details for the calculations

Acronyms:

LDL: Lower detection limit

PSL: Polystyrene size standards

UDL: Upper detection limit

Table S3-1 Symbols.

Symbol	Description	Unit
D	General symbol for particle diameter. Suffixes are used to specify the particular diameter type where needed (e.g. BC mass equivalent diameter, PSL diameter or mobility diameter)	μm
D_{BC}	BC mass equivalent diameter	μm
$D_{\text{BC,min}}, D_{\text{BC,min}}^*$	Minimal mass equivalent diameter of the BC cores in an aqueous sample (*standard)	μm
$D_{\text{BC,max}}, D_{\text{BC,max}}^*$	Maximal mass equivalent diameter of the BC cores in an aqueous sample (*standard)	μm
$D_{\text{BC,LDL}}$	Lower cut-off diameter of the SP2 measurement in terms of BC core mass equivalent diameter ($D_{\text{BC,LDL}}^*$ is assumed to be equal to $D_{\text{BC,LDL}}$)	μm
$D_{\text{BC,UDL}}$	Upper cut-off diameter of the SP2 measurement in terms of BC core mass equivalent diameter ($D_{\text{BC,UDL}}^*$ is assumed to be equal to $D_{\text{BC,UDL}}$)	μm
$D_{\text{BC,ref}}$	Reference BC mass equivalent diameter for calculating the reference nebulizer efficiency, $\eta_{\text{BC,ref}}$, for BC	μm
D_{PSL}	(Nominal) PSL diameter	μm
$D_{\text{PSL,ref}}$	Reference PSL diameter for calculating the reference nebulizer efficiency, $\eta_{\text{PSL,ref}}$, for PSLs	μm

D_{mob}	Mobility diameter of a BC core	μm
$f_{\text{bias}}, f_{\text{bias}}^*$	SP2 calibration bias for the BC type of an aqueous sample (*standard) expressed as a factor.	-
g_{mob2mev}	Diameter conversion function that calculates the mass equivalent diameter of a BC core from its mobility diameter. This conversion function depends on the BC particle type and is only defined for BC types with a fixed mobility diameter to mass relationship.	n.a.
$C_{\text{liq}}, C_{\text{liq}}^*$	BC mass concentration of an aqueous sample (*standard)	$\mu\text{g L}^{-1}$
$M_{\text{liq}}, M_{\text{liq}}^*$	Mass concentration of water-insoluble particulate matter in an aqueous sample (* standard)	$\mu\text{g L}^{-1}$
γ_{BC}^*	BC mass fraction in dried particles of a BC material that is used to prepare aqueous standard suspensions.	-
$c_{\text{air}}, c_{\text{air}}^*$	BC mass concentration of the aerosol from a nebulized aqueous sample (*standard)	$\mu\text{g m}^{-3}$
$c_{\text{SP2}}, c_{\text{SP2}}^*$	BC mass concentration of the aerosol as inferred from the SP2 measurement of a nebulized aqueous sample (*standard)	$\mu\text{g m}^{-3}$
$C_{\text{SP2}}^x, C_{\text{SP2}}^{x,*}$	BC mass concentration in an aqueous sample (*standard) inferred from the SP2 measurement of the nebulized sample (with accounting for the absolute overall nebulizer efficiency). Note, the superscript “x” is a placeholder for indicating the approach that is used to calculate C_{SP2} . “x” can be S1, S2, S η	$\mu\text{g L}^{-1}$
$C_{\text{SP2,low}}^\eta, C_{\text{SP2,low}}^{\eta,*}$	Lower limit of the BC mass concentration in an aqueous sample (*standard) inferred from the SP2 measurement of the nebulized sample (calculated by using the upper limit for the overall nebulizer efficiency)	$\mu\text{g L}^{-1}$
$\frac{dC_{\text{liq}}}{d \log D_{\text{BC}}}(D_{\text{BC}}),$ $\frac{dC_{\text{liq}}^*}{d \log D_{\text{BC}}}(D_{\text{BC}})$	BC mass size distribution of an aqueous sample (*standard)	$\mu\text{g L}^{-1}$
$\frac{d\tilde{C}_{\text{liq}}}{d \log D_{\text{BC}}}(D_{\text{BC}}),$	Normalized BC mass size distribution of an aqueous sample (*standard)	-

3 Optimized method for BC analysis

$\frac{d\tilde{C}_{\text{liq}}^*}{d \log D_{\text{BC}}}(D_{\text{BC}})$		
$\frac{dc_{\text{air}}}{d \log D_{\text{BC}}}(D_{\text{BC}})$,	BC mass size distribution of the aerosol from a nebulized aqueous sample (*standard)	$\mu\text{g m}^{-3}$
$\frac{dc_{\text{air}}^*}{d \log D_{\text{BC}}}(D_{\text{BC}})$		
$\frac{dc_{\text{SP2}}}{d \log D_{\text{BC}}}(D_{\text{BC}})$,	BC mass size distribution measured by the SP2 for a nebulized aqueous sample (*standard)	$\mu\text{g m}^{-3}$
$\frac{dc_{\text{SP2}}^*}{d \log D_{\text{BC}}}(D_{\text{BC}})$		
$\frac{dC_{\text{SP2}}^\eta}{d \log D_{\text{BC}}}(D_{\text{BC}})$,	BC mass size distribution of an aqueous sample (*standard) inferred from the SP2 measurement of the nebulized sample (with accounting for the nebulizer efficiency)	$\mu\text{g L}^{-1}$
$\frac{dC_{\text{SP2}}^{\eta,*}}{d \log D_{\text{BC}}}(D_{\text{BC}})$		
$\Delta\tilde{C}_{\text{LDL}}, \Delta\tilde{C}_{\text{LDL}}^*$	Relative contribution to the total BC mass in an aqueous sample (*standard) from BC cores with sizes below the LDL of the SP2	-
$\Delta\tilde{C}_{\text{UDL}}, \Delta\tilde{C}_{\text{UDL}}^*$	Relative contribution to the total BC mass in an aqueous sample (*standard) from BC cores with sizes above the UDL of the SP2	-
$\eta(D), \eta^*(D)$	Overall nebulizer efficiency for insoluble particles as a function of the particle diameter during the measurement of a sample (*standard)	L m^{-3}
$\eta_{\text{max}}, \eta_{\text{max}}^*$	Maximum possible overall efficiency of a nebulizer during the measurement of an aqueous sample (*standard)	L m^{-3}
$\eta_{\text{BC}}(D_{\text{BC}})$,	Overall nebulizer efficiency for BC as a function of BC mass equivalent diameter during the measurement of an aqueous sample (*standard)	L m^{-3}
$\eta_{\text{BC}}^*(D_{\text{BC}})$		
$\eta_{\text{BC,ref}}, \eta_{\text{BC,ref}}^*$	Reference nebulizer efficiency for BC at the reference BC mass equivalent diameter D_{ref} during the measurement of an aqueous sample (*standard)	L m^{-3}
$\tilde{\eta}_{\text{BC}}(D_{\text{BC}})$,	Normalized overall nebulizer efficiency for BC as a function of BC mass equivalent diameter (*standard)	-
$\tilde{\eta}_{\text{BC}}^*(D_{\text{BC}})$		

$\hat{\eta}_{BC}(D_{mob})$	Overall nebulizer efficiency for BC as a function of the mobility diameter of the BC core.	-
$\eta_{PSL}(D_{PSL})$	Overall nebulizer efficiency for PSLs as a function of PSL diameter	L m ⁻³
$\eta_{PSL,ref}$	Reference nebulizer efficiency for PSLs at the reference PSL diameter $D_{PSL,ref}$	L m ⁻³
$\tilde{\eta}_{PSL}(D_{PSL})$	Normalized overall nebulizer efficiency for PSLs as a function of PSL diameter	-
$N_{liq,PSL}(D_{PSL})$	Number concentration of PSLs with nominal diameter D_{PSL} in an aqueous standard	L ⁻¹
$n_{air,PSL}(D_{PSL})$	Number concentration of PSLs with nominal diameter D_{PSL} in the aerosol from a nebulized aqueous standard	cm ⁻³
$\varepsilon_{drop}, \varepsilon_{drop}^*$	Fraction of the supplied aqueous sample that is transformed into droplets and successfully transferred towards the aerosol sample outlet of the nebulizer during the measurement of an aqueous sample (*standard)	-
$\varepsilon_{loss}(D)$, $\varepsilon_{loss}^*(D)$	Size-dependent factor accounting for all kind of losses during the measurement of a sample (*standard) in the complete nebulizer unit including everything between the sample vial and the SP2 inlet	-
$q_{air,supply}, q_{air,supply}^*$	Air flow rate at the purge air inlet of the nebulizer during the measurement of an aqueous sample (*standard)	L min ⁻¹
$q_{air,aerosol}, q_{air,aerosol}^*$	Air flow rate of the aerosol outlet of the nebulizer during the measurement of an aqueous sample (*standard)	L min ⁻¹
$q_{air,drain}, q_{air,drain}^*$	Air flow rate through the drain channel from the nebulizer chamber during the measurement of an aqueous sample (*standard)	L min ⁻¹
$Q_{liq,supply}, Q_{liq,supply}^*$	Flow rate of the aqueous sample supplied to the nebulizer during the measurement of an aqueous sample (*standard)	mL min ⁻¹
$Q_{liq,drain}, Q_{liq,drain}^*$	Flow rate of water that is drained from the nebulizer chamber without being nebulized during the measurement of an aqueous sample (*standard)	mL min ⁻¹
ρ_{bulkBC}	Void free material density of BC	kg m ⁻³

$\rho_{\text{eff,BC}}(D_{\text{mob}})$ Effective density of BC particles as a function of particle mobility diameter kg m^{-3}

S.1 General definitions and equations

S.1.1 Nebulizer efficiency for BC

The size-dependent overall nebulizer efficiency for BC as a function of BC mass equivalent diameter during the measurement of an aqueous BC sample is defined as the ratio of the BC mass size distribution in the aerosol from the nebulized aqueous sample, $\frac{dc_{\text{air}}}{d \log D_{\text{BC}}}$, to the BC

mass size distribution in the aqueous sample, $\frac{dC_{\text{liq}}}{d \log D_{\text{BC}}}$, at the same BC mass equivalent diameter, D_{BC} :

$$\eta_{\text{BC}}(D_{\text{BC}}) := \frac{\frac{dc_{\text{air}}}{d \log D_{\text{BC}}}(D_{\text{BC}})}{\frac{dC_{\text{liq}}}{d \log D_{\text{BC}}}(D_{\text{BC}})} \quad (\text{S1})$$

The reference nebulizer efficiency for BC, $\eta_{\text{BC,ref}}$, at the arbitrarily chosen BC mass equivalent reference diameter, $D_{\text{BC,ref}}$, is defined as:

$$\eta_{\text{BC,ref}} := \eta_{\text{BC}}(D_{\text{BC,ref}}) \quad (\text{S2})$$

and the normalized overall nebulizer efficiency for BC as a function of BC mass equivalent diameter is defined as:

$$\tilde{\eta}_{\text{BC}}(D_{\text{BC}}) := \frac{\eta_{\text{BC}}(D_{\text{BC}})}{\eta_{\text{BC,ref}}} \quad (\text{S3})$$

Note, from Eqs. (S2) and (S3) follows: $\tilde{\eta}_{\text{BC}}(D_{\text{BC,ref}}) = 1$.

Rearranging Eq. (S3) provides an alternative form for the overall nebulizer efficiency for BC (as a function of BC mass equivalent diameter):

$$\eta_{\text{BC}}(D_{\text{BC}}) = \eta_{\text{BC,ref}} \tilde{\eta}_{\text{BC}}(D_{\text{BC}}) \quad (\text{S4})$$

The definitions for the nebulizer efficiency during the measurement of an aqueous BC standard are equivalent to Eqs. (S1) to (S4) (obtained with substituting η_{BC} , $\tilde{\eta}_{BC}$, c_{air} and C_{liq} for η_{BC}^* , $\tilde{\eta}_{BC}^*$, c_{air}^* and C_{liq}^* , respectively).

S.1.2 Nebulizer efficiency for PSLs

The size-dependent overall nebulizer efficiency for PSLs as a function of PSL diameter is defined as the ratio of the number concentration of PSLs in the aerosol from the nebulized aqueous standard, $n_{air,PSL}$, to the number concentration of PSLs in the aqueous standard, $N_{liq,PSL}$, with the same nominal diameter D_{PSL} :

$$\eta_{PSL}(D_{PSL}) := \frac{n_{air,PSL}(D_{PSL})}{N_{liq,PSL}(D_{PSL})} \cdot 10^6 \quad (S5)$$

where the factor 10^6 accounts for the units as defined in the list of all symbols. This definition for the nebulizer efficiency for PSLs is equivalent to the definition for the nebulizer efficiency for BC (Eq. S1). The reference nebulizer efficiency for PSLs, $\eta_{PSL,ref}$, at the arbitrarily chosen reference PSL diameter, $D_{PSL,ref}$, is defined as:

$$\eta_{PSL,ref} := \eta_{PSL}(D_{PSL,ref}) \quad (S6)$$

and the normalized overall nebulizer efficiency for PSLs as a function of PSL diameter is defined as:

$$\tilde{\eta}_{PSL}(D_{PSL}) := \frac{\eta_{PSL}(D_{PSL})}{\eta_{PSL,ref}} \quad (S7)$$

Note, from Eqs. (S6) and (S7) follows: $\tilde{\eta}_{PSL}(D_{PSL,ref}) = 1$

Rearranging Eq. (S7) provides an alternative form for the overall nebulizer efficiency for PSLs (as a function of PSL diameter):

$$\eta_{PSL}(D_{PSL}) = \eta_{PSL,ref} \tilde{\eta}_{PSL}(D_{PSL}) \quad (S8)$$

5.1.3 Particle losses in a nebulizer and upper limit for the nebulizer efficiency

The efficiency of a nebulizer during the measurement of an aqueous BC sample depends on several factors. The overall nebulizer efficiency for insoluble particles in suspension, as defined in Eqs. (S1) and (S5) for BC and PSLs, respectively, can be written as:

$$\eta(D) = \frac{\varepsilon_{\text{drop}} Q_{\text{liq, supply}}}{q_{\text{air, aerosol}}} \varepsilon_{\text{loss}}(D) \quad (\text{S9})$$

This equation is valid for nebulizers where the main nebulizer chamber only has two inputs for the aqueous sample and purge air supply and two outlets for the aerosol sample and the chamber drain (additional drains or vents between the aerosol sample outlet from the main chamber nebulizer chamber and the SP2 inlet such as e.g. drains from the dryer do not matter as they don't change the aerosol concentration). The factor $\varepsilon_{\text{drop}}$ accounts for the fraction of the supplied aqueous sample, fed to the nebulizer with a flow rate of $Q_{\text{liq, supply}}$, that is transformed into droplets and successfully transferred towards the aerosol sample outlet of the nebulizer. $q_{\text{air, aerosol}}$ is the air flow rate at the aerosol outlet of the nebulizer. The factor $\varepsilon_{\text{loss}}$ accounts for any kind of losses of insoluble particles in the complete nebulizer unit, i.e. between the sample vial and the SP2 inlet.

$\varepsilon_{\text{drop}}$ can be expressed with the flow rate of water in the drain line, $Q_{\text{liq, drain}}$:

$$\varepsilon_{\text{drop}} = \frac{Q_{\text{liq, supply}} - Q_{\text{liq, drain}}}{Q_{\text{liq, supply}}} \quad (\text{S10})$$

$Q_{\text{liq, drain}}$ is the flow rate of the portion of the supplied aqueous sample that leaves the nebulizer chamber directly through the drain line without giving a contribution to the aerosol at the nebulizer outlet. Any drain water from the dryer section of the nebulizer must not be included in $Q_{\text{liq, drain}}$.

$q_{\text{air, aerosol}}$ can alternatively be expressed with the flow rates of the purge air, $q_{\text{air, supply}}$, and the air in the drain line from the nebulizer chamber, $q_{\text{air, drain}}$:

$$q_{\text{air, aerosol}} = q_{\text{air, supply}} - q_{\text{air, drain}} \quad (\text{S11})$$

$q_{\text{air, drain}}$ only includes the air flow that leaves the nebulizer chamber directly through the drain line. Any air flow at additional drain ports for e.g. removing water from the dryer section of the

nebulizer must not be included in $q_{\text{air,drain}}$. Often, $q_{\text{air,drain}}$ is much smaller than $q_{\text{air,supply}}$, such that $q_{\text{air,aerosol}} \approx q_{\text{air,supply}}$.

$\varepsilon_{\text{loss}}$ is the only unknown quantity in Eq. (D9) for any nebulizer type where $Q_{\text{liq,supply}}$, $Q_{\text{liq,drain}}$, and $q_{\text{air,aerosol}}$ can be measured. An upper limit for the maximal possible efficiency of a nebulizer, η_{max} , is:

$$\eta_{\text{max}} = \frac{\varepsilon_{\text{drop}} Q_{\text{liq,supply}}}{q_{\text{air,aerosol}}} = \frac{(Q_{\text{liq,supply}} - Q_{\text{liq,drain}})}{q_{\text{air,aerosol}}} \approx \frac{(Q_{\text{liq,supply}} - Q_{\text{liq,drain}})}{q_{\text{air,supply}}} \quad (\text{S12})$$

Inserting Eq. (S12) into Eq. (D9) provides:

$$\eta(D) = \eta_{\text{max}} \varepsilon_{\text{loss}}(D) \Leftrightarrow \varepsilon_{\text{loss}}(D) = \frac{\eta(D)}{\eta_{\text{max}}} \quad (\text{S13})$$

where η is the true efficiency of the nebulizer. Given the fact that $\varepsilon_{\text{loss}}(D) \leq 1$ confirms that η_{max} is indeed an upper limit for $\eta(D)$.

Note, $\varepsilon_{\text{loss}}(D)$ is likely to depend on the properties (density, shape, etc.) of the insoluble particles.

Equations (D9) to (S13) are equivalent for the measurement of an aqueous standard (obtained with substituting $Q_{\text{liq,supply}}$, $Q_{\text{liq,drain}}$, $q_{\text{air,supply}}$, $q_{\text{air,drain}}$, $q_{\text{air,aerosol}}$, $\varepsilon_{\text{drop}}$, $\varepsilon_{\text{loss}}$, η and η_{max} for $Q_{\text{liq,supply}}^*$, $Q_{\text{liq,drain}}^*$, $q_{\text{air,supply}}^*$, $q_{\text{air,drain}}^*$, $q_{\text{air,aerosol}}^*$, $\varepsilon_{\text{drop}}^*$, $\varepsilon_{\text{loss}}^*$, η^* and η_{max}^* , respectively).

S.1.4 BC mass size distribution and mass concentration of an aqueous BC sample and the corresponding nebulized aerosol

The aim of measuring the aerosol from a nebulized aqueous sample with the SP2 is to determine the total BC mass concentration, C_{liq} , and the BC mass size distribution, $dC_{\text{liq}}/d\log D_{\text{BC}}$, in the aqueous sample. These two quantities are related as follows:

$$C_{\text{liq}} = \int_{D_{\text{BC,min}}}^{D_{\text{BC,max}}} \frac{dC_{\text{liq}}}{d\log D_{\text{BC}}} (D_{\text{BC}}) d\log D_{\text{BC}} \quad (\text{S14})$$

where $D_{\text{BC,min}}$ and $D_{\text{BC,max}}$ are the minimal and maximal BC core mass equivalent diameters in the sample.

3 Optimized method for BC analysis

The primary measurements of the SP2 are the total BC mass concentration, c_{SP2} , and the BC mass size distribution, $dc_{\text{SP2}}/d\log D_{\text{BC}}$, of the aerosol from the nebulized aqueous sample, which are related as follows:

$$c_{\text{SP2}} = \int_{D_{\text{BC,LDL}}}^{D_{\text{BC,UDL}}} \frac{dc_{\text{SP2}}}{d\log D_{\text{BC}}}(D_{\text{BC}}) d\log D_{\text{BC}} \quad (\text{S15})$$

$D_{\text{BC,LDL}}$ and $D_{\text{BC,UDL}}$ are the LDL and UDL of the SP2 in terms of BC mass equivalent diameter.

The detection efficiency of the SP2 is unity within its detection limits. BC cores smaller than the LDL of the SP2 may still be detected but with a detection efficiency below unity. BC cores larger than the UDL of the SP2 are properly counted but their BC mass cannot be quantified (due to detector saturation).

Any SP2 measurement of BC mass is potentially biased. The size-dependent calibration bias for BC mass, f_{bias} , can be defined as:

$$f_{\text{bias}}(D_{\text{BC}}) = \frac{\frac{dc_{\text{SP2}}}{d\log D_{\text{BC}}}(D_{\text{BC}})}{\frac{dc_{\text{air}}}{d\log D_{\text{BC}}}(D_{\text{BC}})} \quad (\text{S16})$$

where $dc_{\text{air}}/d\log D_{\text{BC}}$ is the true BC mass size distribution of the aerosol from the nebulized aqueous sample. If the calibration bias is assumed to be a constant, i.e. independent of BC core size, within the detection range of the SP2, follows:

$$\frac{dc_{\text{SP2}}}{d\log D_{\text{BC}}}(D_{\text{BC}}) = f_{\text{bias}} \frac{dc_{\text{air}}}{d\log D_{\text{BC}}}(D_{\text{BC}}) \quad \forall D_{\text{BC}} \in [D_{\text{BC,LDL}}, D_{\text{BC,UDL}}] \quad (\text{S17})$$

The normalized BC mass size distribution of the aqueous sample is defined as:

$$\frac{d\tilde{C}_{\text{liq}}}{d\log D_{\text{BC}}}(D_{\text{BC}}) := \frac{1}{C_{\text{liq}}} \frac{dC_{\text{liq}}}{d\log D_{\text{BC}}}(D_{\text{BC}}) \quad (\text{S18})$$

The relative contribution from BC cores with sizes below the LDL of the SP2 to the total BC mass in the aqueous sample is (use Eq. S18 to obtain the right hand side):

$$\Delta\tilde{C}_{\text{LDL}} = \frac{1}{C_{\text{liq}}} \int_{D_{\text{BC,min}}}^{D_{\text{BC,LDL}}} \frac{dC_{\text{liq}}}{d\log D_{\text{BC}}}(D_{\text{BC}}) d\log D_{\text{BC}} = \int_{D_{\text{BC,min}}}^{D_{\text{BC,LDL}}} \frac{d\tilde{C}_{\text{liq}}}{d\log D_{\text{BC}}}(D_{\text{BC}}) d\log D_{\text{BC}} \quad (\text{S19})$$

The relative contribution from BC cores with sizes above the UDL of the SP2 to the total BC mass in the aqueous sample is (use Eq. S18 to obtain the right hand side):

$$\Delta \tilde{C}_{UDL} = \frac{1}{C_{liq}} \int_{D_{BC,UDL}}^{D_{BC,max}} \frac{dC_{liq}}{d \log D_{BC}}(D_{BC}) d \log D_{BC} = \int_{D_{BC,UDL}}^{D_{BC,max}} \frac{d\tilde{C}_{liq}}{d \log D_{BC}}(D_{BC}) d \log D_{BC} \quad (S20)$$

From Eqs. (S14), (S18), (S19) and (S20) follows:

$$\int_{D_{BC,LDL}}^{D_{BC,UDL}} \frac{d\tilde{C}_{liq}}{d \log D_{BC}}(D_{BC}) d \log D_{BC} = 1 - \Delta \tilde{C}_{LDL} - \Delta \tilde{C}_{UDL} \quad (S21)$$

From the above definition of the nebulizer efficiency for BC follows (Eqs. S1 and S4):

$$\frac{dc_{air}}{d \log D_{BC}}(D_{BC}) = \eta_{BC}(D_{BC}) \frac{dC_{liq}}{d \log D_{BC}}(D_{BC}) = \eta_{BC,ref} \tilde{\eta}_{BC}(D_{BC}) \frac{dC_{liq}}{d \log D_{BC}}(D_{BC}) \quad (S22)$$

Inserting Eq. (S17) into Eq. (S22) provides:

$$\begin{aligned} \frac{dc_{SP2}}{d \log D_{BC}}(D_{BC}) &= f_{bias} \eta_{BC}(D_{BC}) \frac{dC_{liq}}{d \log D_{BC}}(D_{BC}) \\ &= f_{bias} \eta_{BC,ref} \tilde{\eta}_{BC}(D_{BC}) \frac{dC_{liq}}{d \log D_{BC}}(D_{BC}) \end{aligned} \quad (S23)$$

$\forall D_{BC} \in [D_{BC,LDL}, D_{BC,UDL}]$

Inserting Eq. (S23) into Eq. (S15) provides the following relationship between the total BC mass concentration measured by the SP2 and the BC mass size distribution in the aqueous sample:

$$c_{SP2} = f_{bias} \int_{D_{BC,LDL}}^{D_{BC,UDL}} \eta_{BC,ref} \tilde{\eta}_{BC}(D_{BC}) \frac{dC_{liq}}{d \log D_{BC}}(D_{BC}) d \log D_{BC} \quad (S24)$$

The central equation for inferring the BC mass size distribution in an aqueous sample, $dC_{SP2}^{\eta}/d \log D_{BC}$, from the SP2 measurement of the nebulized sample, if the absolute nebulizer efficiency is known, is:

$$\frac{dC_{SP2}^{\eta}}{d \log D_{BC}}(D_{BC}) := \frac{1}{\eta_{BC}(D_{BC})} \frac{dc_{SP2}}{d \log D_{BC}}(D_{BC}) = \frac{1}{\eta_{BC,ref} \tilde{\eta}_{BC}(D_{BC})} \frac{dc_{SP2}}{d \log D_{BC}}(D_{BC}) \quad (S25)$$

3 Optimized method for BC analysis

Inserting Eqs. (S17) and (S22) into Eq. (S25) provides:

$$\begin{aligned} \frac{dC_{SP2}^{\eta}}{d \log D_{BC}}(D_{BC}) &= f_{\text{bias}} \frac{1}{\eta_{BC}(D_{BC})} \frac{dc_{\text{air}}}{d \log D_{BC}}(D_{BC}) \\ &= f_{\text{bias}} \frac{dC_{\text{liq}}}{d \log D_{BC}}(D_{BC}) \quad \forall D_{BC} \in [D_{BC,\text{LDL}}, D_{BC,\text{UDL}}] \end{aligned} \quad (\text{S26})$$

This confirms that Eq. (S25) indeed provides the correct result for all BC core sizes within the detection range of the SP2, if the size dependent nebulizer efficiency for BC is known and if the potential SP2 calibration bias is small (i.e. $f_{\text{bias}} \approx 1$).

The central equation for inferring the total BC mass concentration in an aqueous sample, C_{SP2}^{η} , from the SP2 measurement of the nebulized sample, if the absolute nebulizer efficiency is known, is obtained by integrating Eq. (S25):

$$\begin{aligned} C_{SP2}^{\eta} &:= \int_{D_{BC,\text{LDL}}}^{D_{BC,\text{UDL}}} \frac{dC_{SP2}^{\eta}}{d \log D_{BC}}(D_{BC}) d \log D_{BC} \\ &= \int_{D_{BC,\text{LDL}}}^{D_{BC,\text{UDL}}} \frac{1}{\eta_{BC}(D_{BC})} \frac{dc_{SP2}}{d \log D_{BC}}(D_{BC}) d \log D_{BC} \\ &= \int_{D_{BC,\text{LDL}}}^{D_{BC,\text{UDL}}} \frac{1}{\eta_{BC,\text{ref}} \tilde{\eta}_{BC}(D_{BC})} \frac{dc_{SP2}}{d \log D_{BC}}(D_{BC}) d \log D_{BC} \end{aligned} \quad (\text{S27})$$

Inserting Eqs. (S26), (S18), and (S21) into Eq. (S27) provides:

$$\begin{aligned} C_{SP2}^{\eta} &= \int_{D_{BC,\text{LDL}}}^{D_{BC,\text{UDL}}} \frac{dC_{SP2}^{\eta}}{d \log D_{BC}}(D_{BC}) d \log D_{BC} \\ &= \int_{D_{BC,\text{LDL}}}^{D_{BC,\text{UDL}}} f_{\text{bias}} \frac{dC_{\text{liq}}}{d \log D_{BC}}(D_{BC}) d \log D_{BC} \\ &= f_{\text{bias}} C_{\text{liq}} \int_{D_{BC,\text{LDL}}}^{D_{BC,\text{UDL}}} \frac{d\tilde{C}_{\text{liq}}}{d \log D}(D_{BC}) d \log D_{BC} = f_{\text{bias}} C_{\text{liq}} (1 - \Delta\tilde{C}_{\text{LDL}} - \Delta\tilde{C}_{\text{UDL}}) \end{aligned} \quad (\text{S28})$$

This confirms that Eq. (S27) indeed provides the correct result for the total BC mass concentration of BC cores within the detection range of the SP2, if the size-dependent nebulizer efficiency for BC is known and if the potential SP2 calibration bias is small (i.e. if $f_{\text{bias}} \approx 1$).

No aqueous BC standard is required as a reference for the approach with using Eq. (S27) for inferring the total BC mass concentration in the aqueous sample. However, Eq. (S27) can only be

evaluated if the size-dependent overall efficiency of the nebulizer for BC is known and if it is different from zero in the size range between $D_{BC,LDL}$ and $D_{BC,UDL}$, i.e. if:

$$\tilde{\eta}_{BC}(D_{BC}) \neq 0 \quad \forall \quad D_{BC} \in [D_{BC,LDL}, D_{BC,UDL}] \quad (S29)$$

For nebulizers with a sharp efficiency drop towards zero above a certain diameter, such as e.g. observed for the CETAC ultrasonic nebulizer, the integration in Eq. (S27) must be additionally restricted to diameters below which the nebulizer is sufficiently efficient (i.e. diameters for which Eq. (S29) is fulfilled). This would potentially increase the unaccounted portion of BC mass, $C_{liq} \Delta \tilde{C}_{UDL}$, if the nebulizer cut-off is below the upper end of the BC size distribution.

If the BC mass fraction of BC cores in the aqueous sample with sizes outside the detection range of the SP2 is small, i.e. if:

$$\Delta \tilde{C}_{LDL} + \Delta \tilde{C}_{UDL} \ll 1 \quad (S30)$$

then follows from Eq. (S28) that Eq. (S27) correctly provides the total BC mass concentration in the aqueous sample of BC cores with any core size, except for the potential calibration bias:

$$C_{SP2}^{\eta} \approx f_{bias} C_{liq} \quad (S31)$$

Typically, the absolute nebulizer efficiency is not known. In such cases it is still possible to obtain an estimate of the lower limit of the total BC mass concentration in an aqueous sample, $C_{SP2,low}^{\eta}$, from the SP2 measurement of the nebulized sample by substituting the true nebulizer efficiency (η_{BC}) with the upper limit of the nebulizer efficiency (η_{max}) in Eq. (S27):

$$C_{SP2,low}^{\eta} := \frac{1}{\eta_{max}} \int_{D_{BC,LDL}}^{D_{BC,UDL}} \frac{dc_{SP2}}{d \log D_{BC}}(D_{BC}) d \log D_{BC} = \frac{1}{\eta_{max}} c_{SP2} \quad (S32)$$

With $\eta_{max} \geq \eta_{BC}(D_{BC})$ follows:

$$C_{SP2,low}^{\eta} \leq C_{SP2}^{\eta} \quad (S33)$$

which confirms that Eq. (S32) indeed provides a lower limit for C_{SP2}^{η} .

3 Optimized method for BC analysis

Equations (S14) to (S33) are equivalent for the measurement of an aqueous BC standard (obtained with substituting C_{liq} , $D_{\text{BC,min}}$, $D_{\text{BC,max}}$, $dC_{\text{liq}}/d \log D_{\text{BC}}$, c_{SP2} , $dc_{\text{SP2}}/d \log D_{\text{BC}}$, etc. for C_{liq}^* , $D_{\text{BC,min}}^*$, $D_{\text{BC,max}}^*$, $dC_{\text{liq}}^*/d \log D_{\text{BC}}$, c_{SP2}^* , $dc_{\text{SP2}}^*/d \log D_{\text{BC}}$, etc., respectively).

S.2 Approach of using aqueous standards as a reference for the measurement of unknown samples

The nebulizer efficiency is often not known. In such cases it is common to relate the BC mass concentration measurement of an aqueous sample to the measurement of an aqueous BC standard of known concentration, C_{liq}^* . The assumption behind this approach is that the nebulizer efficiency remains stable between the measurement of the sample and the standard, i.e.:

$$\eta_{\text{BC}}(D_{\text{BC}}) = \eta_{\text{BC}}^*(D_{\text{BC}}) \quad \forall D_{\text{BC}} \quad (\text{S34})$$

The following simple rule of proportion is then commonly used to infer the BC mass concentration, $C_{\text{SP2}}^{\text{S1}}$, of the aqueous sample of interest from the SP2 measurements of the nebulized sample and standard:

$$C_{\text{SP2}}^{\text{S1}} := c_{\text{SP2}} \frac{C_{\text{liq}}^*}{c_{\text{SP2}}^*} \quad (\text{S35})$$

Drifts of the aqueous sample and/or air flow rates between the measurement of the aqueous BC sample and standard (i.e. if $Q_{\text{liq,supply}} \neq Q_{\text{liq,supply}}^*$, $Q_{\text{liq,drain}} \neq Q_{\text{liq,drain}}^*$, $q_{\text{air,supply}} \neq q_{\text{air,supply}}^*$ and/or $q_{\text{air,aerosol}} \neq q_{\text{air,aerosol}}^*$), which can occur depending on the nebulizer type, will result in a drift of the overall nebulizer efficiency (see Eqs. D9 to S11), thus turning Eq. (S34) invalid. However, the particle losses in the nebulizer system may not be affected by moderate changes of the water and air flow rates, such that the factor $\varepsilon_{\text{loss}}$ may still be assumed to remain stable between the measurement of the sample and the standard, i.e.:

$$\varepsilon_{\text{loss}}(D_{\text{BC}}) = \varepsilon_{\text{loss}}^*(D_{\text{BC}}) \quad \forall D_{\text{BC}} \quad (\text{S36})$$

In such cases it is possible to account for drifts of $Q_{\text{liq,supply}}$, $q_{\text{air,aerosol}}$ and/or $\varepsilon_{\text{drop}}$, for nebulizer types where these quantities can be monitored, by using the following equation (as an alternative to Eq. S35):

$$C_{SP2}^{S2} := C_{SP2,low}^{\eta} \frac{C_{liq}^*}{C_{SP2,low}^{\eta,*}} \quad (S37)$$

From Eq. (S32) follows:

$$\frac{C_{SP2,low}^{\eta}}{C_{SP2,low}^{\eta,*}} = \frac{\eta_{max}^*}{\eta_{max}} \frac{c_{SP2}}{c_{SP2}^*} \quad (S38)$$

and by inserting Eqs. (S35) and (S37) into Eq. (S38) it follows that:

$$C_{SP2}^{S2} = \frac{\eta_{max}^*}{\eta_{max}} C_{SP2}^{S1} \quad (S39)$$

From Eq. (S39) follows that the approaches of using Eq. (S35) or (S37) are equal except for the factor η_{max}^*/η_{max} , which is normally close to unity (the factor η_{max}^*/η_{max} reflects the slightly different underlying assumptions, i.e. Eq. S34 for Eq. S35 and Eq. S36 for Eq. (S37)). If this factor was substantially different from unity, i.e. if the nebulizer system was operated with substantially different water and air flow rates when measuring the standard and the sample, then Eq. (S34) is not sufficiently well satisfied, thus turning Eq. (S35) invalid (see also below). In such cases, it is important to account for differences between η_{max} and η_{max}^* by applying Eq. (S37) instead. However, if the water and air flow rates differ substantially between measuring the standard and the sample, then it is also possible that Eq. (S36) is not fulfilled anymore, thereby potentially making the approach of Eq. (S37) imprecise or even invalid, too.

The use of Eqs. (S18) and (S24) as well as the assumption of Eq. (S34) yields:

$$\begin{aligned} \frac{C_{SP2}}{C_{SP2}^*} &= \frac{f_{bias} \int_{D_{BC,LDL}}^{D_{BC,UDL}} \eta_{BC,ref} \tilde{\eta}_{BC}(D_{BC}) \frac{dC_{liq}}{d \log D_{BC}}(D_{BC}) d \log D_{BC}}{f_{bias}^* \int_{D_{BC,LDL}}^{D_{BC,UDL}} \eta_{BC,ref}^* \tilde{\eta}_{BC}^*(D_{BC}) \frac{dC_{liq}^*}{d \log D_{BC}}(D_{BC}) d \log D_{BC}} \\ &= \frac{C_{liq} f_{bias} \int_{D_{BC,LDL}}^{D_{BC,UDL}} \tilde{\eta}_{BC}(D_{BC}) \frac{d\tilde{C}_{liq}}{d \log D_{BC}}(D_{BC}) d \log D_{BC}}{C_{liq}^* f_{bias}^* \int_{D_{BC,LDL}}^{D_{BC,UDL}} \tilde{\eta}_{BC}(D_{BC}) \frac{d\tilde{C}_{liq}^*}{d \log D_{BC}}(D_{BC}) d \log D_{BC}} \end{aligned} \quad (S40)$$

3 Optimized method for BC analysis

Inserting Eq. (S40) into Eq. (S35) provides:

$$C_{SP2}^{S1} = C_{liq} \frac{\int_{D_{BC,LDL}}^{D_{BC,UDL}} \tilde{\eta}_{BC}(D_{BC}) \frac{d\tilde{C}_{liq}}{d \log D_{BC}}(D_{BC}) d \log D_{BC}}{\int_{D_{BC,LDL}}^{D_{BC,UDL}} \tilde{\eta}_{BC}(D_{BC}) \frac{d\tilde{C}_{liq}^*}{d \log D_{BC}}(D_{BC}) d \log D_{BC}} \frac{f_{bias}}{f_{bias}^*} \frac{D_{BC,LDL}}{D_{BC,UDL}} \quad (S41)$$

Equation (S41) can be written as:

$$C_{SP2}^{S1} = C_{liq} \frac{f_{bias}}{f_{bias}^*} k_{S1} \quad (S42)$$

with:

$$k_{S1} := \frac{\int_{D_{BC,LDL}}^{D_{BC,UDL}} \tilde{\eta}_{BC}(D_{BC}) \frac{d\tilde{C}_{liq}}{d \log D_{BC}}(D_{BC}) d \log D_{BC}}{\int_{D_{BC,LDL}}^{D_{BC,UDL}} \tilde{\eta}_{BC}(D_{BC}) \frac{d\tilde{C}_{liq}^*}{d \log D_{BC}}(D_{BC}) d \log D_{BC}} \quad (S43)$$

From Eqs. (S39) and (S42) it follows that:

$$C_{SP2}^{S2} = C_{liq} \frac{f_{bias}}{f_{bias}^*} k_{S2} \quad (S44)$$

with:

$$k_{S2} := \frac{\eta_{max}^*}{\eta_{max}} k_{S1} = \frac{\int_{D_{BC,LDL}}^{D_{BC,UDL}} \varepsilon_{loss}(D_{BC}) \frac{d\tilde{C}_{liq}}{d \log D_{BC}}(D_{BC}) d \log D_{BC}}{\int_{D_{BC,LDL}}^{D_{BC,UDL}} \varepsilon_{loss}(D_{BC}) \frac{d\tilde{C}_{liq}^*}{d \log D_{BC}}(D_{BC}) d \log D_{BC}} \quad (S45)$$

The factor $\frac{f_{bias}}{f_{bias}^*} k_{S1}$ in Eq. (S42) quantifies the total error introduced when using the simple

Eq. (S35) to infer the BC mass concentration of an aqueous sample from the SP2 measurements of the aqueous sample and an aqueous standard with known concentration (under the

assumption of Eq. S34). Likewise, the factor $\frac{f_{bias}}{f_{bias}^*} k_{S2}$ in Eq. (S44) quantifies the total error

introduced when using the simple Eq. (S37) to infer the BC mass concentration of an aqueous sample from the SP2 measurements of the aqueous sample and an aqueous standard with

known concentration (under the slightly less stringent assumption of Eq. S36). From Eq. (S45) and the fact that $\eta_{\max}^*/\eta_{\max}$ is close to unity, follows that k_{S1} and k_{S2} are almost equal. Consequently, the conditions under which Eqs. (S35) and (S37) are valid are similar (the difference being the underlying assumptions, i.e. Eq. S34 for Eq. S35 and Eq. S36 for Eq. S37) and thus these conditions are only discussed for the approach of Eq. (S35) in the following.

The ratio $f_{\text{bias}}/f_{\text{bias}}^*$ in Eq. (S42) quantifies the contribution of SP2 calibration error for the BC in the sample and the standard to the total error when using the simple Eq. (S35). The sensitivity of the SP2 can differ substantially between different BC types (see Moteki and Kondo, 2010, and Laborde et al., 2012) for a detailed discussion of SP2 sensitivity). The factor $f_{\text{bias}}/f_{\text{bias}}^*$ only becomes unity if the correct SP2 calibration curves are applied to evaluate both the measurements of the sample and the standard, or if the calibration biases cancel each other by chance (i.e. if $f_{\text{bias}} \approx f_{\text{bias}}^*$). If the correct calibration is known for the standard only (i.e. $f_{\text{bias}}^* \approx 1$), then the uncertainty introduced by the factor $f_{\text{bias}}/f_{\text{bias}}^*$ reduces to (f_{bias}). Likewise, if the correct calibration is known for the sample only (i.e. $f_{\text{bias}} \approx 1$), then the uncertainty introduced by the factor $f_{\text{bias}}/f_{\text{bias}}^*$ reduces to $(f_{\text{bias}}^*)^{-1}$. If the SP2 sensitivity is neither known for the sample nor the standard, then the same internal SP2 calibration curve should be applied for evaluating the SP2 data from both the sample and standard. Using this strategy, the bias factor in the BC mass concentration inferred with Eq. (S35), which is introduced by the factor $f_{\text{bias}}/f_{\text{bias}}^*$ in Eq. (S42), will be unity, if the SP2 is equally sensitive to the BC in the sample and the standard, or it will otherwise reflect the ratio of the SP2 sensitivity to the sample and the standard, as the absolute magnitude of the sensitivities is cancelled.

When applying Eq. (S35), the factor k_{S1} in Eq. (S42) quantifies the error in the determination of the BC mass concentration of the aqueous sample that is associated with the differences in the shape of the mass size distributions of the sample and the standard (note that the values of $D_{\text{BC,LDL}}$ and $D_{\text{BC,UDL}}$ and the size dependence of the efficiency only matter if there is such a difference). Unfortunately, k_{S1} is generally not unity nor can it be evaluated if the BC mass size distributions and $\tilde{\eta}_{\text{BC}}(D)$ are unknown. Equation (S42) thus shows that an error of unknown magnitude is introduced when using Eq. (S35) to infer the BC mass concentration of an aqueous sample from the SP2 measurements of the sample and standard. However, it will be shown in the following that it is possible to further constrain the factor k_{S1} under certain conditions such that Eq. (S35) (and Eq. S37) becomes a valid approach.

S.2.1 Nebulizers with size-dependent efficiency for BC

It has been shown above (Eq. S42) that working with aqueous BC standard suspensions is difficult if the nebulizer efficiency depends on BC size, i.e. if $\eta_{BC}(D_{BC}) \neq \text{const}$. An exception is the special case when the shapes of the BC mass size distributions of the aqueous sample and the aqueous standard are equal, i.e. if:

$$\frac{d\tilde{C}_{\text{liq}}}{d \log D_{BC}}(D_{BC}) \approx \frac{d\tilde{C}_{\text{liq}}^*}{d \log D_{BC}}(D_{BC}) \quad \forall D_{BC} \quad (\text{S46})$$

In this case the factor k_{SI} becomes approximately equal to unity and Eq. (S35) becomes valid for any kind of size-dependent nebulizer efficiency. In principle, it is sufficient to relax the condition of Eq. (S46) to:

$$\frac{d\tilde{C}_{\text{liq}}}{d \log D_{BC}}(D_{BC}) \approx \frac{d\tilde{C}_{\text{liq}}^*}{d \log D_{BC}}(D_{BC}) \quad \forall D_{BC} \in [D_{BC,\text{LDL}}, D_{BC,\text{UDL}}] \quad (\text{S47})$$

However, the condition in Eq. (S47) is equivalent to the following pair of conditions (Eqs. S14, S18, S19, and S20):

$$\frac{dC_{\text{liq}}}{d \log D_{BC}}(D_{BC}) \propto \frac{dC_{\text{liq}}^*}{d \log D_{BC}}(D_{BC}) \quad \forall D_{BC} \in [D_{BC,\text{LDL}}, D_{BC,\text{UDL}}] \quad (\text{S48})$$

and

$$\Delta\tilde{C}_{\text{LDL}} + \Delta\tilde{C}_{\text{UDL}} \approx \Delta\tilde{C}_{\text{LDL}}^* + \Delta\tilde{C}_{\text{UDL}}^* \quad (\text{S49})$$

These two conditions are hardly fulfilled if the shapes of the BC mass size distributions of the sample and the standard differ outside the detection range of the SP2. Thus the more restrictive condition (Eq. S46) of agreement between the size distribution shapes of sample and standard must essentially be fulfilled over the whole size range of BC cores for the validity of Eq. (S35), if the nebulizer efficiency is size-dependent.

The factor k_{SI} (Eq. S43) only contains the relative size dependence of the nebulizer efficiency, $\tilde{\eta}_{BC}(D)$, while the factor for the absolute efficiency, $\eta_{BC,\text{ref}}$, got cancelled. This indicates that using an aqueous standard as a reference can provide quantitative results if the relative size dependence of the nebulizer efficiency for BC is known. In such cases, the following equation can be used to infer the BC mass concentration, $C_{\text{SP2}}^{S\eta}$, in the aqueous sample of interest from the

SP2 measurements of the nebulized sample and standard, taking into account the relative size dependence of the nebulizer efficiency:

$$C_{\text{SP2}}^{S\eta} := \frac{\int_{D_{\text{BC,LDL}}}^{D_{\text{BC,UDL}}} \frac{1}{\tilde{\eta}_{\text{BC}}(D)} \frac{dc_{\text{SP2}}}{d \log D}(D) d \log D}{\int_{D_{\text{BC,LDL}}}^{D_{\text{BC,UDL}}} \frac{1}{\tilde{\eta}_{\text{BC}}(D_{\text{BC}})} \frac{dc_{\text{SP2}}^*}{d \log D_{\text{BC}}}(D_{\text{BC}}) d \log D_{\text{BC}}} \frac{C_{\text{liq}}^*}{C_{\text{SP2}}^{\eta,*}} \quad (\text{S50})$$

Inserting Eq. (S27) into Eq. (S50) in a first step and Eq. (S28) in a second step provides:

$$C_{\text{SP2}}^{S\eta} = C_{\text{SP2}}^{\eta,*} \frac{C_{\text{liq}}^*}{C_{\text{SP2}}^{\eta,*}} = C_{\text{liq}} \frac{f_{\text{bias}}}{f_{\text{bias}}^*} \frac{(1 - \Delta\tilde{C}_{\text{LDL}} - \Delta\tilde{C}_{\text{UDL}})}{(1 - \Delta\tilde{C}_{\text{LDL}}^* - \Delta\tilde{C}_{\text{UDL}}^*)} \quad (\text{S51})$$

Equation (S51) can be written as:

$$C_{\text{SP2}}^{S\eta} = C_{\text{liq}} \frac{f_{\text{bias}}}{f_{\text{bias}}^*} k_{\text{fract}} \quad (\text{S52})$$

with:

$$k_{\text{fract}} := \frac{1 - \Delta\tilde{C}_{\text{LDL}} - \Delta\tilde{C}_{\text{UDL}}}{1 - \Delta\tilde{C}_{\text{LDL}}^* - \Delta\tilde{C}_{\text{UDL}}^*} \quad (\text{S53})$$

The factor $\frac{f_{\text{bias}}}{f_{\text{bias}}^*} k_{\text{fract}}$ in Eq. (S52) quantifies the total error introduced when using Eq. (S50) to

infer the BC mass concentration of an aqueous sample from the SP2 measurements of the aqueous sample and an aqueous standard with known concentration and with accounting for the relative size dependence of the nebulizer efficiency (note that the assumption of Eq. S34 needs to be satisfied for Eq. S52 to be valid). The ratio $f_{\text{bias}}/f_{\text{bias}}^*$ quantifies the contribution of SP2 calibration errors for the BC in the sample and the standard to the total error, as already discussed above. The factor k_{fract} quantifies the contribution to the total error associated with BC cores in the sample and/or standard outside the detection range of the SP2.

If the contribution of BC cores outside the detection range of the SP2 to the total BC mass is negligible for both the sample and the standard (Eq. S30 is fulfilled for the sample and the standard) then it follows that $k_{\text{fract}} \approx 1$. Thus, Eqs. (S52) and (S53) show that Eq. (S50) can be used to accurately determine the BC mass in the aqueous sample, except for potential SP2 calibration errors, by relating it to the measurement of an aqueous BC standard, if the relative

3 Optimized method for BC analysis

size dependence of the nebulizer efficiency for BC is known and if the SP2 measurement covers the full range of the BC mass size distributions in both the sample and the standard (i.e. if Eq. (S30) is fulfilled for the sample and the standard). Additionally, the nebulizer efficiency for BC must be different from zero across the measurement range of the SP2 (i.e. Eq. S29 must be fulfilled). Otherwise, the integration in Eq. (S50) must be restricted to the range across which the nebulizer is sufficiently efficient, thereby potentially increasing the unaccounted BC mass fraction of the sample and/or the standard.

If the BC mass size distribution of the aqueous sample extends beyond the detection range of the SP2 (Eq. S30 is not fulfilled for the sample), it follows from Eqs. (S52) and (S53) that Eq. (S50) still provides an accurate value for the BC mass concentration in the aqueous sample within the detection range of the SP2 (as long as Eq. S30 is fulfilled for the standard, i.e. if the aqueous standard fully falls within the detection range of the SP2).

It also follows from Eqs. (S52) and (S53) that the BC mass concentration in an aqueous sample within the detection range of the SP2 is overestimated by the factor $(1 - \Delta\tilde{C}_{LDL}^* - \Delta\tilde{C}_{UDL}^*)^{-1}$ when applying Eq. (S50) and using an aqueous standard with a substantial portion of the BC mass outside the detection range of the SP2 (Eq. S30 is not fulfilled for the standard).

S.2.2 Nebulizers with size-independent efficiency for BC

Nebulizers with size-independent efficiency for the nebulization of BC fulfill:

$$\begin{aligned} \eta_{BC}(D_{BC}) &\approx \eta_{BC,ref} \Leftrightarrow \tilde{\eta}_{BC}(D_{BC}) \\ &\approx 1 \quad \forall \quad D_{BC} \in [\min(D_{BC,min}, D_{BC,min}^*), \max(D_{BC,max}, D_{BC,max}^*)] \end{aligned} \quad (S54)$$

The assumption of Eq. (S54) together with Eqs. (S21), (S43) and (S53) yields:

$$k_{S1} \approx \frac{\int_{D_{BC,LDL}}^{D_{BC,UDL}} \frac{d\tilde{C}_{liq}}{d \log D_{BC}}(D_{BC}) d \log D_{BC}}{\int_{D_{BC,LDL}}^{D_{BC,UDL}} \frac{d\tilde{C}_{liq}^*}{d \log D_{BC}}(D_{BC}) d \log D_{BC}} = \frac{1 - \Delta\tilde{C}_{LDL} - \Delta\tilde{C}_{UDL}}{1 - \Delta\tilde{C}_{LDL}^* - \Delta\tilde{C}_{UDL}^*} = k_{fract} \quad (S55)$$

Equation (S42) then simplifies to:

$$C_{SP2}^{S1} \approx C_{liq} \frac{f_{bias}}{f_{bias}^*} k_{fract} \quad (S56)$$

where k_{fract} is defined in Eq. (S53).

The ratio $f_{\text{bias}}/f_{\text{bias}}^*$ in Eq. (S56) quantifies the contribution of SP2 calibration errors, as discussed above, for the BC in the sample and the standard to the total error when using the approach of Eq. (S35) for a size-independent nebulizer efficiency. If the contribution of BC cores outside the detection range of the SP2 to the total BC mass is negligible for both the sample and the standard (Eq. S30 is fulfilled for the sample and the standard), it follows that $k_{\text{fact}} \approx 1$. Equation (S56) thus shows that Eq. (S35) can be used to determine the BC mass concentration of an aqueous sample from the SP2 measurements of the nebulized sample and standard, if the nebulizer efficiency is independent of particle size and if the BC cores smaller and larger than the LDL and UDL of the SP2, respectively, only give a negligible contribution to the total BC mass for both the aqueous sample and the aqueous standard.

If the BC mass size distribution of the aqueous sample extends beyond the detection range of the SP2 (Eq. S30 is not fulfilled for the sample), then follows from Eqs. (S53) and (S56) that Eq. (S35) still provides an accurate value for the BC mass concentration in the aqueous sample within the detection range of the SP2 (as long as Eq. S30 is fulfilled for the standard, i.e. if the aqueous standard fully falls within the detection range of the SP2).

It also follows from Eqs. (S53) and (S56) that the BC mass concentration in an aqueous sample within the detection range of the SP2 is overestimated by the factor $(1 - \Delta\tilde{C}_{\text{LDL}}^* - \Delta\tilde{C}_{\text{UDL}}^*)^{-1}$ when applying Eq. (S35) and using an aqueous standard with a substantial portion of the BC mass outside the detection range of the SP2 (Eq. S30 is not fulfilled for the standard). Thus, Eq. (S35) can generally not be applied for such standards without introducing a bias.

An exception, where Eq. (S35) is valid even if Eq. (S30) is not fulfilled for the standard, is when the shapes of the BC mass size distributions of the aqueous sample and the aqueous standard are equal for all diameters (i.e., Eq. (S46) is fulfilled, which also implies $D_{\text{min}} \approx D_{\text{min}}^*$ and $D_{\text{max}} \approx D_{\text{max}}^*$). In this case follows $1 - \Delta\tilde{C}_{\text{LDL}} + \Delta\tilde{C}_{\text{UDL}} \approx 1 - \Delta\tilde{C}_{\text{LDL}}^* + \Delta\tilde{C}_{\text{UDL}}^*$ and hence $k_{\text{fact}} \approx 1$, such that only potential calibration biases remain left in Eq. (S56):

$$C_{\text{SP2}}^{\text{S1}} \approx C_{\text{liq}} \frac{f_{\text{bias}}}{f_{\text{bias}}^*} \quad (\text{S57})$$

S.3 Measurement of the nebulizer efficiency

S.3.1 Nebulizer efficiency for PSLs

It is quite straightforward to produce a PSL standard suspensions from PSL size standards (see Sect. 2.4.2 in main text), i.e. an aqueous suspension with known number concentration of PSL spheres, $N_{\text{liq,PSL}}$, of a well-defined diameter, D_{PSL} . The aerosol obtained by nebulizing such a standard contains the PSL spheres with diameter D_{PSL} and, for the most part, very small particles that emerge from the residual solutes in each droplet. The residual particles can be distinguished from the PSL spheres based on their size. Therefore, the number concentration of the target PSL particles, $n_{\text{air,PSL}}$, can be measured by the SP2 using the light scattering detector (the SP2 has a detection efficiency of unity for purely scattering particles with sizes above the LDL of the light scattering detector). The nebulizer efficiency for PSLs is then directly obtained with Eq. (S5). Figure 3.2a in the main text shows the normalized overall nebulizer efficiency for PSLs, $\tilde{\eta}_{\text{PSL}}$, for the three investigated nebulizer types. Normalization was done according to Eqs. (S6) and (S7), where different reference diameters, $D_{\text{PSL,ref}}$, are chosen for the different nebulizers in such a manner that $\tilde{\eta}_{\text{PSL}}$ is unity at the PSL diameter with maximal efficiency. The reference PSL diameters, normalization factors and coefficients for the fitted efficiency curves are provided in Table S3-2 for all nebulizers.

Logarithmic functions were used to fit the efficiency curves of the APEX and Collison-type nebulizers:

$$\tilde{\eta}_{\text{PSL}}^{\text{APEX-PSI}}(D_{\text{PSL}}) = c_0 + c_1 \ln(D_{\text{PSL}}) \quad (\text{S58})$$

and

$$\tilde{\eta}_{\text{PSL}}^{\text{Collison-PSI}}(D_{\text{PSL}}) = c_0 + c_1 \ln(D_{\text{PSL}}) \quad (\text{S59})$$

The efficiency curve of PSI's CETAC nebulizer was fitted with a skewed Gauss function:

$$\tilde{\eta}_{\text{PSL}}^{\text{CETAC-PSI}}(D_{\text{PSL}}) = 2f_{\text{Gauss}}(D_{\text{PSL}}, c_0, c_1, c_2) f_{\text{GaussCDF}}(c_3(D_{\text{PSL}} - c_2), c_1) \quad (\text{S60})$$

with the Gauss function

$$f_{\text{Gauss}}(x, N, \sigma, \bar{x}) = \frac{N}{\sqrt{2\pi\sigma^2}} \exp\left(-\frac{(x - \bar{x})^2}{2\sigma^2}\right) \quad (\text{S61})$$

and the cumulative Gauss function

$$f_{\text{GaussCDF}}(x, \sigma) = \frac{1}{2} \left(1 + \operatorname{erf} \left(\frac{x}{\sigma\sqrt{2}} \right) \right) \quad (\text{S62})$$

where erf denotes the error function.

The efficiency curve of CWU's CETAC nebulizer was fitted with a Hill-equation:

$$\tilde{\eta}_{\text{PSL}}^{\text{CETAC-CWU}}(D_{\text{PSL}}) = c_0 + \frac{c_1 - c_0}{1 + \left(\frac{c_3}{D_{\text{PSL}}} \right)^{c_2}} \quad (\text{S63})$$

Table S3-2 Efficiency curves of the different nebulizers for PSLs.

Nebulizer	$D_{\text{PSL,ref}}$ [μm]	$\eta_{\text{PSL,ref}}$ [-]	c_0	c_1	c_2	c_3
APEX-PSI ^a	1.000	$3.16 \cdot 10^{-2}$	1	0.107	-	-
Collison-PSI ^a	0.100	$4.78 \cdot 10^{-3}$	0.356	-0.280	-	-
CETAC-PSI ^a	0.405	$4.80 \cdot 10^{-2}$	0.556	0.296	0.245	1.39
CETAC-CWU ^b	0.220	0.108	1	-0.0259	5.76	0.589

^avalid for the PSL diameter range 0.1–1.0 μm

^bvalid for the PSL diameter range 0.22–1.025 μm

S.3.2 Quantifying the losses of PSL particles in the CETAC nebulizer

All relevant water and air flow rates, $Q_{\text{liq,supply}}$, $Q_{\text{liq,drain}}$, and $q_{\text{air,aerosol}}$, can be measured when using a CETAC nebulizer, such that an upper limit for the overall nebulizer efficiency, $\eta_{\text{max,CETAC}}$, can be calculated with Eq. (S12). Substituting $\eta_{\text{max,CETAC}}$ for $\eta_{\text{BC}}(D_{\text{BC}})$ in Eq. (S27) thus provides a lower limit for the true BC mass concentration of the sample (Eq. S32). However, the true BC mass concentration will be substantially higher than the lower limit obtained in this way, as $\varepsilon_{\text{loss,CETAC}}$ is substantially smaller than unity. Eqs. (S12) and (S13) were used to calculate $\varepsilon_{\text{loss,CETAC}}$ from the overall nebulizer efficiency, $\eta_{\text{PSL,CETAC}}(D_{\text{PSL}})$, measured for the PSL standards (see above). Figure S3-1 reveals that the fraction of lost particles, $\varepsilon_{\text{loss,CETAC}}$, differs significantly between the PSI- and CWU nebulizer. Consequently, it is not possible to rely on literature values for the CETAC nebulizer efficiency. Instead every nebulizer needs to be tested

(and stable performance also needs to be ensured) if the shape and/ or absolute values of the nebulizer efficiency curve is relevant. Both nebulizers have in common that $\epsilon_{\text{loss,CETAC}}$ remains below $\sim 0.2\text{--}0.3$ at any diameter (i.e. at least 70–80% losses) and that $\epsilon_{\text{loss,CETAC}}$ sharply drops above PSL diameters of $\sim 450\text{--}500$ nm. ϵ_{loss} depends on (1) potential losses of insoluble particles between the aqueous sample and the point of nebulization, (2) on the probability that an insoluble particle is incorporated into a droplet if the portion of aqueous sample where it resides is nebulized, i.e. that it is not lost during the process of droplet generation at e.g. the ultrasonic membrane of the ultrasonic nebulizer, as well as (3) on potential losses of insoluble particles between the point of nebulization and the aerosol outlet of the nebulizer unit including the dryer.

It is not possible to quantify the loss factor ϵ_{loss} for the APEX or Collison type nebulizers applied in this study in a similar manner, as not all aqueous and air flow rates required to calculate ϵ_{loss} are known.

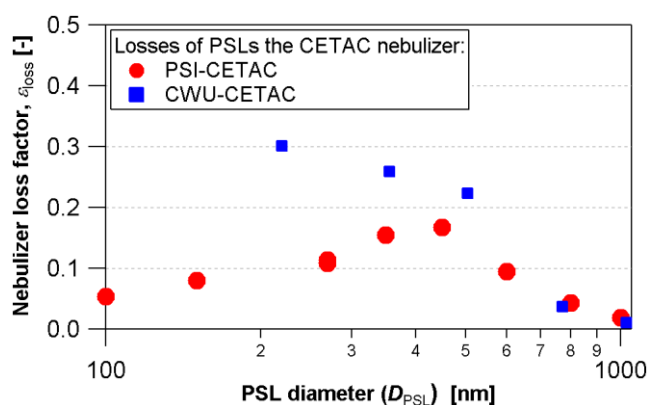


Figure S3-1 Losses in the PSI- and CWU-CETAC nebulizer as derived from the measurements of the PSL standard suspensions.

S.3.3 Nebulizer efficiency for BC

Both PSL spheres and BC particles are insoluble in water, but they typically have a different material density and shape. Thus, the nebulizer efficiency for BC particles may potentially differ from that for PSL spheres. The loss processes in the nebulizer may for example depend on the mobility diameter, mass equivalent diameter or aerodynamic diameter of a particle. It is, therefore, not quite clear which type of diameter should be used to estimate the nebulizer efficiency for BC particles from the measured efficiency for PSL spheres.

The nebulizer efficiency for BC particles cannot be directly measured, as no aqueous standards containing a known number concentration of BC particles with a well-defined size are available. It is also not straightforward to infer it from measurements of the nebulizer efficiency for PSL spheres, as the loss processes in the nebulizer may depend on the mobility diameter, mass equivalent diameter, aerodynamic diameter and/or further particle properties.

Nevertheless, the aerosols produced with two different nebulizers from the same aqueous BC sample makes it possible to test whether BC particles behave similar to PSL particles. Taking the ratio of the BC mass size distributions measured by the SP2 for two nebulizers “neb1” and “neb2” and inserting Eq. (S23) provides:

$$\frac{\frac{dc_{SP2}^{neb1}}{d \log D_{BC}}(D_{BC})}{\frac{dc_{SP2}^{neb2}}{d \log D_{BC}}(D_{BC})} = \frac{\eta_{BC}^{neb1}(D_{BC}) \frac{dC_{liq}}{d \log D_{BC}}(D_{BC})}{\eta_{BC}^{neb2}(D_{BC}) \frac{dC_{liq}}{d \log D_{BC}}(D_{BC})} \quad (S64)$$

Solving for η_{BC}^{neb1} provides:

$$\eta_{BC}^{neb1}(D_{BC}) = \eta_{BC}^{neb2}(D_{BC}) \frac{\frac{dc_{SP2}^{neb1}}{d \log D_{BC}}(D_{BC})}{\frac{dc_{SP2}^{neb2}}{d \log D_{BC}}(D_{BC})} \quad (S65)$$

Fortunately, the efficiency of the APEX nebulizer depends only weakly on particle size (see Sect. 3.1.1 in main text), such that it can be assumed that its efficiency for BC (as a function of BC mass equivalent diameter) is approximately equal to that for PSL spheres (as a function of PSL diameter), i.e.:

$$\eta_{BC}^{APEX}(D_{BC}) \approx \eta_{PSL}^{APEX}(D_{PSL}) \quad (S66)$$

From Eq. (S65) and (S66) (and defining the APEX as the second nebulizer) follows:

$$\eta_{BC}^{neb1}(D_{BC}) \approx \eta_{PSL}^{APEX}(D_{PSL}) \frac{\frac{dc_{SP2}^{neb1}}{d \log D_{BC}}(D_{BC})}{\frac{dc_{SP2}^{APEX}}{d \log D_{BC}}(D_{BC})} \quad (S67)$$

Equation (S67) can be used to determine the efficiency of any nebulizer “neb1” expressed as a function of BC mass equivalent diameter (D_{BC}) to a degree of approximation which depends on the validity of the assumption made in Eq. (S66).

3 Optimized method for BC analysis

The mobility diameter, D_{mob} , of a BC particle normally differs from its mass equivalent diameter, D_{BC} , as they are typically non-spherical. The relationship between D_{BC} and D_{mob} can be expressed as:

$$D_{\text{BC}} = D_{\text{mob}} \left(\frac{\rho_{\text{eff,BC}}(D_{\text{mob}})}{\rho_{\text{bulkBC}}} \right)^{1/3} \quad (\text{S68})$$

where ρ_{bulkBC} is the void-free material density of BC ($1'800 \text{ kg m}^{-3}$) and $\rho_{\text{eff,BC}}$ is the size-dependent effective density of the BC particles as defined in Gysel et al. (2011).

The nebulizer efficiency for BC particles, $\hat{\eta}_{\text{BC}}$, as a function of the mobility diameter of the BC core is related to the efficiency as a function of the mass equivalent diameter:

$$\hat{\eta}_{\text{BC}}(D_{\text{mob}}) = \eta_{\text{BC}} \left(D_{\text{mob}} \left(\frac{\rho_{\text{eff,BC}}(D_{\text{mob}})}{\rho_{\text{bulkBC}}} \right)^{1/3} \right) \quad (\text{S69})$$

Inserting Eq. (S69) into Eq. (S65) provides:

$$\hat{\eta}_{\text{BC}}^{\text{neb1}}(D_{\text{mob}}) = \hat{\eta}_{\text{BC}}^{\text{neb2}}(D_{\text{mob}}) \frac{\frac{dc_{\text{SP2}}^{\text{neb1}}}{d \log D} \left(D_{\text{mob}} \left(\frac{\rho_{\text{eff,BC}}(D_{\text{mob}})}{\rho_{\text{bulkBC}}} \right)^{1/3} \right)}{\frac{dc_{\text{SP2}}^{\text{APEX}}}{d \log D} \left(D_{\text{mob}} \left(\frac{\rho_{\text{eff,BC}}(D_{\text{mob}})}{\rho_{\text{bulkBC}}} \right)^{1/3} \right)} \quad (\text{S70})$$

Similar to Eq. (S66), it can be argued that

$$\hat{\eta}_{\text{BC}}^{\text{APEX}}(D_{\text{mob}}) \approx \eta_{\text{PSL}}^{\text{APEX}}(D_{\text{mob}}) \quad (\text{S71})$$

is likely fulfilled in good approximation. Combining Eqs. (S70) and (S71) provides:

$$\hat{\eta}_{\text{BC}}^{\text{neb1}}(D_{\text{mob}}) \approx \eta_{\text{PSL}}^{\text{APEX}}(D_{\text{mob}}) \frac{\frac{dc_{\text{SP2}}^{\text{neb1}}}{d \log D} \left(D_{\text{mob}} \left(\frac{\rho_{\text{eff,BC}}(D_{\text{mob}})}{\rho_{\text{bulkBC}}} \right)^{1/3} \right)}{\frac{dc_{\text{SP2}}^{\text{APEX}}}{d \log D} \left(D_{\text{mob}} \left(\frac{\rho_{\text{eff,BC}}(D_{\text{mob}})}{\rho_{\text{bulkBC}}} \right)^{1/3} \right)} \quad (\text{S72})$$

Equation (S72) can be used to determine the efficiency of any nebulizer “neb1” expressed as a function of the mobility diameter in good approximation, provided that Eq. (S71) is fulfilled and that the effective density is known for the BC sample that is used to test the nebulizers.

In this study AQ was used to determine the nebulizer efficiency for BC particles, as the effective density for AQ particles is available in the literature (Gysel et al., 2011). Equations (S67) and (S72) were then used to infer η_{BC} and $\hat{\eta}_{BC}$, respectively, for the CETAC and Collision type nebulizers (see Sect. 3.1.1 in main text).

S.3.4 Testing the approach of using standards for the CETAC nebulizer

Above it has been shown that it is, under certain circumstances, possible to use standard suspensions with known BC concentrations as a reference for the measurement of aqueous BC samples of unknown concentration (Eqs. (S35) or (S37)). Some tests to confirm the validity of this approach include e.g. the measurement of different types of BC standards or of dilution series (i.e. equal BC material but variable concentration). This has been done using CWU’s CETAC nebulizer in order to test whether or not the factor $C_{liq}^*/C_{SP2,low}^{\eta,*}$ in Eq. (S37) is independent of BC standard concentration and standard material. The results provided in the main text (Sect. 3.2) revealed considerable differences in the factor $C_{liq}^*/C_{SP2,low}^{\eta,*}$ determined with different BC standards. The reasons for this will be elucidated in the following.

From Eqs. (S14), (S32), and (S23) follows:

$$\frac{C_{liq}^*}{C_{SP2,low}^{\eta,*}} = \frac{\int_{D_{BC,min}^*}^{D_{BC,max}^*} \frac{dC_{liq}^*}{d \log D_{BC}} (D_{BC}) d \log D_{BC}}{\frac{1}{\eta_{max}^*} \int_{D_{BC,LDL}}^{D_{BC,UDL}} f_{bias}^* \eta_{BC}^* (D_{BC}) \frac{dC_{liq}^*}{d \log D_{BC}} (D_{BC}) d \log D_{BC}} \quad (S73)$$

Further inserting Eqs. (S13) and (S18) into Eq. (S73) provides:

$$\frac{C_{liq}^*}{C_{SP2,low}^{\eta,*}} = \frac{1}{f_{bias}^*} \frac{1}{\int_{D_{BC,LDL}}^{D_{BC,UDL}} \varepsilon_{loss}^* (D_{BC}) \frac{d\tilde{C}_{liq}^*}{d \log D_{BC}} (D_{BC}) d \log D_{BC}} \quad (S74)$$

3 Optimized method for BC analysis

Equation (S74) can be simplified if the losses of particles in the whole nebulizer system are independent of particle size, i.e. if:

$$\varepsilon_{\text{loss}}^*(D_{\text{BC}}) \approx \varepsilon_{\text{loss}}^* = \text{const.} \quad \forall D_{\text{BC}} \in [D_{\text{BC,LDL}}, D_{\text{BC,UDL}}] \quad (\text{S75})$$

Inserting Eq. (S75) into Eq. (S74) provides (with inserting Eq. S21):

$$\begin{aligned} \frac{C_{\text{liq}}^*}{C_{\text{SP2,low}}^{\eta,*}} &\approx \frac{1}{f_{\text{bias}}^*} \frac{1}{\varepsilon_{\text{loss}}^*} \frac{1}{\int_{D_{\text{BC,LDL}}}^{D_{\text{BC,UDL}}} \frac{d\tilde{C}_{\text{liq}}^*}{d \log D_{\text{BC}}} (D_{\text{BC}}) d \log D_{\text{BC}}} \\ &= \frac{1}{f_{\text{bias}}^*} \frac{1}{\varepsilon_{\text{loss}}^*} \frac{1}{1 - \Delta\tilde{C}_{\text{LDL}}^* - \Delta\tilde{C}_{\text{UDL}}^*} \end{aligned} \quad (\text{S76})$$

If there is no bias of the SP2 calibration for the BC type in the aqueous BC standard, one has:

$$f_{\text{bias}}^* \approx 1 \Leftrightarrow f_{\text{bias}}^{*-1} \approx 1 \quad (\text{S77})$$

If the whole BC mass size distribution of the aqueous standard falls within the detection range of the SP2, i.e. if Eq. (S30) is fulfilled for the BC standard, follows:

$$(1 - \Delta\tilde{C}_{\text{LDL}}^* - \Delta\tilde{C}_{\text{UDL}}^*)^{-1} \approx 1 \quad (\text{S78})$$

If both Eqs. (S77) and (S78) are fulfilled, then Eq. (S76) finally simplifies to:

$$\frac{C_{\text{liq}}^*}{C_{\text{SP2,low}}^{\eta,*}} \approx \frac{1}{\varepsilon_{\text{loss}}^*} \geq 1 \quad (\text{S79})$$

Equation (S79) is independent of the choice made for the type of aqueous BC standard (independence of $\varepsilon_{\text{loss}}^*$ on the type of BC is an assumption that is inherently required when working with BC standards), while this does not apply for Eqs. (S74) and (S76). This implies that applying Eq. (S37) cannot provide accurate results by using an aqueous BC standard unless the BC standard fulfills Eqs. (S77) and (S30) (i.e. there is no bias of the SP2 calibration to the BC type in the aqueous BC standard and the whole BC mass size distribution of the aqueous standard falls within the detection range of the SP2), and the nebulizer system fulfills Eq. (S75) (i.e. the nebulizer losses are independent of particle size). It further implies that Eqs. (S77) and (S30) are the only conditions to be fulfilled by an aqueous standard from a mathematical point of view (other reasons such as stability of the aqueous suspension also play a role when choosing a material for the aqueous BC standards).

Unknown sensitivity of the SP2 to the BC type of the aqueous BC standard results in an uncertainty of the magnitude f_{bias}^{*-1} (see e.g. Moteki and Kondo, 2010, and Laborde et al., 2012, for a detailed discussion of SP2 sensitivity). If the aqueous BC standard contains substantial contribution to the total BC mass from BC cores with sizes outside the detection range of the SP2 (i.e. Eq. S30 is not fulfilled for the standard), then the factor $(1 - \Delta\tilde{C}_{\text{LDL}}^* - \Delta\tilde{C}_{\text{UDL}}^*)^{-1}$ becomes greater than unity and it follows from Eq. (S76) that the BC mass concentration inferred with Eq. (S37) overestimates the true value.

Equation (S76) shows that the ratio $C_{\text{liq}}^*/C_{\text{SP2,low}}^{\eta,*}$ essentially characterizes the particle losses in the nebulizer system. However, if the particle losses in the nebulizer system depend on particle size (Eq. S75 is not fulfilled), then the ratio $C_{\text{liq}}^*/C_{\text{SP2,low}}^{\eta,*}$ contains a factor representing a “weighted average of $\varepsilon_{\text{loss}}^*(D_{\text{BC}})$ over all diameters between $D_{\text{BC,LDL}}$ and $D_{\text{BC,UDL}}$ with the shape of the BC mass size distribution of the standard as a weighting function” (see Eq. S74). The ratio $C_{\text{liq}}^*/C_{\text{SP2,low}}^{\eta,*}$ then becomes dependent on the choice of the aqueous BC standard, thereby introducing uncertainty when applying the approach of Eq. (S37). The conclusion drawn here about the factors that make the ratio $C_{\text{liq}}^*/C_{\text{SP2,low}}^{\eta,*}$ dependent on the choice of the aqueous BC standard, reflect a subset of the complete set of conditions under which the approaches of Eqs. (S35) and (S37) are valid (see earlier section).

S.4 Correct treatment of non-BC matter in BC standard materials

Not all BC materials available for preparing aqueous BC standard suspensions are pure BC. The BC mass fraction, γ_{BC}^* , of Fullerene Soot is almost 100% (Gysel et al., 2011; Moteki and Kondo, 2010), while of dried AQ particles it is only around 70.5% (this study; similar to the 76% found in Gysel et al. (2011)). This fact must be considered when working with aqueous BC standards for the quantification of BC in aqueous samples using Eqs. (S35) or (S37), specifically when determining the factor $C_{\text{liq}}^*/c_{\text{SP2}}^*$ or $C_{\text{liq}}^*/C_{\text{SP2,low}}^{\eta,*}$, respectively. Practically, this means that the BC mass concentration of an aqueous BC standard (C_{liq}^*) must be calculated from the mass concentration of water-insoluble particulate matter in an aqueous standard (M_{liq}^*):

$$C_{\text{liq}}^* = \gamma_{\text{BC}}^* M_{\text{liq}}^* \quad (\text{S80})$$

At the same time, the SP2 response to the standard particles must be calibrated for the BC mass in the particles rather than the total particle mass, i.e. when selecting the standard particles by an aerosol particle mass analyzer to provide particles of a well defined mass to the SP2 during internal calibration of the SP2 (such as e.g. described in Gysel et al., 2011). It is important to correct this nominal mass of the selected particles with the factor γ_{BC}^* in order to get the BC mass in these particles. The factor γ_{BC}^* gets cancelled in the ratio C_{liq}^*/c_{SP2}^* or $C_{liq}^*/C_{SP2,low}^{\eta,*}$ because it shows up both in the nominator and the denominator. Consequently, it is also possible to ignore the factor γ_{BC}^* for the preparation of an aqueous BC standard and in the internal SP2 calibration curve applied in the analysis of the SP2 measurement of the standard. This reflects the fact that the ratio C_{liq}^*/c_{SP2}^* or $C_{liq}^*/C_{SP2,low}^{\eta,*}$ is simply used to quantify the nebulizer efficiency for insoluble particles and it is in principle possible to use any insoluble material that is detectable by the SP2 in a quantitative manner and that fulfils the other requirements for preparing an aqueous standard. However, materials with a substantial mass fraction of water-soluble components are not suitable for preparing aqueous standards, because water-soluble matter is redistributed in an uncontrolled manner between droplets with/without insoluble inclusion, when producing an aerosol by nebulization of an aqueous suspension.

S.5 The SP2 sensitivity to different BC types and associated measurement uncertainties

The sensitivity of the SP2 to BC mass depends on the chemical structure of the BC, i.e. graphitic versus disordered. Previous studies (Laborde et al., 2012; Moteki and Kondo, 2010) indicate that the sensitivity of the SP2 to BC in diesel exhaust, wood combustion exhaust and atmospheric particles is similar to its sensitivity to fullerene soot, while it is more sensitive to AQ particles (i.e. ~40% more sensitive without accounting for the non-BC matter in AQ, ~80% more sensitive with accounting for this). Thus, fullerene soot has been recommended as an SP2 calibration material for atmospheric applications (Baumgardner et al., 2012).

The value c_{SP2} or $C_{SP2,low}^{\eta}$ in Eqs. (S35) or (S37), respectively, must always be evaluated with an SP2 calibration that matches the SP2 sensitivity to BC mass of the BC type in the sample under investigation as close as possible (i.e. in order to keep the factor f_{bias} in Eqs. (S42) or (S44) as close as possible to unity). The SP2 has a broadband and narrowband incandescence detector. The signal ratio in the two channels, commonly referred to as band ratio or colour ratio, also

differs between different BC types. Ambient BC often exhibits the same band ratio as fullerene soot, while that of AQ is different. However, the band ratio of ambient BC is occasionally more similar to that of AQ. Likewise, the band ratio of BC from ice core and snow samples sometimes resembles that of fullerene soot, sometimes that of AQ. If the band ratio of a sample under investigation differs from the band ratio of the material used for internal calibration of the SP2, then follows that applying such calibration data will result in biased BC mass measurements for at least one incandescence channel (possibly even both). Inversely, it might be interpreted as evidence that a calibration material is suitable, if its band ratio matches that of the sample under investigation, though this is not a proof. Consequently, it is suggested to apply fullerene soot calibration curves for the evaluation of aqueous samples that exhibit the same band ratio as fullerene soot. If the band ratio of an aqueous sample is more similar to that of AQ, then it is suggested to apply an AQ calibration. Whether or not to correct the AQ calibration curve for the BC mass fraction in AQ particles is difficult to answer. From a conceptual point of view this correction should be done. However, the uncorrected AQ calibration falls in between the two extremes corresponding to fullerene soot calibration and the corrected AQ calibration (which differ by 80%). Thus, applying the uncorrected AQ calibration might be better in order to keep the potential calibration bias within $\sim\pm 40\%$ if the true calibration is not really known. If the band ratio is not available or does not give any indication for the choice of the calibration material, then it is suggested to apply the fullerene soot calibration as recommended by Baumgardner et al. (2012). However, the measurement bias in such cases may be as high as 40–80%. The discussion above solely affects the choice of the internal SP2 calibration curve that is to be applied for the evaluation of the measurements of the aqueous sample, i.e. to determine C_{SP2}^{η} , c_{SP2} or $C_{SP2,low}^{\eta}$ when working with the approaches of Eqs. (S27), (S35) or (S37), respectively. However, it does not affect the choice of the BC material that is used to prepare aqueous BC standards. Any BC material with known SP2 sensitivity, which is suitable for preparing aqueous standards, can be used when working with the approaches of Eqs. (S35) or (S37), but it is important to apply the internal SP2 calibration curve for the standard material when calculating c_{SP2}^* or $C_{SP2,low}^*$, respectively, in order to keep the factor f_{bias}^* in Eqs. (S42) or (S44) as close as possible to unity (see also previous discussion above). If the SP2 sensitivity to the BC type in the standard material is not known, then a measurement uncertainty of at least 40% is introduced.

References

Baumgardner, D., Popovicheva, O., Allan, J., Bernardoni, V., Cao, J., Cavalli, F., Cozic, J., Diapouli, E., Eleftheriadis, K., Genberg, P. J., Gonzalez, C., Gysel, M., John, A., Kirchstetter, T. W., Kuhlbusch, T. A. J., Laborde, M., Lack, D., Müller, T., Niessner, R., Petzold, A., Piazzalunga, A., Putaud, J. P., Schwarz, J., Sheridan, P., Subramanian, R., Swietlicki, E., Valli, G., Vecchi, R. and Viana, M.: Soot reference materials for instrument calibration and intercomparisons: a workshop summary with recommendations, *Atmospheric Measurement Techniques*, 5(8), 1869–1887, doi:10.5194/amt-5-1869-2012, 2012.

Gysel, M., Laborde, M., Olfert, J. S., Subramanian, R. and Groehn, A. J.: Effective density of Aquadag and fullerene soot black carbon reference materials used for SP2 calibration, *Atmospheric Measurement Techniques*, 4(12), 2851–2858, doi:10.5194/amt-4-2851-2011, 2011.

Laborde, M., Mertes, P., Zieger, P., Dommen, J., Baltensperger, U. and Gysel, M.: Sensitivity of the Single Particle Soot Photometer to different black carbon types, *Atmospheric Measurement Techniques*, 5(5), 1031–1043, 2012.

Moteki, N. and Kondo, Y.: Dependence of laser-induced incandescence on physical properties of black carbon aerosols: Measurements and theoretical interpretation, *Aerosol Science and Technology*, 44(8), 663–675, 2010.

4 800 year ice-core record of nitrogen deposition in Svalbard linked to ocean productivity and biogenic emissions

I. A. Wendl^{1,2,3}, A. Eichler^{1,2}, E. Isaksson⁴, T. Martma⁵, M. Schwikowski^{1,2,3}

¹Laboratory of Radiochemistry and Environmental Chemistry, Paul Scherrer Institut, 5232 Villigen PSI, Switzerland

²Oeschger Centre for Climate Change Research, University of Bern, Switzerland

³Department of Chemistry and Biochemistry, University of Bern, Switzerland

⁴Norwegian Polar Institute, Framsenteret, 9296 Tromsø, Norway

⁵Institute of Geology, Tallinn University of Technology, Estonia

Manuscript submitted to Atmospheric Chemistry and Physics Discussions

Abstract

We present the records of the two nitrogen species nitrate (NO_3^-) and ammonium (NH_4^+) analysed in a new ice core from Lomonosovfonna, Svalbard, in the Eurasian Arctic covering the period 1222-2009. We investigate the emission sources and the influence of melt on the records. During the 20th century both records are influenced by anthropogenic pollution from Eurasia. In pre-industrial times NO_3^- is highly correlated with methane-sulphonate (MSA) on decadal time-scales, which we explain by a fertilising effect. Enhanced atmospheric NO_3^- concentrations and the corresponding nitrogen input to the ocean trigger the growth of dimethyl-sulphide-(DMS)-producing phytoplankton. Increased DMS production results in elevated fluxes to the atmosphere where it is oxidised to MSA. Eurasia was presumably the main source area also for pre-industrial NO_3^- , but a more exact source apportionment could not be performed based on our data. This is different for NH_4^+ , where biogenic ammonia (NH_3) emissions from Siberian boreal forests were identified as the dominant source of pre-industrial NH_4^+ . Changes in melt at the Lomonosovfonna glacier are excluded as major driving force for the decadal variations of the investigated compounds.

4.1 Introduction

The Arctic is generally a nutrient limited region (Dickerson, 1985). Nutrients originate from lower latitudes and reach the remote polar areas via long-range transport, local sources are sparse. The major source for bio-available nitrogen in the Arctic is the deposition of reactive atmospheric nitrogen that is present primarily as peroxyacetyl nitrate (PAN), but also as nitrate (NO_3^-) and ammonium (NH_4^+) (Björkman et al., 2013; Kühnel et al., 2012). Those species are predominantly removed from the atmosphere by wet deposition (Bergin et al., 1995). NO_3^- is the oxidation product of emitted NO_x (NO and NO_2). In general, major NO_3^- sources include biomass burning, emissions from microbial processes in soils, ammonia oxidation, stratospheric injection, lightning, as well as fossil fuel and biofuel combustion, and aircraft emissions (Fibiger et al., 2013; Galloway et al., 2004; Hastings et al., 2004; Wolff, 2013). NH_4^+ derives from biogenic emissions of ammonia (NH_3) from terrestrial and marine sources, biomass burning, agriculture, and livestock breeding (Fuhrer et al., 1996; Galloway et al., 2004; Wolff, 2013). Both NO_3^- and NH_4^+ concentrations in the atmosphere have varied greatly with time and space due to changing emissions and the short atmospheric lifetimes of a few days (Adams et al., 1999; Feng and Penner, 2007). Generally, concentrations were low in pre-industrial times and increased due to stronger emissions with beginning of the industrialisation and intensification of agricultural activities (Galloway et al., 2004). The deposition of NO_3^- and NH_4^+ in the Arctic is an important

nutrient source. Varying concentrations thus greatly affect the nitrogen budget in the Arctic where nutrient supply is limited.

Ice cores represent an invaluable archive of past atmospheric composition. Ice core studies from the Arctic clearly reveal an anthropogenic influence on the concentrations of NO_3^- and NH_4^+ approximately during the last 150 years (Fischer et al., 1998; Fuhrer et al., 1996; Goto-Azuma and Koerner, 2001; Kekonen et al., 2002, 2005; Legrand and Mayewski, 1997; Matoba et al., 2002; Simões and Zagorodnov, 2001). North America was identified as major pollutant source for south Greenland, both North America and Eurasia for central and north Greenland, and Eurasia for Svalbard (Goto-Azuma and Koerner, 2001; Hicks and Isaksson, 2006). However, the pre-industrial sources of NO_3^- and NH_4^+ are still fairly unknown (Legrand and Mayewski, 1997; Wolff, 2013). Eichler et al. (2011) identified forest fires as major source of NO_3^- in a Siberian Altai ice core from the mid-latitudes. In studies on Greenland ice NO_3^- was also associated with forest fires (Whitlow et al., 1994; Wolff et al., 2008). Pre-industrial NH_4^+ in ice cores from the mid-latitudes was attributed to biogenic emissions (Eichler et al., 2009; Kellerhals et al., 2010). Similarly, long-term trends in Greenland ice cores have been attributed to changing biogenic emission from North America, whereas short-term NH_4^+ changes were found to correlate with forest fires (Fuhrer et al., 1996; Whitlow et al., 1994; Zennaro et al., 2014).

Whereas a few records exist from Greenland, there is less information available from the Eurasian Arctic. The NO_3^- and NH_4^+ records of a previous ice core from Lomonosovfonna, Svalbard, retrieved in 1997 (Lomo97, for location see Figure 4.1), cover the last 1000 years (Divine et al., 2011; Kekonen et al., 2002, 2005). For both species a clear anthropogenic impact is observed in the second half of the 20th century, but the pre-industrial sources remain largely unidentified due to potential runoff that biased the ion records before the mid-16th century (Kekonen et al., 2002, 2005). Nevertheless, the fairly stable concentrations in the NO_3^- record from the mid-16th to the mid-19th century are interpreted as input from natural NO_3^- sources (Kekonen et al., 2002). An anthropogenic influence in the 20th century is also visible in the NO_3^- and NH_4^+ records of other Eurasian Arctic ice cores (see Figure 4.1 for locations) from Høltedahlfonna (Holte05), Svalbard (Beaudon et al., 2013), Snøfjellaafonna, Svalbard (Goto-Azuma and Koerner, 2001), and Severnaya Zemlya (Weiler et al., 2005). The industrial records from these cores are discussed in detail, but pre-industrial sources and concentration changes of the inorganic nitrogen species remain unexplained.

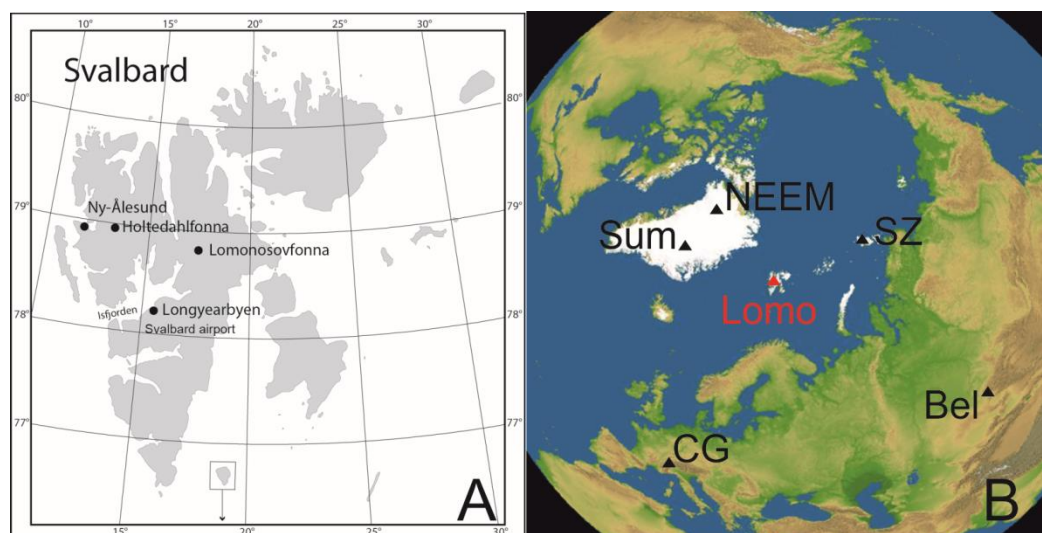


Figure 4.1 (A) Map of Svalbard with the locations of Lomonosovfonna and Holtedahlfonna. (B) Map with all ice core locations discussed in the text: Lomo = Lomonosovfonna (red triangle); NEEM, Sum = Summit, SZ = Severnaya Zemlya, Bel = Belukha, and CG = Colle Gnifetti (black triangles). Satellite image in (B) © PlanetObserver, extracted from DVD-ROM "Der Große 3D-Globus 4.0 Premium," #2008 United Soft Media Verlag GmbH, Munich.

The interpretation of NO_3^- and NH_4^+ as paleo-environmental proxies may be hampered by the fact that both undergo post-depositional processes leading to loss from or relocation within the snow pack even at temperatures well below the melting point (Pohjola et al., 2002). NO_3^- can be relocated or lost by photolysis and/or evaporation of nitric acid (HNO_3) (Honrath et al., 1999; Röthlisberger et al., 2002). This loss can be severe at low accumulation sites such as Dome C, Antarctica (Röthlisberger et al., 2000, 2002). At sites with higher accumulation rates such as Summit in Greenland or Weissfluhjoch in the European Alps the majority of NO_3^- is preserved (Baltensperger et al., 1993; Fibiger et al., 2013). Many studies reveal that NH_4^+ and NO_3^- are preserved in snow and firn cores with respect to percolating melt water (Eichler et al., 2001; Ginot et al., 2010; Moore and Grinsted, 2009; Pohjola et al., 2002), but others report a preferential elution of these species compared to other major ions (Brimblecombe et al., 1985; Moore and Grinsted, 2009; Pohjola et al., 2002). The underlying mechanism is not well understood, except from the fact that it depends on the overall ion composition.

In this paper we discuss the records of the two nitrogen species NO_3^- and NH_4^+ analysed in a new ice core drilled on Lomonosovfonna, Svalbard, in 2009. The study focuses on the investigation of the major sources of NO_3^- and NH_4^+ deposited in the Eurasian Arctic which highly affects the nutrient budget in the region, along with the effect of melt on the geochemical records of these nitrogen species which will gain importance due to the ongoing global warming.

4.2 Methods

4.2.1 Drilling site and meteorological setting

In 2009, a 149.5 m long ice core was drilled on Lomonosovfonna, Svalbard (1202 m asl; 78°49'24"N, 17°25'59"E), using the Fast Electromechanical Lightweight Ice Coring System (FELICS) (Ginot et al., 2002). The 2009 drilling site is 4.6 km south of that in 1997 (Isaksson et al., 2001). Bedrock was not reached but a radar survey suggested it to be at around 200 m (Pettersson, unpublished data). Svalbard is located at a climatically sensitive area being surrounded by the Arctic Ocean, the Barents Sea and the Atlantic Ocean, and situated at the southerly edge of the permanent Arctic sea ice and close to the over-turning point of the North Atlantic thermohaline circulation. Further, it is relatively close to the industrialised areas of Eurasia which were found to highly affect the chemical composition of air reaching the archipelago, especially in spring during the Arctic Haze (Eleftheriadis et al., 2009; Eneroth et al., 2003; Forsström et al., 2009; Goto-Azuma and Koerner, 2001; Law and Stohl, 2007; Stohl et al., 2007). The Arctic Haze describes a phenomenon of increased aerosol concentration in the end of winter to early spring (Greenaway, 1950; Quinn et al., 2007; Shaw, 1995). At that time of the year temperatures in the Arctic become very low which leads to a thermally very stable stratification with strong surface inversions (Shaw, 1995; Stohl, 2006). This cold stratified air forms a dome over the Arctic that hinders warm air masses from lower latitudes to enter. The boundary of this dome that acts as a transport barrier is called Arctic or Polar Front whose position shifts between summer and winter due to temperature. In summer only the more northern parts of the Northern Hemisphere are cold enough to cause a stable stratification of the atmosphere, whereas in winter temperatures in more southern parts are cold enough so that the Arctic Front is located as far south as 40°N. Then large areas of Eurasia and partly North America are included in the Arctic dome, facilitating transport of pollution from those regions. In addition, since both dry and wet deposition is reduced within the Arctic dome in winter, aerosols have very long lifetimes once within the Arctic dome (Stohl, 2006).

4.2.2 Sampling and analyses

The Lomonosovfonna 2009 ice core (Lomo09) was processed in the cold room (-20°C) at Paul Scherrer Institut, Switzerland, resulting in 3997 samples with a depth resolution of 3-4 cm (details on the method in Eichler et al., 2000). The resolution was adapted to layer thinning with depth, so that even in the deepest and oldest part of the core each year is at least represented by one sample. The inner part of the core was sampled for the analysis of water soluble major ions and the water stable isotopes $\delta^{18}\text{O}$ and δD . Outer core sections were analysed for ^3H and ^{210}Pb used for dating purposes (Eichler et al., 2000).

Concentrations of water soluble major ions, including NO_3^- and NH_4^+ , were determined using ion chromatography (Metrohm 850 Professional IC combined with a 872 Extension Module and a 858 Professional Sample Processor autosampler). A list of the measured ionic species, their detection limits and median concentrations are given in Table 4.1. Values were not blank corrected.

Table 4.1 Detection limits and median values [$\mu\text{eq/L}$] for the ions analysed with the Metrohm 850 Professional IC. Pre-ind. = pre-industrial time from 1222-1859; Ind. = industrial time from 1860-2009; MSA = CH_3SO_3^- .

Anions	Detection limit	Median		Cations	Detection limit	Median	
		Pre-ind.	Ind.			Pre-ind.	Ind.
MSA	0.005	0.09	0.05	Na⁺	0.02	8.77	7.18
Cl⁻	0.02	10.48	8.92	NH₄⁺	0.02	0.50	0.74
NO₃⁻	0.01	0.54	0.65	K⁺	0.02	0.25	0.19
SO₄²⁻	0.02	2.08	2.63	Mg²⁺	0.03	2.10	1.32
				Ca²⁺	0.04	1.43	1.02

4.2.3 Ice-core dating

The Lomo09 ice core covers the time period of 1222 to 2009 (Figure 4.2). It was dated with a combination of reference horizons, annual layer counting (ALC), ^{210}Pb decay, and a simple glacier flow model. The reference horizons include the tritium peak indicating the year 1963, and the major volcanic eruptions of Bezymianny (1956), Katmai (1912), Tambora (1815), Laki (1783), Hekla (1766), Kuwae (1458/59; Sigl et al., 2013), and Samalas (1257/58; Lavigne et al., 2013) marked by high non-sea-salt sulphate concentrations and high values for the sulphate-residual of the multiple linear regression of all measured ions, a method previously described in Moore et al. (2012). Annual layer counting was performed down to a depth of ~ 79.7 m weq (= 1750) using the pronounced seasonality of $\delta^{18}\text{O}$ and Na^+ (Figure S4-1). A simple glacier flow model (Thompson et al., 1998) was fitted through the volcanic reference horizons. This was used to date the core below ~ 79.7 m weq where ALC was limited due to strong layer thinning. The dating uncertainty for the core down to a depth of ~ 68 m weq is estimated to be ± 1 year within ± 10 years of the reference horizons and increases to ± 3 years in between. Down to a depth of ~ 80 m weq the dating uncertainty enlarges to ± 3 years also in proximity of the reference horizons, and below ~ 80 m weq it increases to ± 10 years. This was calculated using

the difference of the year of the volcanic eruptions and the modelled date. The average annual accumulation rate is 0.58 ± 0.13 m weq.

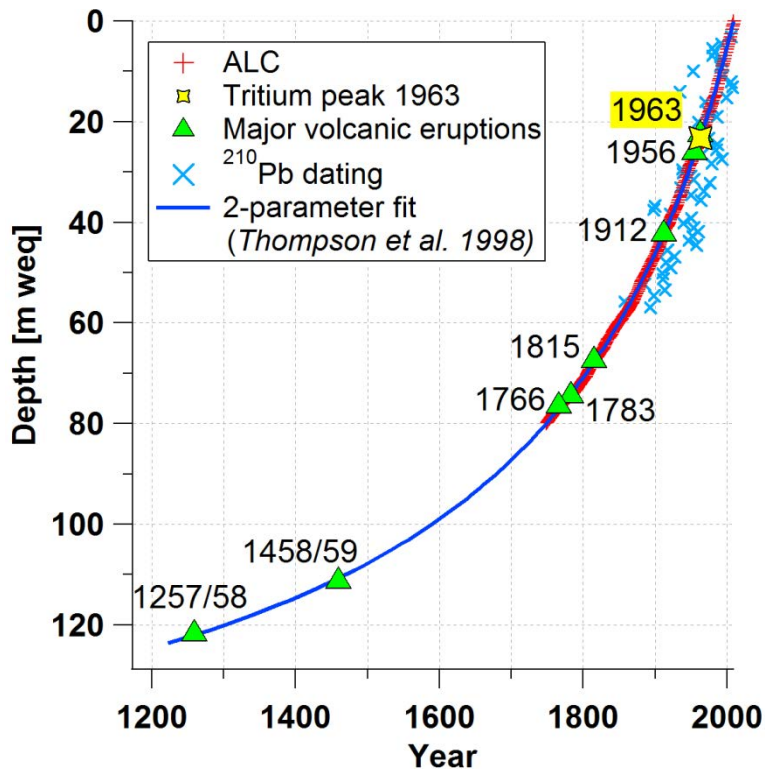


Figure 4.2 Depth-age relationship of the Lomo09 ice core showing all dating methods applied. Depth is given in m weq to account for density variation.

4.2.4 Calculation of annual melt percent

Melt features are formed when surface snow melts and the melt water percolates into deeper layers where it fills the pores and refreezes under the formation of a layer of ice poor or free of air bubbles. The percentage of annual melt in the Lomo09 core was calculated from the thickness of melt features observed during processing of the core (similar to Henderson et al., 2006). Clear and bubbly ice appears as transparent area when the core is backlit. If the melt did not affect the whole core diameter, this was accounted for by multiplying the length of the melt feature with the percentage of the core diameter it covered. If for example a melt feature was 20 cm long but only affected one fifth of the core diameter, this melt feature would count the same as a four centimetre long melt feature affecting the whole core diameter. The observed melt features were then summed up per year to calculate the annual melt percent.

4.3 Results and discussion

The records of NO_3^- and NH_4^+ of the Lomo09 core both show the highest concentrations during the period of approximately 1940 to 1980 (Figure 4.3), similar to findings from other Arctic

sites (Goto-Azuma and Koerner, 2001). This clearly indicates a strong influence of anthropogenic emissions in recent decades on the chemical composition of aerosols reaching Lomonosovfonna. Both records show a significant decrease after 1980, a trend similarly observed in the NO_3^- and NH_4^+ records of ice cores from the Siberian Altai (Eichler et al., 2009, 2011) (Figure 4.4) and Severnaya Zemlya (Opel et al., 2013; Weiler et al., 2005) influenced mainly by Eurasian pollution. In contrast, NO_3^- concentrations in records from Summit, Greenland, and Colle Gnifetti, Swiss Alps (see Figure 4.1 for locations), affected by Northern American and Western European air masses, respectively, kept rising into the 21st century (Figure 4.4). This suggests that the major sources for the increased concentrations of NO_3^- and NH_4^+ in the Lomo09 core are similar to those for the Siberian Altai and Severnaya Zemlya, whereas the influence of emissions in North America and Europe is of minor importance. We thus attribute the observed trend in NO_3^- to higher NO_x emissions from traffic, energy production, and industrial activities, and in NH_4^+ to enhanced NH_3 emissions from agriculture and livestock mainly in Eurasia (Eichler et al., 2009; Weiler et al., 2005). The anthropogenic impact is also seen in the NO_3^- and- less pronounced- in the NH_4^+ record of the Lomo97 core (Divine et al., 2011; Kekonen et al., 2005) (Figure 4.3), which underlines the spatial representativeness of the Lomo09 ice core data. The NO_3^- records of the Lomo09 and Lomo97 cores agree well. This is not the case for the NH_4^+ records, where the Lomo97 shows higher concentrations, especially before 1900 (Figure 4.3). We cannot explain this difference, but NH_4^+ is known to be prone to contamination during analysis (Jauhiainen et al., 1999; Kaufmann et al., 2010; Legrand et al., 1984, 1993, 1999; Udisti et al., 1994). The 300 year records of NO_3^- and NH_4^+ from Holtedahlfonna (Beaudon et al., 2013) are in reasonable agreement with the Lomo09 data (Figure 4.3).

In order to investigate sources of NH_4^+ and NO_3^- and other ionic species in the Lomo09 ice core we performed a principal component analysis (PCA). We used 10-year-averages to account for dating uncertainties and smoothing effects by melt-water relocation. Previous studies on the Lomo97 core suggested that the percolation lengths at the site can reach two to eight annual layers in the warmest years (Moore et al., 2005; Pohjola et al., 2002). Additionally, we included the 10-year-average record of melt percent in the PCA to examine the influence of melt on the NH_4^+ and NO_3^- records. The PCA was performed only for pre-industrial times (1222-1859) to exclude anthropogenic influences on the ion concentrations. Sulphate (SO_4^{2-}) from anthropogenic sources has been shown to increase already during the second half of the 19th century (Moore et al., 2006).

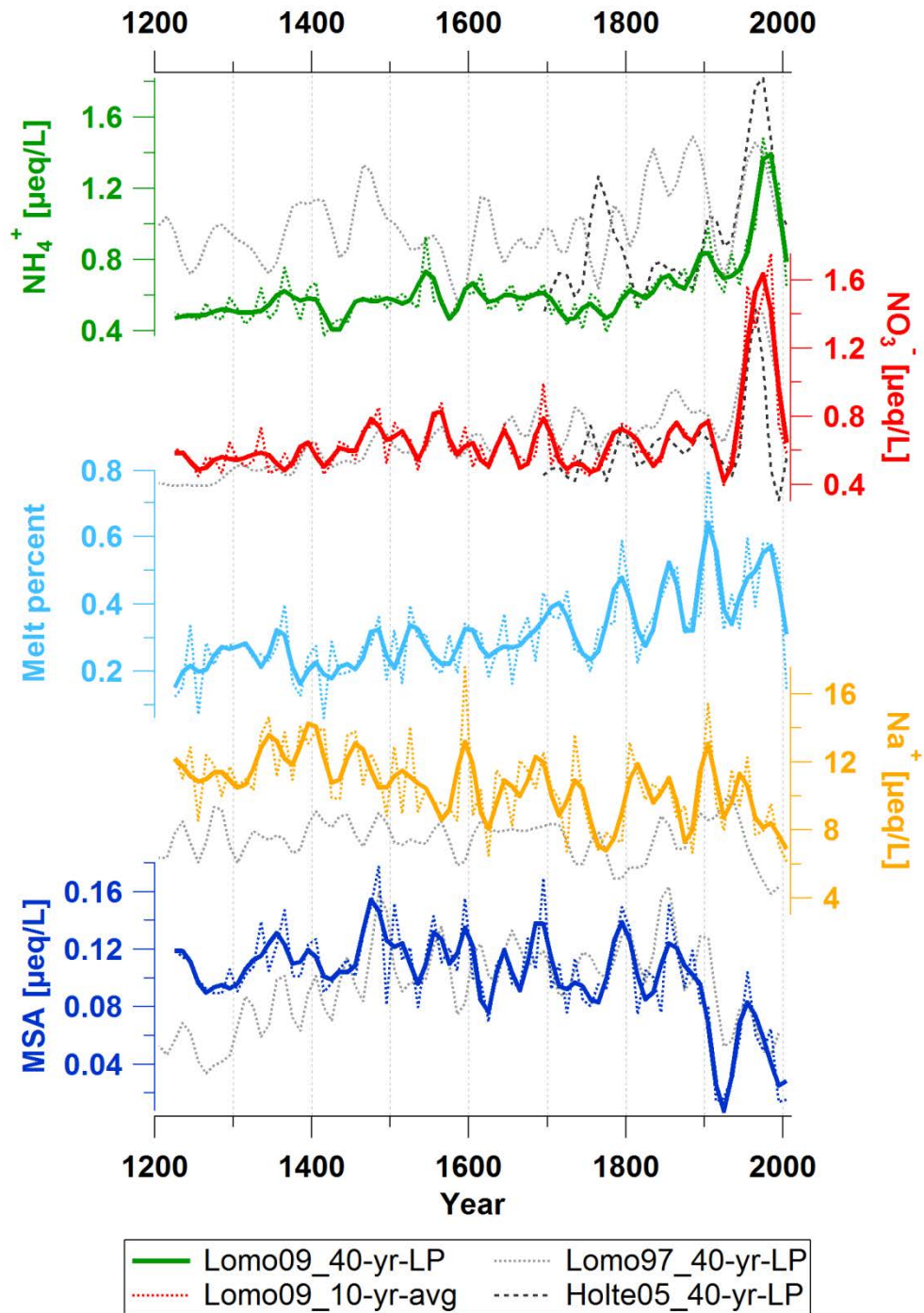


Figure 4.3 Records of NH_4^+ (green), NO_3^- (red), melt percent (light blue), Na^+ (yellow), and MSA (dark blue) of the Lomo09 ice core. Bold lines are 40-year-lowpass-filtered (40-yr-LP); dashed lines are 10-year averages (10-yr-avg). Raw data are available in the supplementary material (Figures S4-2 and S4-3). Grey dashed lines are 40-year-lowpass-filtered records of NH_4^+ , NO_3^- , Na^+ , and MSA of the Lomo97 ice core (Kekonen et al., 2005) calculated with the updated chronology of Divine et al. (2011). Black dashed lines are 40-year-lowpass-filtered records of NH_4^+ and NO_3^- of the Holte05 ice core (Beaudon et al., 2013).

We obtained six principal components (PCs) from the PCA (Table 4.2). PC1 has high loadings of sodium (Na^+), potassium (K^+), magnesium (Mg^{2+}), and chloride (Cl^-). This component explains 38% of the total variance and contains species that are directly emitted by sea spray. PC2 has

high loadings of methane-sulphonate ($\text{MSA} = \text{CH}_3\text{SO}_3^-$) and NO_3^- . MSA has a strictly marine biogenic source. It results from the oxidation of gaseous dimethyl-sulphide (DMS) which is produced by phytoplankton and emitted from the ocean to the atmosphere. This gas release across the sea-air interface differs distinctly from the way sea salt species are emitted to the atmosphere via sea spray because no droplets are involved (Stefels et al., 2007; Vogt and Liss, 2009). PC3 has a high loading of NH_4^+ , representing biogenic emissions. Calcium (Ca^{2+}) is the only species that has a high loading in PC4. This suggests that PC4 represents a mineral dust component. The melt percent is the only parameter that has a high loading in PC5. This shows that decadal ion concentration averages are not influenced by melt, which is in agreement with Pohjola et al. (2002) and Moore et al. (2005). PC6 has a high loading of SO_4^{2-} , indicating a volcanic source because the marine part of SO_4^{2-} is covered by the sea spray component PC1.

Table 4.2 Results of the principal component analysis (PCA) after VARIMAX rotation. Time period: 1222-1859; data: 10-year averages; MSA = CH_3SO_3^- ; melt% = melt percent. Values >0.8 marked in bold.

	PC1	PC2	PC3	PC4	PC5	PC6
Na⁺	0.97	0.06	0.05	0.11	-0.03	0.08
K⁺	0.88	0.18	0.00	-0.04	-0.07	0.16
Mg²⁺	0.82	0.37	0.02	0.27	0.07	0.19
Cl⁻	0.97	0.08	0.06	0.12	0.01	0.08
MSA	0.33	0.80	0.13	0.22	0.23	0.11
NO₃⁻	0.11	0.89	0.22	0.16	0.09	0.22
NH₄⁺	0.06	0.23	0.96	-0.02	0.17	0.02
Ca²⁺	0.18	0.27	-0.02	0.92	0.07	0.19
Melt%	-0.05	0.19	0.16	0.07	0.96	0.07
SO₄²⁻	0.29	0.28	0.02	0.21	0.08	0.88
Variance explained [%]	38	19	11	11	11	10

The results of the PCA are in good correspondence with those of a correlation analysis of the 10-year-averaged records of the ionic species and the melt percent for the pre-industrial period (Table 4.3). Strong correlation is observed for the sea spray related ions Na^+ , K^+ , Mg^{2+} , and Cl^- ($0.59 < r^2 < 0.98$). Furthermore, MSA and NO_3^- are highly correlated and share 60% of data variability. NH_4^+ , Ca^{2+} , melt percent and SO_4^{2-} are not significantly correlated with any other species.

Table 4.3 R² values of the correlation analysis of the ionic species and the melt percent (Melt%). Time period: 1222-1859; data: 10-year averages; MSA = CH₃SO₃⁻; 0.5 < r² < 1 marked in bold.

r ²	Na ⁺	K ⁺	Mg ²⁺	Cl ⁻	MSA	NO ₃ ⁻	NH ₄ ⁺	Ca ²⁺	Melt%	SO ₄ ²⁻
Na ⁺	1									
K ⁺	0.71	1								
Mg ²⁺	0.71	0.59	1							
Cl ⁻	0.98	0.67	0.78	1						
MSA	0.17	0.16	0.41	0.20	1					
NO ₃ ⁻	0.04	0.08	0.27	0.06	0.60	1				
NH ₄ ⁺	0.01	0.01	0.03	0.02	0.14	0.19	1			
Ca ²⁺	0.09	0.06	0.27	0.10	0.26	0.21	0.00	1		
Melt%	0.00	0.00	0.02	0.00	0.15	0.11	0.13	0.04	1	
SO ₄ ²⁻	0.16	0.18	0.33	0.17	0.26	0.26	0.02	0.24	0.04	1

4.3.1 Nitrate and methane-sulphonate (NO₃⁻ and MSA)

In the Lomo09 ice core NO₃⁻ is highly correlated with MSA before around 1900. The records (Figures 4.3 and 4.5) are similar with shared peaks around 1395, 1475, 1560, 1645, 1695, and 1795. After around 1900 there is a decoupling of both species with enhanced NO₃⁻ concentrations from anthropogenic Eurasian NO_x emissions (see above) and strongly decreased MSA concentrations. Whereas marine biogenic sources for MSA in the Arctic are well known (Legrand, 1997), major pre-industrial NO₃⁻ sources in this region are still not fully understood (e.g., Wolff et al., 2008).

Varying atmospheric MSA concentrations have been related to changing sea ice conditions. Studies from Arctic and Antarctic ice cores found positive (Becagli et al., 2009; Legrand et al., 1997), but also negative correlations of MSA and sea ice extent (Rhodes et al., 2009; Sharma et al., 2012). After 1920 the Lomo97 core MSA correlates negatively with summer (August) sea-ice extent and sea surface temperature in the Barents Sea (O'Dwyer et al., 2000) and positively with the instrumental summer temperature record from Svalbard (Isaksson et al., 2005). During the period 1600-1920 Isaksson et al. (2005) detected a positive correlation of the Lomo97 MSA and winter (April) sea ice extent in the Barents Sea (Divine and Dick, 2006; Vinje, 2001). The Lomo97 MSA record reveals a pattern with twice as high values prior to about 1920 compared

to those of the later 20th century (Isaksson et al., 2005). They suggest that it results from a change of source and/or more favourable growing conditions for the DMS-producing phytoplankton in a more extensive sea ice environment before 1920.

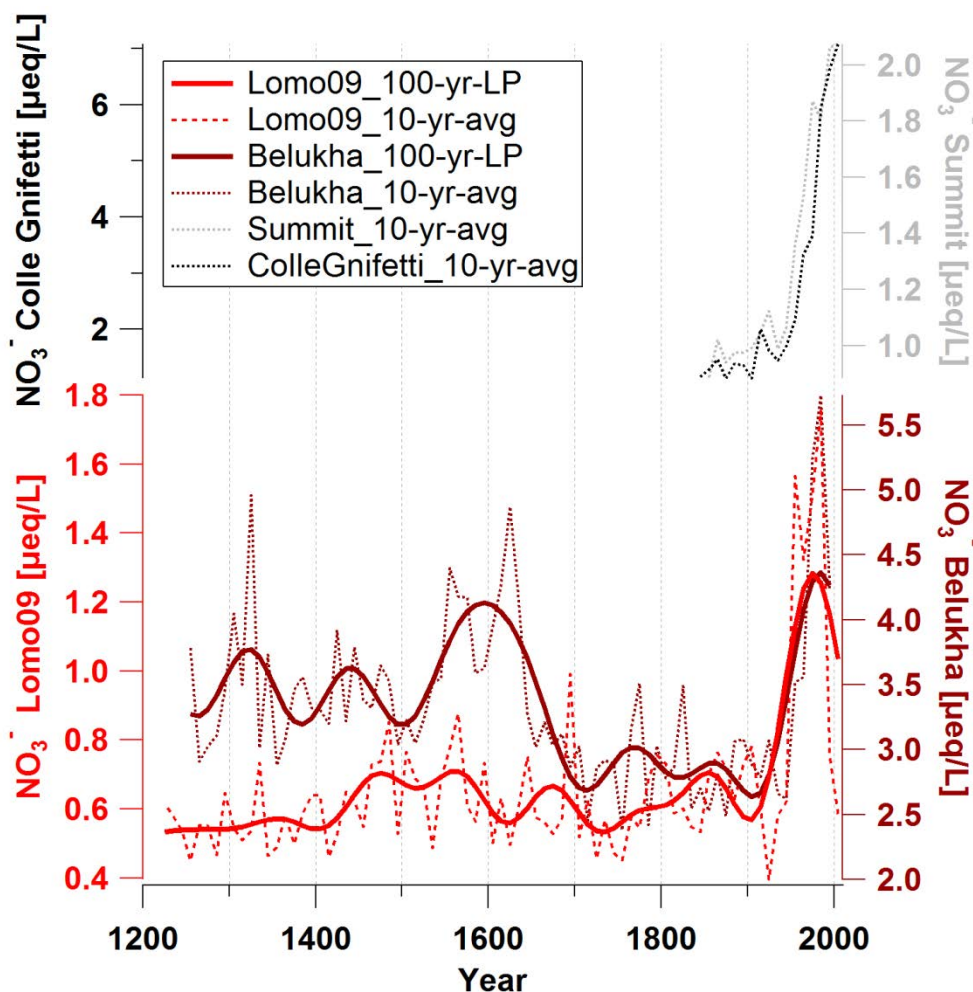


Figure 4.4 NO_3^- records from Lomo09 (red), Belukha (dark red; Eichler et al., 2009), Summit, Greenland (grey; Geng et al., 2014), and Colle Gnifetti, Swiss Alps (black; Sigl, 2009). Bold lines are 100-year-lowpass-filtered (100-yr-LP); dashed lines are 10-year averages (10-yr-avg).

In the MSA record of the Lomo09 core we find a similar pattern as in the Lomo97 core with higher concentrations prior to the 20th century and a decreasing trend since around 1900 (Figures 4.3 and 4.5). Hence, we investigate if a coupling of MSA with sea ice conditions around Svalbard exists, using three long-term reconstructions of sea ice extent. These reconstructions include the winter (April) ice extent in the Western Nordic Seas covering the last 800 years (Macias Fauria et al., 2010), the summer (August) location of the sea ice edge in the Barents Sea (BS) that covers the last 400 years (Kinnard et al., 2011), and the summer sea ice extent in the Arctic Seas extending back to the year 563 (Kinnard et al., 2011). The best agreement was observed between the 40-year-lowpass-filtered records of Lomo09 MSA and winter (April) Western Nordic Seas ice extent (Macias Fauria et al., 2010) (Figure 4.5; $r=0.56$, $p<0.001$). The

most striking feature in both records is the pronounced decrease starting around 1890 which is not seen in any of the summer (August) ice records before around 1910 (Figure 4.5). Furthermore, the pronounced minimum around 1710 and the peak around 1640 in the BS ice record are not reflected in the Lomo09 MSA record. Thus, our data do not support the connection of MSA at Lomonosovfonna and the BS ice extent stated in O'Dwyer et al. (2000) for the period 1920-1997, nor the assumption of Isaksson et al. (2005) that the MSA sources prior and after 1920 were the same, i.e. the BS. We explain the positive correlation of Lomo09 MSA and Western Nordic Sea ice extent as follows. The marginal ice zone is known to be the area of highest DMS production (Perrette et al., 2011). The larger the sea ice area, the more ice edge area is available for phytoplankton growth and thus DMS production. Furthermore, more ice leads to higher freshwater inflow by melting ice. This results in a stronger stratification of the ocean water (Perrette et al., 2011) which keeps the phytoplankton in the euphotic zone. The good correspondence of the Lomo09 MSA record with the Western Nordic Sea ice extent but not with that of the BS is well supported by the findings of Beaudon et al. (2013) pointing to the Greenland Sea as the main source for biogenic related MSA in Svalbard.

The sources of pre-industrial NO_3^- in the Arctic are not well understood. In previous studies NO_3^- was found to correlate with non-sea-salt- Ca^{2+} (nss- Ca^{2+}) (Legrand et al., 1999; Röthlisberger et al., 2000, 2002), suggesting that nss- Ca^{2+} prevents NO_3^- from being re-emitted from the snowpack. However, those studies are from Greenland, consider glacial timescales, and include e.g. the last glacial maximum (LGM) with much higher nss- Ca^{2+} concentrations. Other studies observed a correlation of NO_3^- and Ca^{2+} in summer and with sea salt in winter but they considered only industrial times (Beine et al., 2003; Geng et al., 2010; Teinilä et al., 2003). The empirical orthogonal function (EOF) analysis performed on the ion data of the Lomo97 core suggests in general no correlation between Ca^{2+} and NO_3^- , but in some parts of the last 200 years the two species are clearly associated (Kekonen et al., 2002). Kekonen et al. (2002) found NO_3^- and NH_4^+ to covariate during the last 100 years. However, the EOF of the whole core did not show a clear association of NH_4^+ and NO_3^- . Nevertheless, they suggested that before 1920 and after 1960 ammonium nitrate (NH_4NO_3) has been common at Lomonosovfonna. They explain this in recent years to be due to Arctic Haze and significant natural sources of NH_4NO_3 during the earlier period. At Holtedahlfonna, Svalbard, NH_4^+ was also associated with NO_3^- before 1880 which Beaudon et al. (2013) interpreted as evidence for NH_4NO_3 to be present. Teinilä et al. (2003) also discovered a correlation of NO_3^- and NH_4^+ in recent times which they concluded to result from anthropogenic emissions. Our data neither support a correlation of NO_3^- and Ca^{2+} , nor of NO_3^- and the sea salt species Na^+ , nor of NO_3^- and NH_4^+ in pre-industrial times. Instead, they clearly suggest an association of NO_3^- with MSA. Three hypotheses for the high correlation

are discussed: (1) post-depositional processes caused by melt water percolation affecting NO_3^- and MSA in the same way, (2) a common source of NO_3^- and MSA, and (3) NO_3^- fertilisation of the ocean which triggers phytoplankton growth and thus DMS and MSA formation.

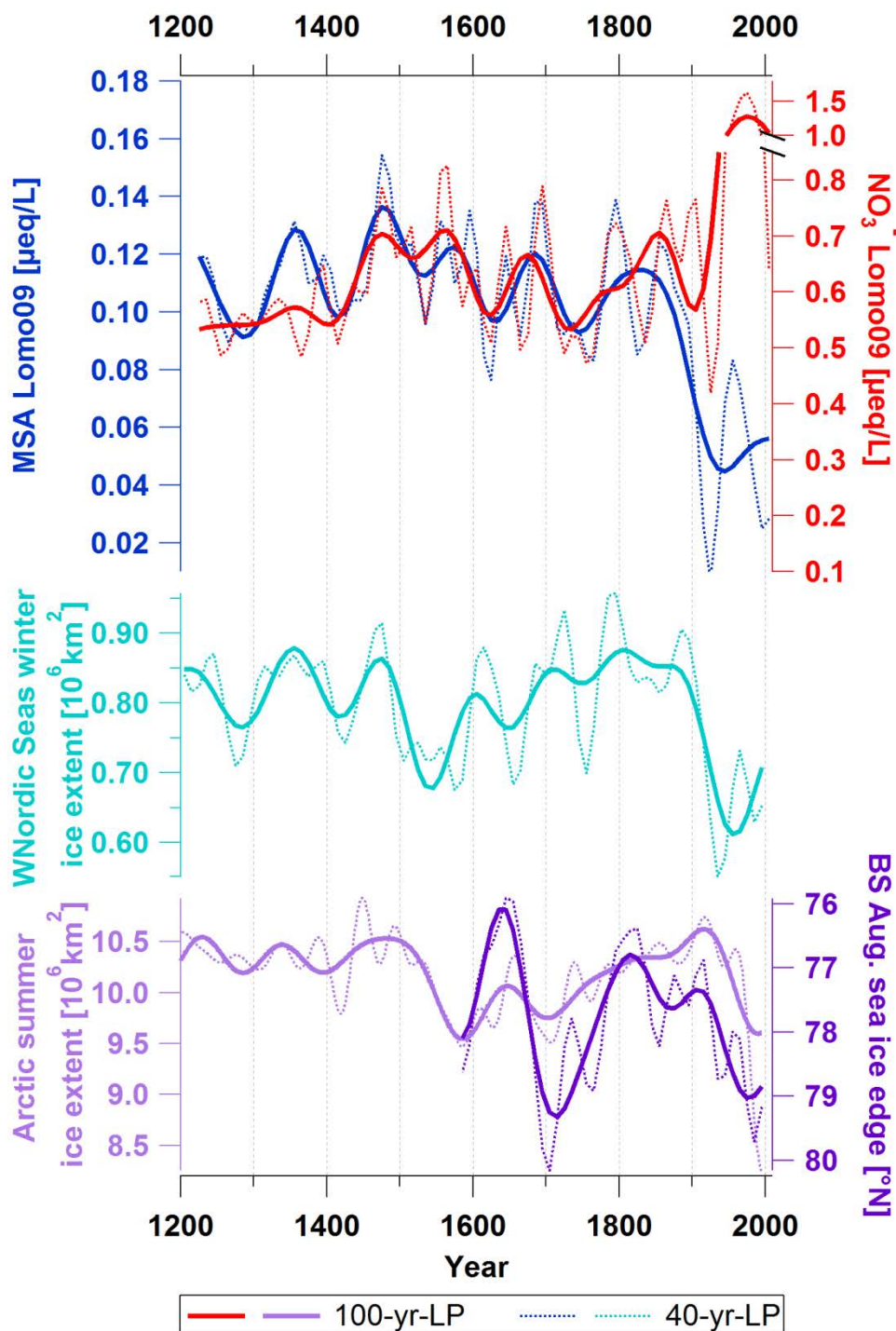


Figure 4.5 Records of Lomo09 MSA (dark blue), pre-industrial NO_3^- (red), Western Nordic Seas winter (April) ice extent (turquoise; Macias Fauria et al., 2010), Arctic summer (August) sea ice extent (light purple; Kinnard et al., 2011), and August sea ice edge position in the Barents Sea (BS; dark purple; Kinnard et al., 2011). Bold lines are 100-year-lowpass-filtered (100-yr-LP); dashed lines are 40-year-lowpass-filtered (40-yr-LP).

(1) The pre-industrial record of the melt percent does share some features with NO_3^- and MSA but there is no significant correlation with NO_3^- or MSA ($r^2=0.1$ with either NO_3^- or MSA) (Table 4.3, Figure 4.3). This is also seen in the PCA where the melt percent and the two ionic species have their highest loadings in different PCs (Table 4.2). Thus, the correlation of NO_3^- and MSA is not a result of similar relocation during melt events on the decadal time scales considered here.

(2) If both species have a common source this would have to be the ocean because MSA results only from marine DMS production and its oxidation in the atmosphere. NO_3^- is only a minor component in sea water with concentrations in the micro-molar range (Chester and Jickells, 2012; Codispoti et al., 2013). The ice core $\text{NO}_3^-/\text{Na}^+$ ratio of ~ 0.066 in the Lomo09 core is up to a factor of ten higher than the sea water ratio of 0.006 to 0.038 (Keene et al., 1986). Additionally, we can exclude NO_3^- to be derived from sea spray because NO_3^- and the major sea spray components Na^+ , K^+ , Mg^{2+} , and Cl^- (PC1) do not correlate as seen in the PCA and the correlation analysis (Tables 4.2 and 4.3). Thus, the major NO_3^- source is not the ocean which excludes a common source to cause the strong correlation of NO_3^- and MSA.

(3) Elevated atmospheric NO_3^- concentrations due to high NO_x emissions and/or enhanced transport to the Arctic in the end of winter lead to an increased amount of NO_3^- dissolved in the ocean surface water. Nutrient supply in the Arctic is known to be limited and nitrate depletion is common during the vegetative season (Codispoti et al., 2013). Hence, an increased nitrogen input by dissolved NO_3^- leads to a fertilisation of the phytoplankton (Duce et al., 2008). As soon as light becomes available this results in an enhanced production of DMS and finally higher MSA concentrations in the atmosphere. This process takes weeks to months (Codispoti et al., 2013; Sharma et al., 2012). However, such a potential short time lag cannot be resolved from our data.

We suggest the fertilising effect to be the dominant cause for the high correlation of NO_3^- and MSA in pre-industrial times. In industrial times the records of NO_3^- and MSA diverge with increasing NO_3^- and decreasing MSA concentrations. This reveals that during the 20th century the effect of decreasing MSA concentrations following reduction in ice extent in the Western Nordic Seas predominates compared to an expected MSA increase caused by enhanced anthropogenic NO_3^- levels.

The major NO_3^- source region for the industrial time is Eurasia indicated by the similarity of the NO_3^- records observed in the last 30-40 years in the ice cores from Lomo09, the Siberian Altai, and Severnaya Zemlya (Eichler et al., 2009; Weiler et al., 2005) (Figure 4.4). We assume that the source region has not changed from pre-industrial to industrial times. In the period 1250-1940 NO_3^- in the Siberian Altai ice core was ascribed to forest fires and mineral dust as main pre-

industrial sources (Eichler et al., 2011). That NO_3^- record shows a maximum between 1540 and 1680 (see Figure 4.4), attributed to an increased mineral dust input from Central Asian deserts (1540-1600) and enhanced fire activity from Siberian boreal forests (1600-1680). This distinct peak in the 16th and 17th century is not observed in the Lomo09 NO_3^- record and also the general pre-industrial records do not correspond well. We cannot exclude that other regional scale NO_3^- sources in Eurasia had a significant impact on the low pre-industrial concentration level. From our data we can therefore not identify major pre-industrial NO_3^- sources for the Lomo09 core.

4.3.2 Ammonium (NH_4^+)

The Lomo09 NH_4^+ record shows very low concentrations between the 13th and 18th century and an increasing trend from around 1750 onwards (Figure 4.6). The values are on the same order of magnitude as those from other Arctic sites and the Lomo97 ice core (Beaudon et al., 2013; Fuhrer et al., 1996; Kehrwald et al., 2012; Kekonen et al., 2005; Legrand and De Angelis, 1996; Legrand et al., 1992; Whitlow et al., 1994; Zennaro et al., 2014). Another Svalbard core from Høltedahlfonna that spans the last 300 years shows similarly a strong increasing trend in the NH_4^+ record from the 18th century on (Beaudon et al., 2013) (Figure 4.3). The authors interpret the rising concentrations from 1880 as result of anthropogenic mid-latitude pollution reaching the Arctic. However, the earlier increase in NH_4^+ concentrations in the Lomo09 and Holte05 ice core from the 18th century on cannot be related to anthropogenic emissions. As discussed above, anthropogenic NH_3 emissions from Eurasia influence precipitation chemistry in Svalbard only after around 1940.

Pre-industrial NH_4^+ was not studied in details in the Lomo97 core but Kekonen et al. (2002) suggested NH_4NO_3 to have been common at Lomonosovfonna before 1920. Similarly, Beaudon et al. (2013) postulated that at Høltedahlfonna natural NH_4NO_3 was a common aerosol. Our data do not support this hypothesis since NH_4^+ and NO_3^- are not significantly correlated in pre-industrial times (Tables 4.2 and 4.3). In other studies pre-industrial NH_4^+ was attributed mainly to biomass burning (e.g., Fuhrer et al., 1996; Kehrwald et al., 2010; Legrand et al., 1992; Whitlow et al., 1994). North America and Canada were identified as major sources for NH_4^+ in Greenland ice (Fuhrer et al., 1996), whereas Legrand and De Angelis (1996) and Zennaro et al. (2014) suggest an additional Eurasian source. A period of exceptional high fire activity around 1600-1680 in Siberian boreal forests of Eurasia was detected in the ice core fire tracer records from the Siberian Altai and Greenland (Eichler et al., 2011; Zennaro et al., 2014). This unique period did not lead to a maximum in the Lomo09 NH_4^+ record. Therefore, we conclude that biomass burning is not a major source for NH_4^+ arriving at Svalbard.

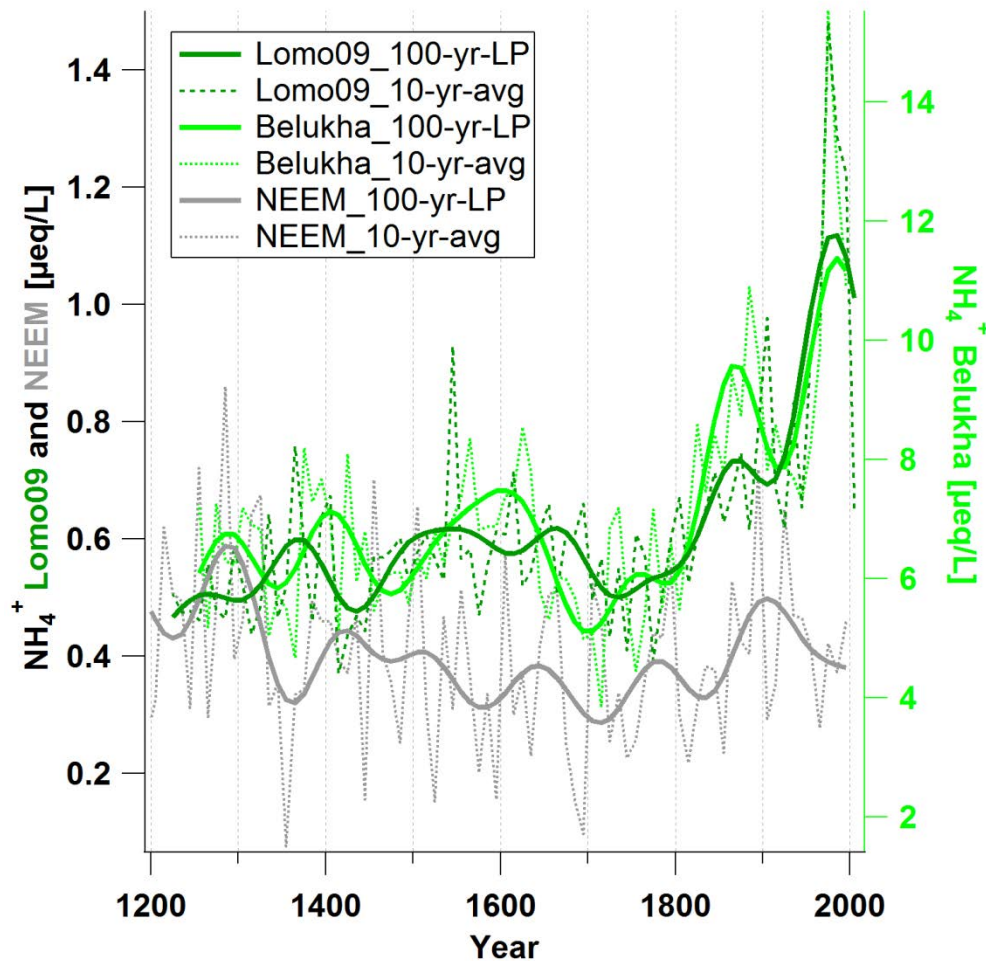


Figure 4.6 NH_4^+ records of the Lomo09 (green), Belukha (light green; Eichler et al., 2009), and the NEEM (grey; Zennaro et al., 2014) ice cores. Bold lines are 100-year-lowpass-filtered (100-yr-LP); dashed lines are the 10-year-averages (10-yr-avg).

The trend in the Lomo09 NH_4^+ record is very similar to that in the ice core from Belukha glacier in the Siberian Altai with increasing concentrations already from around 1750 (Eichler et al., 2009) (Figure 4.6). Furthermore, both records show very low concentrations around 1680 to 1750. At the Belukha site long-term NH_4^+ variations were related to temperature-induced changes of biogenic NH_3 emissions from extended Siberian boreal forests (Eichler et al., 2009). The strong increase after the 18th century was caused by a rise of Siberian temperatures since that time. Hence, from the similarity in the Lomo09 and Siberian Altai NH_4^+ concentration records we conclude that biogenic NH_3 emissions from Siberian boreal forests are the dominant source for NH_4^+ at Lomonosovfonna. Due to the larger distance to the emission sources the NH_4^+ concentrations in the Lomo09 core are about one order of magnitude lower than in the core from Belukha glacier. The NH_4^+ concentrations in a Greenland ice core (NEEM, for location see Figure 4.1) do not show the increase after the 18th century (Zennaro et al., 2014) (Figure 4.6), implying that biogenic emission trends in Northern America and Eurasia differ.

4.4 Summary

We presented the 800 year records of the two nitrogen species NO_3^- and NH_4^+ analysed in a new ice core collected from Lomonosovfonna, Svalbard, in 2009. In general, the NO_3^- and NH_4^+ records of the 2009 ice core reasonably agree with published data from two previous Svalbard ice cores, Lomonosovfonna 1997 (Kekonen et al., 2005) and Høltedahlfonna 2005 (Beaudon et al., 2013). On the decadal time scale considered here melt related effects did not significantly alter the concentrations of the nitrogen compounds. Both species show a clear impact of anthropogenic pollution in the 20th century, with peak concentrations in the 1970s/1980s. This temporal trend points to source regions in Eurasia and the Siberian Arctic, since emissions in Northern America and Western Europe kept rising into the 21st century. In pre-industrial times, i.e. prior to the 20th century, the dominant source of NH_4^+ was biogenic NH_3 emissions from Siberian boreal forests. During the same period NO_3^- was highly correlated to MSA on a decadal time scale. We explained this by a fertilising mechanism where higher atmospheric NO_3^- concentrations yield higher nitrogen input to the ocean, triggering the growth of DMS-producing phytoplankton. Elevated DMS concentrations then result in enhanced concentrations of MSA in the atmosphere. Based on our data it was not possible to resolve major pre-industrial NO_3^- sources for Svalbard.

Acknowledgements

The drilling was funded by the Paul Scherrer Institut and the Norwegian Polar Institute with help from Serla.

We would like to thank Beat Rufibach[†], and Dieter Stampfli for drilling; NPI field logistics personnel, Mats Björkman, Gerit Rotschky, and Carmen Vega for their help during the expedition; Dmitry Divine for the help on the sea ice data, Richard Petterson for providing the ice depth data, John Moore for providing the Lomo97 ion data, Emilie Beaudon for providing the Holte05 NO_3^- and NH_4^+ data, Leonhard Tobler for analysing ^{210}Pb , and Max Rüthi and Jost Eikenberg for analysing tritium, and Audun Igesund for the help on the map in Figure 4.1A.

This is a contribution to cryosphere-atmosphere interactions in a changing Arctic climate (CRAICC), a top-level research initiative (TRI).

References

- Adams, P. J., Seinfeld, J. H. and Koch, D. M.: Global concentrations of tropospheric sulfate, nitrate, and ammonium aerosol simulated in a general circulation model, *Journal of Geophysical Research, Atmospheres*, 104(D11), 13791–13823, doi:10.1029/1999JD900083, 1999.
- Baltensperger, U., Schwikowski, M., Gäggeler, H. W., Jost, D. T., Beer, J., Siegenthaler, U., Wagenbach, D., Hofmann, H. J. and Synal, H. A.: Transfer of atmospheric constituents into an alpine snow field, *Atmospheric Environment Part General Topics*, 27(12), 1881–1890, doi:10.1016/0960-1686(93)90293-8, 1993.
- Beaudon, E., Moore, J. C., Martma, T., Pohjola, V. A., van de Wal, R. S. W., Kohler, J. and Isaksson, E.: Lomonosovfonna and Høltedahlfonna ice cores reveal east–west disparities of the Spitsbergen environment since AD 1700, *Journal of Glaciology*, 59(218), 1069–1083, doi:10.3189/2013JoG12J203, 2013.
- Becagli, S., Castellano, E., Cerri, O., Curran, M., Frezzotti, M., Marino, F., Morganti, A., Proposito, M., Severi, M. and Traversi, R.: Methanesulphonic acid (MSA) stratigraphy from a Talos Dome ice core as a tool in depicting sea ice changes and southern atmospheric circulation over the previous 140 years, *Atmospheric Environment*, 43(5), 1051–1058, 2009.
- Beine, H. J., Dominè, F., Ianniello, A., Nardino, M., Allegrini, I., Teinilä, K. and Hillamo, R.: Fluxes of nitrates between snow surfaces and the atmosphere in the European high Arctic, *Atmospheric Chemistry and Physics*, 3(2), 335–346, doi:10.5194/acp-3-335-2003, 2003.
- Bergin, M. H., Jaffrezo, J.-L., Davidson, C. I., Dibb, J. E., Pandis, S. N., Hillamo, R., Maenhaut, W., Kuhns, H. D. and Makela, T.: The contributions of snow, fog, and dry deposition to the summer flux of anions and cations at Summit, Greenland, *Journal of Geophysical Research Atmospheres*, 100(D8), 16275–16288, doi:10.1029/95JD01267, 1995.
- Björkman, M. P., Kühnel, R., Partridge, D. G., Roberts, T. J., Aas, W., Mazzola, M., Viola, A., Hodson, A., Ström, J. and Isaksson, E.: Nitrate dry deposition in Svalbard, *Tellus B*, 65, 2013.
- Brimblecombe, P., Tranter, M., Abrahams, P. W., Blackwood, I., Davies, T. D. and Vincent, C. E.: Relocation and preferential elution of acidic solute through the snowpack of a small, remote, high-altitude Scottish catchment, *Annals of Glaciology*, 7, 141–147, 1985.
- Chester, R. and Jickells, T. D.: *Marine Geochemistry*, John Wiley & Sons, 2012.
- Codispoti, L. A., Kelly, V., Thessen, A., Matrai, P., Suttles, S., Hill, V., Steele, M. and Light, B.: Synthesis of primary production in the Arctic Ocean: III. Nitrate and phosphate based estimates of net community production, *Progress in Oceanography*, 110, 126–150, doi:10.1016/j.pocean.2012.11.006, 2013.
- Dickerson, R. R.: Reactive nitrogen compounds in the Arctic, *Journal of Geophysical Research Atmospheres*, 90(D6), 10739–10743, doi:10.1029/JD090iD06p10739, 1985.
- Divine, D. V. and Dick, C.: Historical variability of sea ice edge position in the Nordic Seas, *Journal of Geophysical Research Oceans*, 111(C1), doi:10.1029/2004JC002851, 2006.

Divine, D., Isaksson, E., Martma, T., Meijer, H. A. ., Moore, J., Pohjola, V., van de Wal, R. S. and Godtliessen, F.: Thousand years of winter surface air temperature variations in Svalbard and northern Norway reconstructed from ice core data, *Polar Research*, 30, 2011.

Duce, R. A., LaRoche, J., Altieri, K., Arrigo, K. R., Baker, A. R., Capone, D. G., Cornell, S., Dentener, F., Galloway, J., Ganeshram, R. S., Geider, R. J., Jickells, T., Kuypers, M. M., Langlois, R., Liss, P. S., Liu, S. M., Middelburg, J. J., Moore, C. M., Nickovic, S., Oschlies, A., Pedersen, T., Prospero, J., Schlitzer, R., Seitzinger, S., Sorensen, L. L., Uematsu, M., Ulloa, O., Voss, M., Ward, B. and Zamora, L.: Impacts of atmospheric anthropogenic nitrogen on the open ocean, *Science*, 320(5878), 893–897, doi:10.1126/science.1150369, 2008.

Eichler, A., Schwikowski, M., Gäggeler, H. W., Furrer, V., Synal, H.-A., Beer, J., Saurer, M. and Funk, M.: Glaciochemical dating of an ice core from upper Grenzgletscher (4200 m a.s.l.), *Journal of Glaciology*, 46(154), 507–515, doi:10.3189/172756500781833098, 2000.

Eichler, A., Schwikowski, M. and Gäggeler, H. W.: Meltwater-induced relocation of chemical species in Alpine firn, *Tellus B*, 53(2), 192–203, 2001.

Eichler, A., Brütsch, S., Olivier, S., Papina, T., Schwikowski, M.: A 750 year ice core record of past biogenic emissions from Siberian boreal forests, *Geophysical Research Letters*, 36(L18813), L18813, 2009.

Eichler, A., Tinner, W., Brütsch, S., Olivier, S., Papina, T. and Schwikowski, M.: An ice-core based history of Siberian forest fires since AD 1250, *Quaternary Science Reviews*, 30(9–10), 1027–1034, doi:10.1016/j.quascirev.2011.02.007, 2011.

Eleftheriadis, K., Vratolis, S. and Nyeki, S.: Aerosol black carbon in the European Arctic: measurements at Zeppelin station, Ny-Ålesund, Svalbard from 1998–2007, *Geophysical Research Letters*, 36(2), L02809, 2009.

Eneroth, K., Kjellström, E. and Holmén, K.: A trajectory climatology for Svalbard; investigating how atmospheric flow patterns influence observed tracer concentrations, *Physics and Chemistry of the Earth*, 28(28–32), 1191–1203, 2003.

Feng, Y. and Penner, J. E.: Global modeling of nitrate and ammonium: Interaction of aerosols and tropospheric chemistry, *Journal of Geophysical Research Atmospheres*, 112(D1), D01304, doi:10.1029/2005JD006404, 2007.

Fibiger, D. L., Hastings, M. G., Dibb, J. E. and Huey, L. G.: The preservation of atmospheric nitrate in snow at Summit, Greenland, *Geophysical Research Letters*, 40(13), 3484–3489, doi:10.1002/grl.50659, 2013.

Fischer, H., Wagenbach, D. and Kipfstuhl, J.: Sulfate and nitrate firn concentrations on the Greenland ice sheet: 2. Temporal anthropogenic deposition changes, *Journal of Geophysical Research Atmospheres*, 103(D17), 21935–21942, doi:10.1029/98JD01886, 1998.

Forsström, S., Ström, J., Pedersen, C. A., Isaksson, E. and Gerland, S.: Elemental carbon distribution in Svalbard snow, *Journal of Geophysical Research Atmospheres*, 114(D19), doi:10.1029/2008JD011480, 2009.

- Fuhrer, K., Neftel, A., Anklin, M., Staffelbach, T. and Legrand, M.: High-resolution ammonium ice core record covering a complete glacial-interglacial cycle, *Journal of Geophysical Research Atmospheres*, 101(D2), 4147–4164, doi:10.1029/95JD02903, 1996.
- Galloway, J. N., Dentener, F. J., Capone, D. G., Boyer, E. W., Howarth, R. W., Seitzinger, S. P., Asner, G. P., Cleveland, C. C., Green, P. A., Holland, E. A., Karl, D. M., Michaels, A. F., Porter, J. H., Townsend, A. R. and Vöösmary, C. J.: Nitrogen cycles: Past, present, and future, *Biogeochemistry*, 70(2), 153–226, doi:10.1007/s10533-004-0370-0, 2004.
- Geng, H., Ryu, J. Y., Jung, H. J., Chung, H., Ahn, K. H. and Ro, C. U.: Single-particle characterization of summertime Arctic aerosols collected at Ny-Ålesund, Svalbard, *Environmental Science & Technology*, 44(7), 2348–2353, 2010.
- Geng, L., Alexander, B., Cole-Dai, J., Steig, E. J., Savarino, J., Sofen, E. D. and Schauer, A. J.: Nitrogen isotopes in ice core nitrate linked to anthropogenic atmospheric acidity change, *Proceedings of the National Academy of Science*, 201319441, doi: 10.1073/pnas.1319441111, 2014.
- Ginot, P., Stampfli, F., Stampfli, D., Schwikowski, M. and Gäggeler, H. W.: FELICS, a new ice core drilling system for high-altitude glaciers, *Memoirs of the National Institute of Polar Research. Special Issue*, 56, 38–48, 2002.
- Ginot, P., Schotterer, U., Stichler, W., Godoi, M. A., Franco, B. and Schwikowski, M.: Influence of the Tungurahua eruption on the ice core records of Chimborazo, Ecuador, *The Cryosphere*, 4(4), 561–568, doi:10.5194/tc-4-561-2010, 2010.
- Goto-Azuma, K. and Koerner, R. M.: Ice core studies of anthropogenic sulfate and nitrate trends in the Arctic, *Journal of Geophysical Research*, 106, 4959–4969, 2001.
- Greenaway, K. R.: *Experience with Arctic flying weather*, Royal Meteorological Society, Canadian Branch, Toronto, Canada, 1950.
- Hastings, M. G., Steig, E. J. and Sigman, D. M.: Seasonal variations in N and O isotopes of nitrate in snow at Summit, Greenland: Implications for the study of nitrate in snow and ice cores, *Journal of Geophysical Research Atmospheres* 1984–2012, 109(D20), 2004.
- Henderson, K., Laube, A., Gäggeler, H. W., Olivier, S., Papina, T. and Schwikowski, M.: Temporal variations of accumulation and temperature during the past two centuries from Belukha ice core, Siberian Altai, *Journal of Geophysical Research*, 111(D3), D03104, 2006.
- Hicks, S. and Isaksson, E.: Assessing source areas of pollutants from studies of fly ash, charcoal, and pollen from Svalbard snow and ice, *Journal of Geophysical Research-Atmospheres*, 111(D2), doi:10.1029/2005JD006167, 2006.
- Honrath, R. E., Peterson, M. C., Guo, S., Dibb, J. E., Shepson, P. B. and Campbell, B.: Evidence of NO_x production within or upon ice particles in the Greenland snowpack, *Geophysical Research Letters*, 26(6), 695–698, doi:10.1029/1999GL900077, 1999.
- Isaksson, E., Pohjola, V., Jauhiainen, T., Moore, J., Pinglot, J. F., Vaikmaa, R., van de Wal, R. S. W., Hagen, J. O., Ivask, J., Karlöf, L., Martma, T., Meijer, H. A., Mulvaney, R., Thomassen, M. and van

den Broeke, M.: A new ice-core record from Lomonosovfonna, Svalbard: viewing the 1920-97 data in relation to present climate and environmental conditions, *Journal of Glaciology*, 47(157), 335–345, 2001.

Isaksson, E., Kekonen, T., Moore, J. and Mulvaney, R.: The methanesulfonic acid (MSA) record in a Svalbard ice core, *Annals of Glaciology*, 42(1), 345–351, 2005.

Jauhiainen, T., Moore, J., Perämäki, P., Derome, J. and Derome, K.: Simple procedure for ion chromatographic determination of anions and cations at trace levels in ice core samples, *Analytica Chimica Acta*, 389(1-3), 21–29, 1999.

Kaufmann, P., Fundel, F., Fischer, H., Bigler, M., Ruth, U., Udisti, R., Hansson, M., de Angelis, M., Barbante, C., Wolff, E. W., Hutterli, M. and Wagenbach, D.: Ammonium and non-sea salt sulfate in the EPICA ice cores as indicator of biological activity in the Southern Ocean, *Quaternary Science Reviews*, 29(1–2), 313–323, doi:10.1016/j.quascirev.2009.11.009, 2010.

Keene, W. C., Pszenny, A. A. P., Galloway, J. N. and Hawley, M. E.: Sea-salt corrections and interpretation of constituent ratios in marine precipitation, *Journal of Geophysical Research Atmospheres*, 91(D6), 6647–6658, doi:10.1029/JD091iD06p06647, 1986.

Kehrwald, N., Zangrando, R., Gambaro, A. and Barbante, C.: Fire and climate: Biomass burning recorded in ice and lake cores, *EPJ Web Conferences*, 9, 105–114, doi:10.1051/epjconf/201009008, 2010.

Kehrwald, N., Zangrando, R., Gabrielli, P., Jaffrezo, J.-L., Boutron, C., Barbante, C. and Gambaro, A.: Levoglucosan as a specific marker of fire events in Greenland snow, *Tellus Series B-Chemical and Physical Meteorology*, 64, doi:10.3402/tellusb.v64i0.18196, 2012.

Kekonen, T., Moore, J. C., Mulvaney, R., Isaksson, E., Pohjola, V. and van de Wal, R. S. W.: A 800 year record of nitrate from the Lomonosovfonna ice core, Svalbard, *Annals of Glaciology*, 35(1), 261–265, 2002.

Kekonen, T., Moore, J., Perämäki, P., Mulvaney, R., Isaksson, E., Pohjola, V. and van de Wal, R. S. W.: The 800 year long ion record from the Lomonosovfonna (Svalbard) ice core, *Journal of Geophysical Research*, 110, D07304, 2005.

Kellerhals, T., Brütsch, S., Sigl, M., Knüsel, S., Gäggeler, H. W. and Schwikowski, M.: Ammonium concentration in ice cores: A new proxy for regional temperature reconstruction?, *Journal of Geophysical Research Atmospheres*, 115(D16), D16123, doi:10.1029/2009JD012603, 2010.

Kinnard, C., Zdanowicz, C. M., Fisher, D. A., Isaksson, E., de Vernal, A. and Thompson, L. G.: Reconstructed changes in Arctic sea ice over the past 1,450 years, *Nature*, 479(7374), 509–512, 2011.

Kühnel, R., Roberts, T. J., Björkman, M. P., Isaksson, E., Aas, W., Holmén, K. and Ström, J.: 20-year climatology of NO₃⁻ and NH₄⁺ wet deposition at Ny-Ålesund, Svalbard, *Advances in Meteorology*, 2011, e406508, doi:10.1155/2011/406508, 2012.

- Lavigne, F., Degeai, J.-P., Komorowski, J.-C., Guillet, S., Robert, V., Lahitte, P., Oppenheimer, C., Stoffel, M., Vidal, C. M., Suroño, Pratomo, I., Wassmer, P., Hajdas, I., Hadmoko, D. S. and Belizal, E. de: Source of the great A.D. 1257 mystery eruption unveiled, Samalas volcano, Rinjani Volcanic Complex, Indonesia, *Proceedings of the National Academy of Science*, 110(42), 16742–16747, doi:10.1073/pnas.1307520110, 2013.
- Law, K. S. and Stohl, A.: Arctic air pollution: Origins and impacts, *Science*, 315(5818), 1537–1540, 2007.
- Legrand, M.: Ice-core records of atmospheric sulphur, *Philosophical Transactions of the Royal Society of London. Series B. Biological Sciences*, 352(1350), 241–250, 1997.
- Legrand, M. and De Angelis, M.: Light carboxylic acids in Greenland ice: A record of past forest fires and vegetation emissions from the boreal zone, *Journal of Geophysical Research Atmospheres*, 101(2), 4129–4145, 1996.
- Legrand, M. and Mayewski, P.: Glaciochemistry of polar ice cores: a review, *Reviews of Geophysics*, 35, 219–244, 1997.
- Legrand, M., de Angelis, M. and Delmas, R. J.: Ion chromatographic determination of common ions at ultratrace levels in Antarctic snow and ice, *Analytica Chimica Acta*, 156, 181–192, doi:10.1016/S0003-2670(00)85549-X, 1984.
- Legrand, M., De Angelis, M., Staffelbach, T., Neftel, A. and Stauffer, B.: Large perturbations of ammonium and organic acids content in the summit-Greenland Ice Core. Fingerprint from forest fires?, *Geophysical Research Letters*, 19(5), 473–475, doi:10.1029/91GL03121, 1992.
- Legrand, M., De Angelis, M. and Maupetit, F.: Field investigation of major and minor ions along Summit (Central Greenland) ice cores by ion chromatography, *Journal of Chromatography A*, 640(1–2), 251–258, doi:10.1016/0021-9673(93)80188-E, 1993.
- Legrand, M., Hammer, C., Angelis, M. D., Savarino, J., Delmas, R., Clausen, H. and Johnsen, S. J.: Sulfur-containing species (methanesulfonate and SO₄) over the last climatic cycle in the Greenland Ice Core Project (central Greenland) ice core, *Journal of Geophysical Research*, 102(C12), 26663–26,679, doi:10.1029/97JC01436, 1997.
- Legrand, M., Wolff, E. and Wagenbach, D.: Antarctic aerosol and snowfall chemistry: implications for deep Antarctic ice-core chemistry, *Annals of Glaciology*, 29(1), 66–72, doi:10.3189/172756499781821094, 1999.
- Macias Fauria, M., Grinsted, A., Helama, S., Moore, J., Timonen, M., Martma, T., Isaksson, E. and Eronen, M.: Unprecedented low twentieth century winter sea ice extent in the Western Nordic Seas since AD 1200, *Climate Dynamics*, 34(6), 781–795, 2010.
- Matoba, S., Narita, H., Motoyama, H., Kamiyama, K. and Watanabe, O.: Ice core chemistry of Vestfonna ice cap in Svalbard, Norway, *Journal of Geophysical Research*, 107(D23), 4721, 2002.

Moore, J. C. and Grinsted, A.: Ion fractionation and percolation in ice cores with seasonal melting, in *Physics of ice core records II*, vol. 68, edited by Institute of Low Temperature Science, Hokkaido University, pp. 287–298, Hokkaido University Press, Sapporo, Japan, 2009.

Moore, J. C., Grinsted, A., Kekonen, T. and Pohjola, V.: Separation of melting and environmental signals in an ice core with seasonal melt, *Geophysical Research Letters*, 32(10), L10501, 2005.

Moore, J., Kekonen, T., Grinsted, A. and Isaksson, E.: Sulfate source inventories from a Svalbard ice core record spanning the Industrial Revolution, *Journal of Geophysical Research*, 111(D15), 15307, 2006.

Moore, J. C., Beaudon, E., Kang, S., Divine, D., Isaksson, E., Pohjola, V. A. and van de Wal, R. S. W.: Statistical extraction of volcanic sulphate from nonpolar ice cores, *Journal of Geophysical Research*, 117(D3), D03306, 2012.

O'Dwyer, J., Isaksson, E., Vinje, T., Jauhiainen, T., Moore, J., Pohjola, V., Vaikmae, R. and van de Wal, R. S. W.: Methanesulfonic acid in a Svalbard ice core as an indicator of ocean climate, *Geophysical Research Letters*, 27(8), 1159–1162, 2000.

Opel, T., Fritzsche, D. and Meyer, H.: Eurasian Arctic climate over the past millennium as recorded in the Akademii Nauk ice core (Severnaya Zemlya), *Climate of the Past*, 9(5), 2379–2389, doi:10.5194/cp-9-2379-2013, 2013.

Perrette, M., Yool, A., Quartly, G. D. and Popova, E. E.: Near-ubiquity of ice-edge blooms in the Arctic, *Biogeosciences*, 8(2), 515–524, doi:10.5194/bg-8-515-2011, 2011.

Pohjola, V. A., Moore, J. C., Isaksson, E., Jauhiainen, T., van de Wal, R. S. W., Martma, T., Meijer, H. A. J. and Vaikmäe, R.: Effect of periodic melting on geochemical and isotopic signals in an ice core from Lomonosovfonna, Svalbard, *Journal of Geophysical Research*, 107(10.1029), 2002.

Quinn, P. K., Shaw, G., Andrews, E., Dutton, E. G., Ruoho-Airola, T. and Gong, S. L.: Arctic haze: current trends and knowledge gaps, *Tellus B*, 59(1), 99–114, 2007.

Rhodes, R. H., Bertler, N. A. N., Baker, J. A., Sneed, S. B., Oerter, H. and Arrigo, K. R.: Sea ice variability and primary productivity in the Ross Sea, Antarctica, from methylsulphonate snow record, *Geophysical Research Letters*, 36(10), L10704, 2009.

Röthlisberger, R., Hutterli, M. A., Sommer, S., Wolff, E. W. and Mulvaney, R.: Factors controlling nitrate in ice cores: Evidence from the Dome C deep ice core, *Journal of Geophysical Research Atmospheres*, 105(D16), 20565–20572, doi:10.1029/2000JD900264, 2000.

Röthlisberger, R., Hutterli, M. A., Wolff, E. W., Mulvaney, R., Fischer, H., Bigler, M., Goto-Azuma, K., Hansson, M. E., Ruth, U., Siggaard-Andersen, M.-L. and Steffensen, J. P.: Nitrate in Greenland and Antarctic ice cores: a detailed description of post-depositional processes, *Annals of Glaciology*, 35(1), 209–216, doi:10.3189/172756402781817220, 2002.

Sharma, S., Chan, E., Ishizawa, M., Toom-Sauntry, D., Gong, S. L., Li, S. M., Tarasick, D. W., Leaitch, W. R., Norman, A., Quinn, P. K., Bates, T. S., Levasseur, M., Barrie, L. A. and Maenhaut, W.:

Influence of transport and ocean ice extent on biogenic aerosol sulfur in the Arctic atmosphere, *Journal of Geophysical Research*, 117(D12), D12209, doi:10.1029/2011JD017074, 2012.

Shaw, G. E.: The arctic haze phenomenon, *Bulletin of the American Meteorological Society*, 76, 2403–2414, 1995.

Sigl, M.: Ice core based reconstruction of past climate conditions from Colle Gnifetti, Swiss Alps, PhD thesis, University of Bern, Bern, Switzerland, 2009.

Sigl, M., McConnell, J. R., Layman, L., Maselli, O., McGwire, K., Pasteris, D., Dahl-Jensen, D., Steffensen, J. P., Vinther, B., Edwards, R., Mulvaney, R. and Kipfstuhl, S.: A new bipolar ice core record of volcanism from WAIS Divide and NEEM and implications for climate forcing of the last 2000 years, *Journal of Geophysical Research Atmospheres*, doi:10.1029/2012JD018603, 2013.

Simões, J. C. and Zagorodnov, V. S.: The record of anthropogenic pollution in snow and ice in Svalbard, Norway, *Atmospheric Environment*, 35(2), 403–413, 2001.

Stefels, J., Steinke, M., Turner, S., Malin, G. and Belviso, S.: Environmental constraints on the production and removal of the climatically active gas dimethylsulphide (DMS) and implications for ecosystem modelling, *Biogeochemistry*, 83(1-3), 245–275, doi:10.1007/s10533-007-9091-5, 2007.

Stohl, A.: Characteristics of atmospheric transport into the Arctic troposphere, *Journal of Geophysical Research*, 111(D11), D11306, 2006.

Stohl, A., Berg, T., Burkhart, J. F., Forster, C., Herber, A., Hov, Ø., Lunder, C., Mcmillan, W. W., Oltmans, S., Shiobara, M., Simpson, D., Solberg, S., Stebel, K., Ström, J., Tørseth, K., Treffeisen, R., Virkkunen, K. and Yttri, K. E.: Arctic smoke? Record high air pollution levels in the European Arctic due to agricultural fires in Eastern Europe in spring 2006, *Atmospheric Chemistry and Physics*, 7(2), 511–534, 2007.

Teinilä, K., Hillamo, R., Kerminen, V.-M. and Beine, H. J.: Aerosol chemistry during the NICE dark and light campaigns, *Atmospheric Environment*, 37(4), 563–575, doi:10.1016/S1352-2310(02)00826-9, 2003.

Thompson, L. G., Davis, M. E., Mosley-Thompson, E., Sowers, T. A., Henderson, K. A., Zagorodnov, V. S., Lin, P.-N., Mikhailenko, V. N., Campen, R. K., Bolzan, J. F., Cole-Dai, J. and Francou, B.: A 25,000-year tropical climate history from Bolivian ice cores, *Science*, 282(5395), 1858–1864, doi:10.1126/science.282.5395.1858, 1998.

Udisti, R., Bellandi, S. and Piccardi, G.: Analysis of snow from Antarctica: a critical approach to ion-chromatographic methods, *Fresenius Journal of Analytical Chemistry*, 349(4), 289–293, doi:10.1007/BF00323205, 1994.

Vinje, T.: Anomalies and trends of sea-ice extent and atmospheric circulation in the Nordic seas during the period 1864-1998, *Journal of Climate*, 14(3), 255–267, 2001.

Vogt, M. and Liss, P. S.: Dimethylsulfide and climate, in Surface ocean–lower atmosphere processes, edited by C. L. Quéré and E. S. Saltzman, pp. 197–232, American Geophysical Union, 2009.

Weiler, K., Fischer, H., Fritzsche, D., Ruth, U., Wilhelms, F. and Miller, H.: Glaciochemical reconnaissance of a new ice core from Severnaya Zemlya, Eurasian Arctic, *Journal of Glaciology*, 51(172), 64–74, doi:10.3189/172756505781829629, 2005.

Whitlow, S., Mayewski, P., Dibb, J., Holdsworth, G. and Twickler, M.: An ice-core-based record of biomass burning in the Arctic and Subarctic, 1750–1980, *Tellus B*, 46(3), 234–242, 1994.

Wolff, E. W.: Ice sheets and nitrogen, *Philosophical Transactions of the Royal Society Biological Sciences*, 368(1621), 20130127, doi:10.1098/rstb.2013.0127, 2013.

Wolff, E. W., Jones, A. E., Bauguitte, S. J.-B. and Salmon, R. A.: The interpretation of spikes and trends in concentration of nitrate in polar ice cores, based on evidence from snow and atmospheric measurements, *Atmospheric Chemistry and Physics*, 8(18), 5627–5634, doi:10.5194/acp-8-5627-2008, 2008.

Zennaro, P., Kehrwald, N., McConnell, J. R., Schüpbach, S., Maselli, O., Marlon, J., Vallelonga, P., Leuenberger, D., Zangrando, R., Spolaor, A., Borrotti, M., Barbaro, E., Gambaro, A. and Barbante, C.: Fire in ice: two millennia of Northern Hemisphere fire history from the Greenland NEEM ice core, *Climate of the Past Discussions*, 10(1), 809–857, doi:10.5194/cpd-10-809-2014, 2014.

Supplementary Material

Here, an example for the annual layer counting (ALC) for the core section between 0 and 20 m weq (Figure S4-1) is displayed, followed by the raw data for the ionic species (Figure S4-2) and the melt percent (Figure S4-3) of the Lomo09 ice core along depth in m weq.

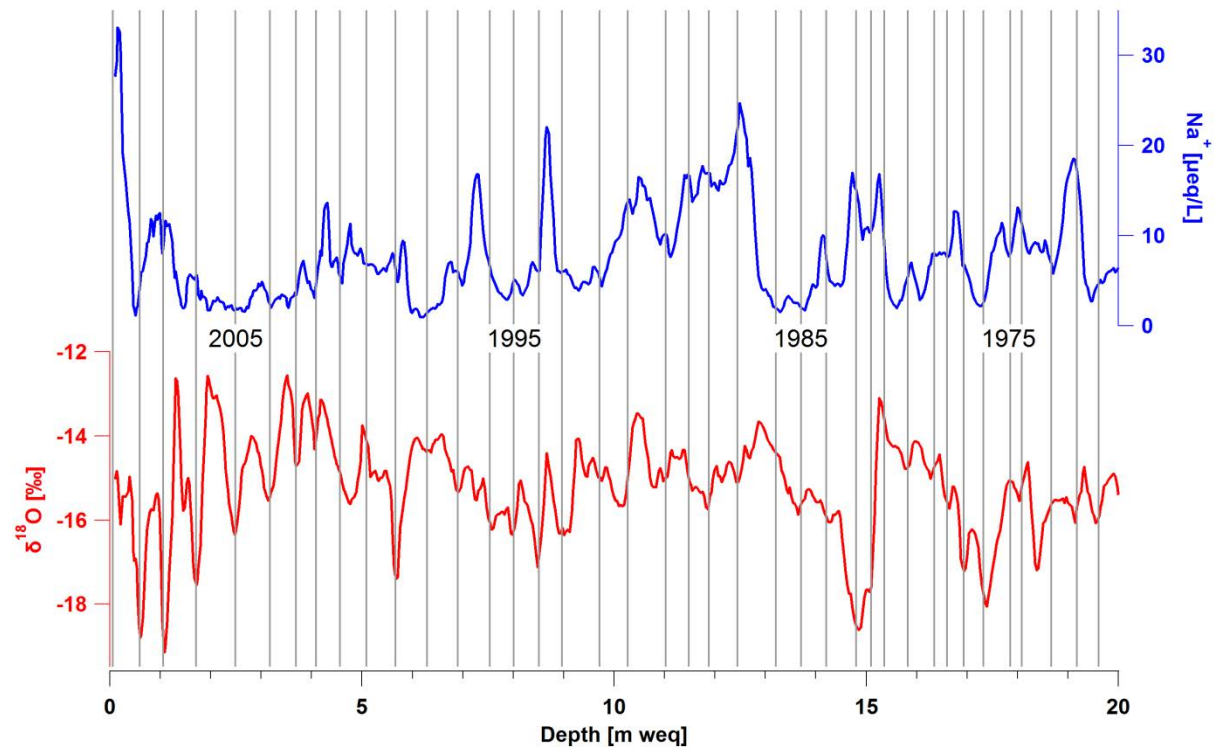


Figure S4-1 Example for annual layer counting (ALC) for the core section between 0 and 20 m weq using the records of $\delta^{18}\text{O}$ and Na^+ . Data are five-point-moving averages. Grey vertical lines indicate the single counted years; numbers within the graph give the resulting year.

4 800 year ice-core record of nitrogen deposition in Svalbard

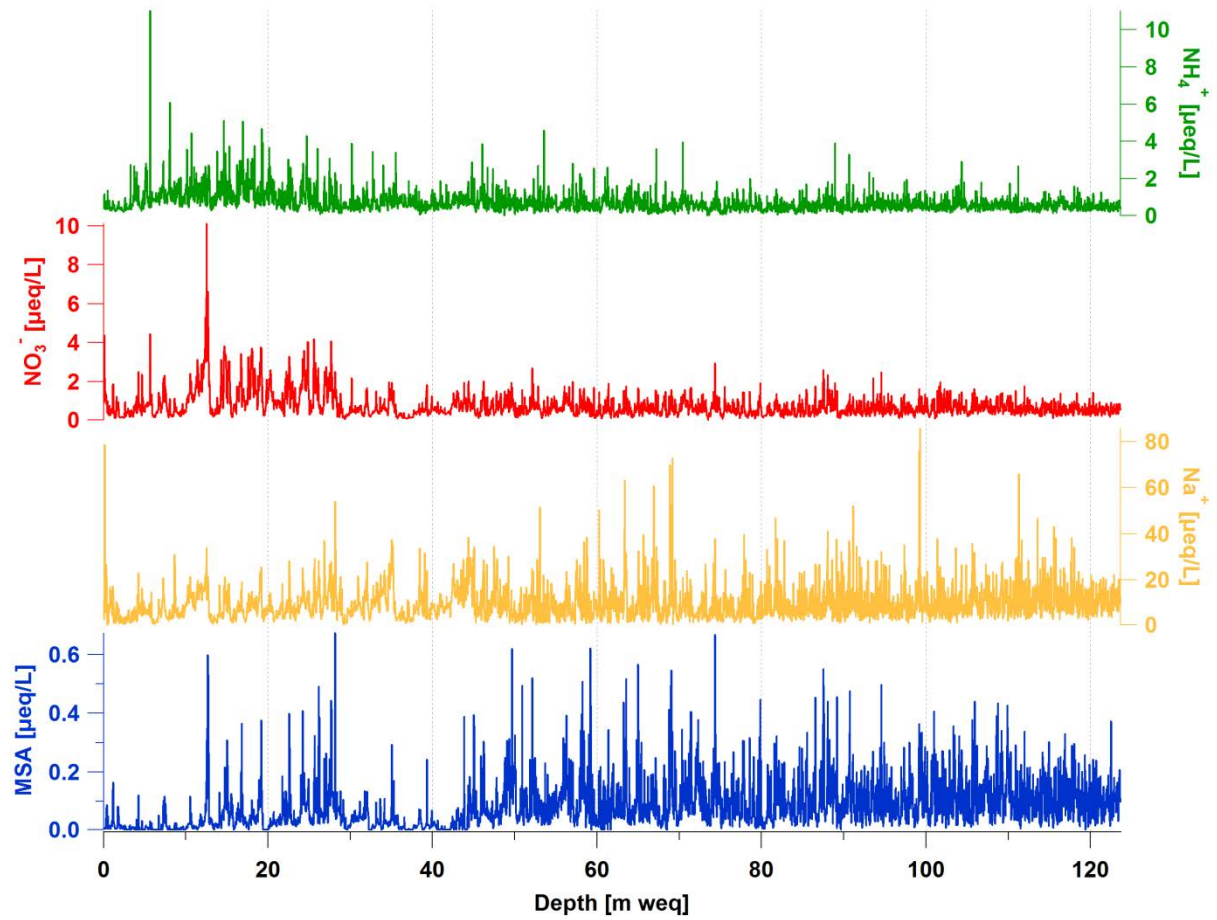


Figure S4-2 Raw data of concentrations of MSA ($=\text{CH}_3\text{SO}_3^-$), Na^+ , NO_3^- , and NH_4^+ of the Lomo09 ice core versus depth in m weq.

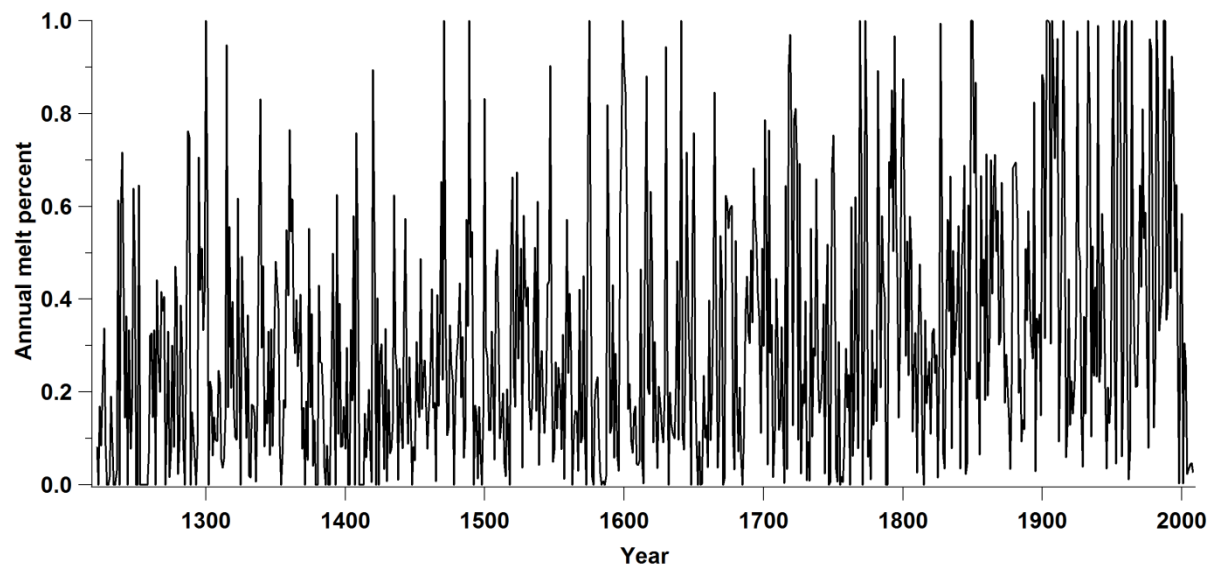


Figure S4-3 Annual melt percent of the Lomo09 ice core versus age.

5 Is the climate and environmental reconstruction from one ice core representative of an entire region? - A case study from Lomonosovfonna, Svalbard

I.A. Wendl^{1,2,3}, A. Eichler^{1,2}, E. Isaksson⁴, T. Martma⁵, M. Schwikowski^{1,2,3}

¹Laboratory of Radiochemistry and Environmental Chemistry, Paul Scherrer Institut, 5232 Villigen PSI, Switzerland

²Oeschger Centre for Climate Change Research, University of Bern, Switzerland

³Department of Chemistry and Biochemistry, University of Bern, Switzerland

⁴Norwegian Polar Institute, Framsenteret, 9296 Tromsø, Norway

⁵Institute of Geology, Tallinn University of Technology, Estonia

Manuscript in preparation

Abstract

We compare the two most recent ice cores from Lomonosovfonna, Svalbard, drilled in 1997 and 2009 (Lomo97 and Lomo09), to test the spatial representativeness of past climate and environmental information from one ice core. Both cores were dated using a multiple parameter approach. Several major volcanic eruptions were identified in both cores, with the 1783 Laki eruption having the most prominent impact on the SO_4^{2-} records. The 1963 tritium peak was clearly imprinted in both cores. The tritium activity and the depth of the peak are in the same range. The largest discrepancy is the age of the deepest core sections, which results from the attribution of the SO_4^{2-} peak detected in the deepest core section to two different major volcanic eruptions, the Hekla 1104 or 1158 for the Lomo97 and the Samalas 1257/58 for the Lomo09. The ion chemistry as well as the concentration trends in the ion records are very similar. The two cores are dominated by the sea salt species of Na^+ , Cl^- , K^+ , and Mg^{2+} that contribute >70% to the ion budget. The anthropogenic influence is observed in both cores, especially in the NO_3^- and SO_4^{2-} records. The correlation of MSA and NO_3^- observed in the Lomo09 core is not seen in the Lomo97, where NO_3^- is correlated with Ca^{2+} . The annual accumulation rates at the sites differ by around 60%, which represents the high spatial variability in the area. The $\delta^{18}\text{O}$ records of the two ice cores are similar, thus the Lomo09 $\delta^{18}\text{O}$ record is thought to correlate best with air temperature near Longyearbyen like the Lomo97 $\delta^{18}\text{O}$ record. The records of the stratigraphic melt index show great similarities in the common period from 1700 to 1997. The records of the melt index $\ln(\text{Na}^+/\text{Mg}^{2+})$ are comparable prior to around 1800. Afterwards, the Lomo09 record resembles more that of the Høltedahlfonna ice core drilled in 2005. This comparison of two ice cores from Lomonosovfonna shows that the climate and environmental reconstruction from one Lomonosovfonna ice core is representative of the glacier, but not necessarily of the entire region of Svalbard.

5.1 Introduction

Ice cores reveal the unique opportunity to reconstruct climatic and environmental history on long time scales. In the Arctic, the number of ice core studies is biased towards the large ice sheet of Greenland, at least partly because it is not affected by seasonal melt as other Arctic sites (e.g., Koerner, 1997). However, the small ice caps and glaciers outside of Greenland add important information to the palaeoclimate reconstruction of the Arctic because they are influenced by different air masses than the high altitude ice sheet of Greenland (AMAP, 2011; Hirdman et al., 2010). The low-altitude ice caps and glaciers receive pollutants from high-latitude Eurasia by low-level transport (AMAP, 2011; Hirdman et al., 2010), in contrast to Greenland which is more connected to transport from lower latitudes (AMAP, 2011).

Additionally, the higher annual accumulation at sites outside of Greenland offers the possibility to gain high time resolved data (Van der Wel et al., 2011; Tarussov, 1992). Thus, ice cores from those sites are well suited to study the impacts and emission source histories during the last centuries.

One of the most important issues for past climate and environmental reconstructions remains the question of the representativeness of a single ice core relative to a single glacier, to a sub-region such as an archipelago, or to a greater region such as the Eurasian Arctic (Kotlyakov et al., 2004). The best way to evaluate this representativeness is using highly-depth-resolved studies on multiple cores from the same location. In the Eurasian Arctic, often two or more cores were recovered from the same glacier (Fritzsche et al., 2002; Isaksson et al., 2001; Kotlyakov et al., 2004; Pinglot et al., 2003; Uchida et al., 1996). However, in most cases the first drilling expeditions took place decades ago and those cores were not analysed in great detail (e.g., Fritzsche et al., 2002). This precluded an in-depth comparison of cores from the same glacier.

Svalbard is located in an area influenced by shifting boundaries in atmosphere and ocean which results in a highly variable climate throughout the year (Isaksson et al., 2003). It is further relatively close to Eurasia, where some of the major sources of anthropogenic pollution are located. Lomonosovfonna is one of the highest ice fields (1250 m asl) in Svalbard and proven to be less affected by melt than other Svalbard glaciers, so that the signals are mainly preserved within an annual strata, but at least within eight annual layers (Gordiyenko et al., 1981; Moore and Grinsted, 2009; Moore et al., 2005; Pohjola et al., 2002a). So far four ice cores have been retrieved from Lomonosovfonna, in 1976, 1982, 1997 and 2009 (Gordiyenko et al., 1981; Isaksson et al., 2001; Kotlyakov et al., 2004). Only the cores drilled in 1997 and 2009 were studied at high resolution and in great detail. Here, we present a first comprehensive comparison of these two cores, retrieved just 4.6 km apart (Isaksson et al., 2001), to assess to what extent the parameters analysed in the cores agree. This comparison is thought to reveal whether the climate and environmental reconstruction from one ice core is representative of an entire region such as the archipelago of Svalbard.

5.2 Drilling and methods

In 1997, a 121 m long ice core was retrieved from the summit of Lomonosovfonna at 78°51'53"N, 17°25'30"E, 1250 m asl (Figure 5.1) (Isaksson et al., 2001). This core almost reached bedrock which ground-penetrating radar measurements indicated to be at ~126.5 m depth. In 2009, a second 149.5 m long ice core from Lomonosovfonna was recovered, only 4.6 km south of the 1997 core (Isaksson et al., 2001) at 78°49'24"N, 17°25'59"E, 1202 m asl (Figure 5.1). The 1997 drilling site was no longer suitable due to a large crevasse that had

5 Is the climate reconstruction of one ice core representative?

opened in the area just before the 2009 drilling expedition and probably affected the records. Thus the drilling site further south was chosen. Bedrock at around 200 m depth- indicated by a radar survey- could not be reached (Pettersen, unpublished data). Hereafter, the cores will be called Lomo97 and Lomo09.

Both ice cores were sampled discretely for the analysis of water soluble major ions, water stable isotopes ($\delta^{18}\text{O}$ and δD), tritium, and ^{210}Pb (details on the sampling methods in Isaksson et al. 2001 and Eichler et al. 2000). The records of the major ions are used to reconstruct climate and pollution on historic time scales, whereas tritium and ^{210}Pb are used for dating. The water stable isotope records are used for both dating and climate reconstruction.

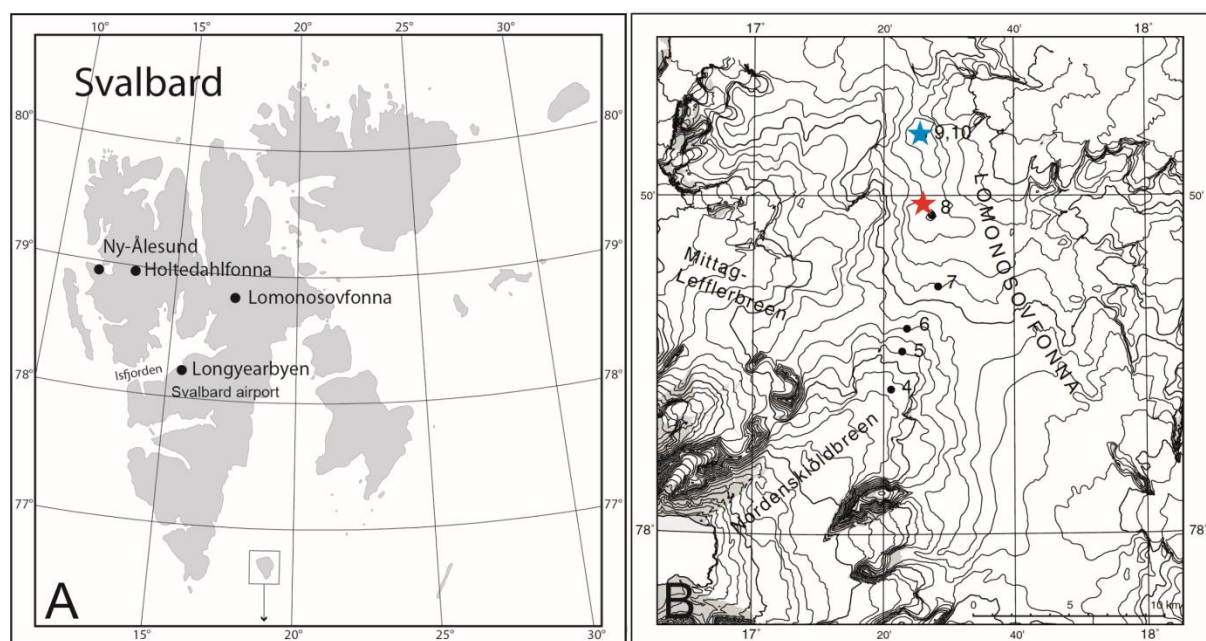


Figure 5.1 Maps showing the location of (A) Lomonosovfonna and (B) the drilling sites in 1997 (blue) and 2009 (red). Graph B modified after Isaksson et al. (2001).

The Lomo97 core was sampled at a resolution of 5 cm for major ion analysis which resulted in >1000 samples (Kekonen et al., 2002). Part of the core was resampled, resulting in 2840 samples for $\delta^{18}\text{O}$ analysis, with up to 23 samples per year in the uppermost part of the core (Divine et al., 2011). Tritium was analysed in 189 samples with a resolution of 5 cm (Van der Wel et al., 2011). For ^{210}Pb analysis the Lomo97 core was sampled down to a depth of around 40 m at a resolution of approximately 1-2 m weq (Pinglot et al., 1999).

The Lomo09 core was sampled for major ion analysis and water stable isotope analysis at a resolution of 3-4 cm to account for layer thinning due to ice flow further down the core. This resulted in 3997 samples for both ion and $\delta^{18}\text{O}/\delta\text{D}$ analysis. In the uppermost part up to 32 samples represent one year, and even in the deepest and oldest core part the sampling

resolution results in at least one sample per year. For tritium the Lomo09 core was sampled between 21 and 43 m first at coarse (60-74 cm) and then at fine (~22 cm) resolution in order to identify the depth of the tritium peak. ^{210}Pb was analysed between 6 and 89 m at a resolution of 16 to 74 cm (one sample per core section).

Both ice cores were analysed for the following major water soluble ions using liquid ion chromatography: the anions methane-sulphonate ($\text{MSA} = \text{CH}_3\text{SO}_3^-$), chloride (Cl^-), nitrate (NO_3^-), and sulphate (SO_4^{2-}), and the cations sodium (Na^+), ammonium (NH_4^+), potassium (K^+), magnesium (Mg^{2+}), and calcium (Ca^{2+}). Details on the major ion and $\delta^{18}\text{O}$ analyses in the Lomo97 core are given elsewhere (Divine et al., 2011; Isaksson et al., 2001; Jauhiainen et al., 1999; Kekonen et al., 2005). The major ions in the Lomo09 core were measured with a Metrohm 850 Professional IC combined with a 872 Extension Module and an autosampler (858 Professional Sample Processor). The anions were determined by a step-wise elution, with a lower concentrated eluent followed by a higher concentrated one. This resulted in the best separation of the single ions and reasonable measuring time. Details on the single components and chemicals are given in Table S5-1 in the Supplementary Material (SM). For every sample batch the instrument was calibrated with different dilutions of in-house reference solutions of 10 ppm. Moreover, after approximately every 20th sample we analysed one of the reference solutions plus an in-house standard (snow from the high altitude research station of Jungfraujoch, Switzerland) to monitor potential drifts. The analysis of $\delta^{18}\text{O}$ and δD for the Lomo09 core was conducted partly using isotopic ratio mass spectrometry (IRMS, Delta V Advantage, Thermo Fisher Scientific, Bremen, Germany), partly using wavelength-scanned cavity ring down spectrometry (WS-CRDS, Picarro L2130-i, Picarro Inc., Santa Clara, CA, USA). In both cases we analysed in-house standards covering the expected value range frequently to monitor stability and potential drifts of the setup. The tritium analysis was performed for both cores using liquid scintillation counting (Pinglot et al., 2003). For the Lomo97 core high-resolution γ -spectrometry was applied for the analysis of ^{210}Pb (Pinglot et al., 2003) and for the Lomo09 we used α -spectrometry, measuring ^{210}Pb indirectly via its decay product ^{210}Po after chemical separation (Gäggeler et al., 1983). The melt features in the Lomo97 core were determined visually at 5 mm resolution in the top 81 m of the core which corresponds to the time period between around 1700 to 1997 (Grinsted et al., 2006). The melt features were classified into four categories to which a specific melt percentage was assigned (Grinsted et al., 2006; Pohjola et al., 2002a). In the Lomo09 core the melt features were also identified visually and the melt percentage was calculated similar to the method described in Henderson et al. (2006). Different from Henderson et al. (2006) the melt features were not categorised but it was accounted for to which extent the melt affected the core diameter. Thus, the length of the melt

feature was multiplied with the percentage of the affected core diameter, summarising the observed melt features of one year to obtain the annual melt percent.

5.3 Results and discussion

In the following we discuss the different aspects of the comparison of the Lomo97 and the Lomo09 ice core. We focus on the dating, the ion chemistry, the accumulation rates, the water stable isotope ratio of $\delta^{18}\text{O}$, and the melt indices of stratigraphic melt index and $\ln(\text{Na}^+/\text{Mg}^{2+})$.

5.3.1 Dating

The two ice cores were dated applying a multiple-parameter approach. The Lomo97 was dated down to 76.2 m weq (= 1613) with a combination of the radioactivity peaks (Pinglot et al., 1999), volcanic reference horizons (Kekonen et al., 2005), and annual layer counting (ALC) using the pronounced $\delta^{18}\text{O}$ summer peaks (Divine et al., 2011). The dating uncertainty for this core section is ± 1 year in the vicinity of the time markers and ± 5 years in between (Divine et al., 2011). For the older core part below 76.2 m weq a simple glacier flow model (Nye, 1963) based on an annual average accumulation rate of 0.36 m weq was applied. This results in an age of 770 ± 150 at the bottom of the core (Figure 5.2; Divine et al., 2011). The Lomo09 core covers the time period from 1222 to 2009 (Figure 5.2; Wendl et al. 2014, submitted to Atmospheric Chemistry and Physics Discussions (ACPD)). Down to a depth of ~ 79.7 m weq (= 1750) the core was dated using a combination of the reference horizons of tritium and several major volcanic eruptions (Table 5.1), and ALC using the pronounced seasonality of the $\delta^{18}\text{O}$ and Na^+ records. A two-parameter glacier flow model (Thompson et al., 1998) was fitted through the volcanic reference horizons, with a modelled average annual accumulation rate of ~ 0.58 m weq and a constant of 1.02. Below ~ 79.7 m weq ALC was limited due to strong layer thinning, so that the flow model was used to date the core. The dating uncertainty of the Lomo09 core ranges from ± 1 year within ± 10 years of the reference horizons in the upper core part to ± 10 years below ~ 80 m weq, calculated using the difference of the year of the volcanic eruption and the modelled date.

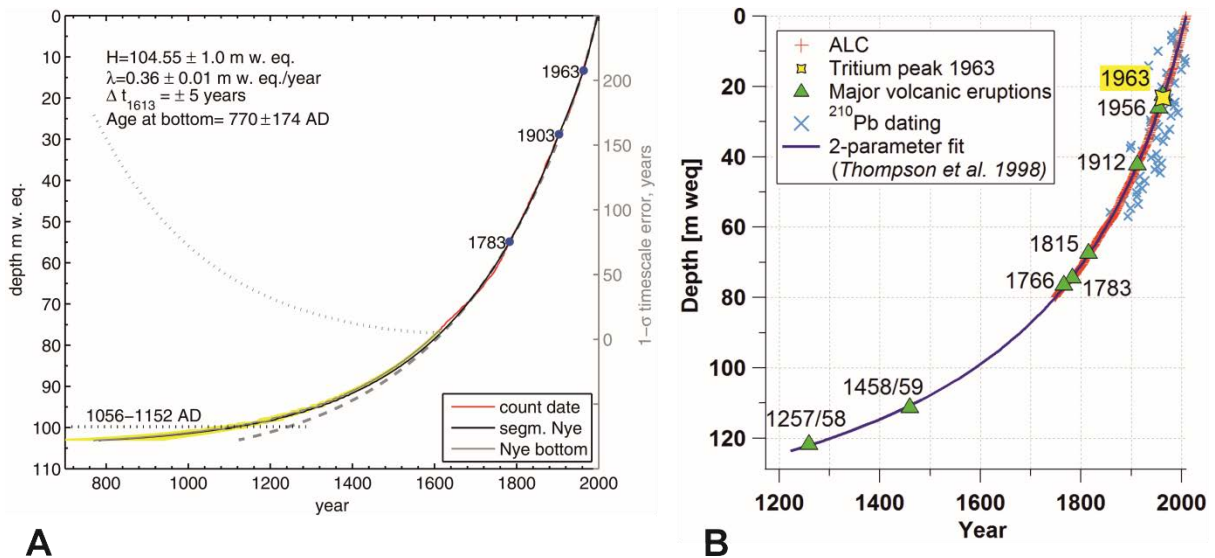


Figure 5.2 Comparison of the dating of the Lomo97 (A; graph adopted from Divine et al. 2011) and Lomo09 core (B; Wendl et al. 2014, submitted to ACPD). ALC = annual layer counting.

The major volcanic eruptions identified in the Lomo97 and Lomo09 core are given in Table 5.1. Several eruptions were detected in both cores with the approach of Moore et al. (2012) using the SO_4^{2-} records. In particular, there is good agreement for the Laki eruption, Iceland, in 1783, which is reflected by the strongest peak in the SO_4^{2-} records of the two cores. The chemical composition of tephra particles retrieved from the Lomo97 core around the depth of this large SO_4^{2-} peak supports the attribution to the 1783 Laki eruption (Kekonen et al., 2005). The largest discrepancy is seen for the eruption identified in the deepest section of the cores. For the Lomo97 this is the eruption of Hekla, Iceland, in 1104 or 1158 at a depth of 117.7 m (= 99.8 m weq), and in the Lomo09 the eruption of Samalas in 1257/58 at a depth of 145.2 m (= 121.8 m weq). Moore et al. (2006) had previously identified the SO_4^{2-} peak at 99.8 m weq in the Lomo97 also as the Samalas eruption. This was revised in Divine et al. (2011) and Moore et al. (2012), based on resampling of the core and an annual accumulation rate that would be far too high to reach 1257/58 at the depth of 99.8 m weq. However, the precise attribution of the SO_4^{2-} peak at 99.8 m weq depth is hampered by discontinuities in the chemical stratigraphy in the bottom part of the Lomo97 core (Divine et al., 2011). In the Lomo09 core the attribution of the SO_4^{2-} peak at a depth of 121.8 m weq to the 1257/58 eruption fits best to the two-parameter model (Thompson et al., 1998) used for the dating below approximately 79.7 m weq. Thus, in order to reach back to 1104 or 1158 for the eruption at 121.8 m weq, the accumulation rate below 79.7 m weq would have to be decreased substantially. We cannot resolve which attribution is to be preferred, because to assign the SO_4^{2-} peak to the other respective eruption would imply an accumulation rate that is out of range for the particular dating.

5 Is the climate reconstruction of one ice core representative?

Table 5.1 Major volcanic eruptions identified in the Lomo97 (Moore et al., 2012) and the Lomo09 ice cores. Volc. erupt. = volcanic eruption. Year = year of eruption. The difference of the year of the Kuwae eruption results from the updated attribution to the years 1458/49 by Sigl et al. (2013) which was incorporated in the Lomo09 dating.

Lomo97			Lomo09		
Volc. erupt.	Depth [m]	Year	Volc. erupt.	Depth [m]	Year
Pinatubo	6.5	1991	Agung/ Sheveluch	32.3	1963/64
Bezymianny	21.1	1956	Bezymianny	36.5	1956
Kharimkotan	29	1934			
Kuril islands	31.5	1928			
Novarupta/ Katmai	36.2	1912	Katmai	55.4	1912
Krakatau	45.5	1883			
Tambora	62.3	1815	Tambora	83.9	1815
Laki	67	1783	Laki	91.8	1783
			Hekla	94.2	1766
Fuji	80.5	1707			
Kuwae	107.5	1453	Kuwae	133.5	1458/59
			Samalas	145.2	1257/58
Hekla	117.7	1104 or 1158			

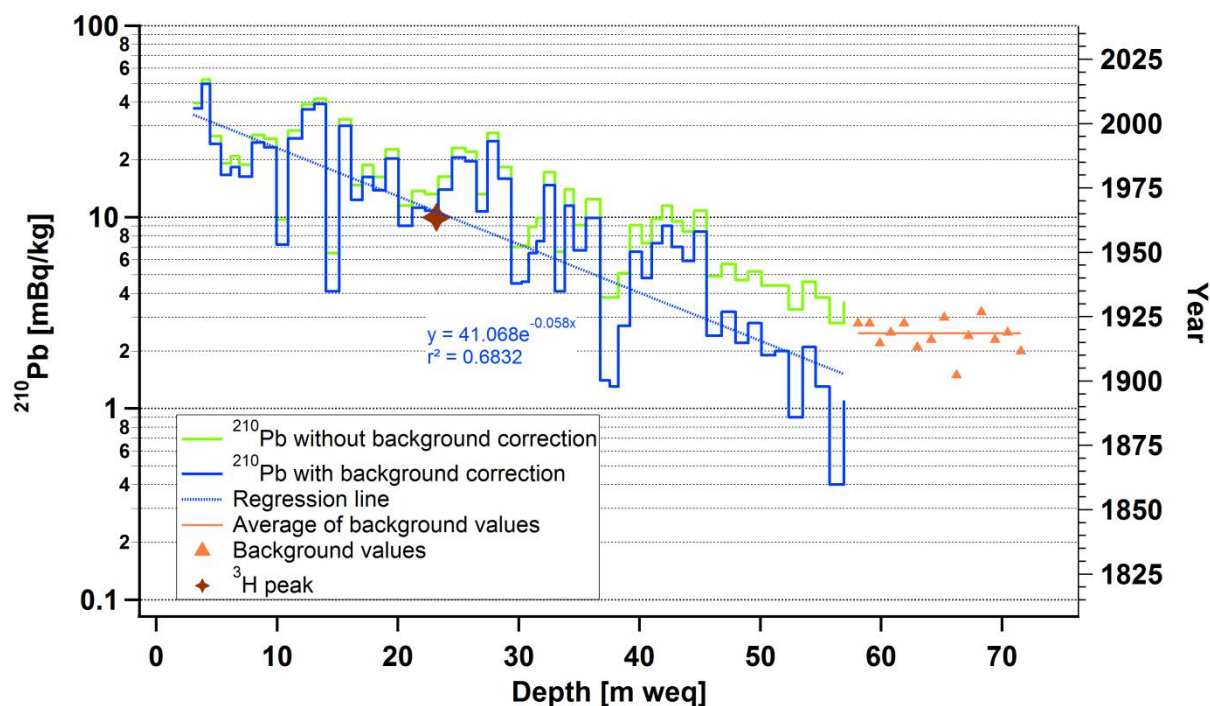


Figure 5.3 Results of the ^{210}Pb analysis of the Lomo09 ice core, with the tritium peak indicated (red cross). The background corrected data (blue line) are included in Figure 5.2B.

The ^{210}Pb analysis for the Lomo97 core was only conducted for the uppermost 25 m weq and did not reveal a decreasing trend (Pinglot et al., 2003). It was thus not used for dating. In the case of the Lomo09 core the ^{210}Pb results show a decrease with time (Figure 5.3) and support the dating by the other methods (Figure 5.2B).

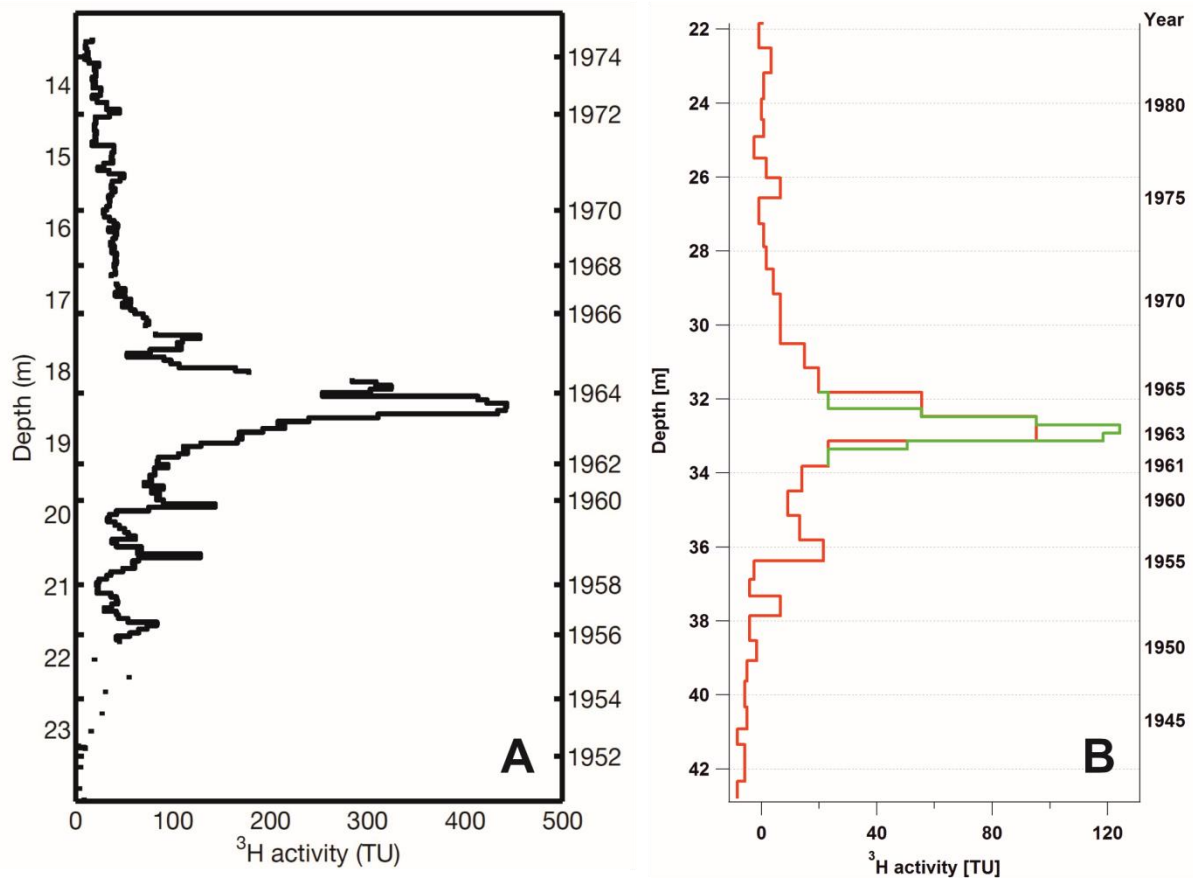


Figure 5.4 Tritium (^3H) records of (A) the Lomo97 (Van der Wel et al., 2011) and (B) the Lomo09 core with the counted years indicated on the right axes. The ^3H activities are not corrected for decay since the year 1963.

The tritium records of the two ice cores both reveal a clear peak, for the Lomo97 core at around 18.5 m depth, and for the Lomo09 core at around 33 m depth (Figure 5.4). The depth of the tritium peak is comparable for the two sites regarding the 12 additional years of snow accumulation for the Lomo09 core. The ^3H activity is also in the same range, the lower values in the Lomo09 core being caused by the longer time period between fallout and analysis.

5.3.2 Ion chemistry

In order to quantify the analytical quality of the ion data determined in the Lomo97 and Lomo09 cores, we consider the ion balances displayed in Figure 5.5. The high r^2 values of the linear fits, 0.91 for Lomo97 and 0.92 for Lomo09, respectively, reveal that the analytical quality for both cores is very good.

5 Is the climate reconstruction of one ice core representative?

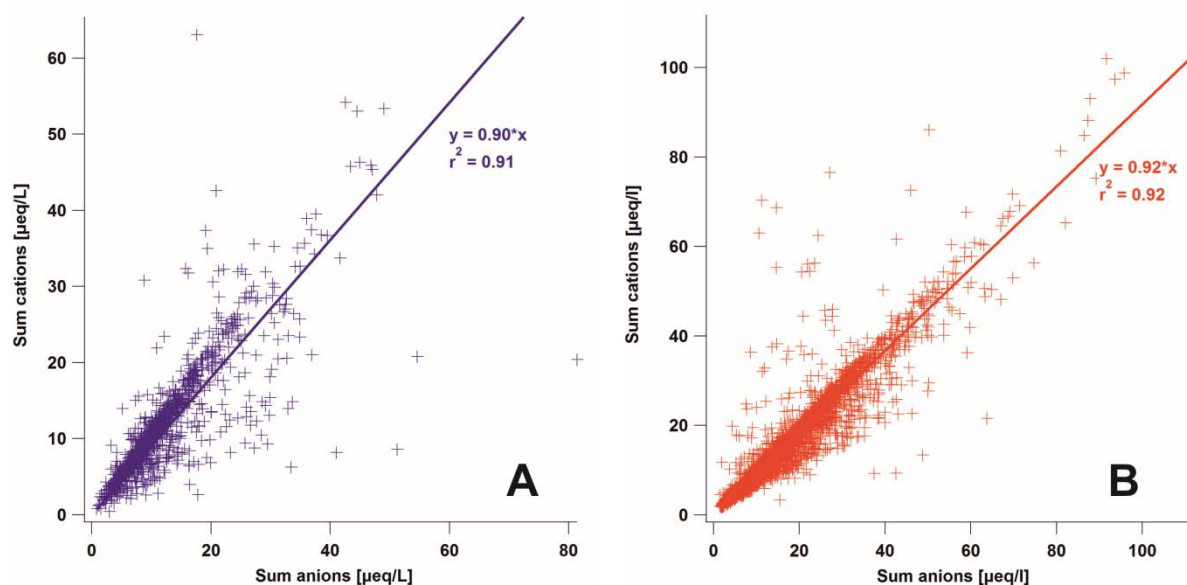


Figure 5.5 Ion balance plots for Lomo97 (A) and Lomo09 (B). The cations considered include Na^+ , NH_4^+ , K^+ , Mg^{2+} , and Ca^{2+} for both cores; the anions include MSA , Cl^- , NO_3^- , and SO_4^{2-} for both cores, for the Lomo09 additionally fluoride, acetate, formate, and oxalate have been included in the ion balance.

The ion records of the Lomo97 and the Lomo09 cores are in the same concentration range for all ionic species (Figures 5.6 and 5.7). In particular, the records of NO_3^- and SO_4^{2-} are in very good agreement (r^2 (10-year-avgs.) = 0.55 and 0.51, respectively). The dominant feature is the peak in concentrations between 1940 and 1990 for NO_3^- and 1920 and 1990 for SO_4^{2-} caused by anthropogenic emissions. The large SO_4^{2-} input by the Laki eruption is indicated by high SO_4^{2-} concentrations around 1780 in both cores. The MSA records agree reasonably well from 1450 onwards (r^2 (10-year-avgs.) = 0.14). Before 1450 the Lomo97 MSA record reveals low concentrations that have previously been explained by potential runoff (Isaksson et al., 2005a; Kekonen et al., 2005). The records of Cl^- , Ca^{2+} , Mg^{2+} , K^+ , and Na^+ are in the same concentration range, but it is noticeable that the records of the Lomo97 core have lower concentrations in the upper- and lowermost part of the core compared to the Lomo09 core. This could be explained by the runoff effect as suggested by Kekonen et al. (2005). We cannot explain why this runoff should only affect the 1997 drill site, but do not find a similar effect for the Lomo09 records. The NH_4^+ records show large differences especially before 1950, with generally higher concentrations in the Lomo97 core. We cannot explain this difference, but NH_4^+ is prone to contamination during analysis (e.g., Jauhiainen et al., 1999; Kaufmann et al., 2010).

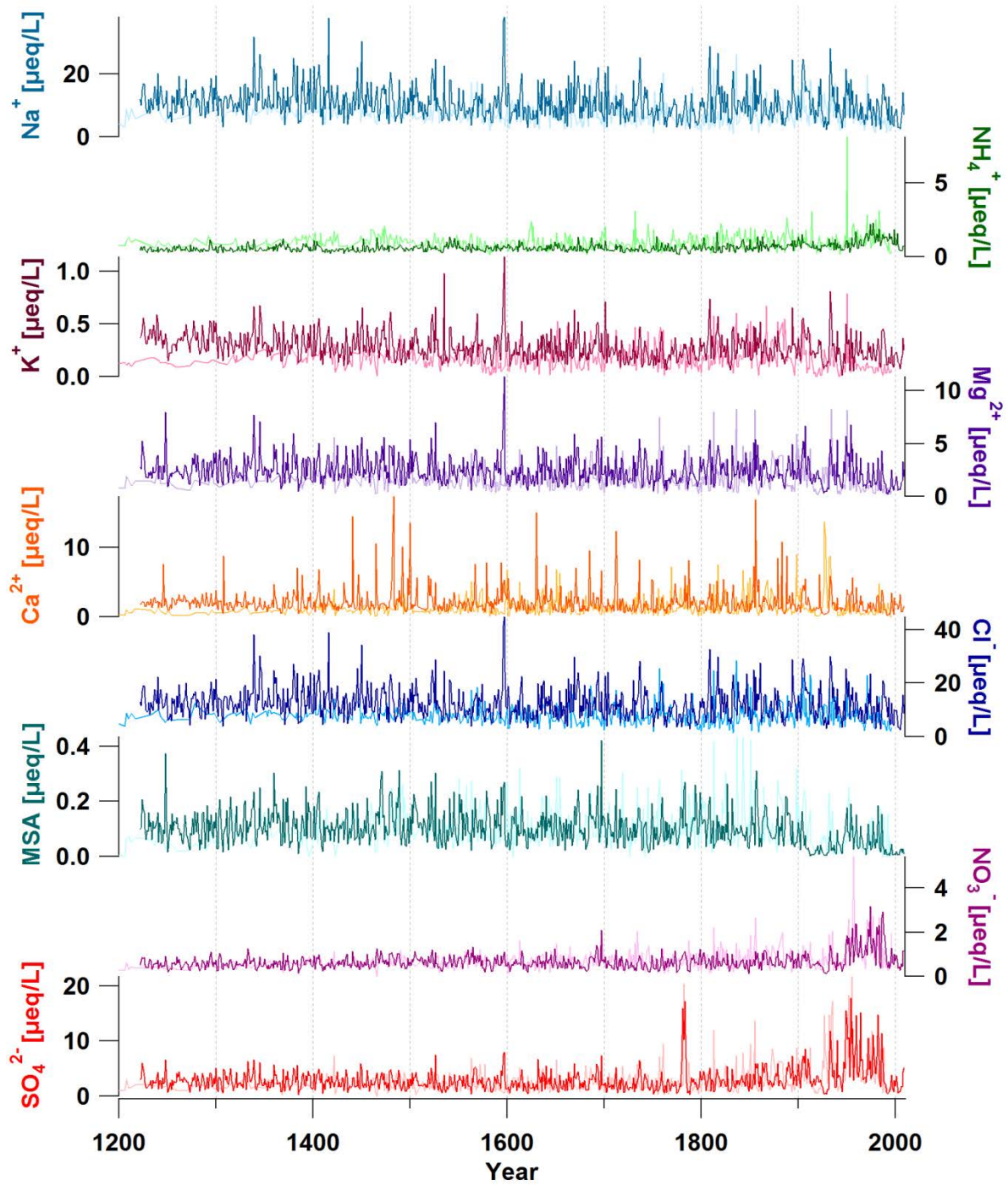


Figure 5.6 Records of the ionic species analysed in the Lomo97 (light colours; data: Kekonen et al. 2005, recalculated with the updated chronology of Divine et al. 2011) and the Lomo09 (dark colours) ice cores. Data are annual averages.

5 Is the climate reconstruction of one ice core representative?

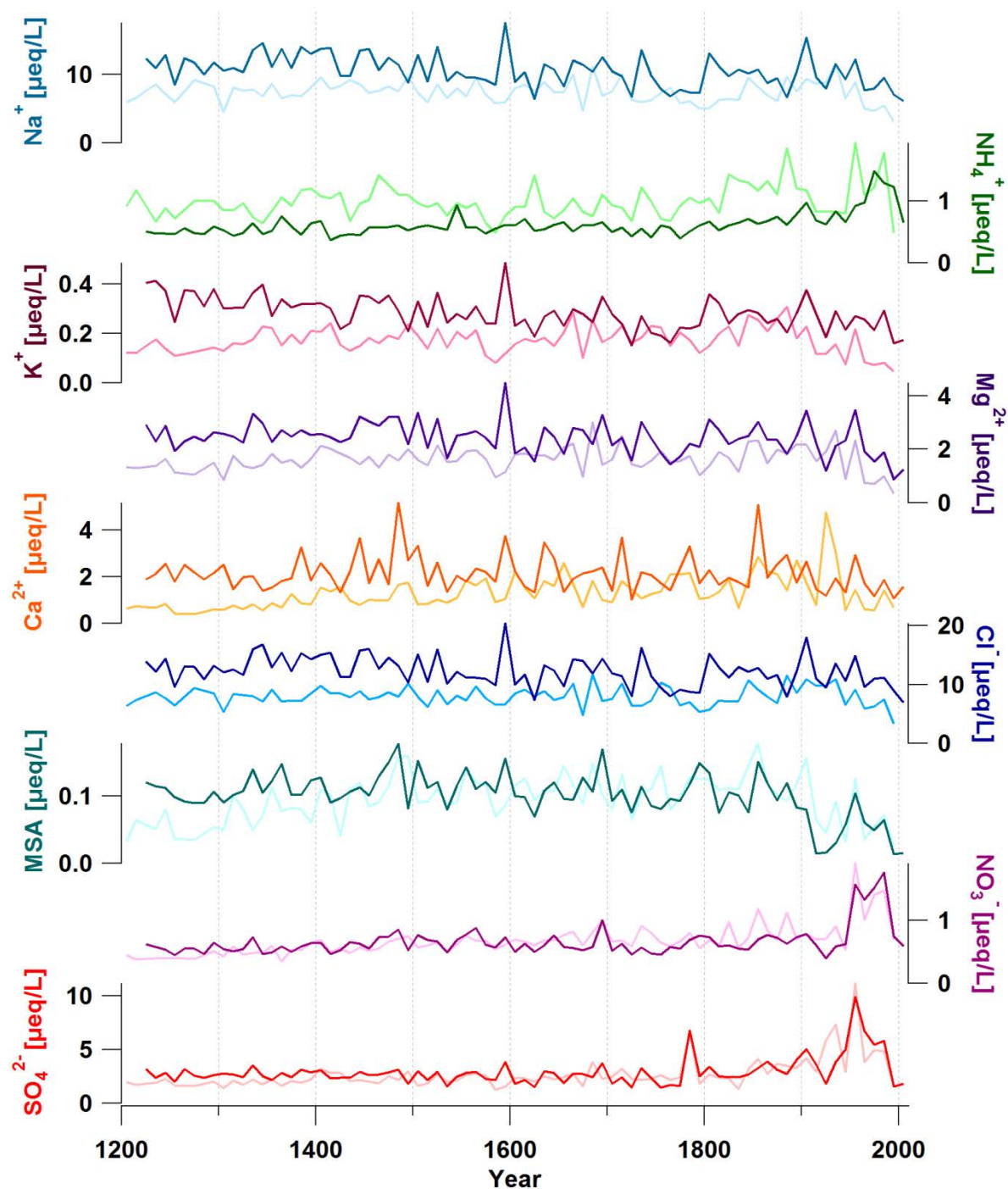


Figure 5.7 Records of the ionic species analysed in the Lomo97 (light colours; data: Kekonen et al. 2005, recalculated with the updated chronology of Divine et al. 2011) and the Lomo09 (dark colours) ice cores. Data are 10-year-averages.

The concentrations of all ionic species have a log-normal mono-modal distribution, apart from NH_4^+ and MSA. Graphs of the frequency distributions can be found in Figures S5-1 and S5-2 in the SM. The broader frequency distribution of NH_4^+ and MSA could be caused by contamination or secondary effects such as melting (Ginot et al., 2006).

We calculated median values for all ionic species in the time period covered by both ice cores (1222-1997) (Table 5.2). Additionally, we calculated the ratio of the medians of the Lomo09 to the Lomo97 core to resolve whether the ionic species behave similarly between the cores.

Table 5.2 Median values [$\mu\text{eq/L}$] for the ionic species determined in both ice cores. Further, the average annual accumulation rate [m/year] and the ratios of the values of Lomo09 to Lomo97 (ratio 09/97) are given. MSA = CH_3SO_3^- . Ann. acc. rate = annual accumulation rate. Ann.acc. rate for Lomo97 from Divine et al. (2011).

1222-1997	Lomo97	Lomo09	Ratio 09/97
MSA	0.07	0.07	1.0
Cl⁻	6.87	10.18	1.5
NO₃⁻	0.63	0.58	0.9
SO₄²⁻	2.25	2.35	1.0
Na⁺	6.18	8.50	1.4
NH₄⁺	0.90	0.57	0.6
K⁺	0.14	0.23	1.6
Mg²⁺	1.26	1.87	1.5
Ca²⁺	0.94	1.29	1.4
Ann. acc. rate	0.36	0.58	1.6

The ion chemistry of both cores is dominated by the sea salt species of Na^+ , Cl^- , K^+ , and Mg^{2+} that contribute >70% to the ion budget. The third most abundant ionic species is SO_4^{2-} which has several sources: (1) sea salt, (2) mineral dust, and (3) anthropogenic and biogenic gases, and volcanic eruptions (Legrand and Mayewski, 1997). Overall, the median values in the Lomo09 core are higher than in the Lomo97 core for all sea salt species and Ca^{2+} , and the same for MSA, NO_3^- and SO_4^{2-} in both cores. The difference of the NH_4^+ ratio can be explained by the potential contamination effect mentioned above. The ratios of the medians of the Lomo09 to the Lomo97 core range from 0.6 to 1.6, which is similar to the ratio of the annual accumulation rates of 1.6. Thus, we suggest the difference in annual accumulation rate to at least partly cause the differences in the concentrations of the ionic species in the two ice cores with larger ion deposition at a higher accumulation rate at the Lomo09 site. This suggests wet deposition to dominate in this region (Alley et al., 1995; Kreutz et al., 2000).

We performed a principal component analysis (PCA) on the Lomo97 and the Lomo09 cores to investigate sources and/ or transport pathways of the ionic species (Table 5.3), similar to Wendl et al. (2014, submitted to ACPD). In order to account for dating uncertainties and smoothing effects by melt-water relocation we used 10-year-averages. We only considered the period 1222-1859 to exclude anthropogenic influences on the ion concentrations. SO_4^{2-} has been

5 Is the climate reconstruction of one ice core representative?

shown to be influenced by anthropogenic emissions already during the second half of the 19th century (Moore et al., 2006).

Table 5.3 Results of the principal component analysis (PCA) after VARIMAX rotation. Time period: 1222-1859; data: 10-year averages; MSA = CH₃SO₃.

	Lomo09						Lomo97					
	PC1	PC2	PC3	PC4	PC5	PC6	PC1	PC2	PC3	PC4	PC5	PC6
Na ⁺	0.97	0.07	0.09	0.04	0.11	-0.07	0.97	0.03	0.03	0.09	0.12	0.03
K ⁺	0.88	0.16	0.01	0.00	0.14	0.38	0.38	0.29	0.18	0.17	0.82	0.15
Mg ²⁺	0.81	0.39	0.27	0.03	0.22	-0.02	0.60	0.33	-0.01	0.37	0.45	0.33
Cl ⁻	0.97	0.11	0.11	0.06	0.12	-0.12	0.95	0.08	0.03	0.12	0.19	0.08
MSA	0.31	0.84	0.20	0.16	0.16	-0.21	0.14	0.53	0.09	0.18	0.19	0.78
NO ₃ ⁻	0.09	0.87	0.19	0.24	0.22	0.22	0.01	0.86	0.24	0.15	0.24	0.20
Ca ²⁺	0.18	0.27	0.93	-0.02	0.19	0.00	0.18	0.81	-0.09	0.36	0.11	0.22
NH ₄ ⁺	0.05	0.23	-0.01	0.97	0.03	0.00	0.04	0.09	0.98	0.04	0.10	0.05
SO ₄ ²⁻	0.27	0.28	0.21	0.03	0.90	0.02	0.20	0.37	0.07	0.87	0.16	0.14
Var.												
[%]	40	21	12	12	11	3	28	24	13	13	12	10

We obtained six principal components (PCs) from the PCA (Table 5.3). For the Lomo09 core the PCA results in a clear grouping of the ionic species. PC1 that explains around 40% of the variance is dominated by the sea salt species Na⁺, K⁺, Mg²⁺, and Cl⁻. PC2 has high loadings of MSA and NO₃⁻, a correlation which suggests a link between NO₃⁻ deposition and ocean productivity (Wendl et al. 2014, submitted to ACPD). PC3 to PC5 are all dominated by a single species: Ca²⁺, NH₄⁺, and SO₄²⁻, respectively. Ca²⁺ derives from terrestrial mineral dust, thus PC3 covers the dust component. The high loading of NH₄⁺ in PC4 suggests biogenic emissions to be represented by this component (details in Wendl et al. 2014, submitted to ACPD). PC5 is dominated by SO₄²⁻ which indicates a volcanic source because the sea salt part of SO₄²⁻ is covered already by PC1. PC6 gives a more diverse picture with higher loadings of K⁺, and partly NO₃⁻ and anti-correlated MSA. The source for this component cannot be defined clearly. The PCA for the Lomo97 core results in a similar picture (Table 5.3). PC1 is also dominated by the sea salt species Na⁺, Mg²⁺, Cl⁻, and K⁺ to a smaller extent. However, PC1 here only explains around 28% of the variance and thus is not as dominant as for the Lomo09 core. PC2 is represented mainly by NO₃⁻ and Ca²⁺ which indicates a terrestrial mineral dust source. PC3 has a high loading of NH₄⁺, representing biogenic emissions. The high loading of SO₄²⁻ in PC4 again indicates a volcanic source because the sea salt SO₄²⁻ part is covered by PC1. PC5 has a high loading of K⁺, which, in combination with

higher loadings of Mg^{2+} and NO_3^- points to a marine, a mineral dust or a fire source. MSA has a high loading in PC6, representing marine biogenic emissions.

Generally, the PCA for both cores supports the dominance of sea salt species reflected in the ion budget. The PCAs agree further for NH_4^+ and SO_4^{2-} that occur separately from the other ionic species. The largest difference is seen for the correlations of MSA, NO_3^- , and Ca^{2+} . In the Lomo09 core MSA is clearly associated with NO_3^- (Wendl et al. 2014, submitted to ACPD), whereas in the Lomo97 core MSA occurs in a separate component and NO_3^- is associated with Ca^{2+} . The latter agrees with previous findings (Beine et al., 2003; Geng et al., 2010; Legrand et al., 1999; Röthlisberger et al., 2000, 2002; Teinilä et al., 2003), but is contrary to the statement by Kekonen et al. (2002) that in general there is no clear association of Ca^{2+} and NO_3^- in the Lomo97 core. The link between NO_3^- and ocean productivity (Wendl et al. 2014, submitted to ACPD) is thus only reflected in the Lomo09 and not in the Lomo97 core.

5.3.3 Annual accumulation rate

The annual accumulation rate of the Lomo97 core has been discussed in several studies. Isaksson et al. (2001) determined a mean annual accumulation rate of 0.36 m weq for the period 1963-1996, based on the depth of the 1963 radioactive layer. They further identified an accumulation gradient from several shallow cores drilled in the vicinity of the 1997 deep core. The lower accumulation rate at the summit of Lomonosovfonna, the Lomo97 drilling site, was attributed rather to a local precipitation feature than strong wind scouring (Isaksson et al., 2001). Pohjola et al. (2002b) reconstructed the accumulation at the Lomo97 drilling site for three centuries based on the record of the water stable isotopes. They determined an average accumulation rate of 0.30 m weq from 1715 to 1950, and an increased accumulation rate of 0.41 m weq on average for the period 1950 to 1997. Pälli et al. (2002) found the average annual accumulation rate at the Lomo97 drilling site with 0.45 m weq between 1986 and 1999 to be about 12% higher than for 1963-86 with 0.38 m weq, based on ground-penetrating radar measurements. They explained this with an increasing precipitation trend also seen in the instrumental records from Longyearbyen. Pälli et al. (2002) further observed a 40-60% spatial variability in snow accumulation on Lomonosovfonna over short distances. They stated this to be caused mainly by local topography, with bedrock depressions leading to increased accumulation. Divine et al. (2011) updated the Lomo97 chronology, based on a partial resampling of the core and a simple glacier flow model (Nye, 1963) fitted through the data. This resulted in the mean accumulation rates of 0.42, 0.32, 0.37, and 0.36 m weq for the time periods 1997-1963, 1963-1903, 1903-1783, and before 1783, respectively.

5 Is the climate reconstruction of one ice core representative?

The average annual accumulation rate for the Lomo09 core was determined to be 0.58 m weq, based on a simple glacier flow model (Thompson et al., 1998) fitted through the reference horizons (see chapter 5.3.1 for details). This model includes further a thinning factor (1.015 for the Lomo09 core) which accounts for layer thinning with depth. Thus, the accumulation rate at the 2009 drilling site is about 60% higher than at the site of the 1997 drilling, leading to higher deposition of the ionic species, as discussed in chapter 5.3.2. This variability in the accumulation rates within a distance of less than 5 km seems realistic. Previous studies already indicated a high spatial variability of the accumulation in the Lomonosovfonna area (Figures S5-3 and S5-4; Claremar, 2013; Isaksson et al., 2001; Pälli et al., 2002).

5.3.4 Water stable isotope ratio $\delta^{18}\text{O}$

$\delta^{18}\text{O}$ has been shown to be a valuable temperature proxy at Lomonosovfonna (Isaksson et al., 2001, 2005b). Divine et al. (2011) used the $\delta^{18}\text{O}$ record of the Lomo97 core to reconstruct 1000 years of winter temperature. The $\delta^{18}\text{O}$ record of the Lomo97 core was further observed to correlate best with the instrumental temperature record from Vardø covering the time back to 1840 (Isaksson et al., 2005b), probably caused by the longer record from Vardø (Grinsted et al., 2006). Grinsted et al. (2006) detected a better correlation for Lomo97 $\delta^{18}\text{O}$ and the Svalbard airport (Longyearbyen) temperature record (Nordli et al., 1996) for the common period of both temperature records (1911 to 1997) than for Lomo97 $\delta^{18}\text{O}$ and Vardø temperature. They interpreted this as temperatures near Longyearbyen being more representative of conditions on Lomonosovfonna than those from Vardø.

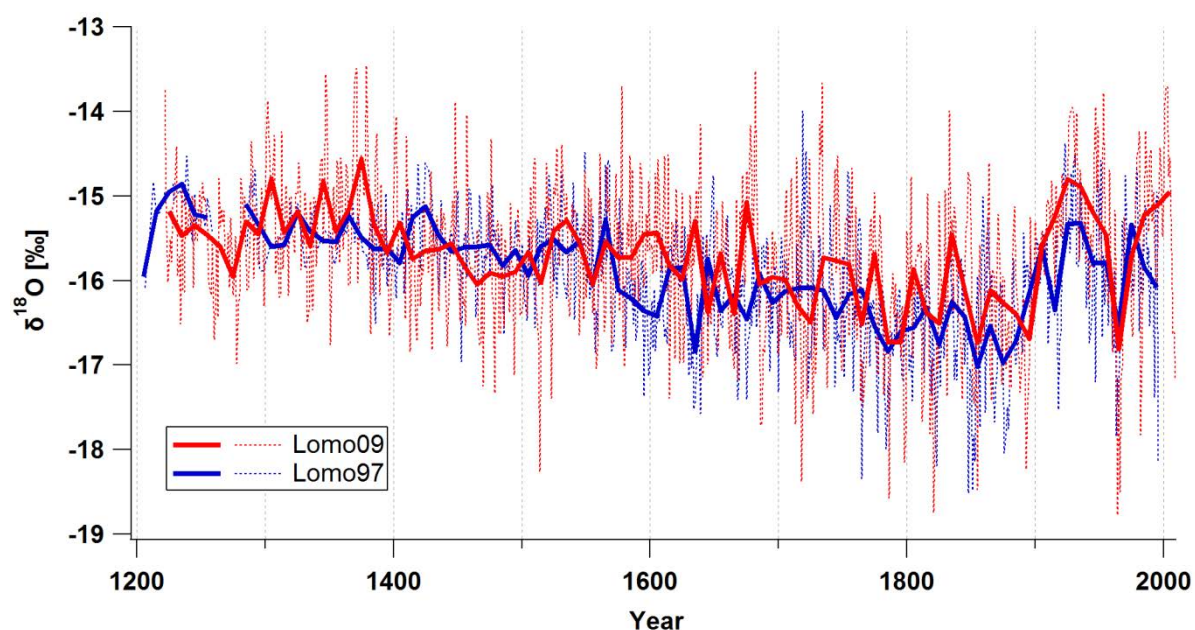


Figure 5.8 Records of $\delta^{18}\text{O}$ of the Lomo97 (blue; Divine et al., 2011) and the Lomo09 ice core (red). Dashed lines are annual averages; bold lines are 10-year-averages.

The $\delta^{18}\text{O}$ records of the Lomo97 and the Lomo09 ice cores agree well with a decreasing trend from 1200 to approximately 1880, highest values between 1900 and 1950, lower values around 1960 and increasing values since then (Figure 5.8). The most negative $\delta^{18}\text{O}$ values and thus the coldest temperatures occur between about 1760 and 1880, as previously noted by Isaksson et al. (2005c). The $\delta^{18}\text{O}$ values are normally distributed, as can be seen in Figure S5-2 in the SM. The great similarity of the two $\delta^{18}\text{O}$ records suggests that the conclusions drawn for the Lomo97 $\delta^{18}\text{O}$ record also apply for the Lomo09 $\delta^{18}\text{O}$ record, although this remains to be studied in detail.

5.3.5 Melt indices stratigraphic melt index and $\ln(\text{Na}^+/\text{Mg}^{2+})$

Low-altitude glaciers in the Arctic are highly affected by seasonal melt (Koerner, 1997) that results in a modified distribution of the chemical species within the ice column, with some species being removed easier than others (Brimblecombe et al., 1985; Davies et al., 1982; Moore and Grinsted, 2009; Pohjola et al., 2002a; Virkkunen et al., 2007). The Lomo97 ice core was found to suffer from modest melt, with an average stratigraphic melt index of ~41% (Pohjola et al., 2002a). The melt index describes how much of an annual layer is affected by melt (Koerner and Fisher, 1990). Despite the high melt index of the Lomo97 core it could be shown that the chemical signals are preserved within two to eight annual layers (Moore et al., 2005; Pohjola et al., 2002a). The melt index of the Lomo09 core is on average 31%. Thus the maximal percolation length is thought to be at the most as high as in the Lomo97 core. On Nordenskjöldbreen, one of the outlet glaciers of Lomonosovfonna, van Pelt et al. (2012) observed that refreezing water contributes 0.27 m weq per year, which is equivalent to 69% of the annual snow accumulation. This is almost twice as high as the refreezing contribution for the Lomo97 and Lomo09 cores, with values of 0.15 and 0.18 m weq per year, respectively. This could be explained by the higher altitude of the drilling sites that are thus less affected by melt.

Previous publications on the Lomo97 core have used either the stratigraphic melt index (Grinsted et al., 2006) or the ratio of Mg^{2+} to Na^+ as index for summer melt (Beaudon et al., 2013; Iizuka et al., 2002). Figure 5.9 compares the stratigraphic melt records of the two cores. For the Lomo97 only 10- or 15-year-moving-averaged data were available (Grinsted et al., 2006; Kekonen et al., 2005). Thus, only a visual comparison was possible. The Lomo97 stratigraphic melt record covers only the time period between around 1700 and 1997, restricted by the applied method (Kekonen et al., 2005). Nevertheless, a reasonable agreement of the two records can be observed, with increased melt around 1790, 1850, 1900 and 1980. However, the highest value for the stratigraphic melt index in the Lomo97 occurs around 1790, whereas melt in the Lomo09 core was even more severe around 1900 than in 1990. Furthermore, the general

5 Is the climate reconstruction of one ice core representative?

increasing trend seen in the Lomo09 record is not depicted in the Lomo97 record, probably due to the shorter time period covered.

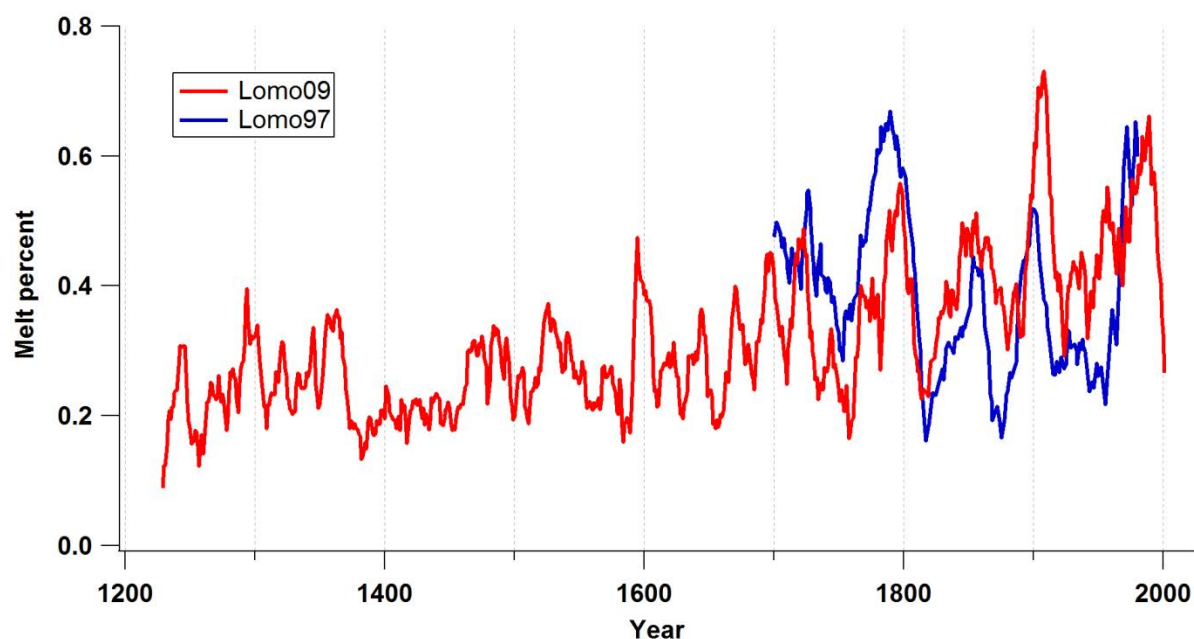


Figure 5.9 The records of the stratigraphic melt index. For the Lomo97 only 10- or 15-year-moving-averaged data were available (Grinsted et al., 2006; Kekonen et al., 2005). Data shown are 15-year-moving averages. Lomo97 data from Grinsted et al. (2006).

We additionally compare the records of the natural logarithm of the ratio Na^+ to Mg^{2+} in the Lomo97 and Lomo09 ice cores (Figure 5.10), an indicator for summer melt previously applied on the Lomo97 and the Høltedahlfonna ice cores (Beaudon et al., 2013).

The records of $\ln(\text{Na}^+/\text{Mg}^{2+})$ of the two ice cores agree reasonably well (r^2 (10-year-avgs.) = 0.09), with the most prominent feature being the increased values from 1810 to 1995 (Figure 5.10). The absolute values and the trends are similar for the two cores. However, the Lomo97 record experiences more or less constantly increasing values for the melt indicator from 1810 to 1995, whereas the Lomo09 record reveals two peaks around 1920 and around 1995. For the Lomo97 core Moore et al. (2005) found that more than 60% of the variance in the ion records is attributed to seasonal melting. In contrast, Wendl et al. (2014, submitted to ACPD), using the stratigraphic melt percent instead of $\ln(\text{Na}^+/\text{Mg}^{2+})$, concluded that melt did not affect the ion records in the Lomo09 core on decadal timescales.

The higher values for $\ln(\text{Na}^+/\text{Mg}^{2+})$ around 1920 and 1995 in the Lomo09 record resemble those detected in the Høltedahlfonna core between 1915 to 1945 and around 1990 (Beaudon et al., 2013). Beaudon et al. (2013) observed a significant correlation of the $\ln(\text{Na}^+/\text{Mg}^{2+})$ melt index with the summer air temperatures (June, July, August) recorded at Svalbard airport (Longyearbyen) since 1911, a correlation not seen for the Lomo97 record. So far we cannot

explain the greater similarity of the melt records of the Lomo09 and the Holtedahlfonna core compared to that of the two cores from Lomonosovfonna.

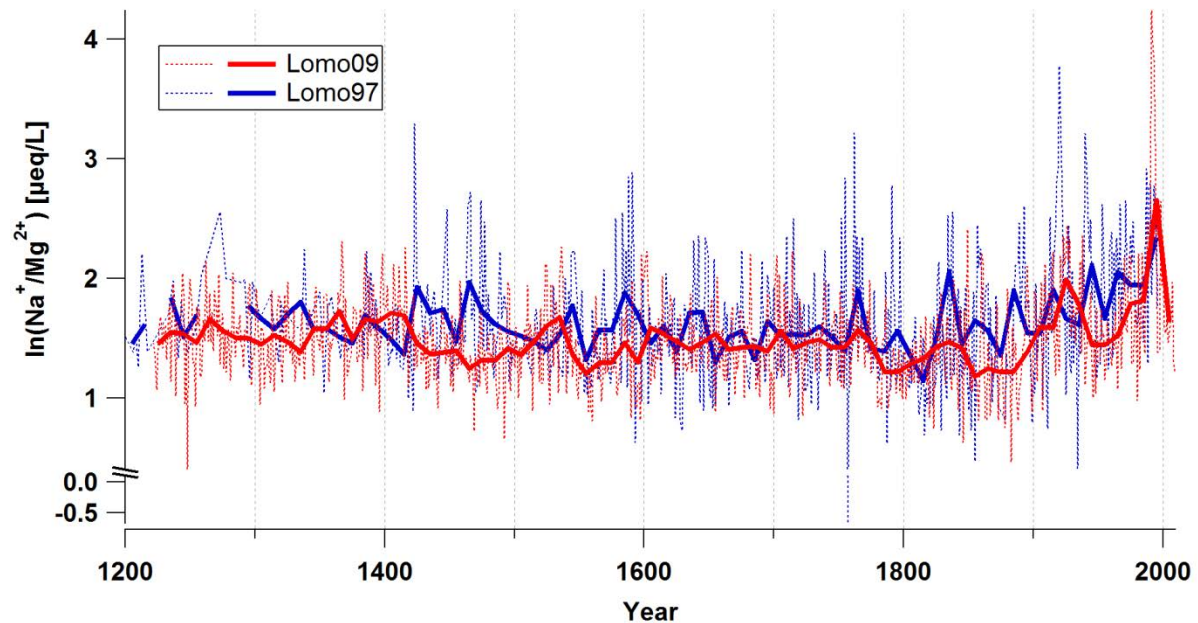


Figure 5.10 Records of $\ln(\text{Na}^+/\text{Mg}^{2+})$ of the Lomo97 (blue; data: Kekonen et al. (2005) calculated with updated chronology of Divine et al. (2011)) and Lomo09 (red) ice core. Dashed lines are annual averages; bold lines are 10-year-averages.

Additionally, we compare the two melt indices stratigraphic melt percent and $\ln(\text{Na}^+/\text{Mg}^{2+})$ of the Lomo09 core (Figure 5.11). This reveals that the two melt indices do not necessarily give the same picture. The general increase in melt with time is visible in both records but the increase in the last 150 years is more pronounced in the $\ln(\text{Na}^+/\text{Mg}^{2+})$ record. Hence the conclusions drawn on either melt index record cannot as such be transferred to the other.

5 Is the climate reconstruction of one ice core representative?

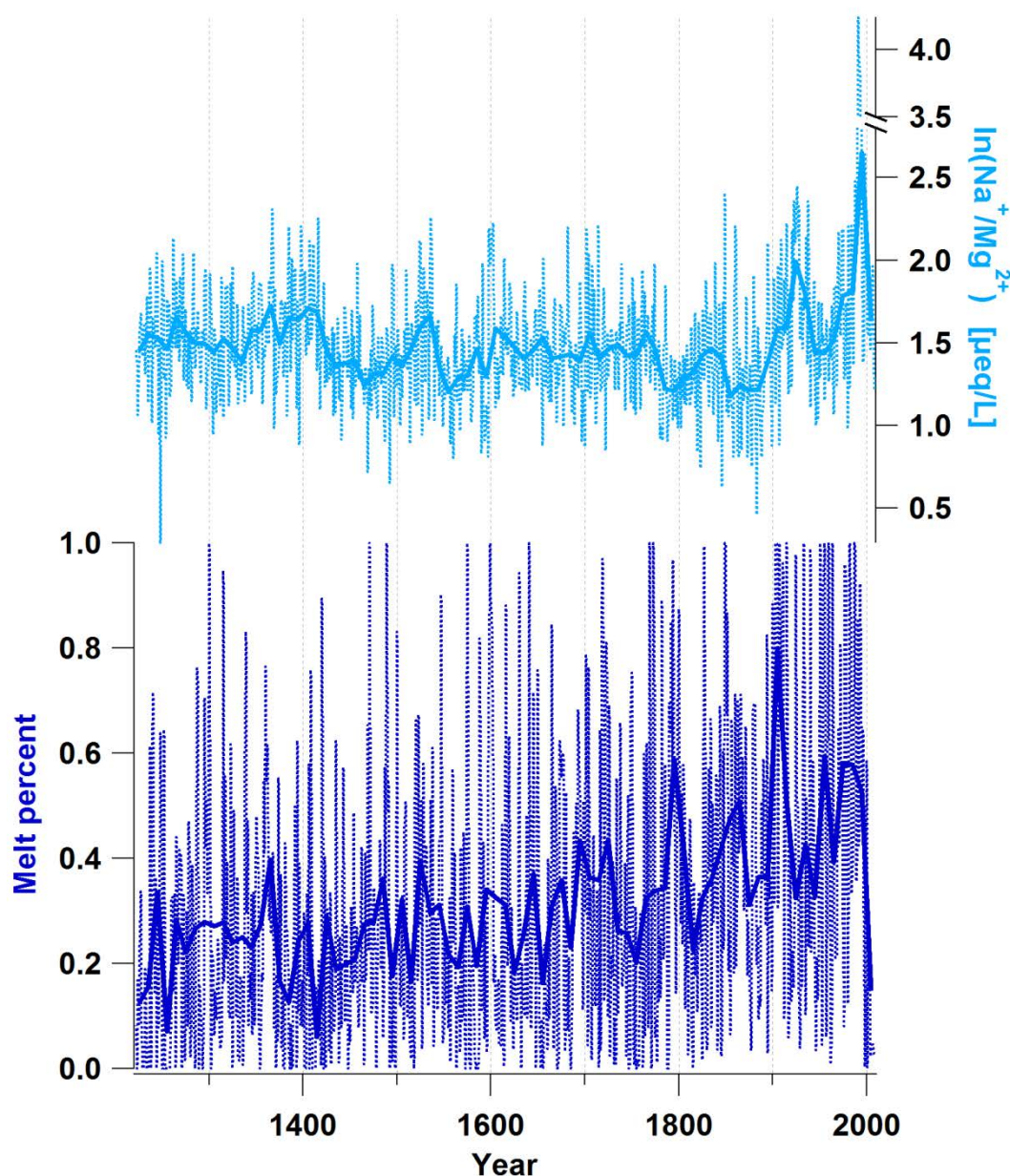


Figure 5.11 Records of the two melt indices stratigraphic melt percent and $\ln(\text{Na}^+/\text{Mg}^{2+})$ for the Lomo09 core. Dashed lines are annual averages; bold lines are 10-year-averages.

5.4 Summary and conclusions

In order to test the spatial representativeness of a climate and environmental reconstruction from one ice core we compared two ice cores from Lomonosovfonna, Svalbard, drilled in 1997 and 2009 (Lomo97 and Lomo09). The results from the detailed analyses of the two cores are reasonably similar in most cases. The ion chemistry agrees well, as do the trends in the records of the ions, of $\delta^{18}\text{O}$, and of the stratigraphic melt index. The ion budgets of the cores are dominated by the sea salt species of Na^+ , Cl^- , K^+ , and Mg^{2+} that contribute >70%. The

anthropogenic influence is clearly seen in the NO_3^- and SO_4^{2-} records, with maximum concentrations from 1940 and 1990 for NO_3^- and 1920 and 1990 for SO_4^{2-} . Due to the great similarity of the two $\delta^{18}\text{O}$ records, $\delta^{18}\text{O}$ in the Lomo09 core is also thought to best correlate with Svalbard airport (Longyearbyen) air temperature.

The differences between the cores appear mainly in the dating. Several major volcanic eruptions could be identified for both cores, but the attribution of the SO_4^{2-} peak detected in the deepest core sections is ambiguous. The peak in the SO_4^{2-} record at 99.8 m weq in the Lomo97 and at 121.8 m weq in the Lomo09 core is assigned to Hekla 1104 or 1158 in the Lomo97 and to Samalas 1257/58 in the Lomo09 core. We cannot resolve whether one is more correct than the other, because in either case the annual accumulation rate to fit the other major volcanic eruption is out of range. Furthermore, the correlation of MSA and NO_3^- observed in the Lomo09 core is not seen in the Lomo97, where NO_3^- is correlated with Ca^{2+} . Thus, NO_3^- in the Lomo97 is not linked to ocean productivity as in the Lomo09 core. The annual accumulation rate at the two sites differs by 60%, which is explained by the high spatial variability already observed in previous studies. The records of the melt index $\ln(\text{Na}^+/\text{Mg}^{2+})$ in the two cores diverge after 1800. The Lomo09 record then resembles more that of the Hoftedahlfonna ice core drilled in 2005, with its two peaks between 1915 to 1945 and around 1990. So far, we cannot explain this resemblance of the Lomo09 melt record with that of the Hoftedahlfonna core.

This first comparison of the two most recent ice cores from Lomonosovfonna reveals that if sample resolution is high, i.e. at least annual, the climate and environmental reconstruction from one ice core may be representative of a single glacier, but not necessarily of an entire region such as Svalbard.

References

- Alley, R., Finkel, R., Nishizumi, K., Anandakrishnan, A., Shuman, C., Mershon, G., Zielinski, G. and Mayewski, P.: Changes in continental and sea-salt atmospheric loadings in central Greenland during the most recent deglaciation: Model-based estimates, *Journal of Glaciology*, 503–514, 1995.
- AMAP: The impact of black carbon on Arctic climate, Arctic Monitoring and Assessment Programme (AMAP), Oslo, 2011.
- Beaudon, E., Moore, J. C., Martma, T., Pohjola, V. A., van de Wal, R. S. W., Kohler, J. and Isaksson, E.: Lomonosovfonna and Holtedahlfonna ice cores reveal east–west disparities of the Spitsbergen environment since AD 1700, *Journal of Glaciology*, 59(218), 1069–1083, doi:10.3189/2013JG12J203, 2013.
- Beine, H. J., Dominè, F., Ianniello, A., Nardino, M., Allegrini, I., Teinilä, K. and Hillamo, R.: Fluxes of nitrates between snow surfaces and the atmosphere in the European high Arctic, *Atmospheric Chemistry and Physics*, 3(2), 335–346, doi:10.5194/acp-3-335-2003, 2003.
- Brimblecombe, P., Tranter, M., Abrahams, P. W., Blackwood, I., Davies, T. D. and Vincent, C. E.: Relocation and preferential elution of acidic solute through the snowpack of a small, remote, high-altitude Scottish catchment, *Annals of Glaciology*, 7, 141–147, 1985.
- Claremar, B.: Relation between meso-scale climate and glacier/snow mass balance on Svalbard, SVALI Deliverable D2.3-11 report, Uppsala University., 2013.
- Davies, T. D., Vincent, C. E. and Brimblecombe, P.: Preferential elution of strong acids from a Norwegian ice cap, *Nature*, 300(5888), 161–163, doi:10.1038/300161a0, 1982.
- Divine, D., Isaksson, E., Martma, T., Meijer, H. A. ., Moore, J., Pohjola, V., van de Wal, R. S. W. and Godtliobsen, F.: Thousand years of winter surface air temperature variations in Svalbard and northern Norway reconstructed from ice core data, *Polar Research*, 30(0), 2011.
- Eichler, A., Schwikowski, M., Gäggeler, H. W., Furrer, V., Synal, H.-A., Beer, J., Saurer, M. and Funk, M.: Glaciochemical dating of an ice core from upper Grenzgletscher (4200 m a.s.l.), *Journal of Glaciology*, 46(154), 507–515, doi:10.3189/172756500781833098, 2000.
- Fritzsche, D., Wilhelms, F., Savatyugin, L. M., Pinglot, J. F., Meyer, H., Hubberten, H.-W. and Miller, H.: A new deep ice core from Akademii Nauk ice cap, Severnaya Zemlya, Eurasian Arctic: first results, *Annals of Glaciology*, 35(1), 25–28, doi:10.3189/172756402781816645, 2002.
- Gäggeler, H., Von Gunten, H. R., Rössler, E., Oeschger, H. and Schotterer, U.: ²¹⁰Pb-dating of cold alpine firn/ice cores from Colle Gnifetti, Switzerland, *Journal of Glaciology*, 29(101), 165–177, 1983.
- Geng, H., Ryu, J. Y., Jung, H. J., Chung, H., Ahn, K. H. and Ro, C. U.: Single-particle characterization of summertime Arctic aerosols collected at Ny-Ålesund, Svalbard, *Environmental Science & Technology*, 44(7), 2348–2353, 2010.

- Ginot, P., Kull, C., Schotterer, U., Schwikowski, M. and Gäggeler, H. W.: Glacier mass balance reconstruction by sublimation induced enrichment of chemical species on Cerro Tapado (Chilean Andes), *Climate of the Past*, 2(1), 21–30, doi:10.5194/cp-2-21-2006, 2006.
- Gordiyenko, F. G., Kotlyakov, V. M., Punning, Y. -K. M. and Vairmäe, R.: Study of a 200-m core from the Lomonosov ice plateau on Spitsbergen and the paleoclimatic implications, *Polar Geography and Geology*, 5(4), 242–251, doi:10.1080/10889378109388695, 1981.
- Grinsted, A., Moore, J. C., Pohjola, V., Martma, T. and Isaksson, E.: Svalbard summer melting, continentality, and sea ice extent from the Lomonosovfonna ice core, *Journal of Geophysical Research*, 111, D07110, 2006.
- Henderson, K., Laube, A., Gäggeler, H. W., Olivier, S., Papina, T. and Schwikowski, M.: Temporal variations of accumulation and temperature during the past two centuries from Belukha ice core, Siberian Altai, *Journal of Geophysical Research*, 111(D3), D03104, 2006.
- Hirdman, D., Sodemann, H., Eckhardt, S., Burkhart, J. F., Jefferson, A., Mefford, T., Quinn, P. K., Sharma, S., Ström, J. and Stohl, A.: Source identification of short-lived air pollutants in the Arctic using statistical analysis of measurement data and particle dispersion model output, *Atmospheric Chemistry and Physics*, 10, 669–693, 2010.
- Iizuka, Y., Igarashi, M., Kamiyama, K., Motoyama, H. and Watanabe, O.: Ratios of Mg²⁺/Na⁺ in snowpack and an ice core at Austfonna ice cap, Svalbard, as an indicator of seasonal melting, *Journal of Glaciology*, 48(162), 452–460, 2002.
- Isaksson, E., Pohjola, V., Jauhiainen, T., Moore, J., Pinglot, J. F., Vaikmaa, R., van de Wal, R. S. W., Hagen, J. O., Ivask, J., Karlöf, L., Martma, T., Meijer, H. A. J., Mulvaney, R., Thomassen, M. and van den Broeke, M.: A new ice-core record from Lomonosovfonna, Svalbard: viewing the 1920-97 data in relation to present climate and environmental conditions, *Journal of Glaciology*, 47(157), 335–345, 2001.
- Isaksson, E., Hermanson, M., Hicks, S., Igarashi, M., Kamiyama, K., Moore, J., Motoyama, H., Muir, D., Pohjola, V., Vaikmäe, R., van de Wal, R. S. W., Watanabe, O.: Ice cores from Svalbard—useful archives of past climate and pollution history, *Physics and Chemistry of the Earth, Parts A/B/C*, 28(28-32), 1217–1228, 2003.
- Isaksson, E., Kekonen, T., Moore, J. and Mulvaney, R.: The methanesulfonic acid (MSA) record in a Svalbard ice core, *Annals of Glaciology*, 42(1), 345–351, doi:10.3189/172756405781812637, 2005a.
- Isaksson, E., Kohler, J., Pohjola, V., Moore, J., Igarashi, M., Karlöf, L., Martma, T., Meijer, H., Motoyama, H., Vaikmäe, R. and van de Wal, R. S. W.: Two ice-cored $\delta^{18}\text{O}$ records from Svalbard illustrating climate and sea-ice variability over the last 400 years, *Holocene*, 15(4), 501–509, doi:10.1191/0959683605h1820rp, 2005b.
- Isaksson, E., Divine, D., Kohler, J., Martma, T., Pohjola, V., Motoyama, H. and Watanabe, O.: Climate oscillations as recorded in Svalbard ice core $\delta^{18}\text{O}$ records between AD 1200 and 1997, *Geografiska Annaler: Series A, Physical Geography*, 87(1), 203–214, 2005c.

5 Is the climate reconstruction of one ice core representative?

Jauhiainen, T., Moore, J., Perämäki, P., Derome, J. and Derome, K.: Simple procedure for ion chromatographic determination of anions and cations at trace levels in ice core samples, *Analytica Chimica Acta*, 389(1-3), 21–29, 1999.

Kaufmann, P., Fundel, F., Fischer, H., Bigler, M., Ruth, U., Udisti, R., Hansson, M., de Angelis, M., Barbante, C., Wolff, E. W., Hutterli, M. and Wagenbach, D.: Ammonium and non-sea salt sulfate in the EPICA ice cores as indicator of biological activity in the Southern Ocean, *Quaternary Science Reviews*, 29(1–2), 313–323, doi:10.1016/j.quascirev.2009.11.009, 2010.

Kekonen, T., Moore, J. C., Mulvaney, R., Isaksson, E., Pohjola, V. and van de Wal, R. S. W.: A 800 year record of nitrate from the Lomonosovfonna ice core, Svalbard, *Annals of Glaciology*, 35(1), 261–265, 2002.

Kekonen, T., Moore, J., Perämäki, P., Mulvaney, R., Isaksson, E., Pohjola, V. and van de Wal, R. S. W.: The 800 year long ion record from the Lomonosovfonna (Svalbard) ice core, *Journal of Geophysical Research*, 110, D07304, 2005.

Koerner, R. M.: Some comments on climatic reconstructions from ice cores drilled in areas of high melt, *Journal of Glaciology*, 43, 90–97, 1997.

Koerner, R. M. and Fisher, D. A.: A record of Holocene summer climate from a Canadian high-Arctic ice core, *Nature*, 343(6259), 630–631, doi:10.1038/343630a0, 1990.

Kotlyakov, V. M., Arkhipov, S. M., Henderson, K. A. and Nagornov, O. V.: Deep drilling of glaciers in Eurasian Arctic as a source of paleoclimatic records, *Quaternary Science Reviews*, 23(11), 1371–1390, 2004.

Kreutz, K. J., Mayewski, P. A., Meeker, L. D., Twickler, M. S. and Whitlow, S. I.: The effect of spatial and temporal accumulation rate variability in west Antarctica on soluble ion deposition, *Geophysical Research Letters*, 27(16), 2517–2520, doi:10.1029/2000GL011499, 2000.

Legrand, M., Wolff, E. and Wagenbach, D.: Antarctic aerosol and snowfall chemistry: implications for deep Antarctic ice-core chemistry, *Annals of Glaciology*, 29(1), 66–72, doi:10.3189/172756499781821094, 1999.

Moore, J. C. and Grinsted, A.: Ion fractionation and percolation in ice cores with seasonal melting, in *Physics of Ice Core Records II*, vol. 68, edited by Institute of Low Temperature Science, Hokkaido University, pp. 287–298, Hokkaido University Press, Sapporo, Japan, 2009.

Moore, J. C., Grinsted, A., Kekonen, T. and Pohjola, V.: Separation of melting and environmental signals in an ice core with seasonal melt, *Geophysical Research Letters*, 32(10), L10501, 2005.

Moore, J., Kekonen, T., Grinsted, A. and Isaksson, E.: Sulfate source inventories from a Svalbard ice core record spanning the industrial revolution, *Journal of Geophysical Research*, 111(D15), 15307, 2006.

Moore, J. C., Beaudon, E., Kang, S., Divine, D., Isaksson, E., Pohjola, V. A. and van de Wal, R. S. W.: Statistical extraction of volcanic sulphate from nonpolar ice cores, *Journal of Geophysical Research*, 117(D3), D03306, 2012.

- Nordli, P. Ø, Hanssen-Bauer, I. and Førland, E. J.: Homogeneity analyses of temperature and precipitation series from Svalbard and Jan Mayen, Norske meteorologiske institutt, 1996.
- Nye, J. F.: Correction factor for accumulation measured by the thickness of the annual layers in an ice sheet, *Journal of Glaciology*, 4(36), 785–788, 1963.
- Pälli, A., Kohler, J. C., Isaksson, E., Moore, J. C., Pinglot, J. F., Pohjola, V. A. and Samuelsson, H.: Spatial and temporal variability of snow accumulation using ground-penetrating radar and ice cores on a Svalbard glacier, *Journal of Glaciology*, 48(162), 417–424, 2002.
- Van Pelt, W. J. J., Oerlemans, J., Reijmer, C. H., Pohjola, V. A., Pettersson, R. and van Angelen, J. H.: Simulating melt, runoff and refreezing on Nordenskiöldbreen, Svalbard, using a coupled snow and energy balance model, *The Cryosphere*, 6(3), 641–659, doi:10.5194/tc-6-641-2012, 2012.
- Pinglot, J. F., Pourchet, M., Lefauconnier, B., Hagen, J. O., Isaksson, E., Vaikmäe, R. and Kamiyama, K.: Accumulation in Svalbard glaciers deduced from ice cores with nuclear tests and Chernobyl reference layers, *Polar Research*, 18(2), 315–321, 1999.
- Pinglot, J. F., Vaikmae, R. A., Kamiyama, K., Igarashi, M., Fritzsche, D., Wilhelms, F., Koerner, R., Henderson, L., Isaksson, E., Winther, J. G., van de Wal, R. S. W., Fournier, M., Bouisset, P. and Meijer, H. A. J.: Ice cores from Arctic sub-polar glaciers: chronology and post-depositional processes deduced from radioactivity measurements, *Journal of Glaciology*, 49(164), 149–158, 2003.
- Pohjola, V. A., Moore, J. C., Isaksson, E., Jauhiainen, T., van de Wal, R. S. W., Martma, T., Meijer, H. A. J. and Vaikmäe, R.: Effect of periodic melting on geochemical and isotopic signals in an ice core from Lomonosovfonna, Svalbard, *Journal of Geophysical Research*, 107(10.1029), 2002a.
- Pohjola, V. A. , Martma, T. A., Meijer, H. A. ., Moore, J. C., Isaksson, E., Vaikmae, R. and van de Wal, R. S. .: Reconstruction of three centuries of annual accumulation rates based on the record of stable isotopes of water from Lomonosovfonna, Svalbard, *Annals of Glaciology*, 35(1), 57–62, 2002b.
- Röthlisberger, R., Hutterli, M. A., Sommer, S., Wolff, E. W. and Mulvaney, R.: Factors controlling nitrate in ice cores: Evidence from the Dome C deep ice core, *Journal of Geophysical Research*, 105(D16), 20565–20572, doi:10.1029/2000JD900264, 2000.
- Röthlisberger, R., Hutterli, M. A., Wolff, E. W., Mulvaney, R., Fischer, H., Bigler, M., Goto-Azuma, K., Hansson, M. E., Ruth, U., Siggaard-Andersen, M.-L. and Steffensen, J. P.: Nitrate in Greenland and Antarctic ice cores: a detailed description of post-depositional processes, *Annals of Glaciology*, 35(1), 209–216, doi:10.3189/172756402781817220, 2002.
- Sigl, M., McConnell, J. R., Layman, L., Maselli, O., McGwire, K., Pasteris, D., Dahl-Jensen, D., Steffensen, J. P., Vinther, B., Edwards, R., Mulvaney, R. and Kipfstuhl, S.: A new bipolar ice core record of volcanism from WAIS Divide and NEEM and implications for climate forcing of the last 2000 years, *Journal of Geophysical Research: Atmospheres*, doi:10.1029/2012JD018603, 2013.
- Tarussov, A.: The Arctic from Svalbard to Severnaya Zemlya: climatic reconstructions from ice cores, in *Climate Since A.D. 1500*, edited by R. S. Bradley and P. D. Jones, pp. 505–516, Routledge, 1992.

5 Is the climate reconstruction of one ice core representative?

Teinilä, K., Hillamo, R., Kerminen, V.-M. and Beine, H. J.: Aerosol chemistry during the NICE dark and light campaigns, *Atmospheric Environment*, 37(4), 563–575, doi:10.1016/S1352-2310(02)00826-9, 2003.

Thompson, L. G., Davis, M. E., Mosley-Thompson, E., Sowers, T. A., Henderson, K. A., Zagorodnov, V. S., Lin, P.-N., Mikhailenko, V. N., Campen, R. K., Bolzan, J. F., Cole-Dai, J. and Franco, B.: A 25,000-year tropical climate history from Bolivian ice cores, *Science*, 282(5395), 1858–1864, doi:10.1126/science.282.5395.1858, 1998.

Uchida, T., Kamiyama, K., Fujii, Y., Takahashi, A., Suzuki, T., Yoshimura, Y., Igarashi, M. and Watanabe, O.: Ice core analyses and borehole temperature measurements at the drilling site on Asgardfonna, Svalbard, in 1993 (scientific paper), *Memoirs of National Institute of Polar Research. Special issue*, 51, 377–386, 1996.

Virkkunen, K., Moore, J. C., Isaksson, E., Pohjola, V., Peramaki, P., Grinsted, A. and Kekonen, T.: Warm summers and ion concentrations in snow: comparison of present day with Medieval Warm Epoch from snow pits and an ice core from Lomonosovfonna, Svalbard, *Journal of Glaciology*, 53(183), 623–634, 2007.

Van der Wel, L. G., Streurman, H. J., Isaksson, E., Helsen, M. M., van de Wal, R. S. W., Martma, T., Pohjola, V. A., Moore, J. C. and Meijer, H. A. J.: Using high-resolution tritium profiles to quantify the effects of melt on two Spitsbergen ice cores, *Journal of Glaciology*, 57(206), 1087–1097, 2011.

Wendl, I.A., Eichler, A., Isaksson, E., Martma, T., Schwikowski, M.: 800 year ice-core record of nitrogen deposition in Svalbard linked to ocean productivity and biogenic emissions, submitted to *Atmospheric Chemistry and Physics Discussions*, 2014.

Supplementary Material

In this supplementary material the details on the single components and chemicals for the ion chromatography (Table S5-1) are given, followed by the frequency distributions of the ionic species and $\delta^{18}\text{O}$ analysed in the Lomo97 and Lomo09 cores (Figures S5-1 and S5-2), and graphs modified after previous studies showing the spatial variability of the accumulation rates in the Lomonosovfonna area (Figures S5-3 and S5-4).

Table S5-1 Components and chemicals used for major ion analysis with the Metrohm 850 Professional IC.

	Cations	Anions
Eluent	2.8 mM HNO_3	A: 1.5 mM Na_2CO_3 / 0.3 mM NaHCO_3 B: 8 mM Na_2CO_3 / 1.7 mM NaHCO_3
Flow rate	1 mL/min	0.9 mL/min
Loop	500 μL	500 μL
Separation column	Metrosep C4	Metrosep A Supp 10
Guard column		Metrosep A Supp 5
Suppression	-	0.05 M H_2SO_4 + 12 g oxalic acid
Detection	conductivity	conductivity

5 Is the climate reconstruction of one ice core representative?

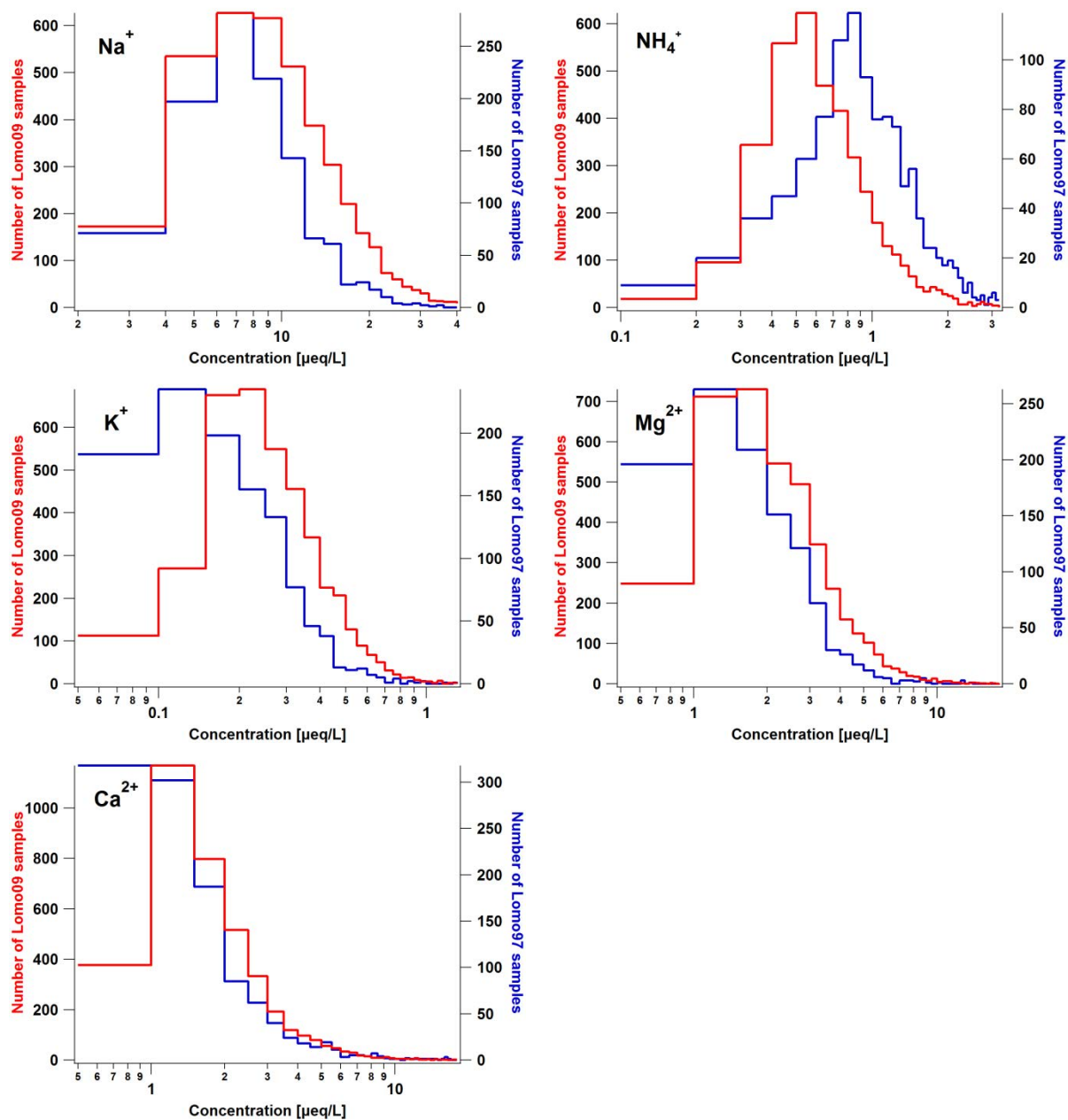


Figure S5-1 Frequency distributions of the cations analysed in the Lomo97 and Lomo09 cores. The red line represents the Lomo09 core; the blue line represents the Lomo97 core.

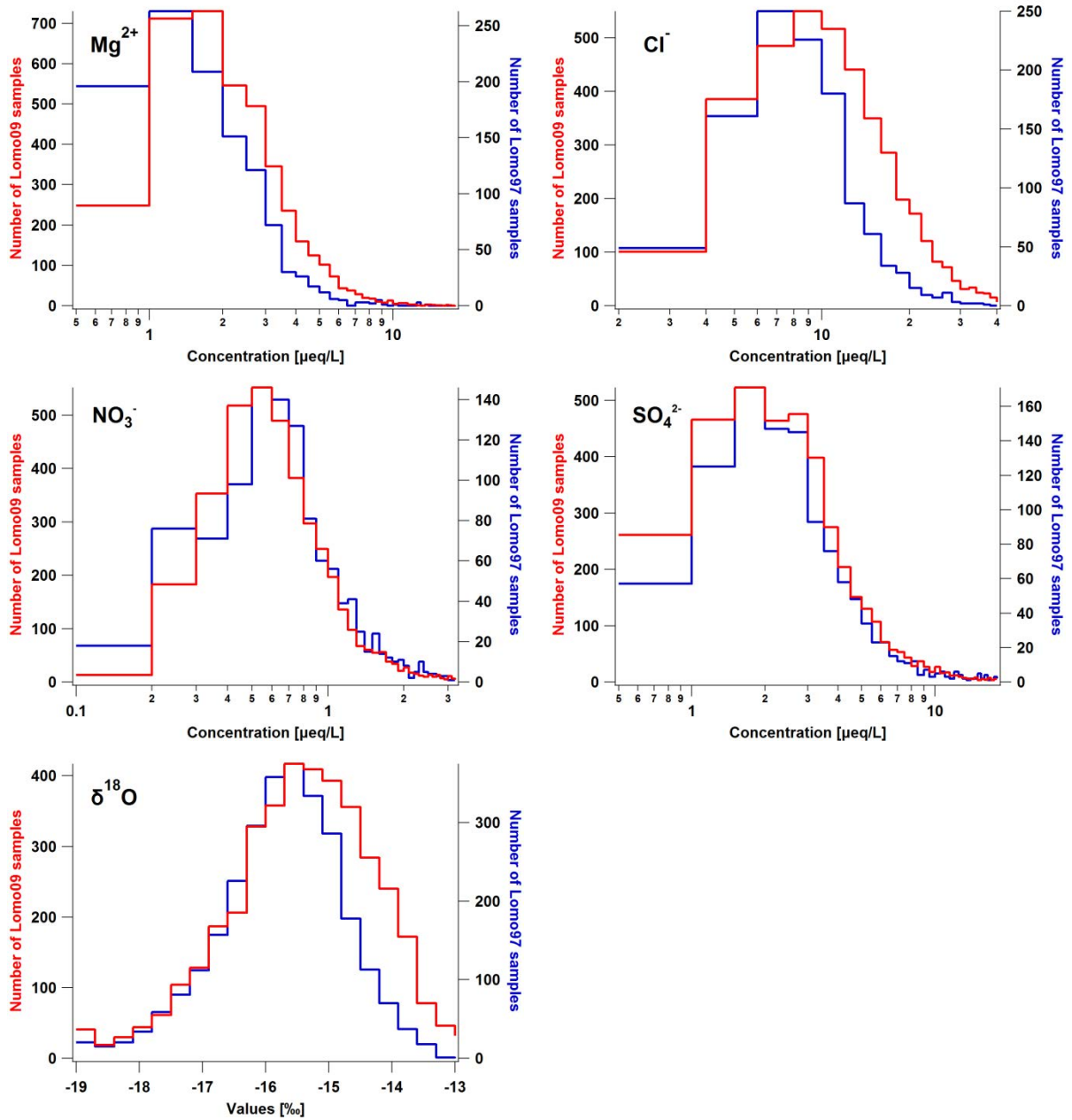


Figure S5-2 Frequency distributions of the anions and $\delta^{18}\text{O}$ analysed in the Lomo97 and Lomo09 cores. The red line represents the Lomo09 core; the blue line represents the Lomo97 core.

5 Is the climate reconstruction of one ice core representative?

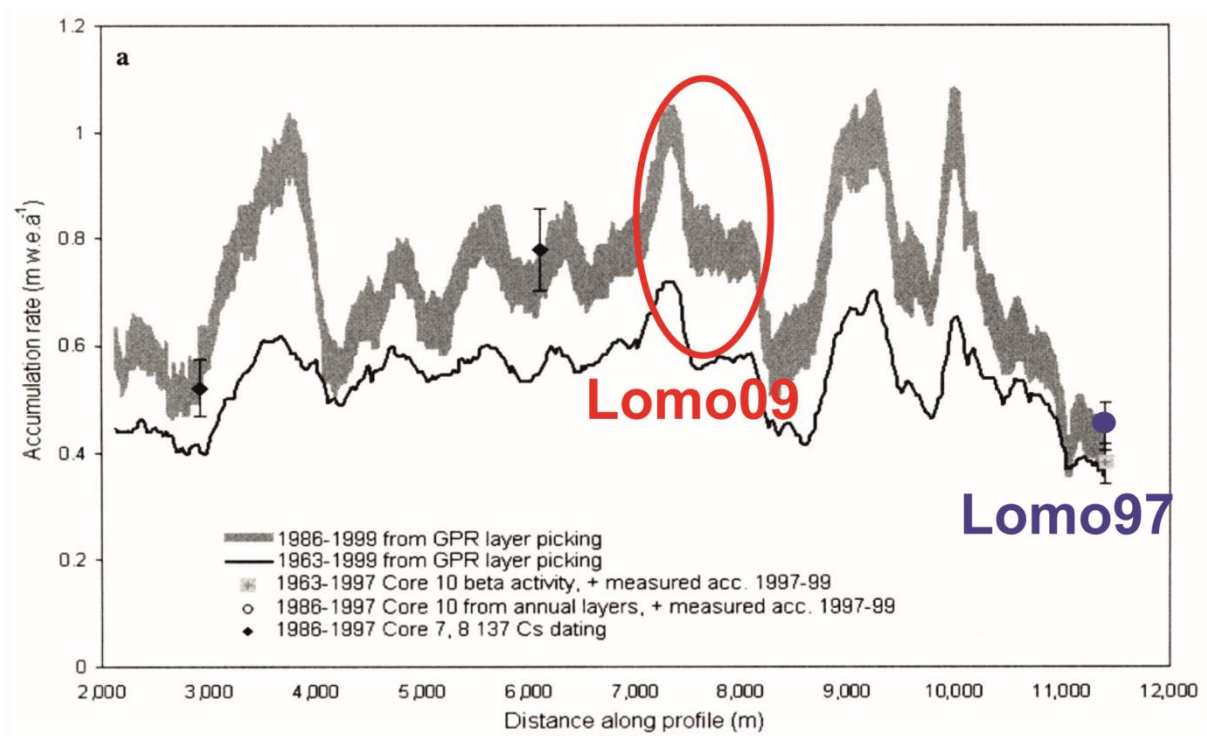


Figure S5-3 Annual accumulation rates vs. distance of the profile along the Lomonosovfonna area. The approximate locations of the 1997 and 2009 drilling sites are indicated. Graph modified after Pälli et al. (2002).

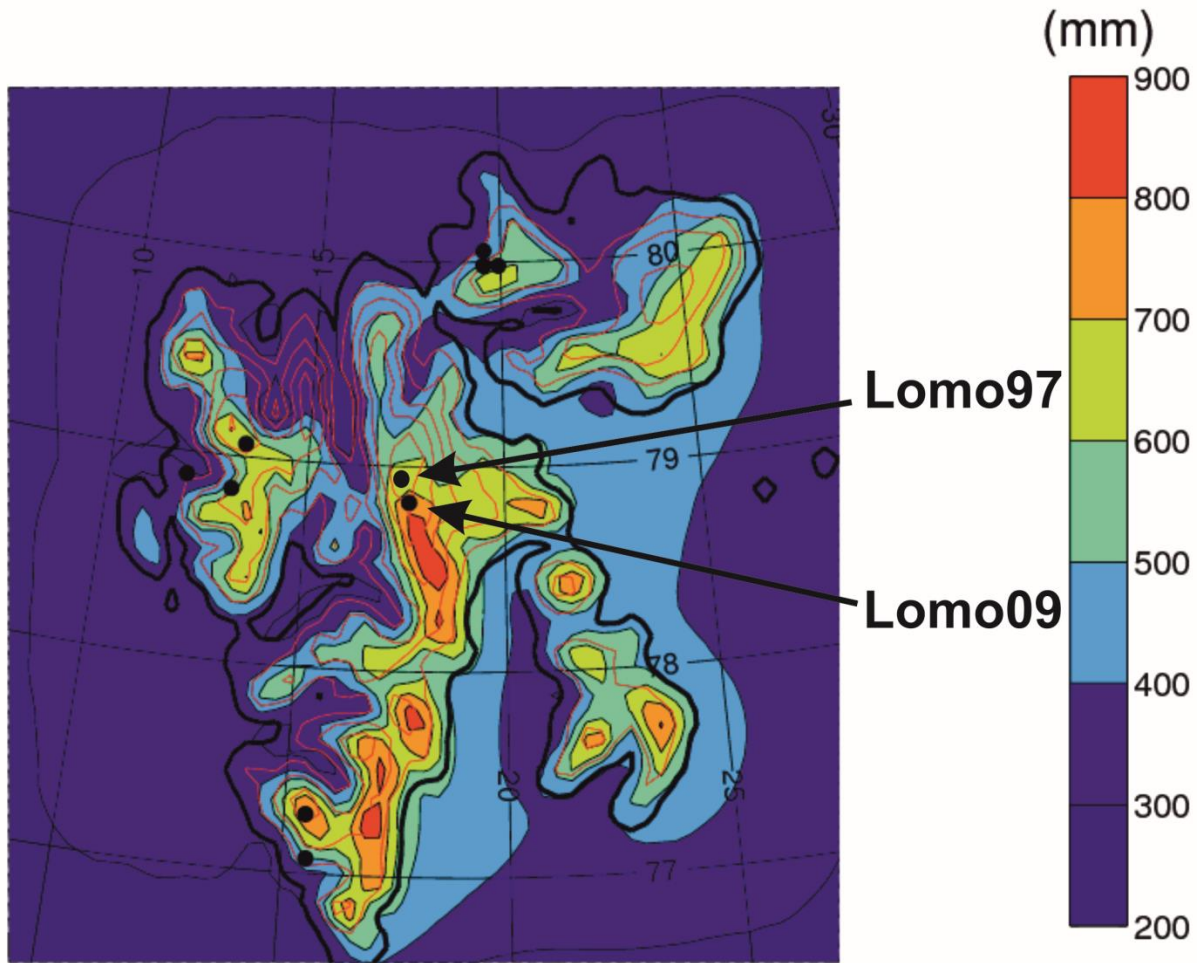


Figure S5-4 Mean annual precipitation in Svalbard. Red contour lines show terrain heights with equidistance of 200 m. The approximate locations of the 1997 and 2009 drilling sites are indicated. Graph modified after Claremar (2013).

6 Black carbon in the Lomonosovfonna 2009 ice core

6.1 Introduction

Light-absorbing impurities such as black carbon (BC) affect the Earth's radiative balance and thus climate change. Black carbon is a by-product of incomplete combustion of biomass and fossil fuels. It has a two-fold climate effect: (1) direct heating of the atmosphere by absorbing the incoming radiation, (2) indirect when deposited on the Earth's surface because it lowers its albedo. The latter effect is particularly important in areas mainly covered by white ice and snow surfaces such as the Arctic, where BC deposition leads to accelerated melt. The surface radiative forcing for the snow albedo effect of BC was estimated to be between 0.01 and 0.09 W/m² (Bond et al., 2013). The efficacy of this forcing was identified to be up to three times greater than that by CO₂ (Flanner et al., 2007). However, not many climate models cover the polar areas that are greatly affected by surface albedo change because of their vast white surfaces including sea ice. Shrinking areas of highly reflective sea ice expose larger areas of darker and more absorbing open water which results in a warming of the ocean (AMAP, 2011; Cubasch et al., 2013). This then leads to further sea ice melt and even more open water, resulting in a self-accelerating process, the so-called ice-albedo feedback (AMAP, 2011).

BC in Arctic snow has been investigated extensively (Aamaas et al., 2011; Clarke and Noone, 1985; Doherty et al., 2010, 2013; Forsström et al., 2009, 2013). The BC concentrations vary from a median of 1 ± 1 µg/L in Greenland summer snow (Doherty et al., 2010) to a median of 88 µg/L in northern Scandinavia (Forsström et al., 2013). The median values for Svalbard are 13 ± 9 and 12-17 µg/L, respectively (Doherty et al., 2010; Forsström et al., 2013). Those values were determined by filter-based methods, such as integrating-sphere/integrating-sandwich (ISSW) spectrophotometry (Doherty et al., 2010) and the thermal-optical technique (Forsström et al., 2013). These methods require large sample volumes and can be biased due to analytical artefacts, such as charring of organic carbon (Soto-Garcia et al., 2011), dust interference (Wang et al., 2012), or filter efficiency (Torres et al., 2014).

In the Arctic, only few long-term BC records exist from ice cores drilled in Greenland (McConnell and Edwards, 2008; McConnell, 2010; McConnell et al., 2007; Zennaro et al., 2014) and Svalbard (Ruppel et al., 2014). Apart from the BC record from NEEM, Greenland, that extends back to more than 2000 years ago (Zennaro et al., 2014), those BC records cover at a maximum the last 300 years (McConnell and Edwards, 2008; McConnell, 2010; McConnell et al., 2007; Ruppel et al., 2014). The Greenland records range from a mean value of 1.7 µg/L for the D4 site prior to 1850

(McConnell et al., 2007) to a mean of around 6-8 $\mu\text{g/L}$ for the NEEM site for the last 2000 years and the ACT2 site for the last 230 years (McConnell and Edwards, 2008; Zennaro et al., 2014). The Svalbard record from Hortedahlfonna reveals mean BC concentrations from $23 \pm 9 \mu\text{g/L}$ prior to 1850 to $45 \pm 19 \mu\text{g/L}$ between 1950 and 2004 (Ruppel et al., 2014).

All Greenland ice core records exhibit increased BC concentrations between around 1880 and 1950 (McConnell and Edwards, 2008; McConnell, 2010; McConnell et al., 2007; Zennaro et al., 2014). The core from Hortedahlfonna also shows elevated BC concentrations after 1850, with a peak around 1910 (Ruppel et al., 2014). In this record the BC concentrations increase again rapidly between 1980 and 2004 (Ruppel et al., 2014). This differs from the Greenland records and from atmospheric measurements at Alert (Canada), Barrow (Alaska), Zeppelin (Svalbard) since 1989 (Ruppel et al., 2014), and at Kevo (Finland) since 1964 (Dutkiewicz et al., 2014). They all indicate decreasing BC concentrations in the Arctic during the last decades. Ruppel et al. (2014) explain the recent rise in the Hortedahlfonna BC concentrations with an increased BC scavenging efficiency induced by rising temperatures.

The differences observed between the BC records from Greenland and Svalbard ice cores may be attributed to varying source areas, dissimilar distance to the sources, and the unlike elevation of the sites (AMAP, 2011; Hirdman et al., 2010; Ruppel et al., 2014). Greenland is affected by pollution sources in the low latitudes, whereas sources in high-latitude Eurasia affect the low-altitude Arctic sites (AMAP, 2011; Hirdman et al., 2010). Thus, the emission trends in the respective BC source regions, that were shown to vary with time and latitude, will result in varying trends in the BC records at the different sites (AMAP, 2011; Skeie et al., 2011). Furthermore, varying methods were applied to determine BC in the ice cores, which may contribute to the diverse values (Ruppel et al., 2014) because the methods may be sensitive to a different part of BC. The Greenland cores were analysed using a Single Particle Soot Photometer (SP2, Droplet Measurement Technology, Inc., Boulder, CO, USA; Schwarz et al., 2006) incorporated in a continuous flow system (e.g., McConnell et al., 2007), whereas Ruppel et al. (2014) analysed filters with the thermal-optical method for the Hortedahlfonna core.

The BC record of the Hortedahlfonna ice core is the only record on historical timescales from outside of Greenland up to now. In order to get a more complete picture of the past BC concentrations in the Arctic, BC was determined in an ice core from Lomonosovfonna, Svalbard, drilled at 1202 m asl in 2009 (hereafter called Lomo09). Details on the drilling and sampling are given in chapters 2.1 and 2.2. Discrete samples were analysed with a setup combining an SP2 and a jet nebulizer system APEX-Q (High Sensitivity Sample Introduction System, Elemental

Scientific Inc., Omaha, NE, USA) (details on the method in chapter 3). Moreover, potential sources for BC in the Lomo09 ice core were tried to be identified.

6.2 Results and discussion

The BC record from the Lomo09 ice core reveals concentrations between 0.1 and 39.0 $\mu\text{g/L}$ in the period from 1950 to 2005, with a median of 1.7 $\mu\text{g/L}$ and an average of 2.6 ± 3.4 $\mu\text{g/L}$. The concentrations vary with time, with maximum concentrations around 1980 (Figure 6.1). Furthermore, the Lomo09 BC record shows a decreasing trend from 1950 to 2005.

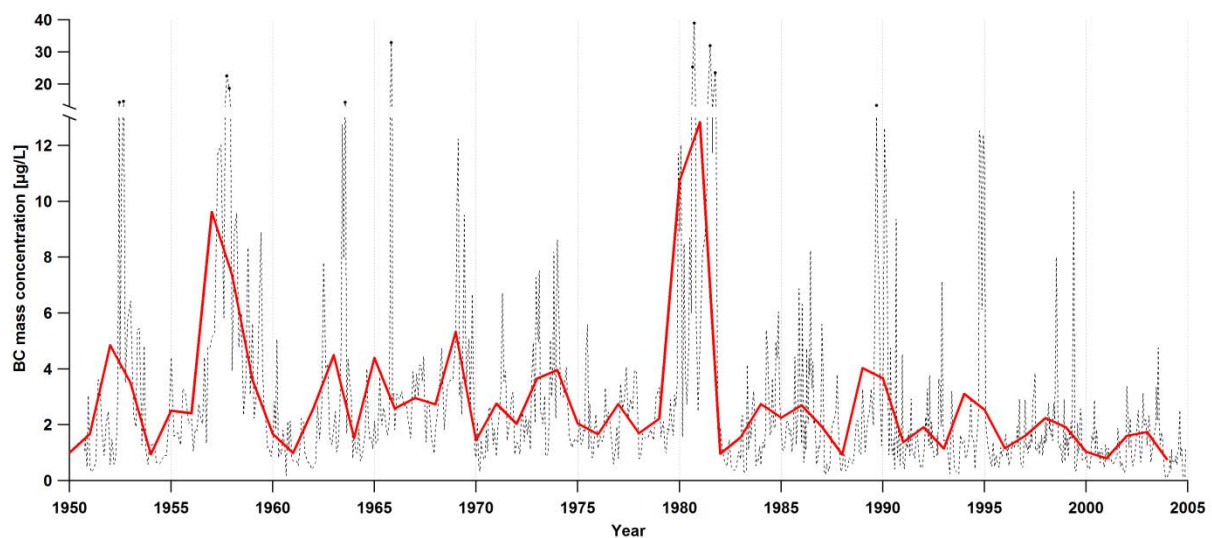


Figure 6.1 Black carbon (BC) record of the Lomonosovfonna 2009 ice core in the time period 1950 to 2005. Dashed black line represents the raw data, bold red line the annual averages.

Sub-annual variations in the BC records can be resolved, as shown by comparison with the records of $\delta^{18}\text{O}$ and Na^+ (Figure 6.2). The $\delta^{18}\text{O}$ record shows pronounced minima in winter caused by lower temperatures, whereas the Na^+ record reveals pronounced maxima in summer due to minimum sea ice extent leading to higher input of Na^+ to the drilling site (Figure 6.2). Those records were used to count annual layers to date the ice core (see chapter 2.7.4). BC is expected to show elevated concentrations in the end of winter/ early spring due to the Arctic Haze phenomenon (Shaw, 1995). Thus, the maximum concentrations in the BC record are expected to correspond to the minima in the $\delta^{18}\text{O}$ record. Indeed, the BC record shows maxima at $\delta^{18}\text{O}$ minima for several years, such as e.g. in 1953, 1958, 1966, 1969, 1973, 1974, 1980, 1981, 1982, 1990, and 1995. However, the seasonality is not as pronounced as in the $\delta^{18}\text{O}$ and Na^+ records.

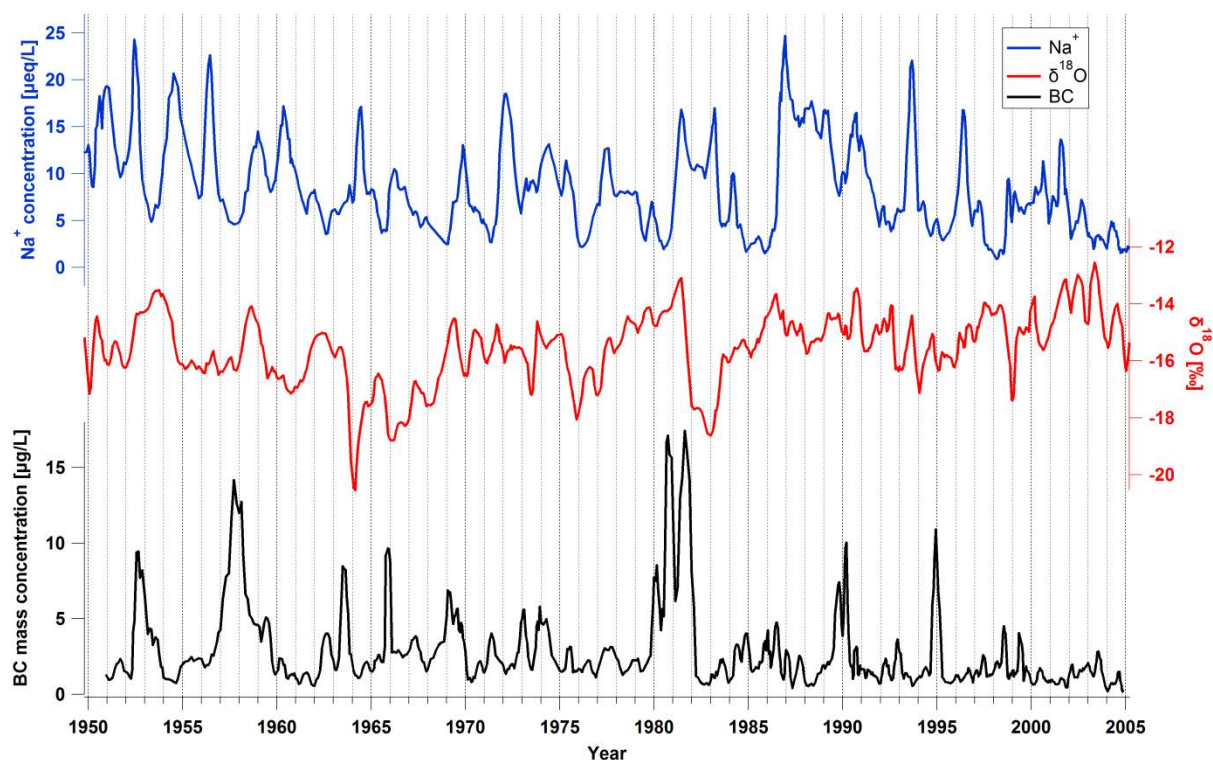


Figure 6.2 Records of concentrations of Na^+ , $\delta^{18}\text{O}$, and BC in the time period between 1950 and 2005. Data shown are five-point-moving-averages. Vertical dashed lines indicate the single counted years.

The median BC concentration of $1.7 \mu\text{g/L}$ in the Lomo09 core is about a factor of ten lower than the values of $13\text{--}17 \mu\text{g/L}$ observed in studies on BC in Svalbard snow (Doherty et al., 2010; Forsström et al., 2013). This can at least partly be explained by the different analytical methods used, because filter-based methods have the potential to over- or underestimate the BC concentrations due to analytical artefacts, see above. Interference with mineral dust as in Wang et al. (2012) can be excluded because Svalbard snow does usually not contain much dust. A bias due to filter efficiency (Torres et al., 2014) would result in lower concentrations with the filter-based method, and thus can be ruled out. The lower values in the Lomo09 core could further result from the different time period considered. Forsström et al. (2013) analysed frequently sampled snow from the spring seasons at various locations in Svalbard in 2007, 2008 and 2009; Doherty et al. (2010) sampled snow near Ny-Ålesund, Svalbard, in spring 2007 and 2009. Those most recent years are not included in the BC record from the Lomo09 core that extends back to 1950. However, the discrepancy in the BC concentrations is most likely explained by the fact that Forsström et al. (2013) and Doherty et al. (2010) only sampled snow in the spring season. Spring is expected to have the highest BC concentrations due to the Arctic Haze phenomenon (e.g., Shaw, 1995).

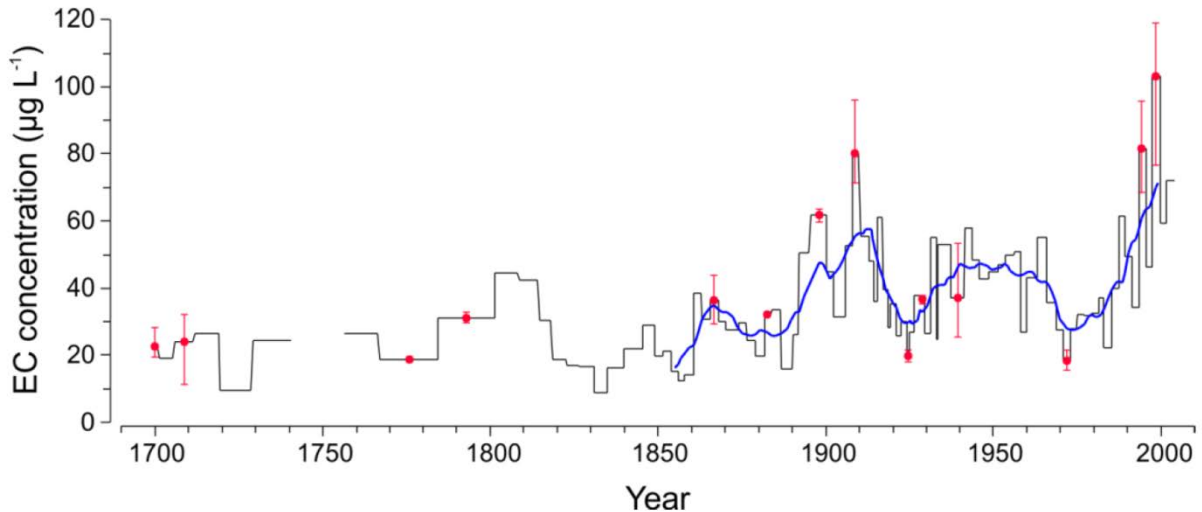


Figure 6.3 Elemental carbon (EC) concentrations in the Holtedahlfonna ice core during the last 300 years (Ruppel et al., 2014). Ruppel et al. (2014) use the term EC due to the thermal-optical measurement technique applied. The black line represents the concentration at sample resolution and the blue line the running 10-year-averages of samples with approximately 2 year resolution. The red dots and error bars indicate the average EC concentration and the absolute errors of samples from which multiple analyses were performed.

In the period between 1950 to 2005 the average BC concentrations of the Lomo09 ice core of $2.6 \pm 3.4 \mu\text{g/L}$ are further about a factor of 20 lower than the mean of $45 \pm 19 \mu\text{g/L}$ of the Holtedahlfonna ice core for the same time period (Ruppel et al., 2014). Moreover, the elevated concentrations in the last 30 years observed in the Holtedahlfonna BC record (Figure 6.3; Ruppel et al., 2014) are not reflected in the Lomo09 BC record. The mean of the Lomo09 core and the lack of the increase in BC concentrations in recent decades resemble rather the BC record of the D4 Greenland ice core with a mean $2.3 \mu\text{g/L}$ for the period from 1952 to 2002 (Figure 6.4; McConnell et al., 2007). The difference between the two Svalbard BC records could at least partly result from the different analytical methods applied, thermal-optical filter-based for the Holtedahlfonna (Ruppel et al., 2014) and SP2-setup for the D4 (McConnell et al. 2007) and the Lomo09 core. However, the D4 site is at ~ 2700 m asl and influenced by more low-latitude sources, whereas the Lomo09 core as a low-altitude site is more affected by BC emissions from high-latitude Eurasia (AMAP, 2011; Hirdman et al., 2010). Moreover, the major pollutant sources for Greenland are North America and Eurasia, whereas Svalbard is affected mainly by Eurasian sources (e.g., Goto-Azuma and Koerner, 2001; Hicks and Isaksson, 2006). BC emissions from Eurasia have decreased constantly over the last 50 years, as shown by several studies (Figure 6.5; Bond et al., 2007; Dutkiewicz et al., 2014; Lamarque et al., 2010; Novakov et al., 2003; Riahi et al., 2011). This decrease is reflected in the Lomo09 BC record, but contrary to the increase observed in the Holtedahlfonna record. Therefore, the assumption of Ruppel et al. (2014) that the BC scavenging efficiency has increased in the last 30 years cannot be

generalised for Svalbard. It is rather likely that the BC concentrations at Lomonosovfonna are influenced mainly by BC emissions in the source region of Eurasia.

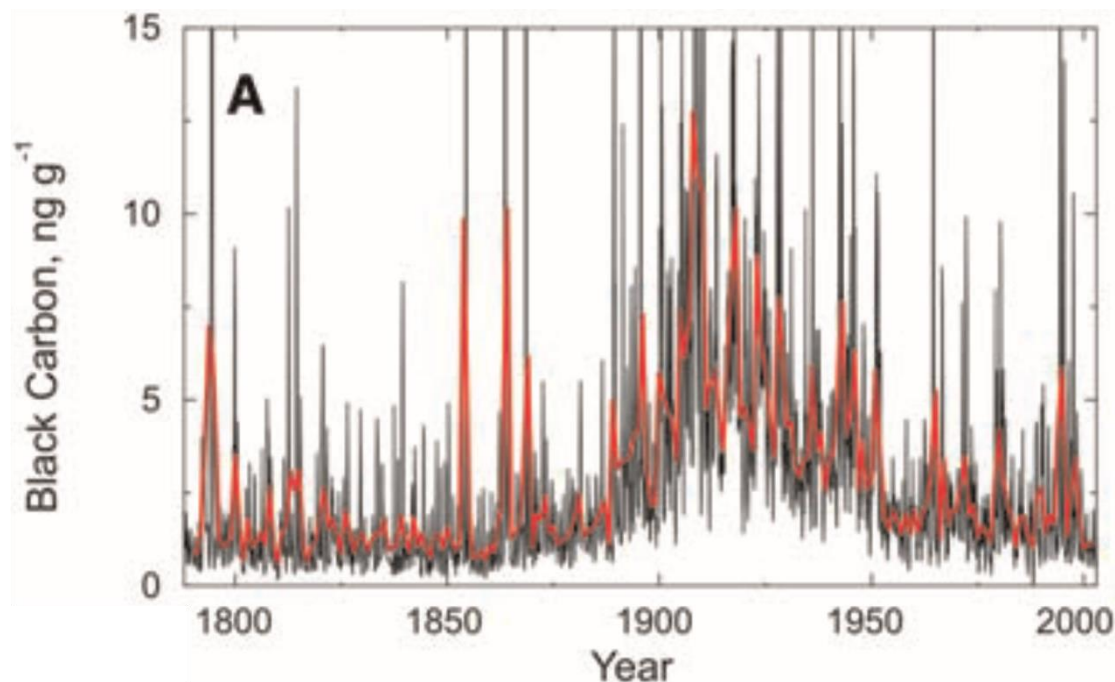


Figure 6.4 Monthly (black) and annual (red) BC concentrations from 1788 through 2002 measured in the Greenland D4 ice core (modified after McConnell et al., 2007).

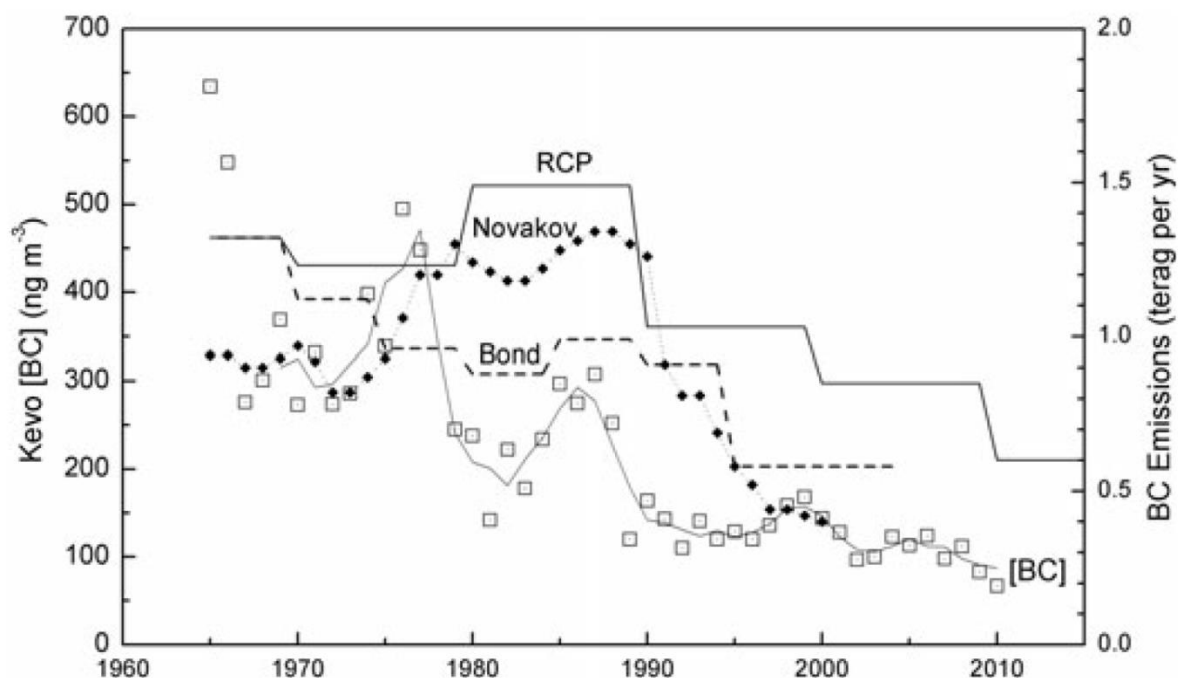


Figure 6.5 Time series plot of [BC] measured at Kevo, Finland, for 1965-2010 compared to selected BC emission estimates given below: Novakov = BC emissions for UK+GER+USSR (Novakov et al., 2003) Bond = BC emissions for OECD Europe+USSR (Bond et al., 2007) RCP = BC emissions for Europe+USSR (Lamarque et al., 2010; Riahi et al., 2011). Graph adopted from Dutkiewicz et al. (2014).

BC has previously been used as tracer for forest fires (e.g., McConnell et al., 2007; Zennaro et al., 2014). The Lomo09 BC record displays a large peak around 1980 and a less prominent one around 1957 (Figures 6.1 and 6.2). Large areas of Russian boreal forest burn every year (Conard and Ivanova, 1997; Dixon and Krankina, 1993). This is one of the potential sources for BC detected in Svalbard. In the particular time periods around 1957 and 1980 where elevated BC concentrations were measured in the Lomo09 core, no major fires could be identified, mainly because the data coverage is scarce, but also because the considered time periods in the studies are often too long to identify single fire events (Oris et al., 2013). However, the large area of boreal forest that burned around 1987-1991 (Conard and Ivanova, 1997; Dixon and Krankina, 1993) is not reflected in the Lomo09 BC record. Anthropogenic emissions from Eurasia do not exhibit higher values for either peak in the Lomo09 BC record (Figure 6.5; Dutkiewicz et al., 2014). Thus, the elevated BC concentrations could be caused by BC emissions from North America that cannot be excluded from affecting BC concentrations in the Lomo09 core. The peak in the Lomo BC record in 1995 (Figures 6.1 and 6.2) resembles, for instance, the peak detected at Summit, Greenland which was attributed to forest fires in North America (Dibb et al., 1996). Furthermore, the BC emissions from North America were elevated around 1980 (Bond et al., 2007), which could have contributed to the elevated BC concentrations around 1980 in the Lomo09 core. Local emissions from Svalbard can be excluded from having influenced the Lomo09 BC record, as shown in the snow pit study in chapter 7.

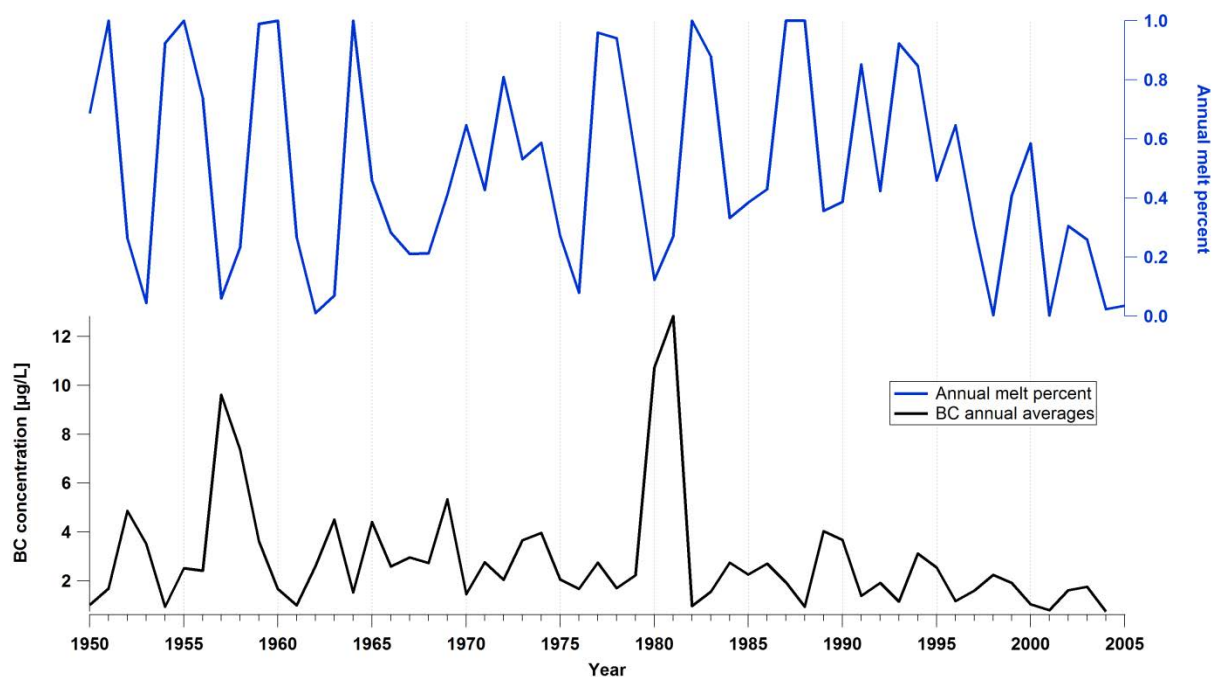


Figure 6.6 Records of the Lomo09 annual BC concentrations and the annual melt percent.

The elevated BC concentrations in the Lomo09 record around 1957 and 1980 could also be caused by relocation of BC due to melt and aggregation at a certain depth. Comparing the records of annual averages of BC and the annual melt percent indicates that there was neither a period of particularly high melt after 1960 nor after 1980 that could have resulted in relocation of BC to greater depth (Figure 6.6). This is supported by the poor correlation of the two records ($r^2 = 0.12$). Thus, melt can be excluded from having influenced the BC concentrations in the Lomo09 core on annual timescales. This is in agreement with Doherty et al. (2013) who state a 10-30% relocation of BC due to meltwater percolation.

6.3 Summary and outlook

The BC record of the 2009 ice core from Lomonosovfonna (Lomo09) covering the time period between 1950 and 2005 is presented. Sub-annual variations can be observed, but a periodic seasonality is not depicted. The BC concentrations in the Lomo09 core are in the same range as those observed in Greenland, but a factor of 10 and 20 lower than those determined in Svalbard snow and the Høltedahlfonna ice core, respectively. This can partly be explained by the different analytical methods applied, SP2-setup for the Lomo09 and thermal-optical filter-based for the snow and the Høltedahlfonna core. The increase in BC concentrations in the Høltedahlfonna record in the last decades is not reflected in the Lomo09 BC record. The Lomo09 BC record rather resembles the records of the Greenland ice cores that agree with the decrease in atmospheric BC in the Arctic in recent decades. The decreasing BC concentrations in the Lomo09 core are probably due to decreasing BC emissions from Eurasia. The source for the elevated BC concentrations in the Lomo09 core around 1957 and 1980 could not be identified unequivocally. BC emissions from North America could have played a role, whereas emissions from Eurasia were not elevated in these particular years. Melt was shown to not have influenced the Lomo09 record on annual timescales.

It is intended to extend the Lomo09 BC record further back in time, enabling a detailed comparison of the existing BC records from Arctic ice cores. In particular, a comparison of the two BC records from Svalbard is important to gain knowledge about past BC concentrations at low-altitude Arctic sites. In addition, the comparison of preindustrial to industrial BC concentrations may enable source apportionment, since forest fires are the only preindustrial source for BC.

The samples for BC analysis were prepared for the entire core, but could not be analysed in the frame of this project due to limited access to the SP2 and the long process of method development. The present BC record lacks the last four years because the samples of the uppermost core part, covering the time period of 2005-2009, had been refrozen and thus were

unsuitable for analysis. However, the Lomo09 BC record will be extended to 2011 using BC samples from a short core drilled on Lomonosovfonna in 2011.

References

Aamaas, B., Bøggild, C. E., Stordal, F., Berntsen, T., Holmén, K. and Ström, J.: Elemental carbon deposition to Svalbard snow from Norwegian settlements and long-range transport, *Tellus B*, 63(3), 340–351, doi:10.1111/j.1600-0889.2011.00531.x, 2011.

AMAP: The Impact of Black Carbon on Arctic Climate, Arctic Monitoring and Assessment Programme (AMAP), Oslo, 2011.

Bond, T. C., Bhardwaj, E., Dong, R., Jogani, R., Jung, S., Roden, C., Streets, D. G. and Trautmann, N. M.: Historical emissions of black and organic carbon aerosol from energy-related combustion, 1850–2000, *Global Biogeochemical Cycles*, 21(2), GB2018, doi:10.1029/2006GB002840, 2007.

Bond, T. C., Doherty, S. J., Fahey, D. W., Forster, P. M., Berntsen, T., DeAngelo, B. J., Flanner, M. G., Ghan, S., Kärcher, B., Koch, D., Kinne, S., Kondo, Y., Quinn, P. K., Sarofim, M. C., Schultz, M. G., Schulz, M., Venkataraman, C., Zhang, H., Zhang, S., Bellouin, N., Guttikunda, S. K., Hopke, P. K., Jacobson, M. Z., Kaiser, J. W., Klimont, Z., Lohmann, U., Schwarz, J. P., Shindell, D., Storelvmo, T., Warren, S. G. and Zender, C. S.: Bounding the role of black carbon in the climate system: A scientific assessment, *Journal of Geophysical Research: Atmospheres*, 118(11), 5380–5552, doi:10.1002/jgrd.50171, 2013.

Clarke, A. D. and Noone, K. J.: Soot in the Arctic snowpack: A cause for perturbations in radiative transfer, *Atmospheric Environment* (1967), 19(12), 2045–2053, 1985.

Conard, S. G. and Ivanova, G. A.: Wildfire in Russian boreal forests—potential impacts of fire regime characteristics on emissions and global carbon balance estimates, *Environmental Pollution*, 98(3), 305–313, doi:10.1016/S0269-7491(97)00140-1, 1997.

Cubasch, U., Wuebbles, D., Chen, D., Facchini, M. C., Frame, D., Mahowald, N. and Winther, J.-G.: Introduction, in *Climate Change 2013: The Physical Science Basis. Contribution of Working Group I to the Fifth Assessment Report of the Intergovernmental Panel on Climate Change*, edited by T. F. Stocker, D. Qin, G.-K. Plattner, M. Tignor, S. K. Allen, J. Boschung, A. Nauels, Y. Xia, V. Bex, and P. M. Midgley, Cambridge University Press, Cambridge, United Kingdom and New York, NY, USA., 2013.

Dibb, J. E., Talbot, R. W., Whitlow, S. I., Shipham, M. C., Winterle, J., McConnell, J. and Bales, R.: Biomass burning signatures in the atmosphere and snow at Summit, Greenland: An event on 5 August 1994, *Atmospheric Environment*, 30(4), 553–561, 1996.

Dixon, R. K. and Krankina, O. N.: Forest fires in Russia: carbon dioxide emissions to the atmosphere, *Canadian Journal of Forest Research*, 23(4), 700–705, doi:10.1139/x93-091, 1993.

Doherty, S. J., Warren, S. G., Grenfell, T. C., Clarke, A. D. and Brandt, R. E.: Light-absorbing impurities in Arctic snow, *Atmospheric Chemistry and Physics*, 10(23), 11647–11680, doi:10.5194/acp-10-11647-2010, 2010.

Doherty, S. J., Grenfell, T. C., Forsström, S., Hegg, D. L., Brandt, R. E. and Warren, S. G.: Observed vertical redistribution of black carbon and other insoluble light-absorbing particles in melting

snow, *Journal of Geophysical Research. Atmospheres*, 118(11), 5553–5569, doi:10.1002/jgrd.50235, 2013.

Dutkiewicz, V. A., DeJulio, A. M., Ahmed, T., Laing, J., Hopke, P. K., Skeie, R. B., Viisanen, Y., Paatero, J. and Husain, L.: Forty-seven years of weekly atmospheric black carbon measurements in the Finnish Arctic: Decrease in black carbon with declining emissions, *Journal of Geophysical Research. Atmospheres*, 119(12), 2014JD021790, doi:10.1002/2014JD021790, 2014.

Flanner, M. G., Zender, C. S., Randerson, J. T. and Rasch, P. J.: Present-day climate forcing and response from black carbon in snow, *Journal of Geophysical Research: Atmospheres*, 112(D11), doi:10.1029/2006JD008003, 2007.

Forsström, S., Ström, J., Pedersen, C. A., Isaksson, E. and Gerland, S.: Elemental carbon distribution in Svalbard snow, *Journal of Geophysical Research: Atmospheres*, 114(D19), doi:10.1029/2008JD011480, 2009.

Forsström, S., Isaksson, E., Skeie, R. B., Ström, J., Pedersen, C. A., Hudson, S. R., Berntsen, T. K., Lihavainen, H., Godtliebsen, F. and Gerland, S.: Elemental carbon measurements in European Arctic snow packs, *Journal of Geophysical Research: Atmospheres*, doi:10.1002/2013JD019886, 2013.

Goto-Azuma, K. and Koerner, R. M.: Ice core studies of anthropogenic sulfate and nitrate trends in the Arctic, *Journal of Geophysical Research*, 106, 4959–4969, 2001.

Hicks, S. and Isaksson, E.: Assessing source areas of pollutants from studies of fly ash, charcoal, and pollen from Svalbard snow and ice, *Journal of Geophysical Research-Atmospheres*, 111(D2), doi:10.1029/2005JD006167, 2006.

Hirdman, D., Sodemann, H., Eckhardt, S., Burkhardt, J. F., Jefferson, A., Mefford, T., Quinn, P. K., Sharma, S., Ström, J. and Stohl, A.: Source identification of short-lived air pollutants in the Arctic using statistical analysis of measurement data and particle dispersion model output, *Atmospheric Chemistry and Physics*, 10, 669–693, 2010.

Lamarque, J. F., Bond, T. C., Eyring, V., Granier, C., Heil, A., Klimont, Z., Lee, D., Liousse, C., Mieville, A., Owen, B., Schultz, M. G., Shindell, D., Smith, S. J., Stehfest, E., Van Aardenne, J., Cooper, O. R., Kainuma, M., Mahowald, N., McConnell, J. R., Naik, V., Riahi, K. and van Vuuren, D. P.: Historical (1850–2000) gridded anthropogenic and biomass burning emissions of reactive gases and aerosols: methodology and application, *Atmospheric Chemistry and Physics*, 10(15), 7017–7039, 2010.

McConnell, J. R.: New Directions: Historical black carbon and other ice core aerosol records in the Arctic for GCM evaluation, *Atmospheric Environment*, 44, 2665–2666, 2010.

McConnell, J. R. and Edwards, R.: Coal burning leaves toxic heavy metal legacy in the Arctic, *Proceedings of the National Academy of Sciences*, 105(34), 12140, 2008.

McConnell, J. R., Edwards, R., Kok, G. L., Flanner, M. G., Zender, C. S., Saltzman, E. S., Banta, J. R., Pasteris, D. R., Carter, M. M. and Kahl, J. D. W.: 20th-century industrial black carbon emissions

altered Arctic climate forcing, *Science*, 317(5843), 1381–1384, doi:10.1126/science.1144856, 2007.

Novakov, T., Ramanathan, V., Hansen, J. E., Kirchstetter, T. W., Sato, M., Sinton, J. E. and Sathaye, J. A.: Large historical changes of fossil-fuel black carbon aerosols, *Geophysical Research Letters*, 30(6), 1324, doi:10.1029/2002GL016345, 2003.

Oris, F., Asselin, H., Ali, A. A., Finsinger, W. and Bergeron, Y.: Effect of increased fire activity on global warming in the boreal forest, *Environmental Reviews*, 1–14, doi:10.1139/er-2013-0062, 2013.

Riahi, K., Rao, S., Krey, V., Cho, C., Chirkov, V., Fischer, G., Kindermann, G., Nakicenovic, N. and Rafaj, P.: RCP 8.5—A scenario of comparatively high greenhouse gas emissions, *Climatic Change*, 109(1-2), 33–57, doi:10.1007/s10584-011-0149-y, 2011.

Ruppel, M. M., Isaksson, E., Ström, J., Beaudon, E., Svensson, J., Pedersen, C. A. and Korhola, A.: Unexpected increase in elemental carbon values over the last 30 years observed in a Svalbard ice core, *Atmospheric Chemistry and Physics Discussions*, 14(9), 13197–13231, doi:10.5194/acpd-14-13197-2014, 2014.

Schwarz, J. P., Gao, R. S., Fahey, D. W., Thomson, D. S., Watts, L. A., Wilson, J. C., Reeves, J. M., Darbeheshti, M., Baumgardner, D. G., Kok, G. L., Chung, S. H., Schulz, M., Hendricks, J., Lauer, A., Kärcher, B., Slowik, J. G., Rosenlof, K. H., Thompson, T. L., Langford, A. O., Loewenstein, M. and Aikin, K. C.: Single-particle measurements of midlatitude black carbon and light-scattering aerosols from the boundary layer to the lower stratosphere, *Journal of Geophysical Research*, 111(D16), 2006.

Shaw, G. E.: The arctic haze phenomenon, *Bulletin of the American Meteorological Society*, 76, 2403–2414, 1995.

Skeie, R. B., Berntsen, T., Myhre, G., Pedersen, C. A., Ström, J., Gerland, S. and Ogren, J. A.: Black carbon in the atmosphere and snow, from pre-industrial times until present, *Atmospheric Chemistry and Physics*, 11(14), 6809–6836, doi:10.5194/acp-11-6809-2011, 2011.

Soto-Garcia, L. L., Andreae, M. O., Andreae, T. W., Artaxo, P., Maenhaut, W., Kirchstetter, T., Novakov, T., Chow, J. C. and Mayol-Bracero, O. L.: Evaluation of the carbon content of aerosols from the burning of biomass in the Brazilian Amazon using thermal, optical and thermal-optical analysis methods, *Atmospheric Chemistry and Physics*, 11(9), 4425–4444, doi:10.5194/acp-11-4425-2011, 2011.

Torres, A., Bond, T. C., Lehmann, C. M. B., Subramanian, R. and Hadley, O. L.: Measuring Organic Carbon and Black Carbon in Rainwater: Evaluation of Methods, *Aerosol Science and Technology*, 48(3), 239–250, doi:10.1080/02786826.2013.868596, 2014.

Wang, M., Xu, B., Zhao, H., Cao, J., Joswiak, D., Wu, G. and Lin, S.: The influence of dust on quantitative measurements of black carbon in ice and snow when using a thermal optical method, *Aerosol Science and Technology*, 46(1), 60–69, 2012.

Zennaro, P., Kehrwald, N., McConnell, J. R., Schüpbach, S., Maselli, O., Marlon, J., Vallelonga, P., Leuenberger, D., Zangrando, R., Spolaor, A., Borrotti, M., Barbaro, E., Gambaro, A. and Barbante, C.: Fire in ice: two millennia of Northern Hemisphere fire history from the Greenland NEEM ice core, *Climate of the Past Discussions*, 10(1), 809–857, doi:10.5194/cpd-10-809-2014, 2014.

7 Snow pit study on black carbon concentrations in Svalbard

7.1 Introduction

In March/April 2010 a snow pit study was conducted in Svalbard, Norway, in order to analyse the winter snow pack of one year for concentrations of black carbon (BC) and water soluble major ions. The study intended to extend the black carbon (BC) record of the 2009 Lomonosovfonna ice core to the year 2010 and to investigate the spatial variation of BC in Svalbard, similar to Aamaas et al. (2011) and Forsström et al. (2009) and (2013). This chapter describes the analysed species and the applied analytical methods only briefly, details can be found in chapters 2.5, 2.6, 3, and 5.

BC, a by-product of incomplete combustion, has light-absorbing properties. This results in a reduction of the albedo when BC is deposited on ice and snow surfaces, which leads to accelerated melting. BC in Svalbard has local sources, such as mining activities, coal and diesel power plants and vehicles, as well as long-range sources in Eurasia (AMAP, 2011; Hirdman et al., 2010). The water soluble ions enable the reconstruction of air composition and pollution history.



Figure 7.1 Map of Svalbard with the location of Foxfonna, Tellbreen and Lomonosovfonna indicated (modified after a map by courtesy of the Norwegian Polar Institute).

Here, the concentrations of BC and Cl⁻ are compared for three Svalbard sites (see Figure 7.1 for locations): Foxfonna, Tellbreen and Lomonosovfonna. Cl⁻, an ionic species derived mainly from sea salt, was chosen because it is one of the major ions in ice from Lomonosovfonna (see chapter 5 for details) and is thus thought to be representative of the total ion composition. Foxfonna and Tellbreen are located in the vicinity of Longyearbyen (12-15 km), the largest town in Svalbard, with a population of 2100, nearby coal mining and a coal and diesel power plant (Aamaas et al., 2011). Furthermore, those two glaciers are close to the ocean (11-15 km) and at an altitude of less than 800 m asl. Lomonosovfonna is a remote site, around 75 km distant from Longyearbyen and even farther from any other settlement. Lomonosovfonna is further located at around 1200 m asl and approximately 20 km from the ocean.

7.2 Methods

Five snow pits were dug in March/April 2010, two on Foxfonna (78°08'N, 16°09'E; 625 m asl), one on Tellbreen (78°15'N, 16°11'E; 460 m asl), and two on Lomonosovfonna (78°24'N, 17°53'E; 1250 m asl). The depth of the snow pits was limited to the depth of the ice layer formed in the previous summer. Thus, the snow pits represent the winter snow pack of one year. On Foxfonna the ice layer was reached at a depth of 1.34 m and 1.48 m, respectively; on Tellbreen the pit had a depth of 1.40 m; and on Lomonosovfonna the ice layer was met in both snow pits at a depth of 1.50 m. At all site, the snow samples were taken at 10 cm resolution according to the ITASE (International Trans-Antarctic Scientific Expedition) sampling protocol (Twickler and Whitlow, 1997). The Tellbreen samples were collected in clean plastic bags, and sub-sampled in pre-cleaned 50 mL polypropylene (PP) vials at UNIS, Svalbard. The samples from Foxfonna and Lomonosovfonna were collected directly in the 50 mL PP vials. All samples were then melted at room temperature and transported in liquid state to the Paul Scherrer Institut (PSI), Switzerland, for analysis.

At PSI, the BC concentrations of the samples were determined with a setup including a Single Particle Soot Photometer (SP2, Droplet Measurement Technology, Inc., Boulder, CO, USA; (Schwarz et al., 2006) and an ultrasonic nebuliser (U5000AT, CETAC Technologies, Omaha, NE, USA), similar as in Kaspari et al. (2011); details can be found in chapter 3. The water soluble major ions were analysed with a Metrohm 850 Professional ion chromatograph combined with an 872 Extension Module and an autosampler (858 Professional Sample Processor); details are given in chapter 2.5.

7.3 Results and discussion

The comparison of the BC concentration records at the three sites indicates that the concentrations at Lomonosovfonna are more than a factor of two lower than those at Foxfonna and Tellbreen (Figure 7.2). This difference probably results from the distance to the local BC sources, because long-range sources are expected to have a similar influence on all three sites. The influence of local BC emissions on sites located in the vicinity of large settlements has been shown previously (Aamaas et al., 2011).

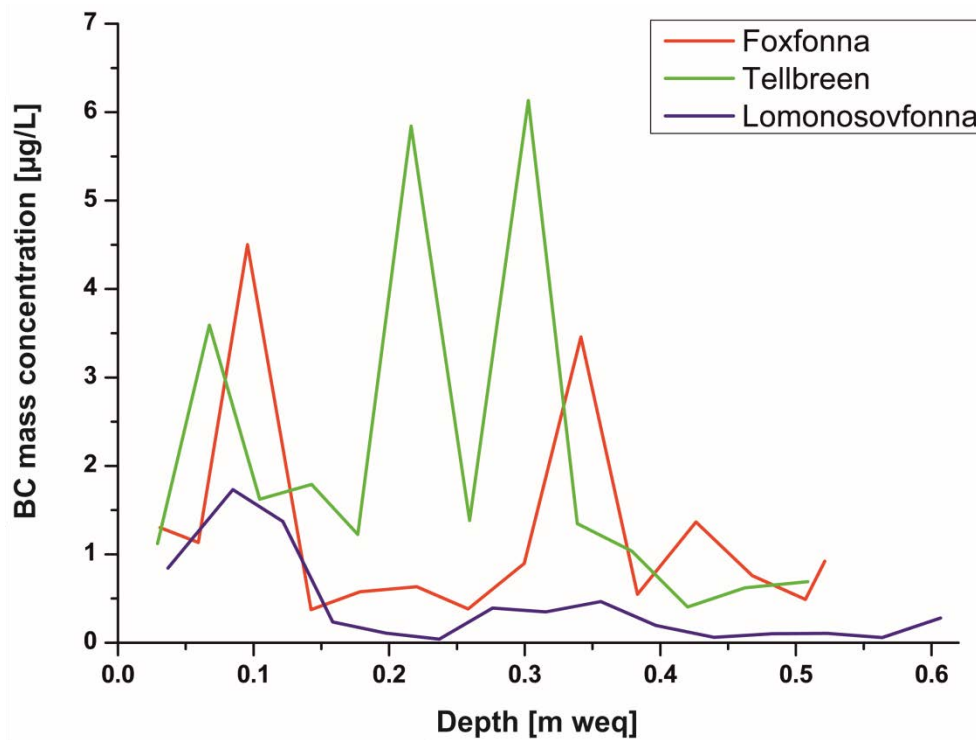


Figure 7.2 Records of BC concentrations at the three sampling sites: Foxfonna (red), Tellbreen (green), and Lomonosovfonna (blue).

A similar effect is seen for the Cl^- concentrations at the three sites, with the concentrations at Lomonosovfonna also being more than a factor of two lower than those at Foxfonna and Tellbreen (Figure 7.3). This is also valid for the other water soluble ions analysed (results not shown). The discrepancy of the concentrations can be explained by the different distance to the ocean. Additionally, the greater altitude of the Lomonosovfonna site has an effect. Air masses reaching the site may have partially lost their coarse sea salt particulate load during the rise due to rapid sedimentation.

The median BC concentration of $0.26 \mu\text{g/L}$ for Lomonosovfonna snow is more than a factor of two lower than those in snow from Foxfonna ($1.02 \mu\text{g/L}$) and Tellbreen ($1.36 \mu\text{g/L}$). Forsström et al. (2013) studied snow at various locations in Svalbard in 2007, 2008 and 2009. They found

median BC concentrations in the range of 1.4 $\mu\text{g/L}$ at Holvedahlfonna in 2007 and 634.0 $\mu\text{g/L}$ at Linnébreen in 2007, the latter being affected by local pollution. At Lomonosovfonna, the median BC concentrations varied between 5.9 $\mu\text{g/L}$ in 2009 and 64.4 $\mu\text{g/L}$ in 2007. The median values obtained in the present study are all well below those of Forsström et al. (2013). This can partly be explained by the different methods applied, with Forsström et al. (2013) using the filter-based thermal-optical method. Furthermore, the snow samples collected at Foxfonna, Tellbreen and Lomonosovfonna in 2010 remained melted and were not stored at cold temperatures for several days before analysis. This results in BC loss as described in chapter 3.

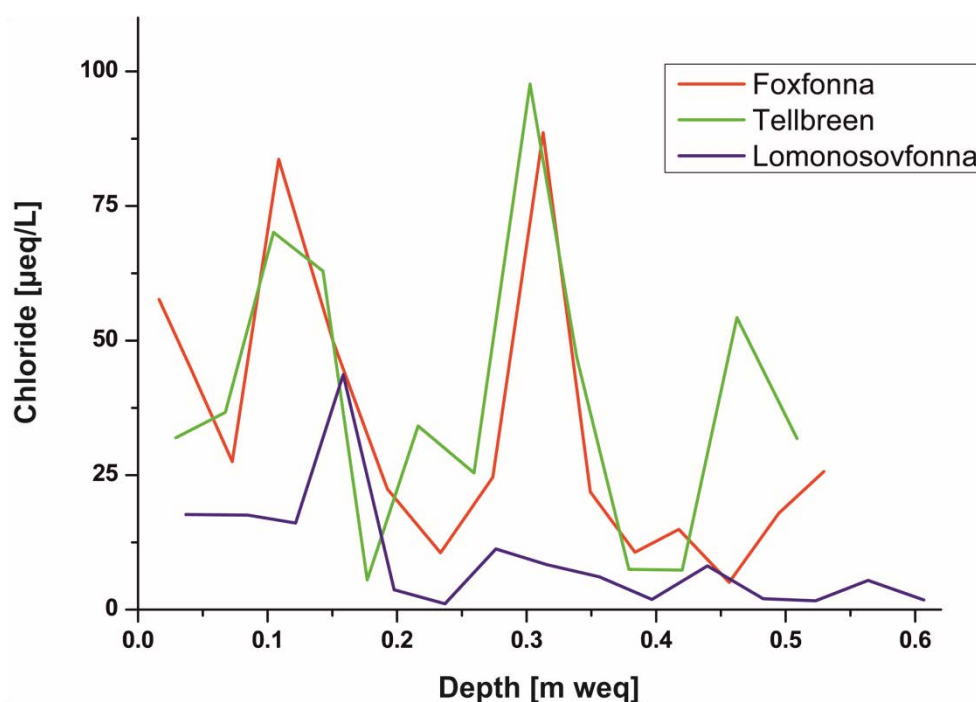


Figure 7.3 Records of the chloride concentrations at the three sampling sites: Foxfonna (red), Tellbreen (green), and Lomonosovfonna (blue).

7.4 Summary

This snow pit study conducted in 2010 compared concentration records of BC and water soluble ions in snow from three Svalbard sites: Foxfonna, Tellbreen, and Lomonosovfonna. Cl⁻, one of the sea salt species, is chosen as representative ionic species because it is one of the major components of the ion budget in ice from Lomonosovfonna. Both BC and Cl⁻ concentrations are more than a factor of two lower at Lomonosovfonna than at the other two sites. This is explained by the greater distance to the ocean and to the local BC sources. The median values for the snow analysed in the present study are well below those previously determined. This is probably due to different analytical methods and inaccurate sample treatment.

Acknowledgements

Thanks to Helgard Anschütz, Mats Björkman, Tõnu Martma, Carmen Vega, and Jakub Zarsky for the help with the sampling.

References

Aamaas, B., Bøggild, C. E., Stordal, F., Berntsen, T., Holmén, K. and Ström, J.: Elemental carbon deposition to Svalbard snow from Norwegian settlements and long-range transport, *Tellus B*, 63(3), 340–351, doi:10.1111/j.1600-0889.2011.00531.x, 2011.

AMAP: The Impact of Black Carbon on Arctic Climate, Arctic Monitoring and Assessment Programme (AMAP), Oslo, 2011.

Forsström, S., Isaksson, E., Skeie, R. B., Ström, J., Pedersen, C. A., Hudson, S. R., Berntsen, T. K., Lihavainen, H., Godtlielsen, F. and Gerland, S.: Elemental carbon measurements in European Arctic snow packs, *Journal of Geophysical Research: Atmospheres*, doi:10.1002/2013JD019886, 2013.

Forsström, S., Ström, J., Pedersen, C. A., Isaksson, E. and Gerland, S.: Elemental carbon distribution in Svalbard snow, *Journal of Geophysical Research: Atmospheres*, 114(D19), doi:10.1029/2008JD011480, 2009.

Hirdman, D., Sodemann, H., Eckhardt, S., Burkhart, J. F., Jefferson, A., Mefford, T., Quinn, P. K., Sharma, S., Ström, J. and Stohl, A.: Source identification of short-lived air pollutants in the Arctic using statistical analysis of measurement data and particle dispersion model output, *Atmospheric Chemistry and Physics*, 10, 669–693, 2010.

Kaspari, S. D., Schwikowski, M., Gysel, M., Flanner, M. G., Kang, S., Hou, S. and Mayewski, P. A.: Recent increase in black carbon concentrations from a Mt. Everest ice core spanning 1860–2000 AD, *Geophysical Research Letters*, 38(4), L04703, 2011.

Schwarz, J. P., Gao, R. S., Fahey, D. W., Thomson, D. S., Watts, L. A., Wilson, J. C., Reeves, J. M., Darbeheshti, M., Baumgardner, D. G., Kok, G. L., Chung, S. H., Schulz, M., Hendricks, J., Lauer, A., Kärcher, B., Slowik, J. G., Rosenlof, K. H., Thompson, T. L., Langford, A. O., Loewenstein, M. and Aikin, K. C.: Single-particle measurements of midlatitude black carbon and light-scattering aerosols from the boundary layer to the lower stratosphere, *Journal of Geophysical Research*, 111(D16), 207, 2006.

Twickler, M. and Whitlow, S.: Appendix B, in Guide for the collection and analysis of ITASE snow and firn samples, edited by P. A. Mayewski and I. D. Goodwin, Past Global Changes (PAGES report 97-1), Bern, Switzerland., 1997.

8 Outlook

In this thesis many aspects for a reconstruction of the climate and environmental history from the 2009 Lomonosovfonna ice core (Lomo09) have been considered. Nevertheless, this work has not yet fully exhausted the potential of the Lomo09 core. Here, some ideas for future work are listed.

8.1 Black carbon (BC)

- Up to now, the BC record covers the time period 1950 to 2005 (chapter 6). Extending the BC analysis for rest of the core will enable not only the reconstruction of past BC deposition on Lomonosovfonna, but also a comparison of the Lomo09 BC record with the other records from Arctic ice cores, such as the D4, ACT2, and Humboldt cores from Greenland (McConnell, 2010; McConnell and Edwards, 2008; McConnell et al., 2007), and the Hortedahlfonna core from Svalbard (Ruppel et al., 2014) on longer timescales. A BC record covering a longer time period will enable the study of changes from pre-industrial to industrial times. Furthermore, the albedo effect of BC could be investigated using the Lomo09 BC record.
- The BC analysis on discrete samples using the APEX/SP2-setup as described in chapter 3 is very time-consuming, at least for samples with low BC concentrations. Furthermore, the samples need to be changed manually. In the future, maybe an autosampler can be incorporated in the setup, although some challenges will arise, e.g. with sonication or time between sample melting and analysis. Maybe it will even be possible to modify the setup as such that a continuous flow device can be integrated, but incorporating a sonication step is also not trivial here.
- In 2011 a Swedish team drilled a short 8 m firn core on Lomonosovfonna, which has been sampled for BC. Those samples are at present at the PSI, Switzerland. Their analysis could extend the Lomo09 BC record to 2011.

8.2 Ice core chemistry

- The water stable isotope ratios of $\delta^{18}\text{O}$ and δD have been analysed for the whole Lomo09 core. However, the interpretation of the records needs further work, as does the comparison with the records from the 1997 Lomonosovfonna (Lomo97) core. It would also be worth considering potential connections of $\delta^{18}\text{O}$ and the North Atlantic Oscillation or Arctic Oscillation index. Additionally, the deuterium excess ($d = \delta\text{D} -$

$\delta^{18}\text{O}$) may be calculated and used as proxy for moisture source conditions (e.g., Jouzel et al., 2005), as done for the Lomo97 core by Divine et al. (2008).

- The analysis of the trace elements in the Lomo09 core could help to further investigate past climate variations, because trace elements are important indicators for biogeochemical cycles, changes in the atmospheric circulation, and pollution sources (Kellerhals et al., 2010; Knüsel et al., 2003).

8.3 Dating methods

- In order to verify the dating of the Lomo09 core particular core sections with high SO_4^{2-} concentrations indicating major volcanic eruptions could be analysed for tephra. The chemical composition and mineralogical characterisation of the tephra could then help to identify specific volcanic eruptions and verify the reference horizons.
- The deepest part of the Lomo09 ice core was dated to 1222, i.e. more than 450 years younger than the deepest ice of the Lomo97 core (Divine et al., 2011). Radiocarbon (^{14}C) dating (Jenk et al., 2009) of the lowermost Lomo09 core part may provide an independent dating method to shed light on this discussion on the age of the deepest ice on Lomonosovfonna.

References

Divine, D., Isaksson, E., Martma, T., Meijer, H. A. ., Moore, J., Pohjola, V., van de Wal, R. S. . and Godtliabsen, F.: Thousand years of winter surface air temperature variations in Svalbard and northern Norway reconstructed from ice core data, *Polar Research*, 30(0), 2011.

Divine, D. V., Isaksson, E., Pohjola, V., Meijer, H., van De Wal, R. S. W., Martma, T., Moore, J., Sjögren, B. and Godtliabsen, F.: Deuterium excess record from a small Arctic ice cap, *Journal of Geophysical Research*, 113, D19104, 2008.

Jenk, T. M., Szidat, S., Bolius, D., Sigl, M., Gäggeler, H. W., Wacker, L., Ruff, M., Barbante, C., Boutron, C. F. and Schwikowski, M.: A novel radiocarbon dating technique applied to an ice core from the Alps indicating late Pleistocene ages, *Journal of Geophysical Research*, 114(D14), D14305, doi:10.1029/2009JD011860, 2009.

Jouzel, J., Masson-Delmotte, V., Stiévenard, M., Landais, A., Vimeux, F., Johnsen, S. J., Sveinbjörnsdottir, A. E. and White, J. W. C.: Rapid deuterium-excess changes in Greenland ice cores: a link between the ocean and the atmosphere, *Comptes Rendus Geoscience*, 337(10–11), 957–969, doi:10.1016/j.crte.2005.05.011, 2005.

Kellerhals, T., Tobler, L., Brütsch, S., Sigl, M., Wacker, L., Gäggeler, H. W. and Schwikowski, M.: Thallium as a Tracer for Preindustrial Volcanic Eruptions in an Ice Core Record from Illimani, Bolivia, *Environmental Science & Technology*, 44(3), 888–893, doi:10.1021/es902492n, 2010.

Knüsel, S., Piguet, D. E., Schwikowski, M. and Gäggeler, H. W.: Accuracy of Continuous Ice-Core Trace-Element Analysis by Inductively Coupled Plasma Sector Field Mass Spectrometry, *Environmental Science & Technology*, 37(10), 2267–2273, doi:10.1021/es026452o, 2003.

McConnell, J. R.: New Directions: Historical black carbon and other ice core aerosol records in the Arctic for GCM evaluation, *Atmospheric Environment*, 44, 2665–2666, 2010.

McConnell, J. R. and Edwards, R.: Coal burning leaves toxic heavy metal legacy in the Arctic, *Proceedings of the National Academy of Sciences*, 105(34), 2008.

McConnell, J. R., Edwards, R., Kok, G. L., Flanner, M. G., Zender, C. S., Saltzman, E. S., Banta, J. R., Pasteris, D. R., Carter, M. M. and Kahl, J. D. W.: 20th-century industrial black carbon emissions altered Arctic climate forcing, *Science*, 317(5843), 1381–1384, doi:10.1126/science.1144856, 2007.

Ruppel, M. M., Isaksson, E., Ström, J., Beaudon, E., Svensson, J., Pedersen, C. A. and Korhola, A.: Unexpected increase in elemental carbon values over the last 30 years observed in a Svalbard ice core, *Atmospheric Chemistry and Physics Discussions*, 14(9), 13197–13231, doi:10.5194/acpd-14-13197-2014, 2014.

9 Appendix

On the following pages the density record of the Lomo09 ice core and those of the raw data of the ionic species and water stable isotopes analysed in the Lomo09 ice core are displayed.

The density record displayed in Figure 9.1 is in agreement with Pohjola et al. (2002).

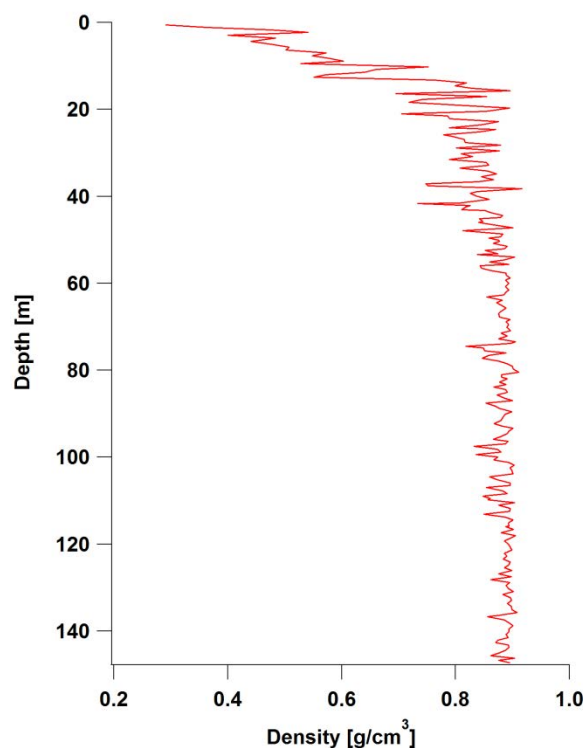


Figure 9.1 Density profile of the Lomo09 core. Density was calculated for each core segment by weighing and measuring section length and diameter. Missing core parts were accounted for.

Reference

Pohjola, V. A., Moore, J. C., Isaksson, E., Jauhiainen, T., van de Wal, R. S. W., Martma, T., Meijer, H. A. J. and Vaikmäe, R.: Effect of periodic melting on geochemical and isotopic signals in an ice core from Lomonosovfonna, Svalbard, *Journal of Geophysical Research*, 107(10.1029), 2002.

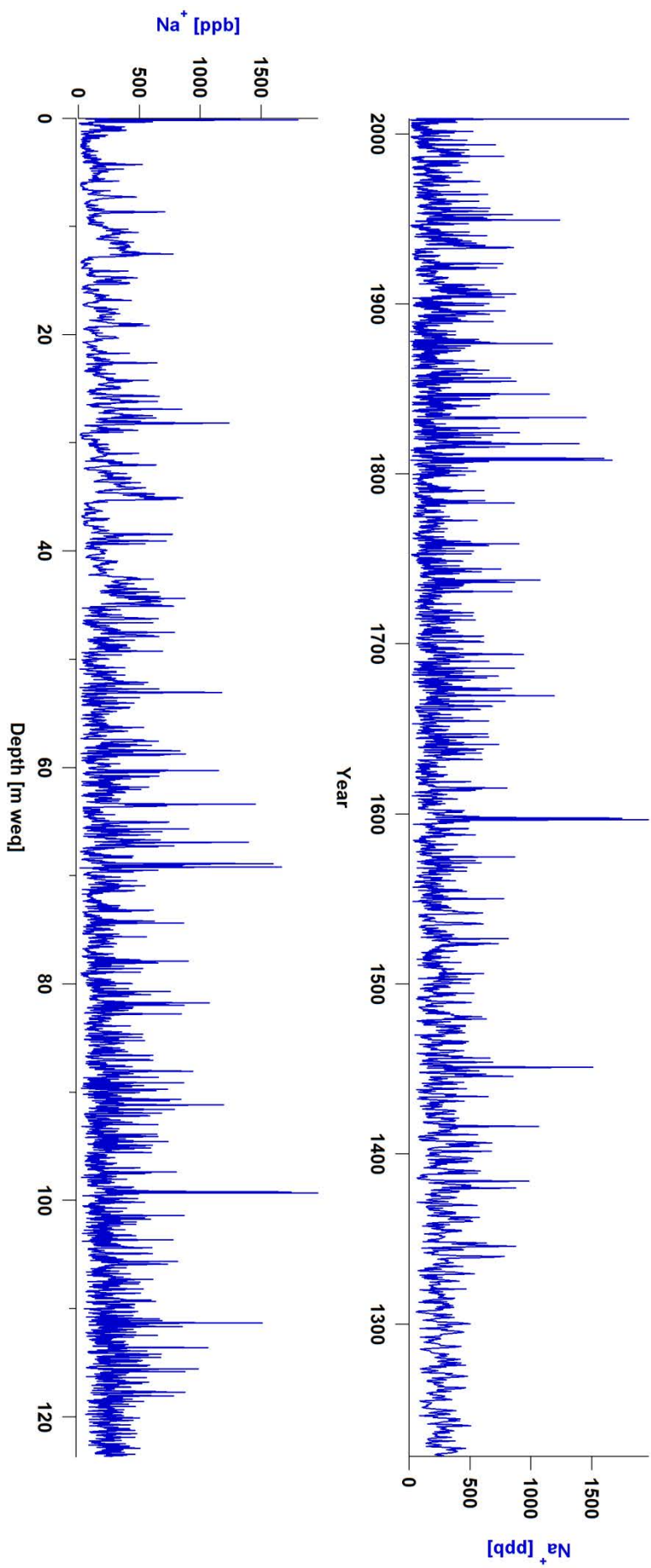


Figure 9.2 Record of the Lomo09 Na⁺ raw data against age (top) and depth (bottom.)

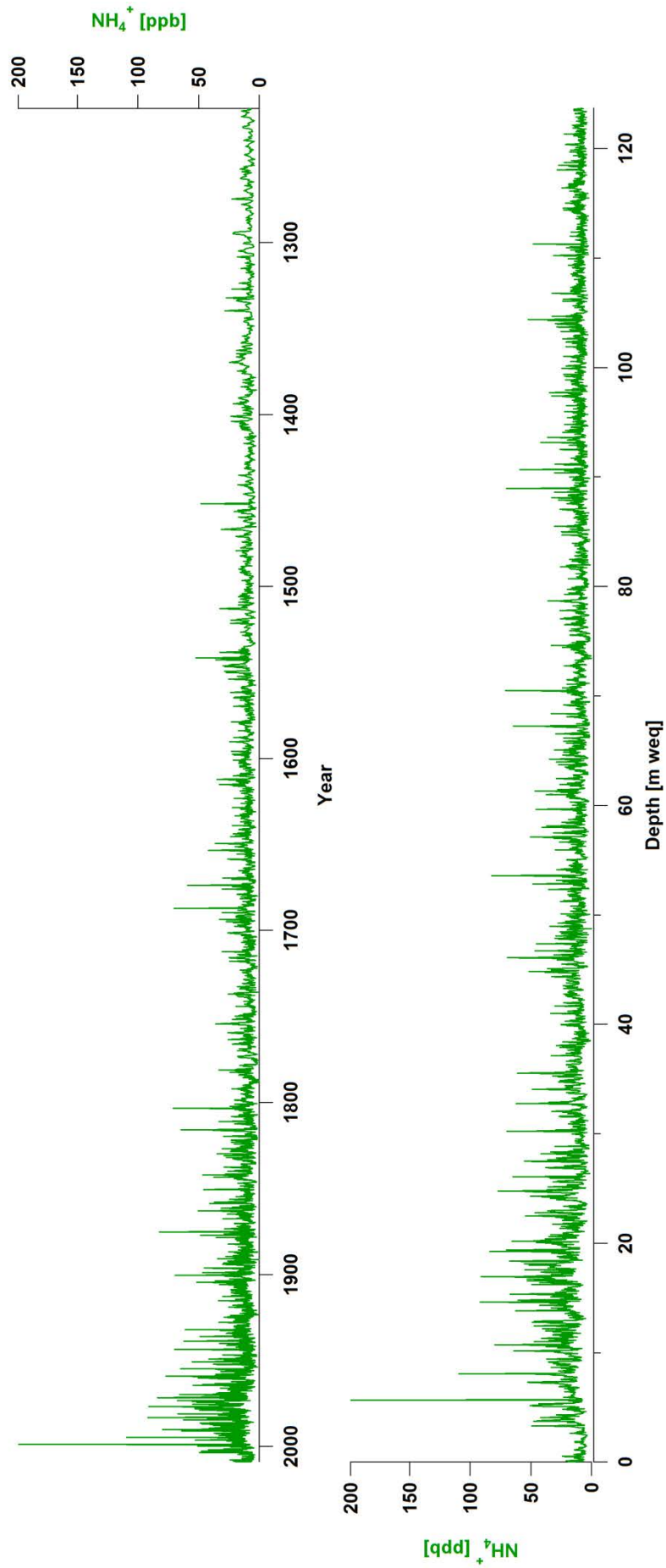


Figure 9.3 Record of the Lomo09 NH_4^+ raw data against age (top) and depth (bottom.)

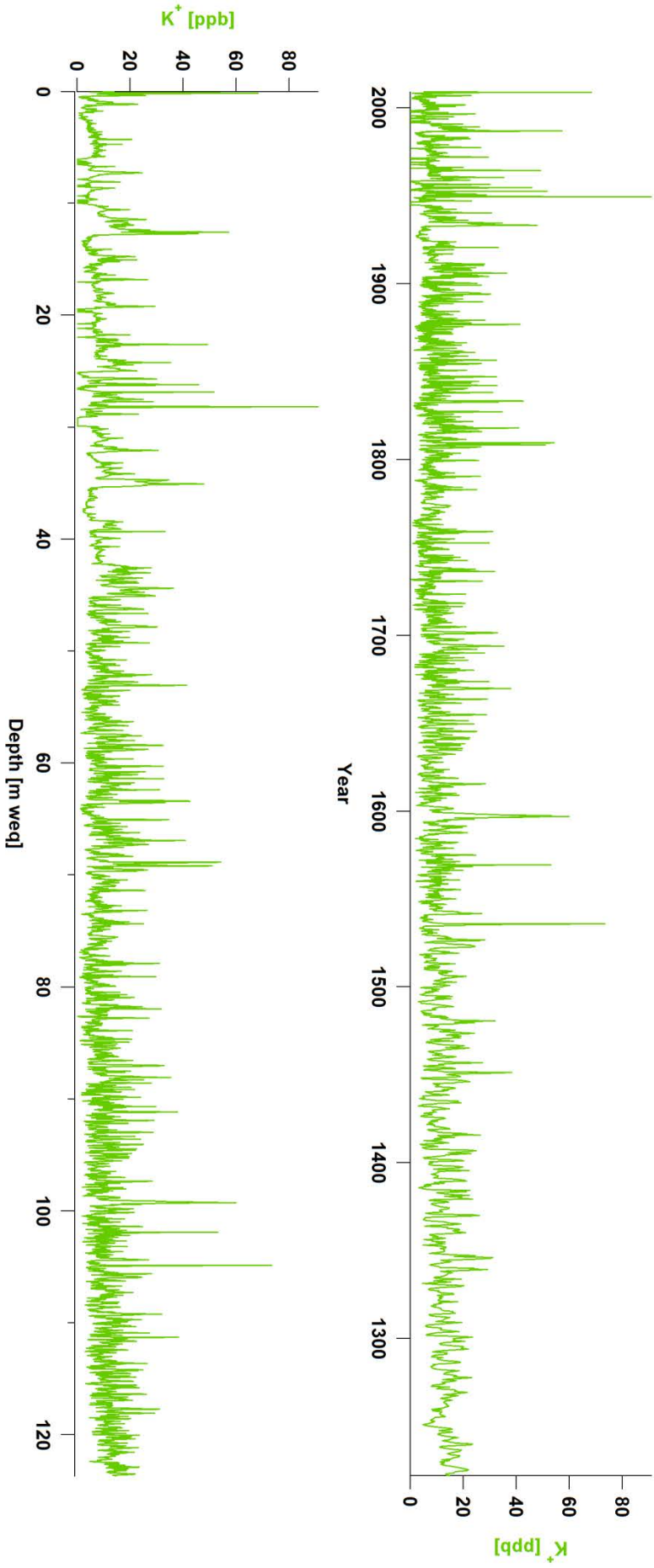


Figure 9.4 Record of the Lomo09 K^+ raw data against age (top) and depth (bottom.)

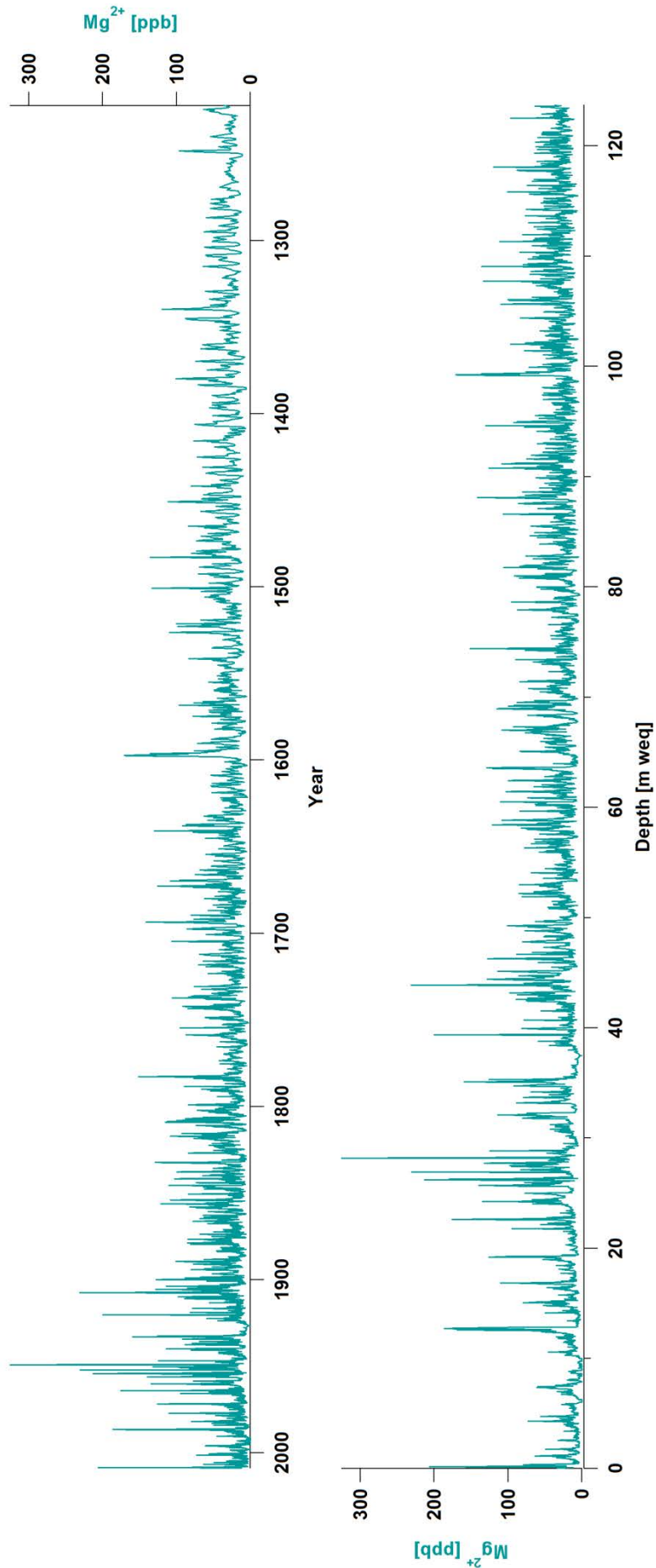


Figure 9.5 Record of the Lomo09 Mg^{2+} raw data against age (top) and depth (bottom.)

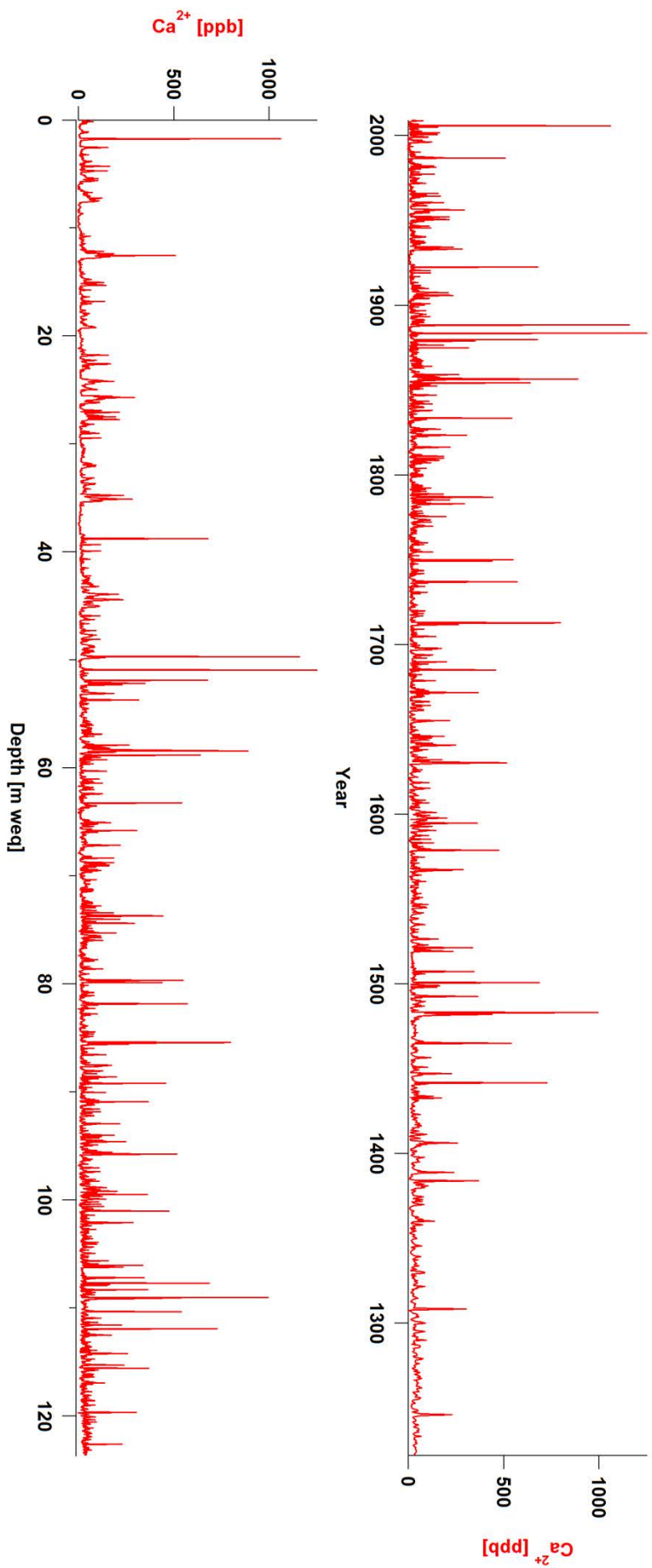


Figure 9.6 Record of the Lomo09 Ca^{2+} raw data against age (top) and depth (bottom.)

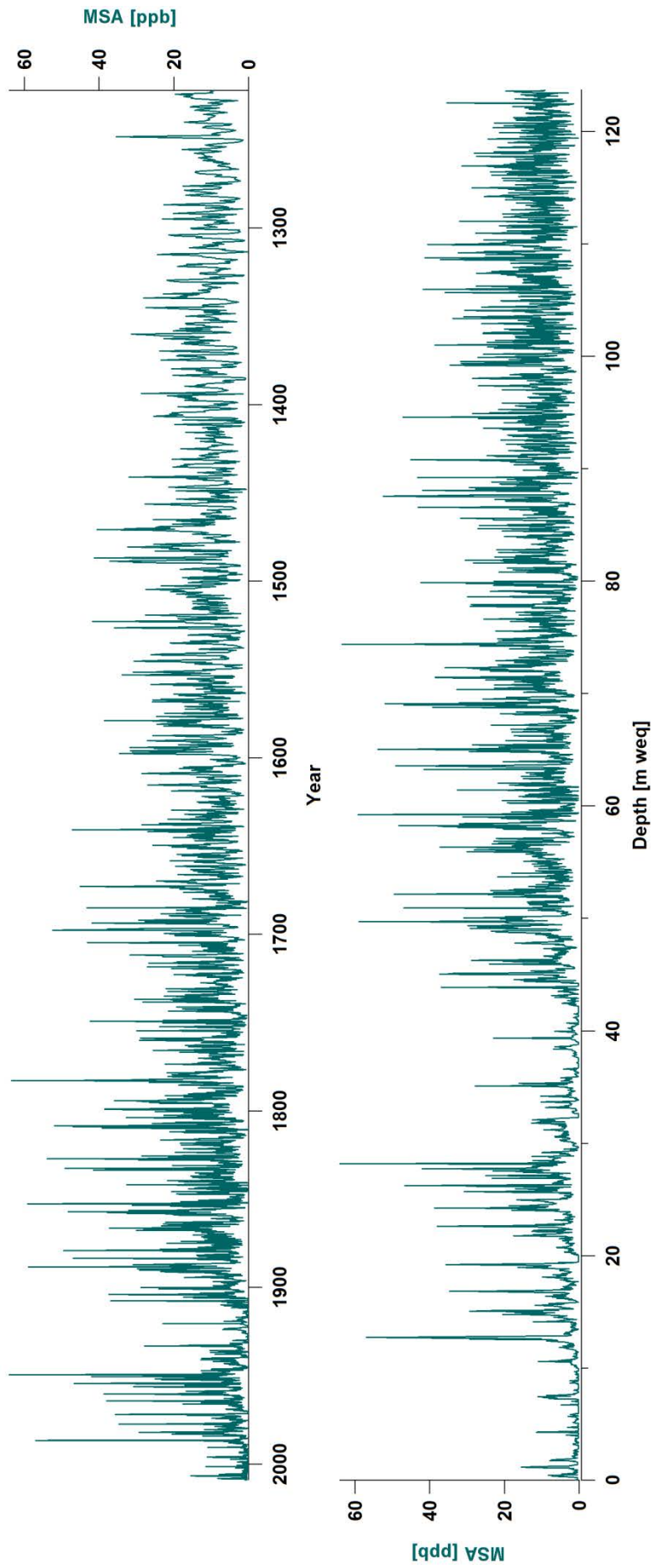


Figure 9.7 Record of the Lomo09 MSA raw data against age (top) and depth (bottom.)

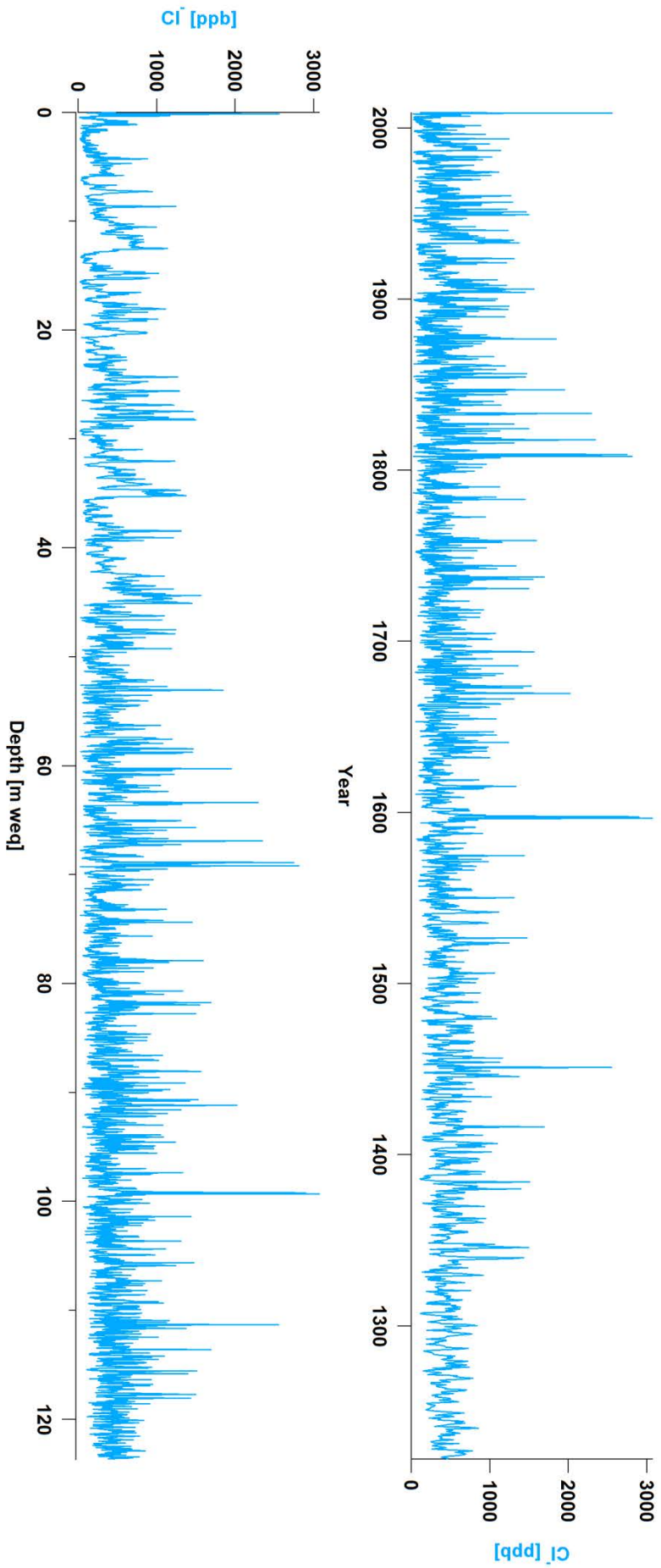


Figure 9.8 Record of the Lomo09 Cl^- raw data against age (top) and depth (bottom.)

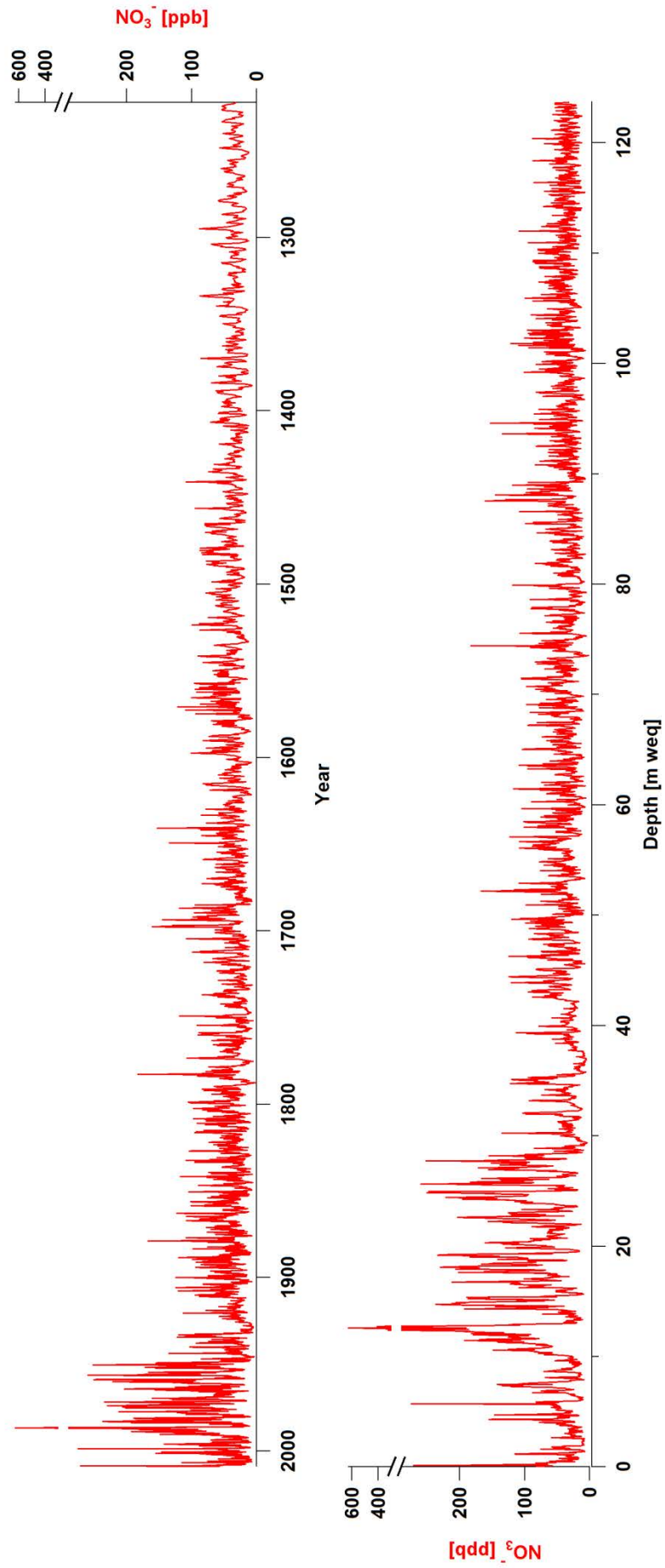


Figure 9.9 Record of the Lomo09 NO_3^- raw data against age (top) and depth (bottom.)

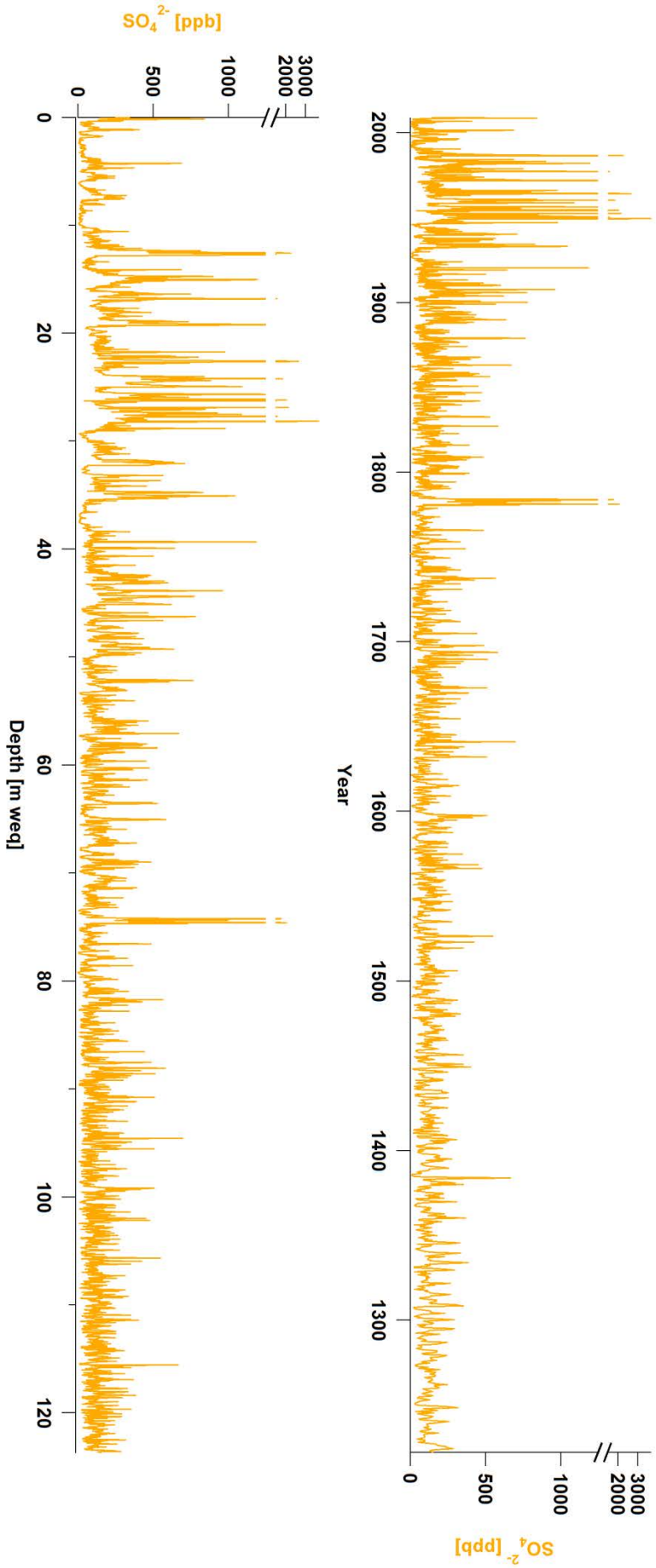


Figure 9.10 Record of the Lomo09 SO_4^{2-} raw data against age (top) and depth (bottom.)

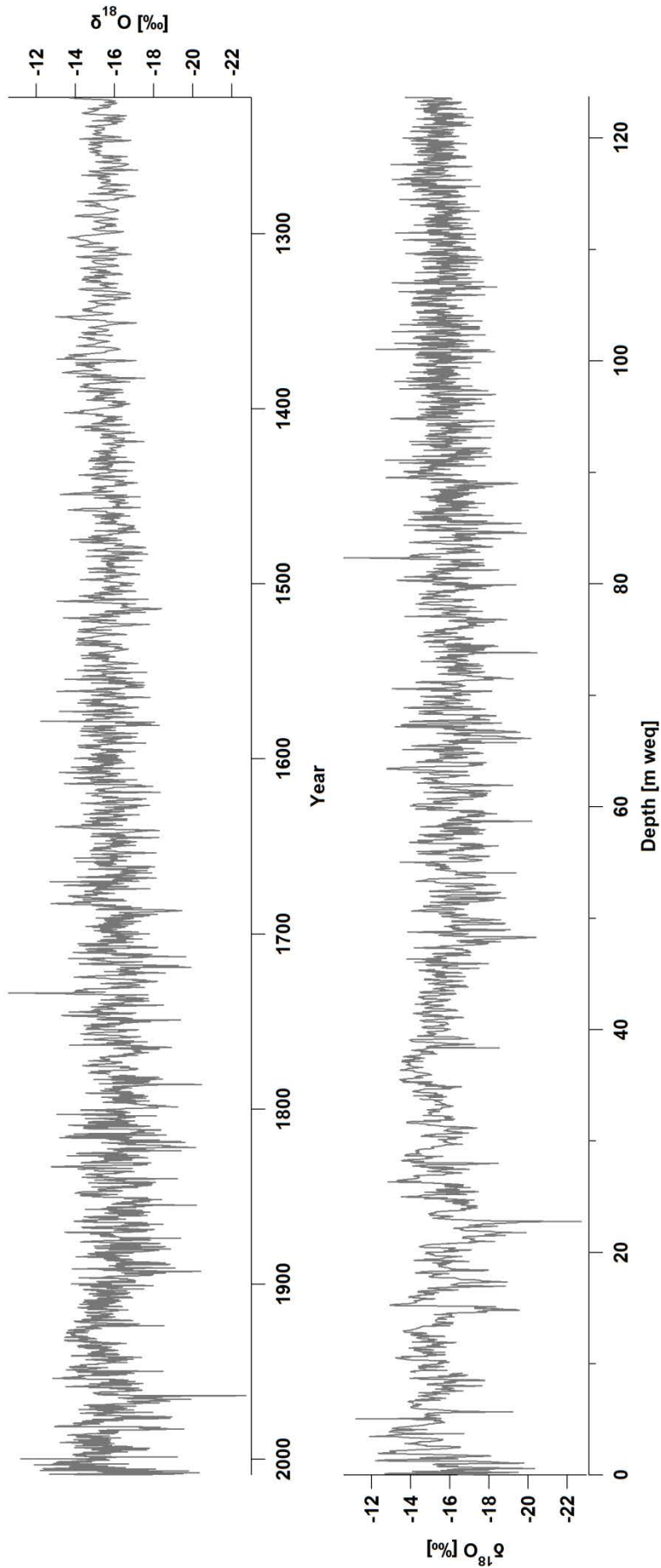


Figure 9.11 Record of the Lomo09 $\delta^{18}\text{O}$ raw data against age (top) and depth (bottom.)

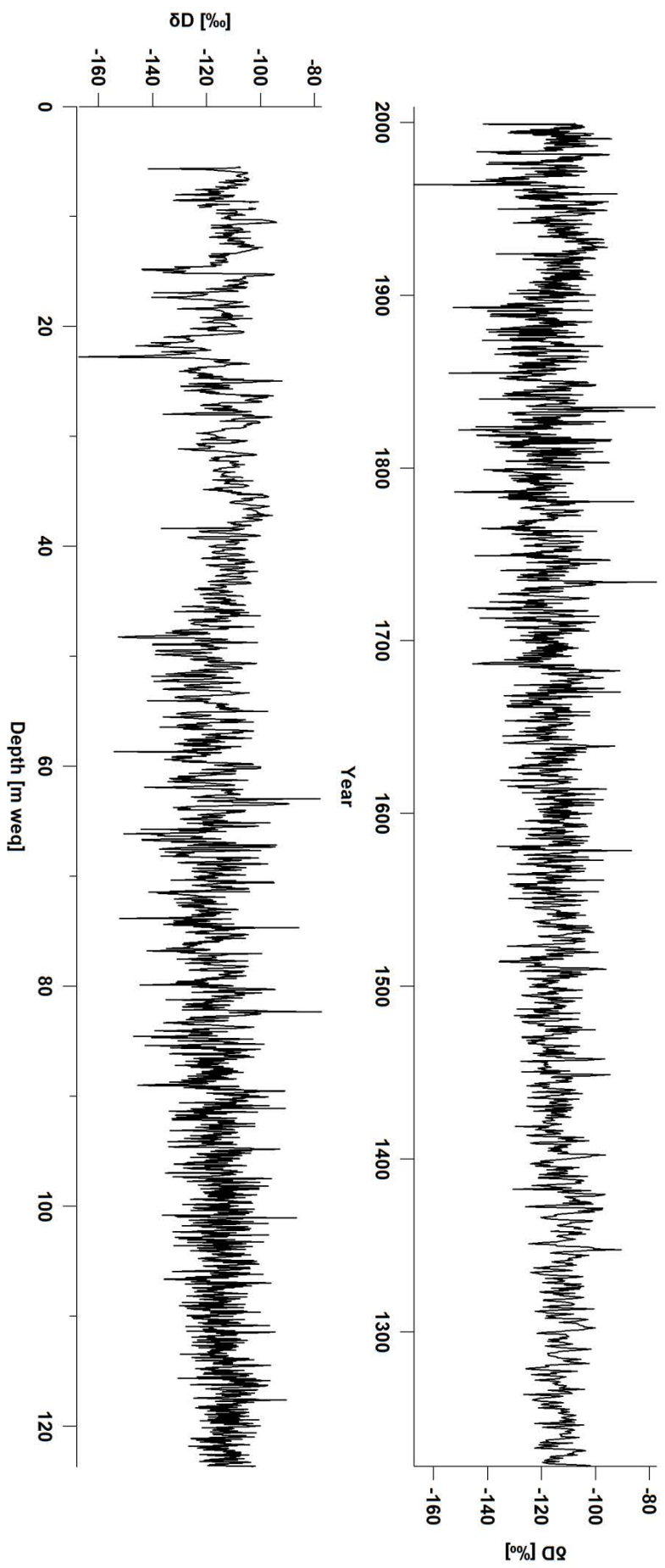


Figure 9.12 Record of Lomo09 dD raw data against age (top) and depth (bottom).

Acknowledgements

This PhD thesis would not have been possible without the help and support from colleagues, family and friends. Thanks to every single one of you. Please forgive me if I forgot to mention one or the other below.

- Margit Schwikowski for her guidance and support throughout the 4.5 years of my PhD. Thanks for always having time to listen and for keeping me on track. Thanks also for giving me the opportunity to work on 'my own ice core', experience the extreme weather in Svalbard, and join the drilling expeditions in the Alps.
- Anja Eichler for her support, fruitful discussions, and a general positive attitude that motivated me whenever I was down.
- Elisabeth Isaksson for her advice and the various very quick and helpful replies to all my questions regarding Svalbard ice core research.
- Marie Laborde and Martin Gysel for their almost endless patience in explaining the SP2 and IGOR to me. Thanks for not getting annoyed even if I asked for the 1000st time.
- Sabina Brüetsch for the help in the lab, especially regarding ion chromatography and water stable isotope analysis with Picarro, and lending me vials when I had run out of clean ones. Thanks for being such a good colleague and friend.
- Tõnu Martma for analysing most of the water stable isotope samples.
- Leo Tobler, Edith Vogel, Max Rüthi and Jost Eikenberg for preparing and analysing my samples for ²¹⁰Pb and tritium. Leo Tobler also for his patience with the broken saw blades and his advice on the APEX.
- Andy Menking and Susan Kaspari for exchanging experiences with the SP2.
- My office mates: Isabella Mariani, Pavlina Pavlova, Johannes Schindler, Pierre-Alain Herren, Cao Fang, and Anna Dal-Farra for a great office atmosphere. Isabella also for the good Italian coffee and for the help with the Picarro.
- Manuel Schläppi for the introduction to ice core sampling and the analytical methods, for the great company in the office during my first year of the PhD, and several running/swimming sessions during lunch break.
- The analytical chemistry group for a great atmosphere and interesting discussions.
- Raphael Färber, Benjamin Wyler, Ivo Budde, Valentine Grimaudo, Dimitri Osmont, and all the other colleagues and students that helped me to process the ice core and obtain the first BC data. I know that you've suffered a lot, especially when being exposed to the

noisy SP2 pump and the unpredictable BC content of the samples that made you stay at PSI till late. Thanks for your endurance and contribution to this work.

- The drilling team that made this PhD possible in the first place: Beat Rufibach[†], Dieter Stampfli, Mats Björkman, Gerit Rotschky, and Carmen Vega.
- Mats Björkman, Carmen Vega and Jakub Zarsky for a great time in Svalbard, and for introducing me to the extreme weather conditions in the high latitudes, frozen fingers included ☺
- Sepp Schreiber and Thorsten Bartels-Rausch for the running sessions during lunch break that gave my brain the chance to breath.
- Dave Piguet for making my trips to PSI during pregnancy way more comfortable.
- Maruta Bunka, Bernadette Hammer, Sabrina Lüthi and Tobias Lorenz for pulling me out of the office to have lunch and for the good coffee that made my days.
- Angela Blattmann for help with all the administrative issues and nice chats in between.
- Darren D’Cruz for keeping me ‘not too German’ and for help on the manuscript.
- My old and new friends: thanks for giving me time to relax, to sing, to chat, or to simply think of something else but work.
- The Laboratory of Radiochemistry and Environmental Chemistry for being great colleagues.

- My family:
 - My wonderful husband Matthias that has accompanied me through all the good and the bad times; thanks for all your love and support; thanks that you never stopped believing in me.
 - Our little daughter Hanna that has been a good girl all way through; thanks for letting me sleep during the nights and giving me strength just by smiling at me.
 - My parents Claudia and Gerhard and my sister Kristina for their endless love and support.
 - My parents-in-law Brigitte and Hans for their support and encouragement, and for covering my back by taking care of Hanna.

Last but not least I would like to thank Alex Zapf, one of my office mates. We’d been sitting next to each other for three years, shared bike rides to PSI, Italian coffee and had good discussions. Last year, he passed away far too early.

Erklärung

gemäss Art. 28 Abs. 2 RSL 05

Name/Vorname: Wendl, Isabel

Matrikelnummer: 09-121-922

Studiengang: Climate Sciences

Bachelor Master Dissertation

Titel der Arbeit: High-resolution records of black carbon and other constituents
from the Lomonosovfonna 2009 ice core

LeiterIn der Arbeit: Prof. Dr. Margit Schwikowski

Ich erkläre hiermit, dass ich diese Arbeit selbständig verfasst und keine anderen als die angegebenen Quellen benutzt habe. Alle Stellen, die wörtlich oder sinngemäss aus Quellen entnommen wurden, habe ich als solche gekennzeichnet. Mir ist bekannt, dass andernfalls der Senat gemäss Artikel 36 Absatz 1 Buchstabe r des Gesetzes vom 5. September 1996 über die Universität zum Entzug des auf Grund dieser Arbeit verliehenen Titels berechtigt ist.

Ich gewähre hiermit Einsicht in diese Arbeit.

.....
Ort/Datum

.....
Unterschrift

Curriculum Vitae

Name: Isabel Wendl, nee Schuck

Birth date: June 14th, 1983

Birth place: Heilbronn, Germany

Citizenship: German

Education

2010-2014 PhD thesis at the Paul Scherrer Institut, Switzerland, and the University of Bern, Switzerland

2009 Position at the Institute of Mineralogy and Geochemistry at the Karlsruhe Institute of Technology (KIT), Germany

2003-2009 Diplom (equivalent to Master) in Geoecology at the University of Karlsruhe, Germany

Diploma thesis entitled 'Mineralogical characterisation and geographic provenance of atmospheric particles in coastal Antarctic ice cores – indicators of past climate variability' in cooperation of the Institute of Mineralogy and Geochemistry, University of Karlsruhe, Germany, and the research institute Geological Nuclear Science (GNS), New Zealand
Advisors: Dr. Thomas Neumann (University of Karlsruhe), Dr. Nancy Bertler (GNS Science, Antarctic Research Centre, Victoria University Wellington)

2002-2003 Studies of Medicine, University of Heidelberg

1993-2002 Secondary School, Heilbronn, Germany

Contribution to conferences

- 2012 Poster at the International Partnerships in Ice Core Sciences (IPICS), First Open Science Conference, Presqu'île de Giens, France, October 1st-5th
- 2011 Poster at the 9th Swiss Geoscience Meeting, ETH Zürich, Switzerland, November 11th-13th
- 2010 Poster at the 9th International NCCR Climate Summer School, 'Adaptation and Mitigation: Responses to Climate Change', Grindelwald, Switzerland, August 29th-September 3rd
- 2010 Participation at the 9th NCCR Young Researchers Meeting, Löwenberg, Switzerland, July 10th-11th
-

Field experience

- 2012 Plaine Morte glacier, Swiss Alps, ice core deep drilling
- 2011 Ewigschneefeld, Swiss Alps, ice core deep drilling
- 2010 Jungfrauoch, Swiss Alps, snow sampling
- 2010 Foxfonna, Svalbard, snow pit sampling
-

Work experience

- 2010-2011 Assistant in the laboratory course in chemistry for biology students
- 2010-2013 Supervision of several students and pupils at the Paul Scherrer Institut including a BSc thesis and an internship
- 2009 Administrative work on a future project including the preparation of a funding proposal
-